THEORETICAL STUDIES ON SOME ASPECTS OF MOLTEN FUEL-COOLANT THERMAL INTERACTION

by

Mujid Suliman Kazimi
B. Eng., University of Alexandria (Egypt)
1969
M.S., Massachusetts Institute of Technology
1971

SUBMITTED IN PARTIAL FULFILLMENT OF THE
REQUIREMENTS FOR THE DEGREE OF
DOCTOR OF PHILOSOPHY
at the

MASSACHUSETTS INSTITUTE OF TECHNOLOGY

June, 1973

Signature of Author _____
Department of Nuclear Engineering
May 4, 1973

Certified by _____ May 4, 1973
Thesis Supervisor

Certified by _____ 4, 1973
Thesis Supervisor

Accepted by _____
Chairman, Departmental Committee on
Graduate Students

THEORETICAL STUDIES ON SOME ASPECTS OF MOLTEN-FUEL-COOLANT THERMAL INTERACTION

by

Mujid S. Kazimi

Submitted to the Department of Nuclear Engineering on May 4, 1973 in partial fulfillment of the requirements for the degree of Doctor of Philosophy.

ABSTRACT

Rapid generation of high pressures and mechanical work may result when thermal energy is transferred from the hot molten nuclear fuel to the coolant in an LMFBR accident. Such energetic thermal interactions are facilitated by the large heat transfer area created when molten fuel is fragmented in the coolant. Two aspects of the molten fuel-coolant interaction problem are investigated: (1) the effects of gas/vapor blanketing of the fuel on post-fragmentation generation of pressure and mechanical work, and (2) the mechanism of the fragmentation of the molten fuel as it contacts the coolant.

A model developed at Argonne National Laboratory to analyze fragmentation-induced energetic fuel-coolant interactions is modified to allow for gas/vapor blanketing of the fuel. The modified model is applied to a hypothetical accident involving an FFTF subassembly. The results indicate that high shock pressures are not necessarily precluded by gas/vapor blanketing of the fuel. However, the generation of mechanical work is greatly reduced.

A model is developed to simulate the dynamic growth of the vapor film around a hot spherical particle which has been suddenly immersed in a coolant. The model is applied to various cases of hot spheres in water and in sodium. A fragmentation mechanism based on the ability of the pressure pulsations of the vapor film to induce internal cavitation in the molten material is shown to predict the reported fragmentation behavior of drops of several hot molten materials in water and sodium.

Thesis Supervisors:

Neil E. Todreas - Associate Professor of Nuclear Engineering

David D. Lanning - Professor of Nuclear Engineering

ACKNOWLEDGEMENTS

I wish to express my sincere appreciation to Professor Neil E. Todreas and Professor David D. Lanning for their encouragement, suggestions and constructive criticism throughout the development of this work, to Professor Warren M. Rohsenow of the Mechanical Engineering Department for his invaluable advice on several considerations in this work, and to Dr. Dae H. Cho of Argonne National Laboratory for his advice on developing the analysis in Chapter 3 and for making available unpublished experimental results.

I am also grateful to Mr. Rateb Abu Eid for his assistance in drawing some of the figures, to Mrs. Virginia O'Keefe and Miss Clare Egan for their patience and skill in converting my scribblings into this manuscript in a short time.

TABLE OF CONTENTS

Page

LIST OF FIGURES

LIST OF TABLES

NOMENCLATURE

A	surface area, a constant or coefficient
A_v	Avogadro's Number
B	constant characteristic pressure of a compressible liquid (Eq. 4.32)
B_v	compressibility coefficient
C	specific heat, sonic velocity or a coefficient
C_p	specific heat, at constant pressure
H	enthalpy or kinetic enthalpy
G	perfect gas constant
L	length of constraining sodium (Chapter 3)
K	coefficient
M	mass or molecular weight
P	pressure
P_∞	ambient pressure
P(T)	saturation pressure at the temperature T
Q	total heat content
R	radius of sphere
R_δ	radius of the film/liquid interface (Chapter 4)
S	cross sectional area of flow (Chapter 3)
T	temperature
T_{sat}	saturation temperature
T^*	minimum temperature of a hot wall to sustain film boiling

U	velocity
V	volume
W	mass of fuel/gm of interacting sodium (Chapter 3) or work of formation of a vapor nucleus (App. H)
Y	generalized variable in Chapter 4
Z	length of the interaction zone in Chapter 3
a	coefficient
c	specific heat or sonic velocity
g	conversion factor
h	specific enthalpy
h*	heat transfer coefficient
h_{fg}	heat of vaporization
h(T)	specific enthalpy at the saturation temperature T
k	thermal conductivity or Boltzman's constant
m	mass of one molecule
n	adiabatic index (for a perfect gas = C_p/C_v)
q"	heat flux
r	radius
t	time
tm	characteristic time for fuel surface area generation in Chapter 3
u	radial velocity at any radius r
v	specific volume

α	thermal diffusivity
α'	thermal expansion coefficient
β	isothermal compressibility
γ	negative pressure required for cavitation
δ	film (blanket) thickness
Δ	thickness of the thermally active region in the liquid (Chapter 4)
ε	emissivity of radiative heat
η	accommodation coefficient
λ	thickness of the thermally active region in the sphere (Chapter 4) or heat of vaporization of one molecule (Appendix H)
μ	viscosity
ρ	density
σ	surface tension

Subscripts

b	blanket
c	defined at the center of the sphere
cr	critical thermodynamic value
f	film
g	gas
gb	blanket gas
in	at the interface

h	hot sphere (Chapter 4)
hi	initial value for the hot sphere
ℓ	liquid
ℓi	initial value for the liquid
ℓv	at the liquid/vapor interface
m.p.	at the melting point
r	radiation
R	at the radius R
s	sodium
s.n.	spontaneous nucleation
u	fuel (UO_2)
v	vapor

Chapter One

INTRODUCTION

Chapter One

INTRODUCTION

1.1 Molten Fuel-Coolant Interaction In LMFBR Safety Analysis

In the current approach to safety analysis of the liquid metal fast breeder reactor (LMFBR), considerable attention is being given to the possibility and consequences of thermal interaction of molten fuel and sodium[1-3]. The consequences of molten fuel-coolant interaction have a larger degree of uncertainty than other key phenomena of interest to LMFBR safety. Thermodynamically, as much as 30% of the thermal energy of the molten fuel may be converted to mechanical work by the transfer of heat from the fuel to sodium[4]. The possibility of producing such a high thermal-to-mechanical energy conversion ratio has been demonstrated in small scale laboratory experiments involving injection of an amount of sodium into molten fuel[5]. However, such high energy conversion ratios have not been observed in each case in which molten fuel and sodium were brought into contact. The pressure pulses and mechanical work generated by molten fuel-sodium thermal interaction seem to depend on the conditions of contact between the molten fuel and sodium. An understanding of the basic physical mechanisms involved in the thermal interaction process is required if an accurate assessment of the influence of the contact conditions on the consequences

of molten fuel-sodium thermal interaction is to be made.

The possibility of producing energetic thermal interactions is not a pecularity of LMFBR materials. Rapid generation of high pressure and mechanical energy has been observed in accidents and experiments involving other hot molten materials and coolants, as will be reviewed in Chapter 2. Such occurrences are often called thermal explosions or vapor explosions. At present, there is no consensus of opinion about the sequence of physical events leading to such explosions.

1.2 The Physical Mechanisms Involved In Explosive Thermal Interactions

The sequence of physical events leading to explosive pressure generation when a hot liquid contacts a relatively cold liquid is not yet completely understood. Two plausible theories have been advanced:

1] Fragmentation-Induced Explosive Interaction

In this theory the explosive pressure generation is due to rapid heating of a constrained volume of the cold liquid. The rapid heat transfer is facilitated by an increase in the heat transfer surface area when either of the two fluids is fragmented and is dispersed in the other fluid[6-8].

2] Nucleation-Induced Explosive Interaction

In this theory the explosive pressure generation

is due to superheating the cold liquid to the temperature at which spontaneous nucleation occurs[9-11]. Vaporization by spontaneous nucleation is rapid enough to cause high pressure pulses. In this case the heating rate of the cold liquid is not controlling as long as the liquid can be heated to the temperature required for spontaneous nucleation.

Fragmentation of molten UO_2 as it contacts sodium has been observed at several laboratories[12,13]. If the thermal energy of the dispersed UO_2 fragments is transferred to a constrained volume of sodium, large pressure pulses and potentially damaging mechanical work can be developed. This is the picture depicted in the Parametric Model for Fuel Coolant Interaction developed at Argonne National Laboratory (ANL-FCI)[14,79]. Parametric studies using the ANL-FCI model have identified several conditions that can prevent the development of high pressures and mechanical work. These conditions include:

1. Limiting the amount of UO_2 and sodium that actually interact.
2. Making available a large expansion volume for the heated sodium.
3. Limiting the heat transfer rate from the fuel to sodium, which can result from either high thermal resistance or limited interface area between the fuel and sodium.

For nucleation-induced vapor explosions to occur in a UO_2/Na system, the sodium must be confined in a zone such that it can be heated up to the spontaneous nucleation temperature. Sodium confinement is necessary since the interface temperature obtained by sudden contact of UO_2 and sodium is far below the spontaneous nucleation temperature of sodium[11]. Additionally, the availability of nucleation sites at the molten UO_2/liquid Na interface or within the sodium will prevent the development of highly superheated sodium. The requirements that the sodium be confined and that nucleation sites be unavailable highly restrict the conditions under which nucleation-induced explosive pressure generation can develop in an LMFBR accident.

The relative roles of both of the afore outlined theories for explosive thermal interactions in the varied configurations of fuel-sodium contact conditions of interest for LMFBR safety analysis is still to be determined.

1.3 The Present Work

The objective of the present work is two-fold:

1] Assessment of the effect of gas/vapor blanketing of the fuel on the pressure pulses and mechanical work that can be generated by a fragmentation-induced vapor explosion.

2] Identification of the physical mechanism inducing

the fragmentation of the molten fuel as it contacts sodium.

The assessment of the effects of gas/vapor blanketing on the thermal interaction is made by modification of the ANL Parametric Model for Fuel-Coolant Interactions. In the original model the thermal resistance to the heat flow from the fuel was assumed to be only that of the fuel fragments. Such an assumption is highly conservative if the fuel fragments become blanketed by non-condensable gases released from the fuel pins or by sodium vapor. The formulation of the modified model and the results of its application to various cases are presented in Chapter 3.

The physical mechanism leading to fragmentation of the molten fuel as it contacts sodium has not been previously identified. In Chapter 5, the fragmentation mechanism is investigated. In this investigation use is made of experiments involving the fragmentation of several molten materials in different liquids. Additionally, use is made of the results of an analytic model developed in the present study to describe the dynamic growth of a vapor film around a spherical particle.

It is hoped that the results of the present work will be useful in the realistic assessment of the consequences of thermal interaction of molten fuel and sodium under LMFBR accident conditions.

Chapter Two

LITERATURE REVIEW: STUDIES OF THERMAL INTERACTIONS OF HOT MOLTEN MATERIALS AND COOLANTS

Chapter Two

LITERATURE REVIEW: STUDIES OF THERMAL INTERACTIONS OF HOT MOLTEN MATERIALS AND COOLANTS

2.1 Introduction

The purpose of this review is to give a comprehensive summary of experimental and theoretical studies presently available in literature related to the nature and consequences of thermal interaction of molten fuel and sodium. The volume of the published studies on the thermal interaction of molten UO_2 and sodium is small but rapidly expanding because of the emphasis in many countries on the development of LMFBR for future production of electrical energy. Additionally, extensive studies on thermal interaction of other hot molten materials and coolants have been undertaken through safety programs of other types of reactors as well as of non-nuclear industries. While this review is not intended to be inclusive of all studies on thermal interactions of hot and cold liquids, an attempt is made to summarize the pertinent results of such studies.

2.2 Experimental Studies on Thermal Interactions of Hot Molten Materials and Coolants

The experimental studies reviewed here have been largely conducted in the U.S.. Results of several experiments conducted abroad are in general agreement with the U.S. findings. Active international experimental programs related to fuel-sodium interactions have been reported at the CREST Meeting on Fuel-Sodium Interaction at Grenoble,

France in January 1972. A summary of the presented papers can be found in Ref.15. Where differences with the U.S. experimental results exist, the results of the non U.S. work are included here.

2.2.1 Incidents of Explosive Thermal Interactions

The production of explosive pressures when a hot molten material contacts a liquid was reported as early as the 19th century. Percy[16] reported in 1864 the occurrence of such accidents in the metal refining industry. As recently as 1966 Lipset[17] reported an explosion when about 100 lb. of molten steel dropped accidentally in a shallow trough containing about 750 gallons of water. Several other incidents involving spillage of molten metals and paper smelt (fused sodium carbonate) onto wet surfaces have been documented by Epstein[18] and Witte et al.[19].

In some nuclear reactor incidents and destructive tests the observations seem to be well explained by the occurrence of energetic thermal interactions between molten nuclear fuel and the coolant. A comprehensive summary of the causes and observations of such accidents and tests has been given by Thompson[20]. The first thermal interaction between molten nuclear fuel and reactor coolant may have been obtained in 1952 as a result of the core meltdown accident of the Canadian NRX test reactor. Although several mechanisms may have contributed to the destructive energy release (nuclear energy release, chemical

energy release, and thermal metal-water interaction), Hurst[21] concluded in his analysis of this accident that the damage to the calandria tubes was a direct result of either uranium-steam or uranium-water interaction and was not nuclear or chemical in nature. Dietrich[22] attributed the high pressures (probably ~ 10,000 psi) observed in the BORAX-I destructive test to the contact of molten metallic fuel elements and water coolant. He found no evidence of chemical reaction, although some of the fuel elements that had melted appeared as spongy globules. Kettel et al.[23] postulated that vaporization of Nak (coolant) entrained in the molten fuel produced the spongy structure observed in the EBR-I meltdown accident. Several other studies have shown that the explosions observed in the SL-1 accident and the SPERT-1D destructive test were most likely the result of rapid generation of vapor from contact of water and molten metals[24-26].

2.2.2 Experiments of Discharging Large Amounts of Hot Molten Materials into Coolants

The occurrence of explosions in the nuclear and non-nuclear industries led to several experimental programs concentrating on the mechanisms involved in the interactions of molten materials and coolants. Elgert and Brown[27], Higgins[28] and Long[6] observed explosive interactions when molten metals were discharged in water. The extent of chemical reactions involved, as evidenced by post-test

examination, did not justify the intensive pressure generation. Epstein[29] showed that the kinetics of chemical reactions between metals and water make the development of some of the observed rapid generation of high pressures impractical by chemical means.

In the experiments of Long[6] involving the discharge of 50 lbs of aluminum in a water tank, explosions were prevented when the bottom of the tank was coated by grease, oil or paint. Long concluded that the explosions were a result of rapid heat transfer from aluminum fragments to water, and that aluminum fragmentation was the result of vaporization of a small amount of water entrapped between the molten aluminum and the bottom of the tank. Experiments with magnesium produced similar results. However, when a mixture of molten sodium chloride and potassium chloride was poured into water, explosions could not be prevented by grease coatings of the water tank. No explanation was provided by Long for the difference in behavior of a salt/H_2O system from a metal/H_2O system. Long's findings from the Al/H_2O experiments were further supported by Hess and Brondyke[30]. Sallack[31], after experiments of paper smelt quenched in green liquor, proposed that spontaneous fragmentation of the quenched molten material results from vaporization of liquid entrained in cracks in the solidified surface of the smelt.

2.2.3 Shock Tube Experiments

Several types of experiments were conducted at TRW Space Technology Laboratories in order to determine the mechanism of creating high pressure levels during a nuclear reactor transient. The earliest tests used a flat plate fuel element and the KEWB reactor as a pulsed heating source[32]. Another group of experiments employed a stainless steel electrical heater which could achieve more rapid thermal transients than the ractor heat source[33]. These tests indicated that the pressures generated by vaporization of water by heat fluxes from solid surfaces are relatively low and further reduced if non-condensable gases were present in the system. Later, Wright[34] conducted experiments involving the use of a shock tube, in which a column of water impacted hot materials held in the bottom of the tube. The water column was 3 ft long and was initially held above the hot material by a diaphragm. Solid and molten aluminum, silver and UO_2 powder were used as heat sources. The impact of the water column on solid metal resulted in low pressure generation. The impact of the water column on molten materials resulted in the generation of pressures as high as 5800 psi and the dispersion of part of the molten materials as fine fragments. The peak pressures would increase as the temperature of the molten metal was increased. The time rise of the pressure was within 0.5 msec from the initial contact of the metal and

the water. The peak pressures observed in the UO_2 powder experiments were lower than those with molten aluminum (same temperature of UO_2 and Al). This was attributed to the existence of compliant space in the discontinuous UO_2 material as well as the lower thermal conductivity of UO_2.

The results of Wright's shock tube experiments have been supported by the recent European experiments of Hillary[15] and Darby[15]. In those experiments, the presence of non-condensable gases in the interaction zone at a pressure of 1 cm Hg prevented the fragmentation of the molten material and inhibited the explosion.

Shock tube experiments employing a sodium column have been reported by Holtbecker et al.[15]. The hot molten material in the reported experiments was alumina at 2670°K. Repeated pressures of small magnitude have been observed. Molten UO_2 instead of alumina is to be used as a heat source in future experiments.

2.2.4 Experiments of Dropping Small Amounts of Hot Molten Materials in Coolants

The fragmentation of hot molten materials in the form of small drops as they contact relatively cold liquids has been observed at several laboratories. A detailed summary of the results of these experiments in included here since these results provide evidence on the nature of the mechanism inducing the fragmentation of molten

UO_2 on free contact with sodium (Discussed in Chapter 5). The data from these experiments is summarized here as quantitatively as could be obtained from the reported literature. The hot drop temperature is usually given at the initial time of dropping and not at the time of actual interaction with the coolant. The drop temperature of interaction would be less than the initial temperature due to cooling during both the fall through the gaseous atmosphere and also through the coolant depth.

2.2.4-a Experiments in Sodium

Experiments of dropping small amounts of materials in a sodium pool have been conducted at ANL by several investigators[12,35-37]. Figure 2.1 summarizes the results of these experiments. The effect of the initial temperature of stainless steel on the size of resulting fragments[37] is shown in Fig. 2.2. Early qualitative observations[36] of dropping 2200°C stainless steel into sodium at 250, 450, 600, 700 and 820°C indicated an enhancement of fragmentation with the increase in the sodium temperature. This conclusion is supported by the more recent quantitative results of Armstrong[12] (shown in Fig. 2.3) and the qualitative observations of Amblard[13].

With the increase in the sodium pool temperature from 200°C to 400°C the peak pressure in the sodium pool as observed by Armstrong[12] increased from 350 psi to 635 psi. The pressure transducer did not operate in 600°C sodium.

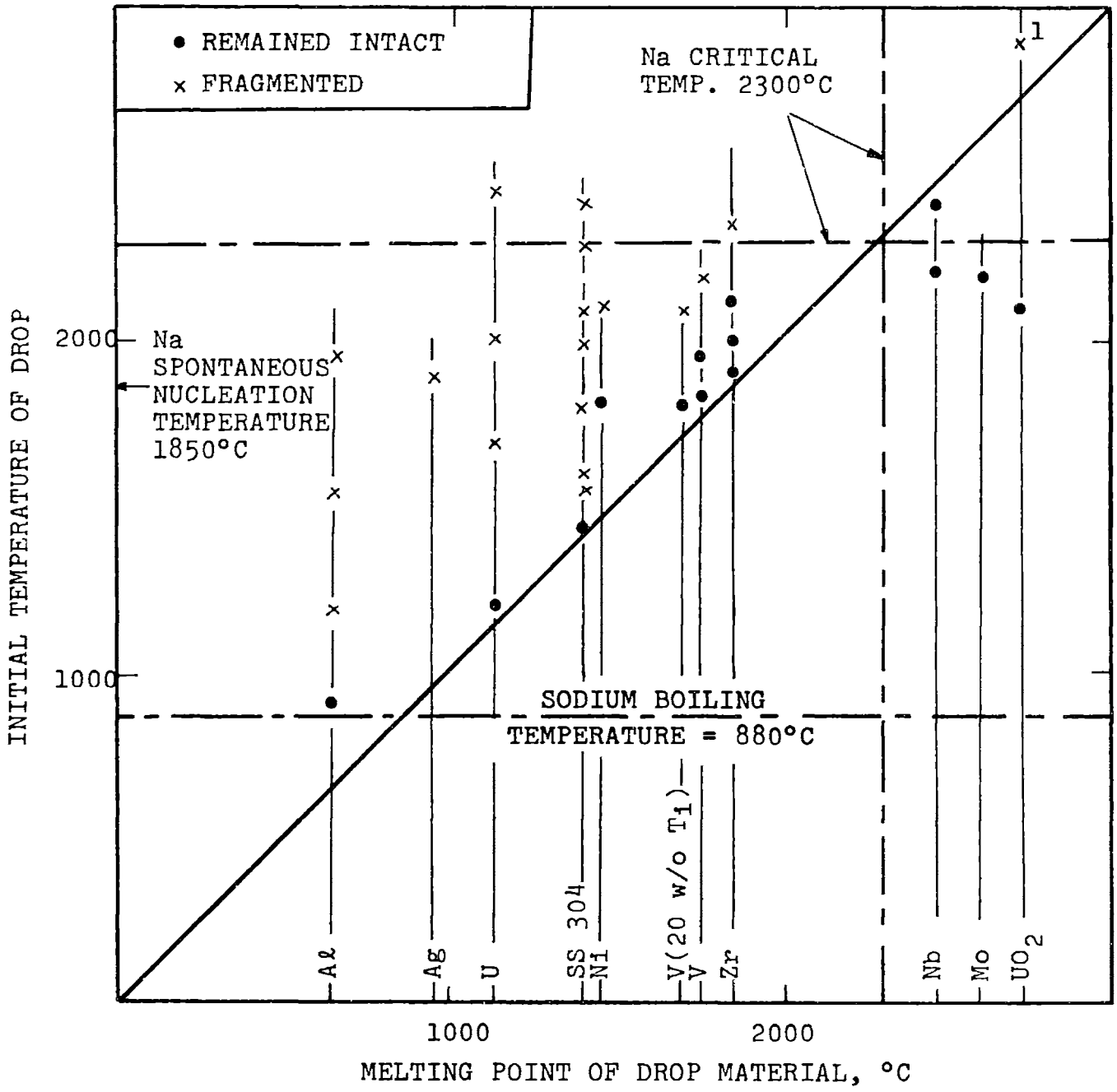

1. OBSERVED IN EXPERIMENTS IN WHICH ~ 1 cm^3 UO_2 WAS DROPPED IN SODIUM AT 200, 400 and 600°C (REF. 12)

FIG. 2.1: RESULTS OF DROPPING VARIOUS MATERIALS INTO SODIUM (REF. 36)

SODIUM TEMPERATURE = 250°C
DROP VOLUME ~ 0.3 cm^3
HEIGHT OF DROPPING = 2 ft.

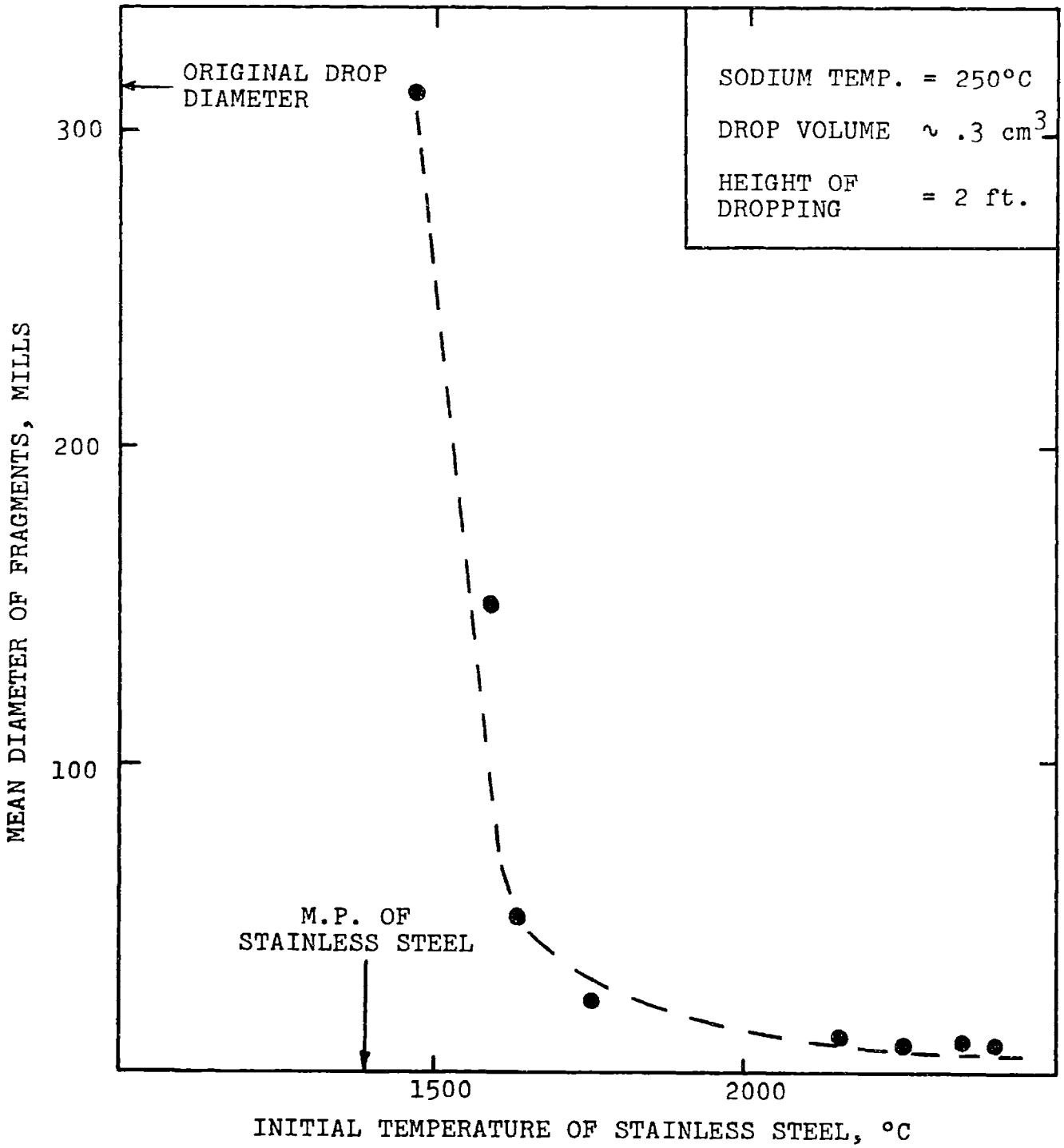

FIG. 2.2: EFFECT OF INITIAL TEMPERATURE OF STAINLESS STEEL ON MEAN DIAMETER OF FRAGMENTS (REF. 37)

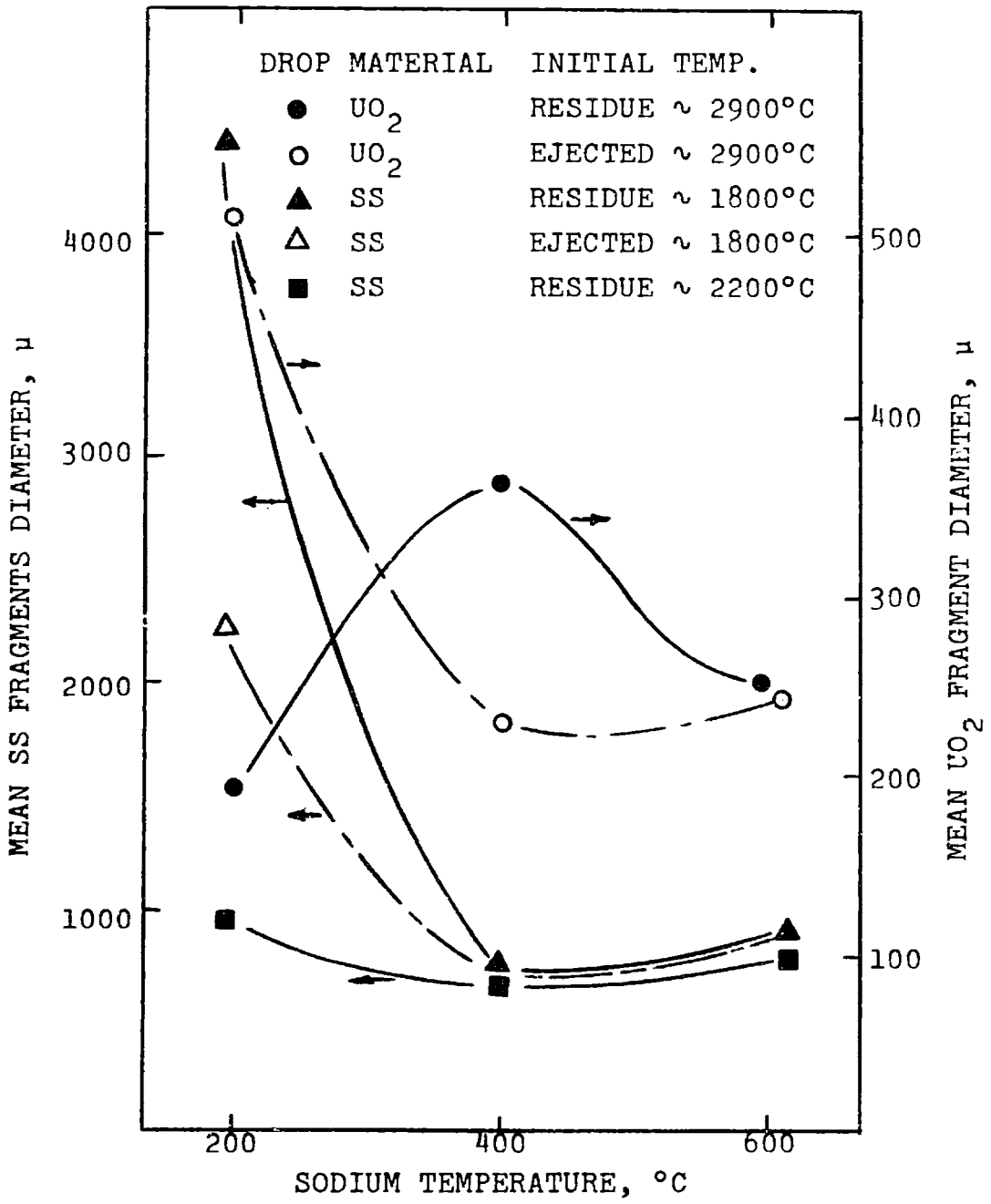

FIG. 2.3: MEAN DIAMETER OF RESIDUE AND EJECTED UO_2 AND STAINLESS STEEL FRAGMENTS AS A FUNCTION OF SODIUM BATH TEMPERATURE (REF. 12) (HEIGHT OF DROPPING NOT REPORTED)

The results of the sodium experiments indicate:

1. Initially solid hot materials do not fragment into sodium.
2. Some degree of sensible heat is required above melting, for fragmentation to occur.
3. At a fixed sodium pool temperature, fragmentation of stainless steel is enhanced by the increase in the initial drop temperature.
4. For a fixed initial drop temperature, fragmentation of stainless steel is enhanced by the increase in the temperature of the sodium pool, within the tested range of 200 to 820°C. The experiments of UO_2 are less definitive in this respect.

2.2.4-b Experiments in Water

Water has been the most extensively used coolant in dropping experiments. In their experiments Swift and Pavlik[35,36] found some of the molten metals will not fragment in water, as shown in Fig. 2.4. Ivins[38] observed an enhancement of the fragmentation with the increase in the "Weber Number" of the drop. The Weber Number is a measure of the ratio of the inertial forces resisting the motion of the drop to the forces of its surface tension. The Weber Number is defined as $N_W = \rho DV^2/\sigma$ where ρ is the coolant density, D is the drop diameter, V is the velocity of the drop as it contacts the coolant and σ is the interfacial surface tension. The existence of a Weber Number effect is an

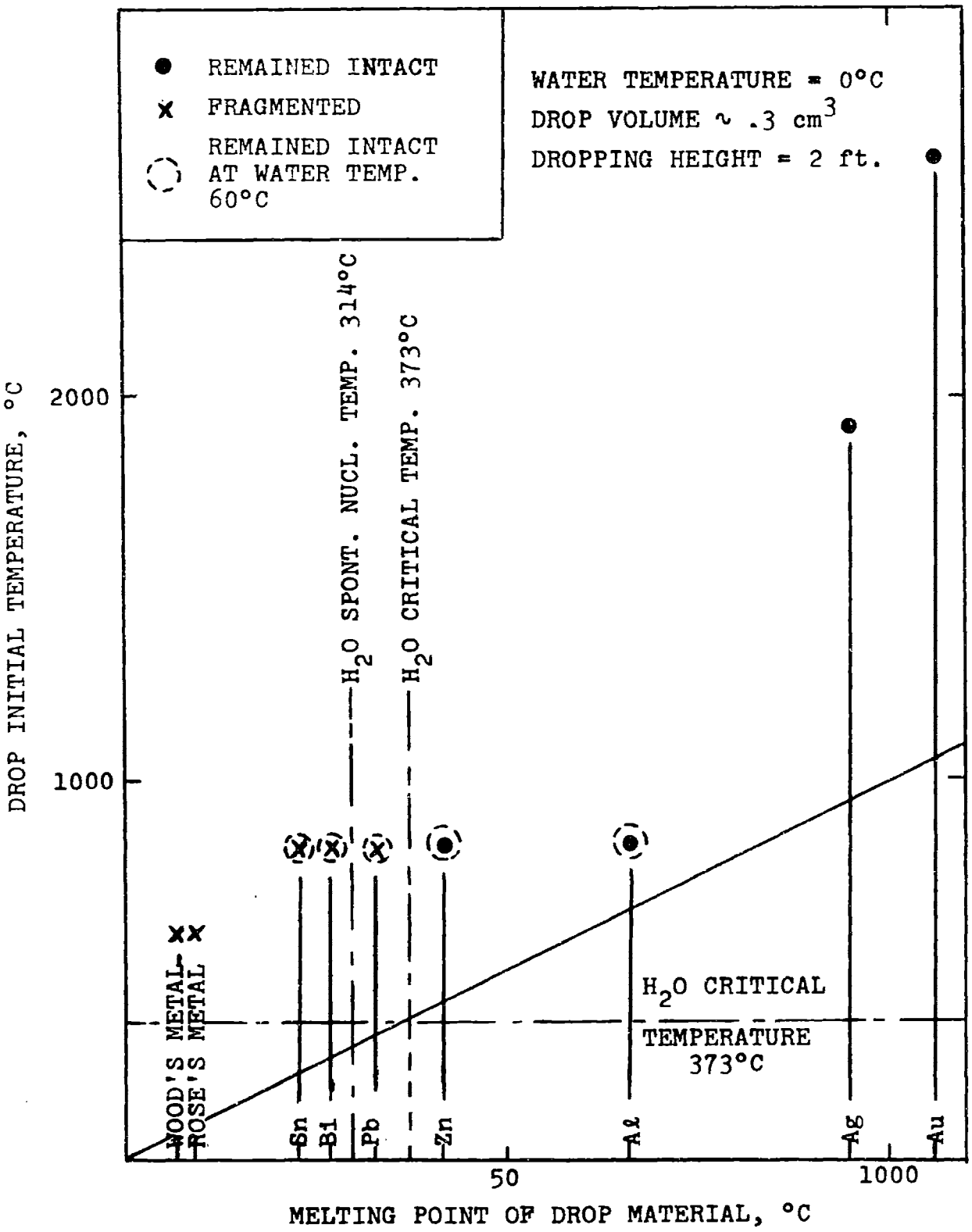

FIG. 2.4: RESULTS OF DROPPING VARIOUS MATERIALS IN WATER (REF. 36)

indication of the influence of a hydrodynamic mode of fragmentation. Hinze[40] has analyzed this mode of fragmentation and shown that the initial forces around a deformable drop may overcome the surface tension of a drop at a critical Weber Number. The fragmentation of mercury in water under isothermal conditions in the experiments of Ivins[38] and Delhaye[15] verify the influence of this mode of fragmentation (See Fig.2.5). The experiments of gallium (See Fig. 2.6) indicate, however, that the Weber Number effect is not the only mechanism inducing fragmentation when the coolant temperature exceeds its boiling point.

The dependence of the extent of fragmentation of the initial temperature of the hot sphere and tne temperature of the coolant for different molten materials dropped in water has been studied by Cho[12,39] Cho's experimental results are shown in Fig. 2.7 thru Fig. 2.11.

The results of ANL experiments in water can be summarized as follows:

1. Some materials that fragment in sodium do not fragment in water, e.g. Ag and Au.
2. Some but not all molten materials fragment in water.
3. The fragmentation of the hot molten material is influenced by two mechanisms: a hydrodynamic mechanism and a thermal mechanism.
4. Fragmentation of the hot material is enhanced by

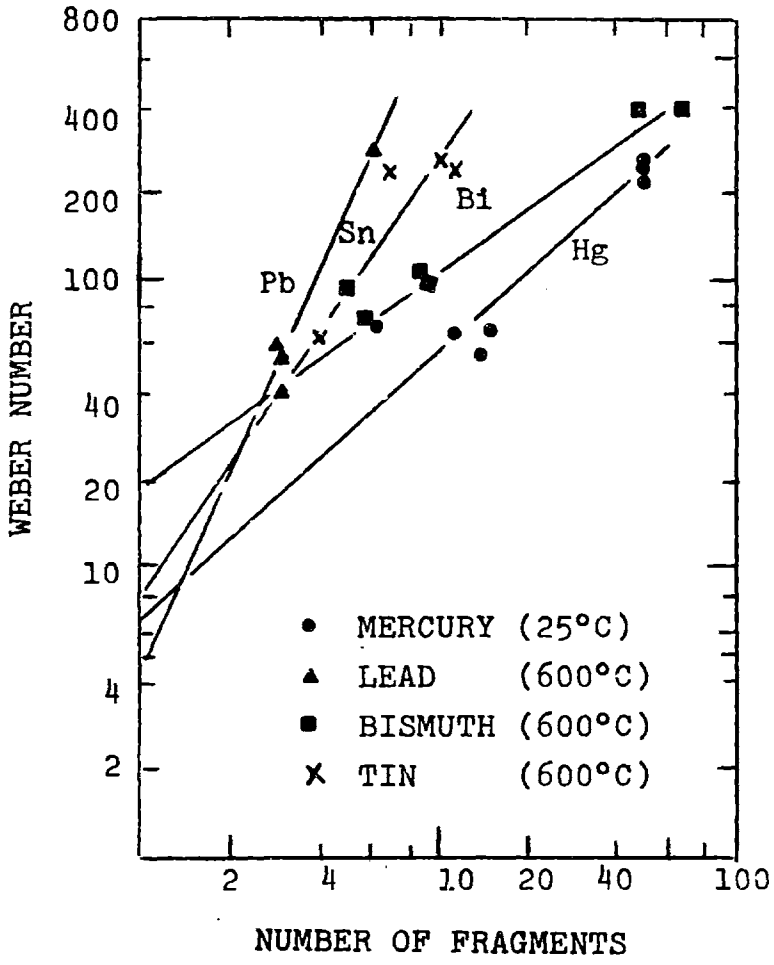

FIG. 2.5: EFFECT OF THE WEBER NUMBER ON FRAGMENTATION OF MOLTEN DROPS IN WATER (REF. 38)

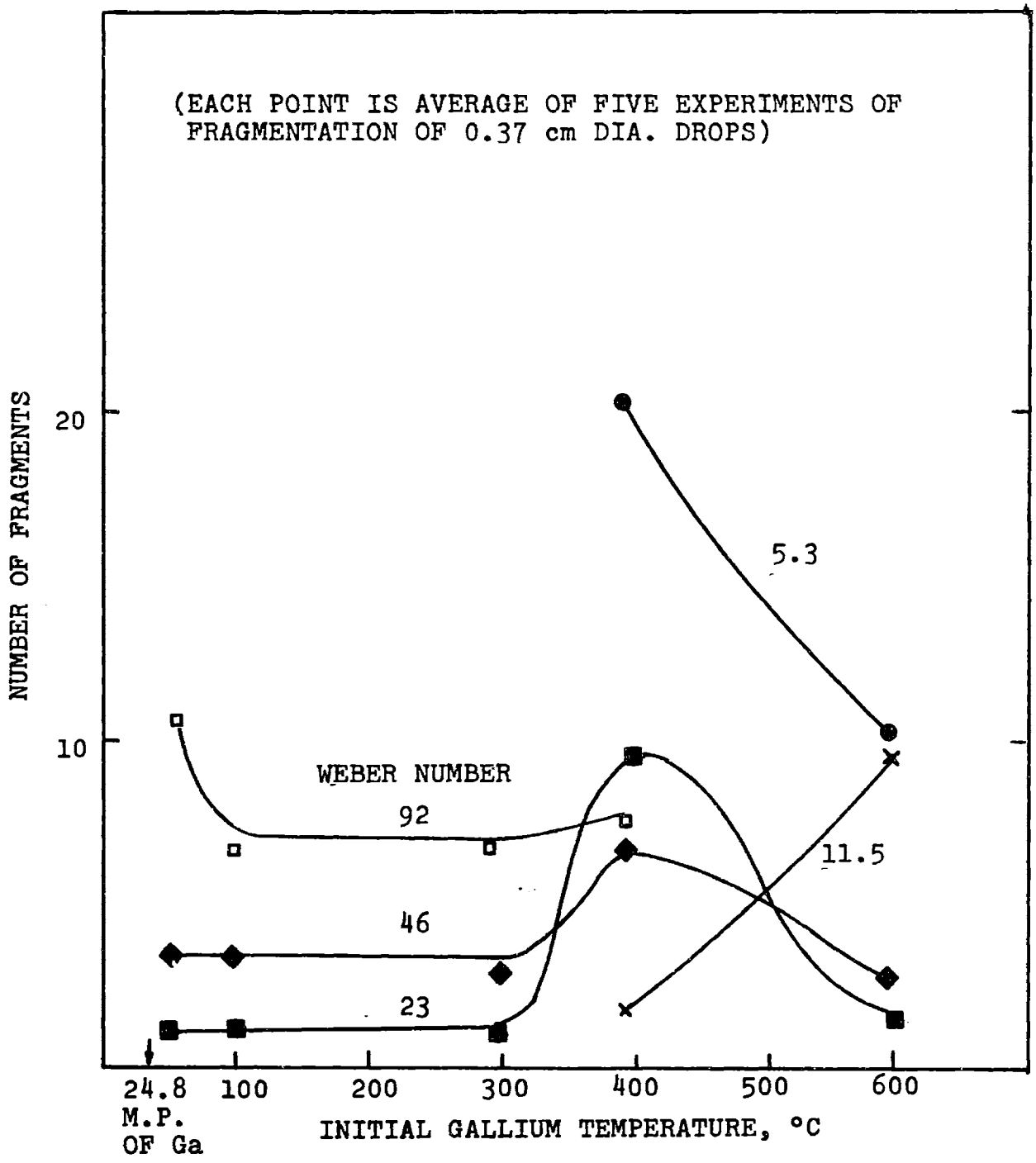

FIG. 2.6: FRAGMENTATION OF LIQUID GALLIUM IN 30°C WATER (REF. 38)

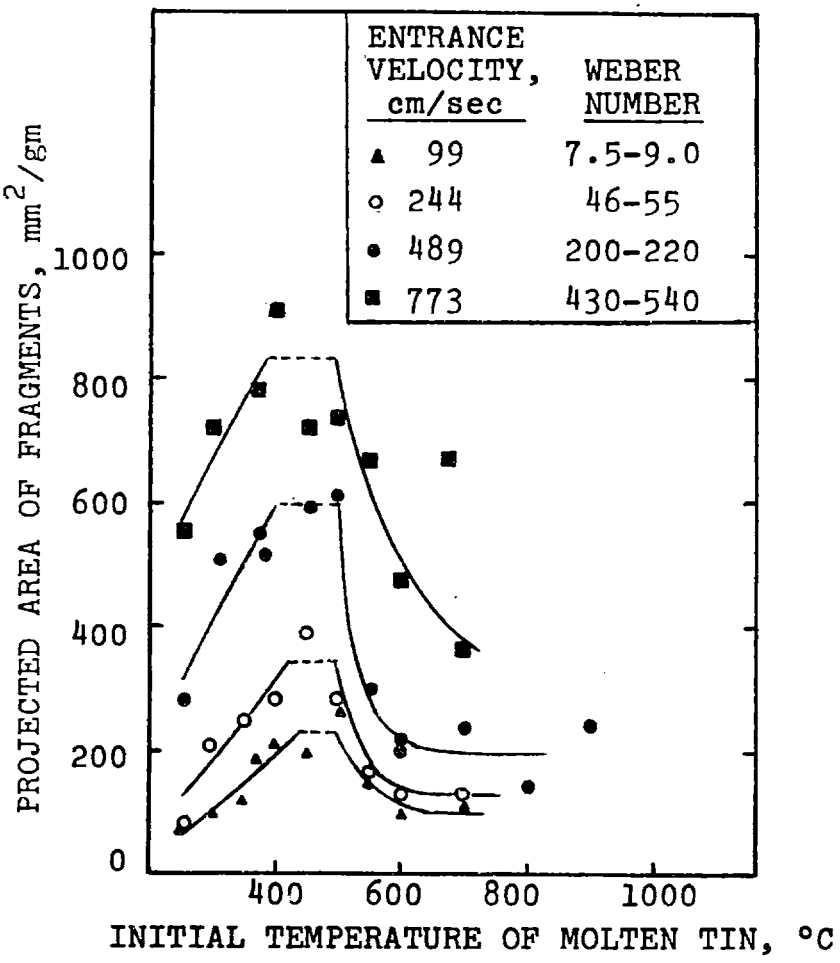

FIG. 2.7: FRAGMENTATION OF MOLTEN TIN QUENCHED IN 22°C WATER (REF. 12)

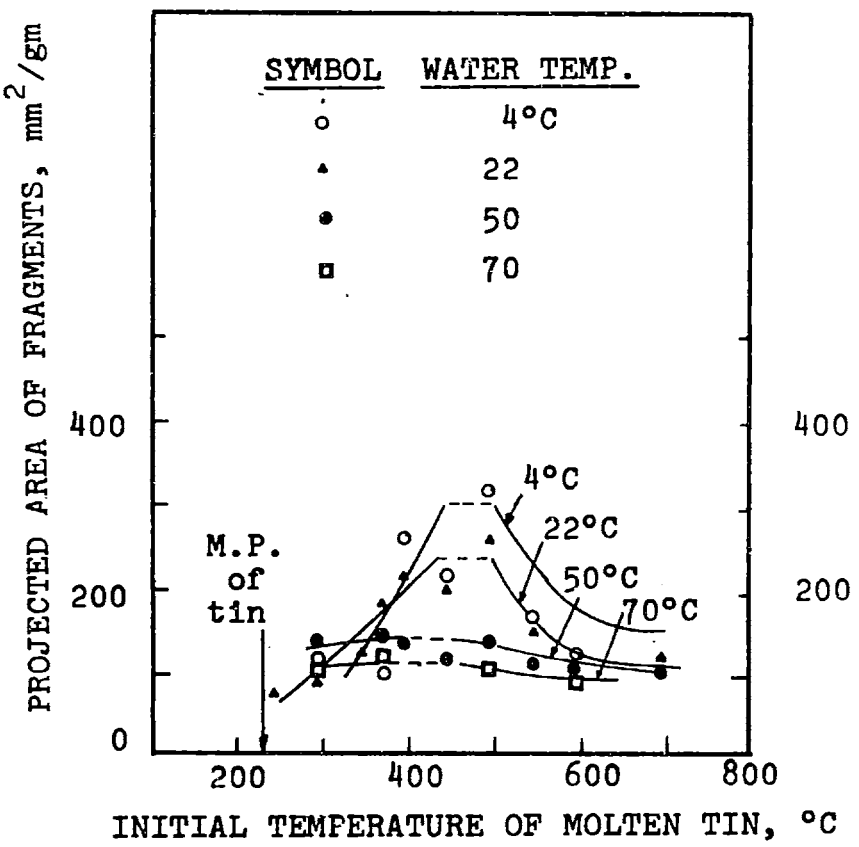

FIG. 2.8: EFFECT OF WATER SUBCOOLING ON FRAGMENTATION OF MOLTEN TIN IN WATER. (REF. 12)

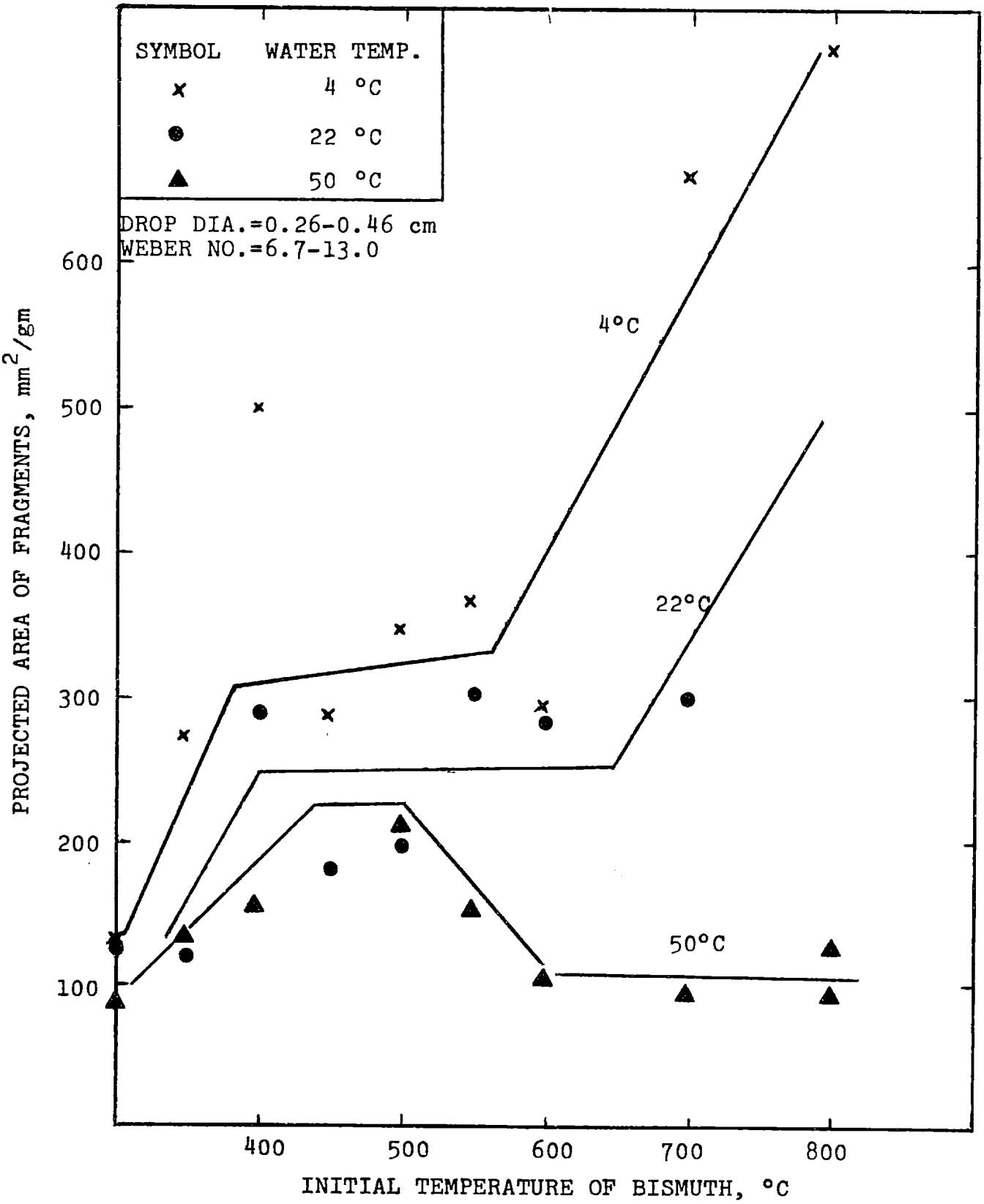

FIG. 2.9: EFFECT OF WATER TEMPERATURE ON FRAGMENTATION OF MOLTEN BISMUTH IN WATER (REF. 39) (MELTING POINT OF BISMUTH 271°C)

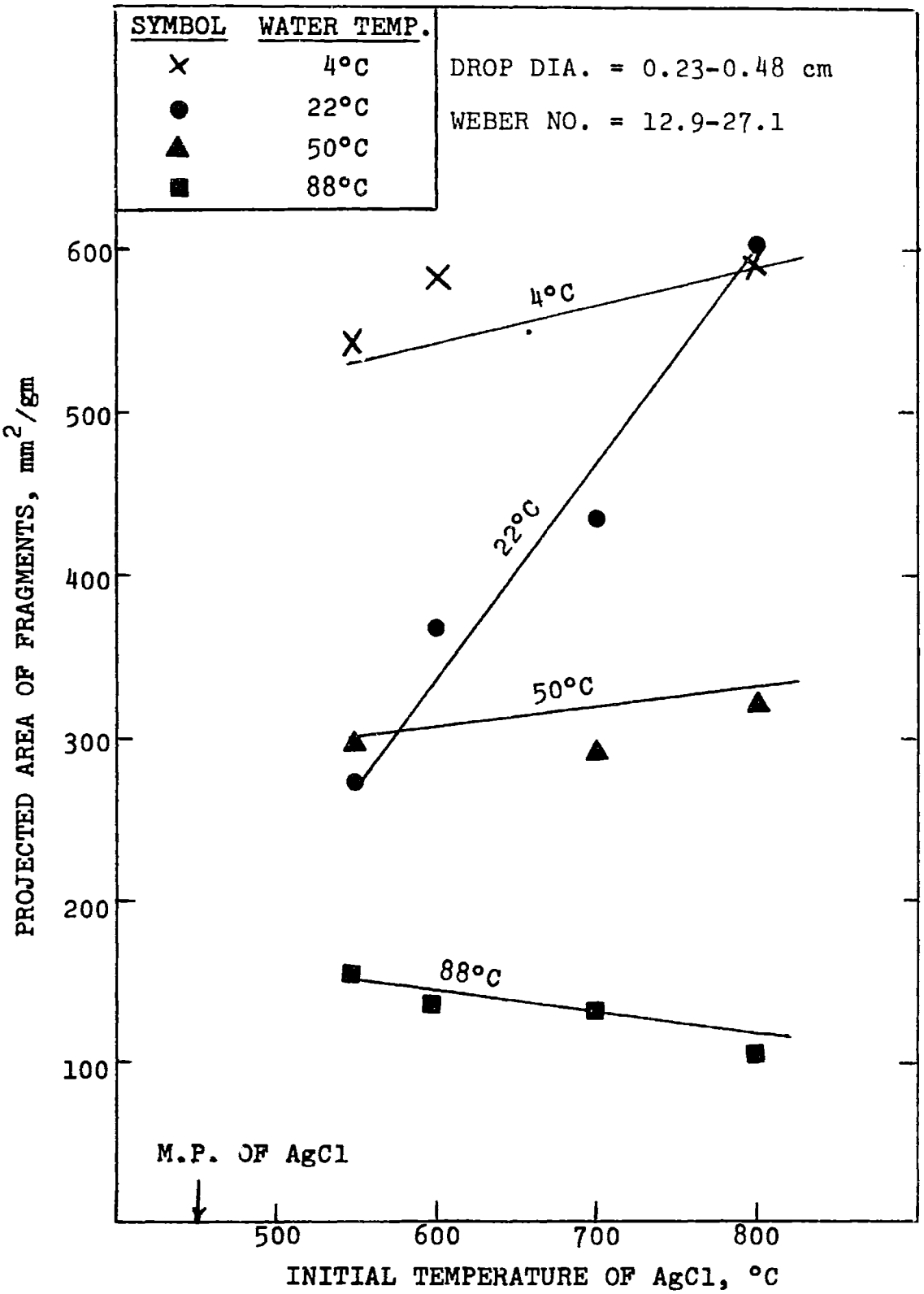

FIG. 2.10: FRAGMENTATION OF AgCl IN WATER (REF. 39)

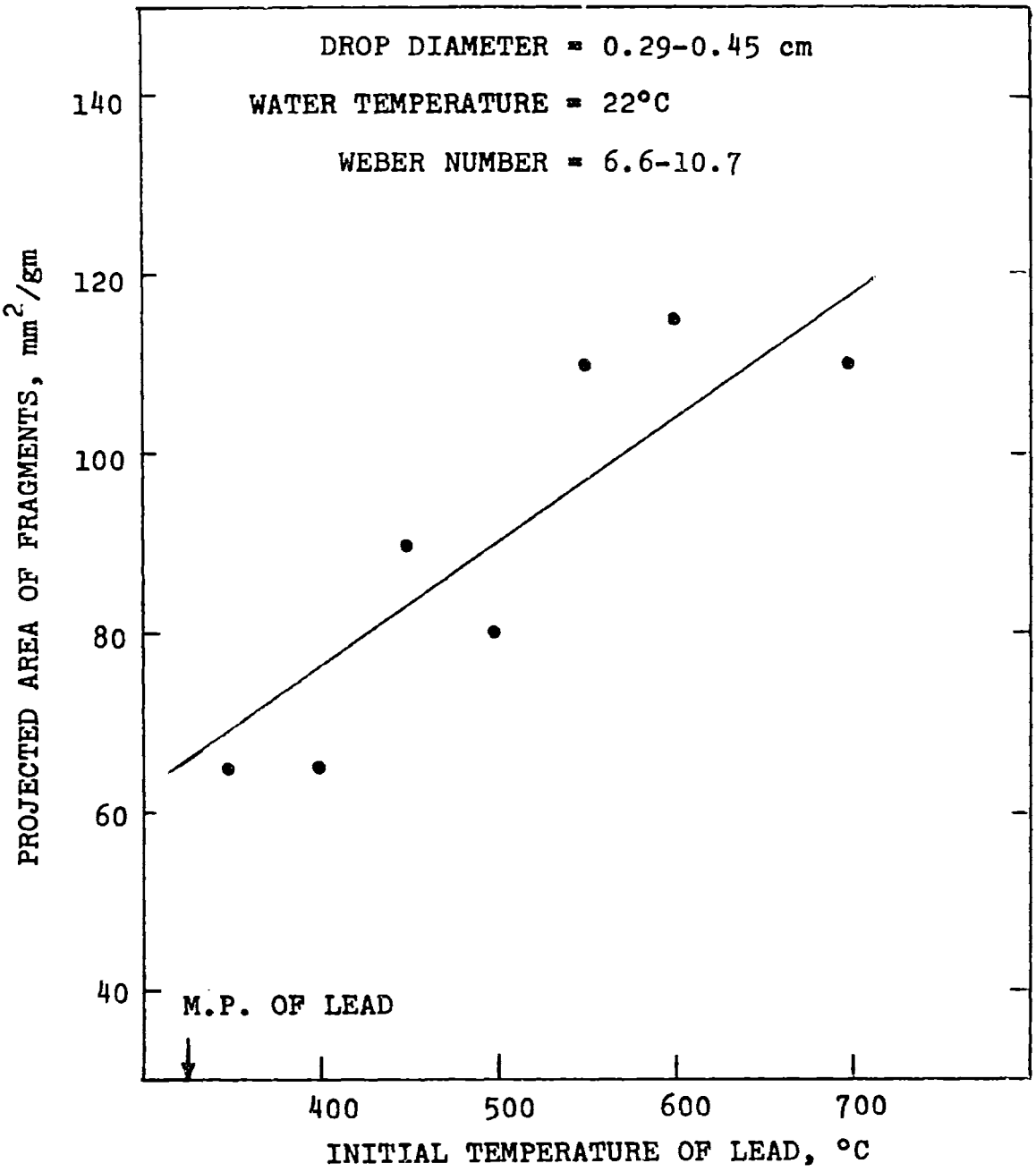

FIG. 2.11: FRAGMENTATION OF MOLTEN LEAD IN WATER (REF. 39)

an increase in the water subcooling (decrease in the water temperature)

5. The extent of fragmentation does not follow a consistent pattern when the initial temperature of the hot drop is increased. The observed Sn behavior indicates the existence of a range of initial drop temperatures for which fragmentation is greatly enhanced. This is supported by the behavior of Bi in 50° water and to a less extent in the experiments with Ga. The experiments of Pb, Bi in $4^{\circ}C$ and $22^{\circ}C$ water and AgCl in $4^{\circ}C$ and $22^{\circ}C$ water show a monotonic increase in the area of fragments with the initial drop temperature.

Based on the early ANL experiments, Swift and Pavlik[35] advanced the hypothesis that fragmentation is associated with the violence of vapor bubble growth and collapse in the nucleate and transition regions of boiling. Thus they expected materials of melting points above the critical temperature of a coolant not to fragment when dropped in that coolant. This criterion was based on the assertion by Westwater[41] that bubbles can not be formed at a surface whose temperature is higher than the critical temperature of the liquid. This criterion, however, does not explain the fragmentation of UO_2 in sodium (Fig. 2.1) or AgCl in water (Fig. 2.10).

In the experiments at University of Kansas[42,43], for which only qualitative results have been reported, molten Al, Pb, Sn, Bi, Zn, Cu, Hg and Wood's Metal were dropped in water. The results support the observations made at ANL of enhanced fragmentation with the increase in the drop Weber Number and with the decrease in the water pool temperature. However, the fragmentation of tin seems to be enhanced with the increase in the initial drop temperature for all the range of tested temperatures (232°C - 950°C). No other metal was tested for such a wide range of temperatures. The following additional observations have been reported by the investigators at University of Kansas[42,43]:

1. There is no evidence of any violent boiling around the hot drops. In the most violent cases fragmentation takes place almost instantaneously upon contact of the metal and water.
2. Fragmentation takes place as an outward burst of the metal. The residues in many cases had a spongy appearance (Fig. 2-12).
3. Many aluminum drops swelled, while under water, into hollow thin-shelled "bubbles". Some of these "bubbles" would burst subsequently (Fig. 2.12).
4. A 50% decrease in the surface tension of molten Al (by the addition of 1% Bi) resulted in a greater tendency for fragmentation, although no actual

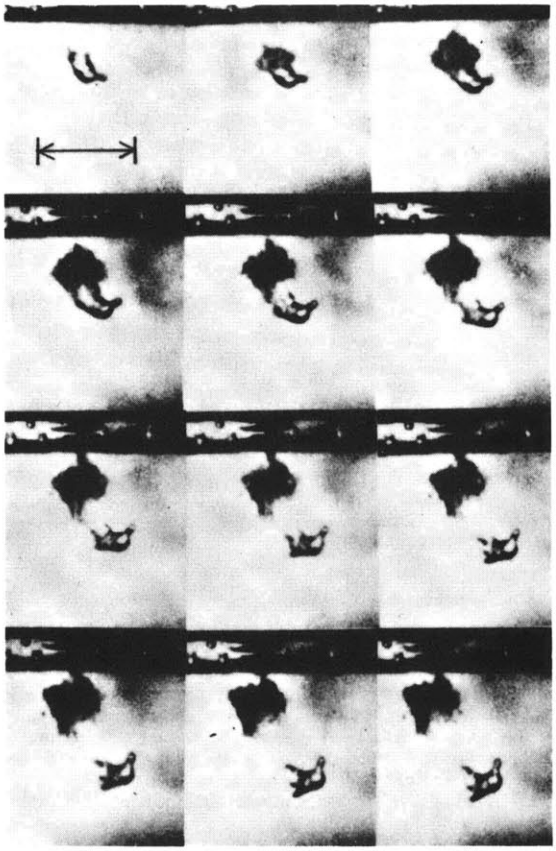

Fig. 12.a Series of frames from film taken of the fragmentation of a lead sample. The frames are 220 μsec apart. Scale line shown represents 2 cm.

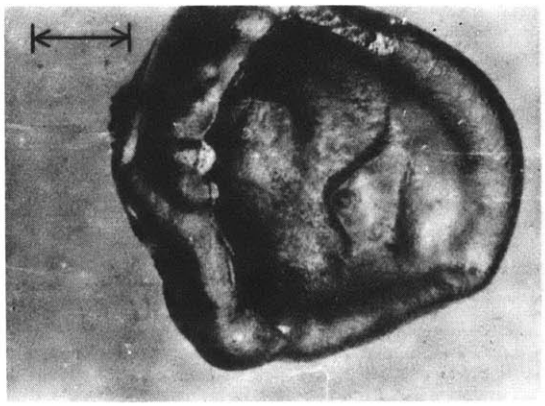

Fig. 12.b Aluminum bubble that collapsed. Scale line shown represents ½ cm.

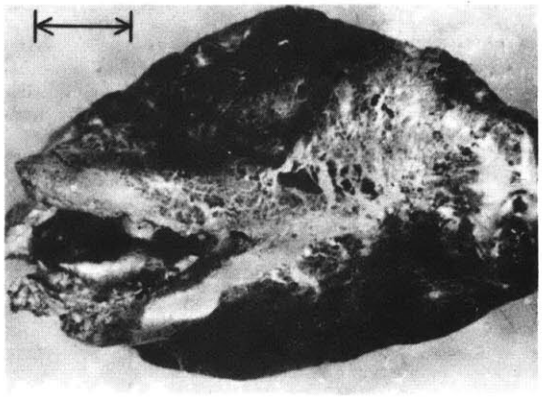

Fig. 12.c Aluminum bubble that burst outward. Scale line shown represents ½ cm.

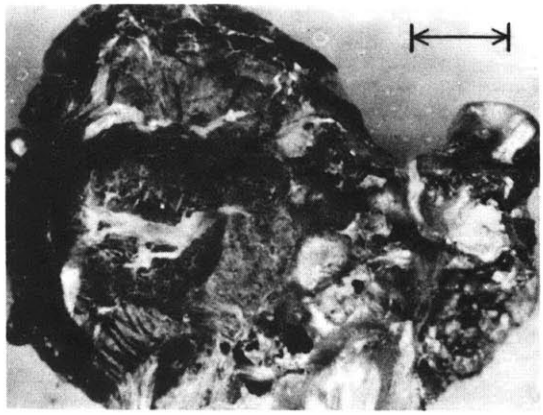

Fig. 12.d Aluminum bubble showing what appears to be interior aluminum that was forced through the outer shell. Scale line shown represents ½ cm.

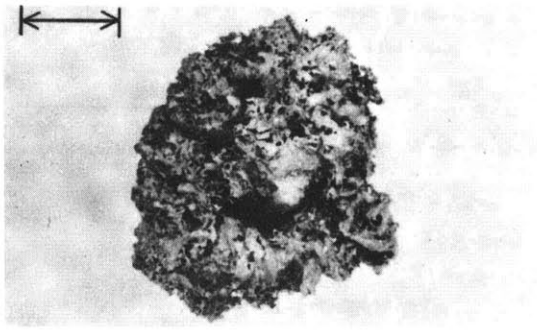

Fig. 12.e Interior of completely mossy lead after fragmentation. Scale line shown represents ½ cm.

Fig. 2.12 Some pictures from the fragmentation experiments of Ref. 42.

explosion occurred.

5. Increasing the viscosity of water approximately five times, by the addition of powdered carboxymethylcellulose, greatly reduced if not prevented the fragmentation of the molten metals.

The experiments were interpreted by the investigators to give evidence of fragmentation due to encapsulation of coolant inside the hot drop as a result of formation of surface instabilities (Helmholtz Instabilities). Other mechanisms have also been proposed for encapsulation of a coolant by a colliding drop[13,31,44].

The results of the Grenoble[13] experiments indicated that UO_2 does not fragment in water. Based on the results of their water and sodium experiments the investigators concluded that UO_2 fragmentation in sodium may be due to two main causes: encapsulation of coolant in UO_2 drops and/or stresses of thermal origin due to high thermal gradients at the drop surface.

Experiments conducted at University of Houston[45] confirmed in general the observations (but not conclusions) of the afore mentioned dropping experiments. In the experiments involving injection of molten metallic jets in water the following observations have been made[46]:

1. The fragmentation seemed to be sensitive to the surface temperature, more so than the bulk temperature, of the molten jet.

2. The blanketing of the jet with a thick vapor shield prevented the initiation of fragmentation from the shielded portion of the jet.
3. "Several of the observed explosions (fragmentation) were preceded by a noticeable bulge in the jet at the point where the explosion (fragmentation) subsequently occurred." This observation is similar to the aluminum swelling phenomenon observed by Flory et al.[43].

In an effort to identify the fragmentation mechanism, the investigators at University of Houston conducted several experiments on transient film boiling and transition boiling around spheres in water[47]. The boiling experiments revealed a phenomenon of very rapid (within 250 microseconds) collapse of the vapor film when the sphere temperature can no longer sustain stable film boiling. The rapid collapse of the film has been suggested as a possible mechanism inducing the fragmentation[47].

Board et al.[48] have recently reported several experiments involving the fragmentation of molten tin in water. In the first type of experiments a few grams of tin were dropped from 2-5 cm above an open tank of water about 30 cm deep. It was found that fragmentation occurred only if both the tin temperature was initially above 400°C and water pool temperature was below 60°C. They reported an explosive interaction between tin at 800°C and water in

20°C. The observations from the fast motion pictures (8000 frames per second) and the pressure pulses indicate a sequence of four interactions with increasing violence took place. In each case the approximately spherical bubble-like region of two-phase coolant and debris would grow and then contract slightly before the next interaction. In a second class of experiments molten tin was introduced in water under reduced pressure. When the external pressure was increased fragmentation with pressure pulses took place. In a third type of experiments a mechanical disturbance was applied to the otherwise stable situation of a tin drop supported on a crucible under water at 80°C. The disturbance was in the form of an impulse transmitted via a steel rod to the loosely-mounted crucible. This resulted in some cases in extensive fragmentation and large pressure pulses. It was shown by a separate experiment with a similarly sized drop of Bi-Pb-Sn-Cd (melting point 70°C and hence molten at the water temperature) that the impulse was not sufficient to cause any dispersion. The investigators conclude that:

1. Fragmentation is triggered by a mechanism that leads to unstable film boiling between the two liquids. This can be produced by transition boiling or some other mechanism depending on the operating conditions.

2. There is a cyclic escalation for the fragmentation (and associated pressure pulses), that is a small perturbation causes a mild fragmentation which then leads to more intensive interaction.
3. Vapor collapse seems to be the main cause of dispersion in thermal interactions. This is possibly done by a small jet of coolant penetrating the molten material and producing fine dispersed coolant in the molten material leading to the fragmentation.

2.2.4-c Experiments with other coolants

No fragmentation resulted when molten Bi, Sn, Pb, Hg and Al were dropped in saturated liquid nitrogen[35,43,45]. Stainless steel is reported to fragment in potassium, mercury and lithium in Swift and Pavlik's experiments. They did not report, however, the temperatures involved in the experiment.

2.2.5 Experiments of Injection of Small Amounts of Coolants Into Hot Molten Materials

Several experiments involving the injection of small amounts of water (1-5 ml) at room temperature into various molten materials (50 ml in ~1" dia steel crucible) were performed at ANL[12]. The water was injected above as well as under the surface of the molten material. In some cases explosions developed. The dynamics of the mixing of water and the transparent molten sodium chloride was studied by high speed motion (2500 frames per second) motion pictures[49].

The explosions, when resulting, would take place after a delay time of several hundred milliseconds, but would develop within one frame (400 μsec). A gas layer between the two fluids seemed to prevent the consistent development of an explosion[50]. Limited number of experiments of injection of small amounts of sodium (~ 0.2 ml) in molten UO_2 (5 - 7 ml) have also been conducted at ANL[5]. Explosions developed in some cases. Again a delay period of a few hundred milliseconds was observed. Anderson and Armstrong hypothesized that the observed explosions result from fragmentation of the coolant followed by extremely rapid mixing with the molten material. Fauske[11], while not excluding the possibility of initial fragmentation of sodium, suggested that the explosions observed in the UO_2/Na injection experiments result from spontaneous nucleation of superheated sodium. Spontaneous nucleation of the cold fluid has been suggested by Nakaniski and Reid[9] and Enger et al.[10] to explain the observed explosions when a cryogenic hydrocarbon is spilled on relatively hot water.

2.2.6 In-Pile Tests of Fuel Pin Failure

Fuel pin failure experiments involving molten fuel-coolant interactions have been performed under thermal reactor safety studies[51-53] as well as the LMFBR safety analysis program[54-59]. The Transient Reactor Test Facility (TREAT) has been used for the on-going LMFBR fuel pin failure studies. These experiments have supplied data on

the threshold of fuel pin failure, movement of fuel and coolant under transient conditions as well as post-failure effects of fuel-sodium interactions. The stagnant sodium piston-autoclave tests (S-series) of ANL have been specifically designed to give information on the pressures and mechanical energy that can be generated by molten fuel-sodium interactions under situations simulating an accidental over-power transient in LMFBR. The fuel melting and pin failure are produced by a nuclear power pulse. The subsequent molten fuel-sodium interaction has been observed to result in extensive fuel fragmentation and a series of pressure pulses. The results indicate that the nuclear-to-mechanical energy conversion ratios obtained under such conditions are several orders of magnitude less than the maximum thermodynamic limit of 30%[4]. Similar low energy conversion ratios have been observed in experiments with flowing sodium (E and H series)[59]. The energy conversion ratios of the UO_2/Na pin failure experiments are comparable to the observed ratios of UO_2/H_2O pin-failure experiments at low values of specific energy inputs[52]. At an energy input of 720 cal/g-UO_2, however, a conversion ratio of 2.8% was reported for water[53]; two orders of magnitude higher than the observed ratio in UO_2/Na experiments with the same specific fission-energy input.

The limited results of the S-series experiments also suggest that the presence of the He-bond gas in the fuel pin reduces the mechanical energy produced by the interaction.

The available limited results of the pin-failure experiments suggest that large scale vapor explosions may not be feasible under reactor conditions. Such a conclusion remains to be verified by experiments simulating other conditions of molten fuel-sodium contact (e.g. sodium re-entry conditions) as well as by analytic studies on the factors affecting the mechanisms involved in energetic thermal interactions.

2.3 Theoretical Studies on Thermal Interactions of Molten Fuel and Sodium

Most of the theoretical work to date has been aimed at calculating the pressures and mechanical work resulting from the thermal interaction of molten fuel and sodium. Some work has been aimed at studying the possible mechanisms involved in the fragmentation of molten fuel. Both types of work are reviewed here.

The theoretical assessment of the consequences of thermal interactions of molten fuel and sodium has developed in three distinct approaches:

1. Thermodynamic Models

2. Rate-limited, parametric models

3. Accident Dependent Models

2.3.1 Thermodynamic Models

The classic work of Hicks and Menzies[4] constituted the first attempt to assess the potentially damaging work that can develop when the thermal energy is transferred from the molten fuel to the relatively cold sodium. In their model the thermal energy is instantaneously shared between the fuel and the sodium, bringing them to a thermal equilibrium. The heated sodium is subsequently expanded to the ambient pressure, and the work is calculated as the difference in the internal energy of sodium between the two ends of the expansion process. Thus the mechanical work was determined as a function of the fuel-to-sodium mass ratio. Their calculations show a maximum work for a mass ratio of $\sim$ 11. Several modifications of their original treatment have been introduced by other authors[60-62]. Notably, Judd[61] has shown the sensitivity of the resultant work to the assumed sodium equation of state.

The thermodynamic approach to the evaluation of the expected work yields high thermal-to-mechanical energy conversion efficiencies which may be prohibitively pessimistic. Additionally, no information is provided by this approach about the time-rate for the pressure and mechanical work generation, which is of significance in the assessment of the consequences of an accident.

2.3.2 Rate limited, Parametric Models

Several models have been developed taking into account the rate limited heat transfer to sodium and the subsequent sodium expansion. In one class of such models sodium is heated at a limited interface with molten UO_2. In a second class of these models the fuel is assumed to fragment and intermix with sodium.

a) First class:

Pfefflerlen[63] estimated the pressure and work accompanying the formation of a shock wave in sodium following the initial contact of molten fuel and sodium. The model is based on a semi-infinite slab geometry and assumes a heat transfer cut-off following vaporization of sodium at the interface. More recently Biasi et al.[64] presented a similar model in spherical geometry. Because vaporization in both models develops in a short time (< 1 microsecond), the amount of heated sodium is limited, and very low values of mechanical work are developed.

b) Second class

Padilla[65] introduced a model in which an amount of sodium is bulk-heated by fuel particles. The fuel particles are assumed to be spherical and uniformly distributed in an "interaction zone" with sodium. The heated sodium in the interaction

zone is constrained from expansion by the surrounding cold sodium. The increase in the specific enthalpy of the volume-constrained sodium raises the pressure in the interaction zone, which accelerates the constraining surroundings. When the pressure in the expanding interaction zone is decreased to the saturation pressure of the prevailing sodium temperature, evaporation is initiated. Evaporation is also initiated when the reflected pressure wave from a free surface reaches the interaction zone. After the initiation of the evaporation no heat is transferred to sodium, and isentropic expansion takes place. Padilla's model has been used to calculate the mechanical work energy of a core disruptive accident for the Fast Flux Test Facility (FFTF).

Several improvements over Padilla's basic assumptions were incorporated in the ANL Parametric Model for Fuel-Coolant Interaction (ANL-FCI) developed by Cho et al.[14]. The ANL-FCI model allows for a rate-limited generation of fuel surface area in the interaction zone, which accounts for the finite rate of fragmentation and mixing of the fuel in sodium. The area of the fuel was taken to change as

$$A(t) = A_o \left(1 - e^{t/tm} \right) \qquad (2.1)$$

This formulation, however, is not based on any physical description of the processes of fragmentation and mixing. The reported parametric studies indicate that the maximum

generated pressure will be larger the higher the rate of surface area generation (shorter tm in Eq. 2.1). Additionally, the compliance of non-condensable gases that may be present in the interaction zone was shown to reduce the maximum pressure and to cause a delay in the generation of the pressure peak. Although the model allowed for extending the calculations beyond the initiation of evaporation, the only thermal resistance that was considered is that of the fuel particles. The treatment of the effect of film blanketing the fuel by non-condensable gas or sodium vapor, which will be described in Chapter 3, has been added to the ANL-FCI for optional use[66].

Several models developed in other countries are based on the same assumptions involved in the ANL-FCI model. Teague[15] reviews the essential features of eight such models. Some differences are worth mentioning here. The British models of Duffy[67] and Randles[68] ignore the initial pressure generation due to heating liquid sodium and consider the pressure generation as due to vapor generation only. Puig and Szeless[69] consider a spherical geometry rather than a one-dimensional cartesian model. They find the ratio of the square of the fuel particle diameter to the radius of the interaction zone a determining factor in the development of mechanical work.

In Caldarola's[70] model, the sodium vapor, when developed, is partitioned between that forming a vapor film around the

fuel particles and that escaping the film to a "vapor zone" within the interaction zone. Caldarola developed a heat transfer coefficient for the vapor film based on the conduction thru the film and a film thickness that is related to the rate of vapor generation. His results indicate the retardation of heat transfer due to vapor film formation reduces the generated pressure and mechanical work.

In all these models, the conditions at which the molten fuel and sodium contact each other (temperature, amounts of masses involved, presence of non-condensable gases) are optional parameters. Additionally, the rate and diameter at which the fuel fragments are produced are optional. Both the conditions of contact and the description of fragmentation have significant effect on the resultant pressure and mechanical work. The rate limited parametric models are, therefore, most useful in sensitivity studies of the effects of the different parameters. The acceptability of the predictions of such models when applied to reactor accidents depends on proper justification of the input parameters.

2.3.3 Accident-Dependent Models

Some models have been developed for specific reactor accidents. In these models the conditions of contact between the molten fuel and sodium are derived from the accident sequence.

Carelli[71] formulated a model for a jet-type ejection of molten fuel through an orifice in a failed fuel rod. Tilbrook[72] used Carelli's model in a whole-core multi-channel analysis model to evaluate the rate at which the fuel is ejected into sodium. The results indicated the pressure generated by the thermal interaction may halt the fuel ejection intermittently. Tilbrook's model also indicated a significant effect of sodium vapor condensation at the liquid/vapor interface on the ejection rate of the sodium slug. A post-fragmentation model has been applied by Cronenberg[73] to the analysis of the H-2 rod-failure test in TREAT. Cronenberg's results also indicated the significance of the condensation of vapor on the cold interface with sodium.

A multichannel power excursion core-disassembly accident model (FISFAX), that utilized in part the formulation of ANL-FCI, has been reported by Lorenzini and Flanagan[74]. An explicit account is made for the motion of the fuel particles in the voided channel. It was found that the fuel motion feed back on reactivity was a main factor in terminating the excursion. This is particularly interesting since the rapid sodium voidage caused by the thermal interaction is a major source of positive reactivity addition in reactor accidents. Mills and Kastenberg[75] find little effect in going from the

point-kinetics model to the more elaborate space-time model for the disassembly accident. Very recently, the mechanistic approach to assessment of molten fuel-sodium interaction has been incorporated in the SAS code developed at ANL for LMFBR hypothetical core disruptive accident analysis[76]. The SAS/FCI model is largely based on the assumptions of ANL-FCI parametric model.

2.3.4 Theoretical Studies on the Mechanism of Fragmentation

The hydrodynamically invoked fragmentation has been thoroughly analyzed by Hinze[40]. His analysis reveals the dependence of the fragmentation process on the Weber Number of the deformable body passing through a fluid. A critical Weber Number is needed for fragmentation to occur. The critical Weber Number was shown to depend on the way in which the relative velocity of the two fluids varies with time. For a sudden exposure of a drop to a parallel velocity field (a case similar to dropping experiments) he found the critical Weber Number to be ~ 13.

Only few attempts have been made at investigating the thermal mechanism leading to fragmentation of hot molten materials into cold liquids. Hsiao et al.[77] considered the pressurization of a solidifying sphere in an infinite cooling medium. They concluded that tangential stresses will exceed the radial stresses for both thermal and pressurization stresses. The maximum stresses were shown to occur as solidification starts, hence rupture should

occur immediately after solidification begins.

Cronenberg[73] considered the energy associated with the creation of the surface area of fuel in sodium. He compared this energy to the inertial energy associated with the fuel particles released from a failed pin, to the energy associated with a shock wave due to sudden heating of the sodium at the interface, and to the energy associated with sodium bubble growth and collapse at the UO_2 surface. He concluded that the energy associated with the nucleate boiling exceeds the other energies by several orders of magnitudes and is therefore more likely to induce fragmentation.

The recent work of Roberts[78] represents a first attempt in describing the mixing that occurs between the two fluids. Roberts considered a jet of coolant penetrating a molten, hot material. He divided the sequence of events into seven stages, allowing for a feed back effect. Following the initial penetration an initial entrainment of the coolant is assumed to take place due to formation of vortices. An increase in the surface area is then assumed to take place due to fluid turbulence. This increase in area is limited by the kinetic energy of the jet and the interfacial surface tension. Assuming the presence of an undefined mechanism by which the heat transfer and the mild pressure pulse can cause further turbulence, he showed how a vast increase in the

surface area can be generated following a delay time. Roberts' model seems appropriate for simulating the shock tube experiments and the jet penetration of a molten drop suggested by Board et al.[48] as a mechanism for fragmentation.

Chapter Three

EFFECT OF GAS/VAPOR BLANKETING OF FUEL ON FRAGMENTATION-INDUCED EXPLOSIVE THERMAL INTERACTION IN LMFBR

Chapter Three

EFFECT OF GAS/VAPOR BLANKETING OF FUEL ON FRAGMENTATION-INDUCED EXPLOSIVE THERMAL INTERACTION IN LMFBR

3.1 Introduction

In the model that has been developed at Argonne National Laboratory to analyze a fragmentation-induced vapor explosion in a hypothetical large scale LMFBR meltdown accident, the rate of heat transfer from the fuel to the sodium is assumed to be limited only by the fuel thermal resistance[14]. Thus any contact resistance that may be established by the presence of non-condensable gases or sodium vapor at the fuel-sodium interface has been neglected. In an operating reactor, non-condensable gases will be present as interstitial gas in the fuel, thermal bond gas, and fission gases released to the plenum. It is therefore conceivable that under reactor accident conditions non-condensable gases will at least partially blanket the fuel surface area. Additionally, once vaporization of sodium takes place, the vapor would most probably be formed at the fuel surface, where sodium is at the highest temperature. The purpose of the present analysis is to assess the effect of the existence of a gas/vapor blanket around the fuel particles on the pressure and mechanical work generated by the fuel-sodium interaction.

The assessment of such an effect is made by modification of the ANL Parametric Fuel-Coolant Interaction Model (ANL-FCI) to account for the blanketing effect. A brief description of the assumptions and formulation of the original ANL-FCI model is given in Section 3.2. The assumptions and formulation of the modified model are given in Section 3.3. The results of the application of the modified model to several cases of fuel-sodium thermal interaction are then discussed in Section 3.4.

3.2 The Original ANL Parametric Model for Fuel-Coolant Interaction

Only the basic assumptions and formulation of the orignial ANL model for fuel-coolant interactions are reviewed here. For more detailed discussions of the model, the reader is referred to Ref. 14 and Ref. 79.

In the ANL model, the thermal interaction process in a volume of fuel-sodium mixture at some location in the core is considered. The heat transfer from the fuel to the interacting sodium increases the sodium specific enthalpy and leads to pressure generation in the "interaction zone". The interaction zone then expands against the constraint provided by the surroundings. The pressure history in the interaction zone is then determined by the two competing processes: the heating of the sodium which produces pressure, and the expansion of the interaction

zone which reduces the pressure. The following assumptions are made in the formulation of the model:

1. The system can be treated in one-dimensional cartesian coordinates (See Fig. 3.1).
2. There is no pressure gradient in the interaction zone.
3. The liquid sodium in the interaction zone has uniform temperature.
4. There is no heat or mass exchange between the interaction zone and the surroundings.
5. The change in the specific volume of the fuel can be neglected at all temperatures.
6. The fuel fragments are uniformly dispersed in the interaction zone. The fragments may be represented by spherical particles of equal size.
7. The surface area of the fuel is generated in the exponential manner:

$$A_u = A_o \left(1 - e^{-t/tm}\right) \qquad 3.1$$

which represents the finite rate of fragmentation and mixing of fuel. The characteristic time, tm, and the asymptotic fuel surface area, A_o, are optional parameters.

8. Non-condensable gases may be present in the interaction zone only away from the fuel-sodium

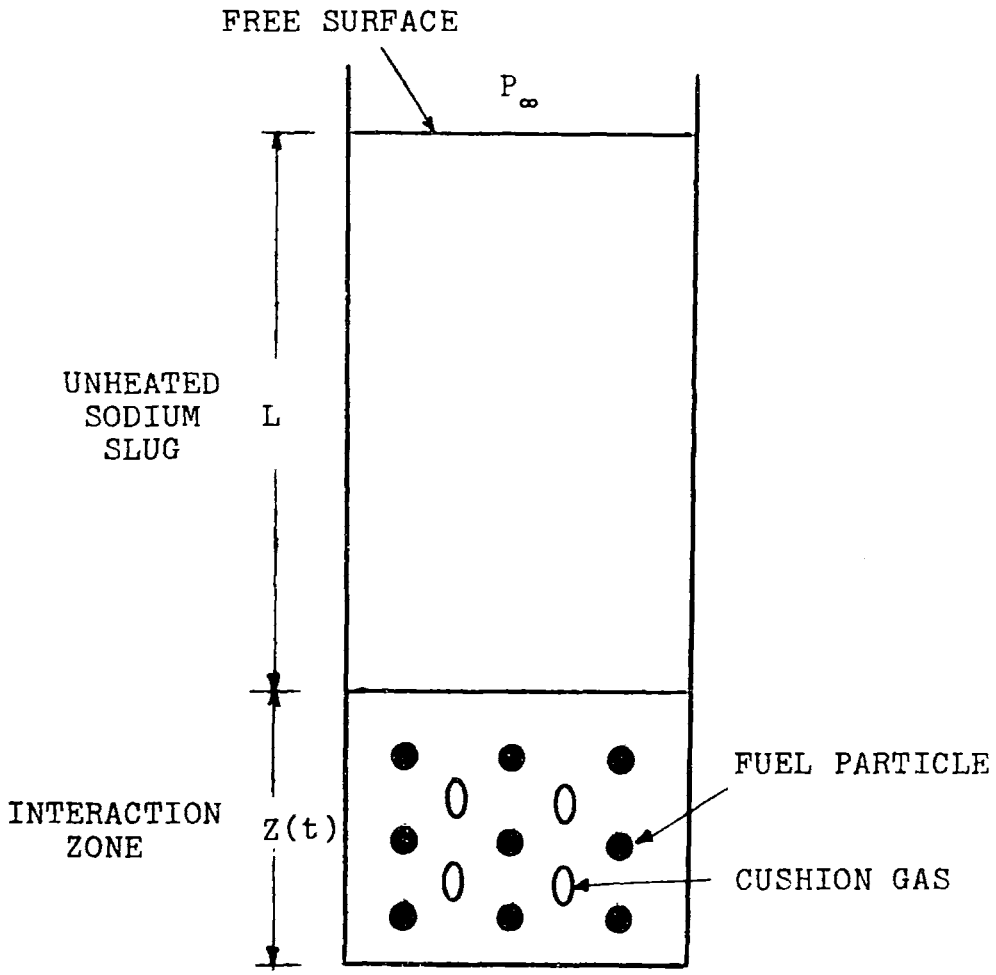

FIG. 3.1: SCHEMATIC DIAGRAM FOR THE SYSTEM DESCRIBED BY THE ORIGINAL ANL PARAMETRIC FUEL-COOLANT INTERACTION MODEL

interface. Hence, the presence of the non-condensable gases does not interfere with the heat transfer in the system. (This type of non-condensable gas will be called "cushion gas" in this study). The non-condensable gas may be treated adiabatically.

9. When sodium vapor is formed in the interaction region, it is uniformly mixed with the liquid. All the vapor can be treated as at thermodynamic equilibrium with the liquid sodium in the interaction zone.

10. The heat transfer from the fuel is limited only by the thermal resistance of the fuel particle. The heat flux from a fuel particle is given by:

$$q'' = h_u^* (T_u - T_s), \qquad 3.2$$

where T_u is the average fuel particle temperature h_u^* is the heat transfer coefficient and is given by

$$h_u^* = \frac{k_u}{\sqrt{\pi \alpha_u t}} + \frac{k_u}{R}, \qquad 3.3$$

where k_u and α_u are the thermal conductivity and diffusivity of the fuel respectively, and R is the fuel particle radius.

The first term in the expression 3.3 for h_u^* represents a "transient" heat transfer coefficient while the second term represents a "steady state" coefficient.

Utilizing the aforementioned assumptions, the problem is then determined by the solution of five simultaneous equations:

a) The rate of heat transfer from fuel to sodium:

$$\frac{dQ}{dt} = h_u^* \; A_u \; (T_u - T_s), \qquad 3.4$$

b) The first law of thermodynamics applied to the sodium in the interacting zone:

$$\frac{dH}{dt} = \frac{dQ}{dt} + \frac{VdP}{dt} \; , \qquad 3.5$$

where H is the enthalpy of sodium,

V is the volume of sodium,

P is the pressure in the interaction zone,

and $\frac{dQ}{dt}$ is the total heat transfer rate from the fuel.

c) The equation of state of sodium:

$$H = H \; (P, \; V), \qquad 3.6$$

d) The constraint equation, relating the rate at which the interaction volume is expanding to the pressure in the interaction zone:

$$P = F \; (V, \; \frac{dV}{dt} \; , \; \frac{d^2V}{dt^2}), \text{ and} \qquad 3.7$$

e) the rate of fuel cooling

$$\frac{dT_u}{dt} = \frac{-1}{C_u W} \; \frac{dQ}{dt} \; , \qquad 3.8$$

where C_u and W are the specific heat and the mass of interacting fuel.

For the constraint equation, two approximate solutions can be used: the inertial approximation and the acoustic approximation. In the inertial approximation the surroundings are considered incompressible. In the acoustic approximation, the surroundings are considered compressible but non-reflecting of pressure waves. In this case the pressure waves generated by the expansion of the interaction zone propagate only outward, away from the interaction zone.

3.3 Modification of the ANL Model to Include the Blanketing Effect

3.3.1. Basic Assumptions

The basic system described by the model (fuel and sodium in an interaction zone expanding against constraints) has not been altered in the present treatment. The basic assumptions 1 through 7 of the original model are also retained. Additionally, the following assumptions are made:

1. Non-condensable gases may be present in the interaction zone at the fuel surface (blanket gas) and/or away from it (cushion gas). The cushion gas may be treated adiabatically (as in the original model). The blanket gas, if present, is of uniform thickness surrounding each fuel particle. (See Fig. 3.2).

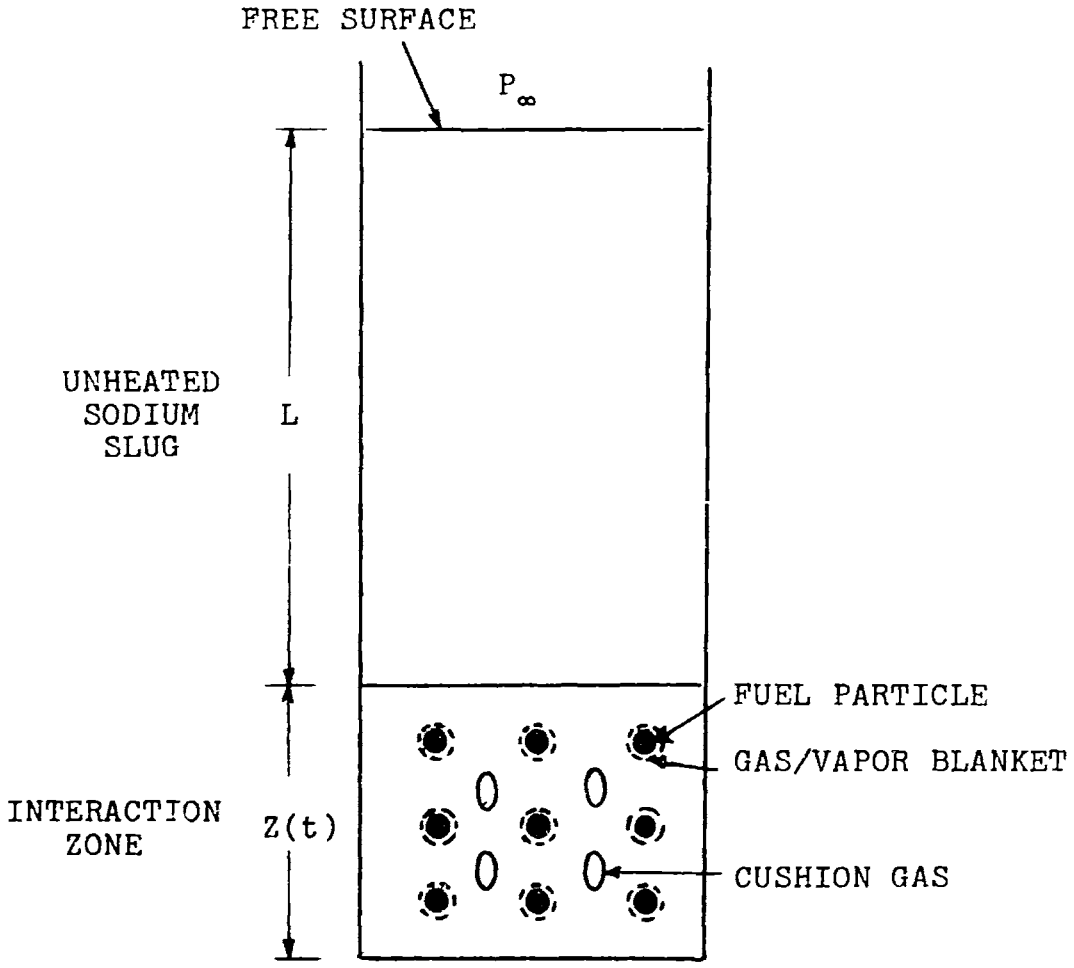

FIG. 3.2: SCHEMATIC DIAGRAM FOR THE SYSTEM DESCRIBED BY THE MODIFIED ANL MODEL FOR FUEL-SODIUM THERMAL INTERACTION

2. The sodium vapor in the interaction zone, whether initially present or generated in the course of the interaction, surrounds the fuel particles as a blanket of uniform thickness. If a gas blanket already exists around the fuel, vapor is added to the blanket uniformly.
3. The temperature profile in the blanket is linear. The vapor is superheated, with respect to the prevailing pressure, everywhere in the blanket except at the blanket/liquid sodium interface.
4. The heat transfer from the fuel is limited by both the thermal resistance of the fuel particle and the blanket. The heat transfer across the blanket is by conduction only. (See Appendix A for an estimate of the contribution of the radiative heat transfer in the cases of interest). The heat transfer coefficient of the blanket is given by k_b/δ, where k_b is the blanket thermal conductivity and δ is the blanket thickness.
5. An average temperature of the gases in the blanket may be given by (See Appendix B)

$$T_b = \frac{T_u + T_s}{2} . \qquad 3.9$$

6. The thermal energy consumed by heating the blanket gas may be neglected compared to that consumed by heating the sodium. However, the

compliance of the blanket gas is taken into account in the pressure calculations.

3.3.2 Mathematical Formulation

Since homogeneity of the interaction zone is assumed, the equations are formulated on the basis of a representative one gram of the interacting sodium.

a) Heat Transfer From the Fuel

The rate of heat transfer from the fuel is given by:

$$\frac{dQ}{dt} = h^* A_u (T_u - T_s), \qquad 3.10$$

where h^* is a composite heat transfer coefficient given by:

$$h^* = \left[\frac{1}{h_u^*} + \frac{\delta}{k_b} \right]^{-1} \qquad 3.11$$

The values of the fuel particle heat transfer coefficient h_u^* has been defined in equation 3.3. The heat transfer area per gram of interacting sodium increases in the exponential form defined in equation 3.1.

At any time, t, the blanket thickness, δ, is given by the total volume of the blanket gas and vapor divided by the surface area of the fuel:

$$\delta = \frac{xV_v + M_g V_{gb}}{A_u}, \qquad 3.12$$

where x is the mass of sodium vapor per gram of the interacting sodium (the quality of the interacting sodium),

M_g is the mass of the blanket gas per gram of interacting sodium,

V_v and V_{gb} are the specific volumes of the vapor and blanket gas respectively.

The gas blanketing is assumed to occur at the same rate as that of surface area generation:

$$M_g = M_{g\ max}\ (1-e^{-t/tm}), \qquad 3.13$$

where $M_{g\ max}$ is the total mass of non-condensable gas available for blanketing per gram of the interacting sodium.

b) <u>The First Law of Thermodynamics Applied to the Interacting Sodium</u>

The first law of thermodynamics applied to the interacting sodium is given by:

$$\frac{dQ}{dt} = \frac{dh_s}{dt} - V_s \frac{dP}{dt}, \qquad 3.14$$

where all the heat transferred from the fuel is assumed to be consumed by sodium only, and where h_s and V_s are the specific enthalpy and specific volume of sodium.

For a single-phase liquid sodium, the change in the enthalpy can be related to the change in the temperature and pressure by the thermodynamic relation

$$dh = C_p dT + v\,(1 - \alpha' T)\,dP, \qquad 3.15$$

where C_p is the specific heat at constant pressure and α' is the thermal expansion coefficient given by:

$$\alpha' = \frac{1}{V}\left(\frac{\partial V}{\partial T}\right)_P \qquad 3.16$$

By substitution from equation 3.15 and 3.16 in equation 3.14, the first law of thermodynamics may be written as:

$$\frac{dQ}{dt} = C_{p\ell}\frac{dT_s}{dt} - V_\ell T_s \alpha'_\ell \frac{dP}{dt} \qquad 3.17$$

where the subscript ℓ refers to liquid sodium.

For a two-phase interacting sodium the specific enthalpy, h_s, and the specific volume, V_s, of the sodium to be used in equation 3.13 are given by:

$$h_s = (1 - x)h_\ell + x\,h_v, \qquad 3.18$$

$$V_s = (1 - x)V_\ell + x\,V_v, \qquad 3.19$$

By substitution from equations 3.18 and 3.19 into equation 3.14, the thermodynamic relation becomes,

$$\frac{dQ}{dt} = (1 - x)\frac{dh_\ell}{dt} + x\frac{dh_v}{dt} + (h_v - h_\ell)\frac{dx}{dt} - [(1 - x)V_\ell + xV_v]\frac{dP}{dt}. \qquad 3.20$$

The values of the specific enthalpies and the specific volumes for liquid and vapor sodium are to be determined from the state equations of sodium.

c) The Equation of State of Sodium

For two-phase sodium, the liquid is assumed to be in equilibrium condition, so that the state equation for saturated liquid are used:

$$h_\ell = h_\ell\ (T_s), \qquad 3.21.a$$

$$V_\ell = V_\ell\ (T_s), \qquad 3.21.b$$

The vapor is assumed to be at an average temperature T_b, higher than the saturation temperature at the prevailing pressure. The thermodynamic properties are therefore given by:

$$h_v = h_v\ (T_s) + C_{pv}\ (T_b - T_s), \qquad 3.21.c$$

$$V_v = \frac{B_v\ G_v\ T_b}{P}, \qquad 3.21.d$$

where $h_v\ (T_s)$ is the saturated vapor specific enthalpy at temperature T_s,

C_{pv} is the vapor specific heat at constant pressure,

G_v is the vapor gas constant, and

B_v is a temperature-dependent compressibility factor.

The blanket average temperature, T_b, has been defined in equation 3.9. The numerical values of the thermodynamic properties of sodium are given in Appendix I.

The state equations are used to determine the relation between the rate of change of the total volume of the interaction zone and the pressurization rate as follows:

The total volume of the interaction zone per one gram of the interacting sodium, V_t, is given by the sum of the volume of sodium, blanket gas, cushion gas, and fuel:

$$V_t = V_s + M_{gmax} V_{gb} + V_{go} \left[\frac{P_o}{P} \right]^{1/n} + \frac{W}{\rho_u}, \qquad 3.22$$

where V_{go} is the initial volume of the cushion gas,

P_o is the initial pressure in the interaction zone,

n is the adiabatic index of the cushion gas (for a perfect gas $n = C_p/C_v$), and

ρ_u is the density of the fuel.

By differentiating equation 3.22 with respect to time, the following relation is obtained:

$$\frac{dV_t}{dt} = \frac{dV_s}{dt} + M_{gmax} \frac{dV_{gb}}{dt} - \frac{V_{go} P_o^{1/n}}{n P^{(1+1/n)}} \frac{dP}{dt}. \qquad 3.23$$

The rate of change of the specific volume of liquid sodium is given by:

$$\frac{dV_\ell}{dt} = \frac{\partial V_\ell}{\partial T_s} \frac{dT_s}{dt} + \frac{\partial V_\ell}{\partial P} \frac{dP}{dt} . \qquad 3.24.a$$

By using the thermal expansion coefficient, α', defined in equation 3.15 and the isothermal compressibility, β defined as

$$\beta = - \frac{1}{V} \left[\frac{\partial V}{\partial P}\right]_T , \qquad 3.25$$

equation 3.24.a may be written in the form

$$\frac{dV_\ell}{dt} = \alpha'_\ell V_\ell \frac{dT_s}{dt} - \beta_\ell V_\ell \frac{dP}{dt} . \qquad 3.24.b$$

For saturated liquid α'_ℓ and β_ℓ are function of temperature only.

The rate of change of the specific volume of vapor sodium is obtained by differentiating equation 3.21.d with respect to time:

$$\frac{dV_v}{dt} = \left[\frac{G_v T_b}{P} \frac{\partial B_v}{\partial T_s} + \frac{B_v G_v}{P} \frac{\partial T_b}{\partial T_s} - \frac{B_v G_v T_b}{P^2} \frac{\partial P}{\partial T_s}\right] \frac{dT_s}{dt} + \frac{B_v G_v}{P} \frac{\partial T_b}{\partial T_u} \frac{dT_u}{dt} . \qquad 3.26$$

The total rate of change of the specific volume of sodium is given by:

i) For single phase liquid sodium

$$\frac{dV_s}{dt} = \frac{dV_\ell}{dt} , \text{ and} \qquad 3.27$$

ii) For two-phase sodium:

$$\frac{dV_s}{dt} = (1-x)\frac{dV_\ell}{dt} + x\frac{dV_v}{dt} + (V_v - V_\ell)\frac{dx}{dt} . \qquad 3.28$$

The rate of change of the specific volume of the blanket gas is given by:

$$\frac{dV_{gb}}{dt} = \frac{d}{dt}\left(\frac{G_{gb}T_b}{P}\right) ,$$

$$\frac{dV_{gb}}{dt} = \frac{G_{gb}}{2P}\frac{dT_s}{dt} + \frac{G_{gb}}{2P}\frac{dT_u}{dt} - \frac{G_{gb}T_b}{P^2}\frac{dP}{dt} , \qquad 3.29$$

where the assumption $T_b = (T_s+T_u)/2$ has been used.

d) The Constraint Equation

Another equation for the rate of change of the total volume of the interaction zone can be obtained by considering the motion of the constraining surrounding due to the pressure generated in the interaction zone. In the original ANL-FCI model, two approximate formulations for the motion are employed for the "constraint equation": the acoustic approximation and the inertial approximation. The two formulations have not been altered in the modified model.

d-1) The acoustic approximation

In this formulation the compressibility of the constraining sodium slug is taken into account. The

formulation allows for the compression waves produced in the surroundings by the expansion of the interaction zone to propagate away from the interaction zone. However, the reflected waves are neglected. Hence, this approximation is appropriate for an initial period of the interaction less than the period $2L/C_o$, where L is the distance to the reflecting surface and C_o is the speed of sound in unheated sodium. In one dimensional cartesian coordinates, the rate at which the interaction zone is expanding is given by

$$\frac{dV_t}{dt} = \frac{SdZ}{dt} , \qquad 3.30$$

where S is the corss sectional area of flow per gram of interacting sodium, and

Z is the length of the interaction zone.

In one dimensional cartesian coordinate, the motion of the compressible liquid sodium induced by propagation of a pressure wave is given by[80]:

$$\frac{d^2Z}{dt^2} = \frac{1}{\rho_o C_o} \frac{d}{dt} (P - P_\infty), \qquad 3.31$$

where ρ_o is the density of the unheated sodium, and

P_∞ is the external pressure (See Fig. 3.2).

Equation 3.31, when integrated with respect to time once, gives:

$$\frac{dZ}{dt} = \frac{P - P_\infty}{\rho_o C_o} \qquad 3.32$$

d-2) The inertial approximation

In this formulation, the constraining unheated sodium is considered incompressible. This formulation is appropriate when the time is larger than $2L/C_o$. The expansion in this case is limited by the inertia of the unheated slug (neglecting any friction or viscous forces). The acceleration of the linear expansion of the interaction zone is given by the familiar Newton's law of motion:

$$\frac{d^2Z}{dt^2} = \frac{P - P_\infty}{\rho_o L} \qquad 3.33$$

The volume expansion rate has been defined in equation 3.30.

e) <u>The Rate of Fuel Cooling</u>

For equal size fuel fragments uniformly distributed in the interaction zone, the average temperature of the particles is reduced at a rate given by equation 3.8:

$$\frac{dT_u}{dt} = -\frac{1}{C_u W}\frac{dQ}{dt} \qquad 3.8$$

3.3.3 The Numerical Solution

The simultaneous solution of equations 3.10, 3.17 (or 3.20), 3.21, 3.23 and 3.30 have been obtained by numerical integration. The equations of the modified formulation were programmed in Fortran IV language and linked to the computer program for the original ANL-FCI model. The parts of the original computer program that supply the numerical values for the thermodynamic properties of sodium and perform the numerical integration have not been altered.

The numerical values for the temperature dependent properties of sodium are based on equations recommended by Golden and Tokar[81]. The validity of the equations, however, is assumed to extend beyond the temperature limit of 1644°K for which date is tabulated in Ref. 81. The equations for sodium properties are given in Appendix I.

The numerical solution is performed by an integration subroutine developed at Argonne National Laboratory. The integration scheme is based on the Bulirsh-Stoer method of extrapolation of rational functions[82].

3.4 Application of the Modified Model: Results and Discussion

Various cases have been investigated using the modified model developed in Section 3.3. The calculations considered a 35 cm long molten zone at the core mid-plane of an FFTF

Table 3.1

Summary of the Varied Conditions in the Investigated Cases

Case	Variable	Cushion Gas[+] Initial Volume (cm^3/gm)	Blanket Gas[+] Initial Thickness (μ)	Vapor* Blanketing	Constraint**
1		---	---	Yes	Acoustic
2		---	10	Yes	Acoustic
3		---	20	Yes	Acoustic
4		0.27	---	No	Acoustic
5		0.27	---	Yes	Acoustic
6		---	---	No	Inertial
7		---	---	Yes	Inertial
8		0.27	---	No	Inertial
9		0.27	---	Yes	Inertial
10		---	10	Yes	Inertial
11		---	20	Yes	Inertial
12		---	---	Heat Transfer Cutoff at Vaporization	Inertial

[+]Assumed to be Xenon.

*Cases without vapor blanketing are calculated by the original model.

**The inertial constraint is taken to be equivalent to 200 cm long unheated sodium slug.

subassembly. The initial conditions and parameters common to all calculations have been chosen equal to a set of values used in the calculations of Ref. 14 utilizing the original model. These values are:

Initial Temperature of Sodium = 1100°K

Initial Temperature of Fuel = 2900°K

Fuel Particle Radius = 117 μ (microns)

Fuel to sodium mass ratio = 8.3

Flow area per gram of interacting sodium, S = 0.077 cm^2

Fragmentation and mixing time constant = 1.0 msec

The fuel particle radius used is the median of the particle radius distribution observed in the dropping experiments of Armstrong[12]. Table 3.1 summarizes the different conditions of the investigated cases.

The pressure histories calculated with an acoustic constraint (cases 1 to 5) are shown in Fig. 3.3 and 3.4. Consider the results shown in Fig. 3.3. In the absence of any gas in the interaction zone (case 1), the pressure rise suppresses vaporization until the peak pressure is relieved. When gases are present in the interaction zone, an initial vaporization process takes place. All the vapor recondenses at a later time, and a high pressure peak develops when all the interacting sodium is in the liquid phase. The results of Fig. 3.3 indicate that gas blanketing results in a delay in the pressure rise time.

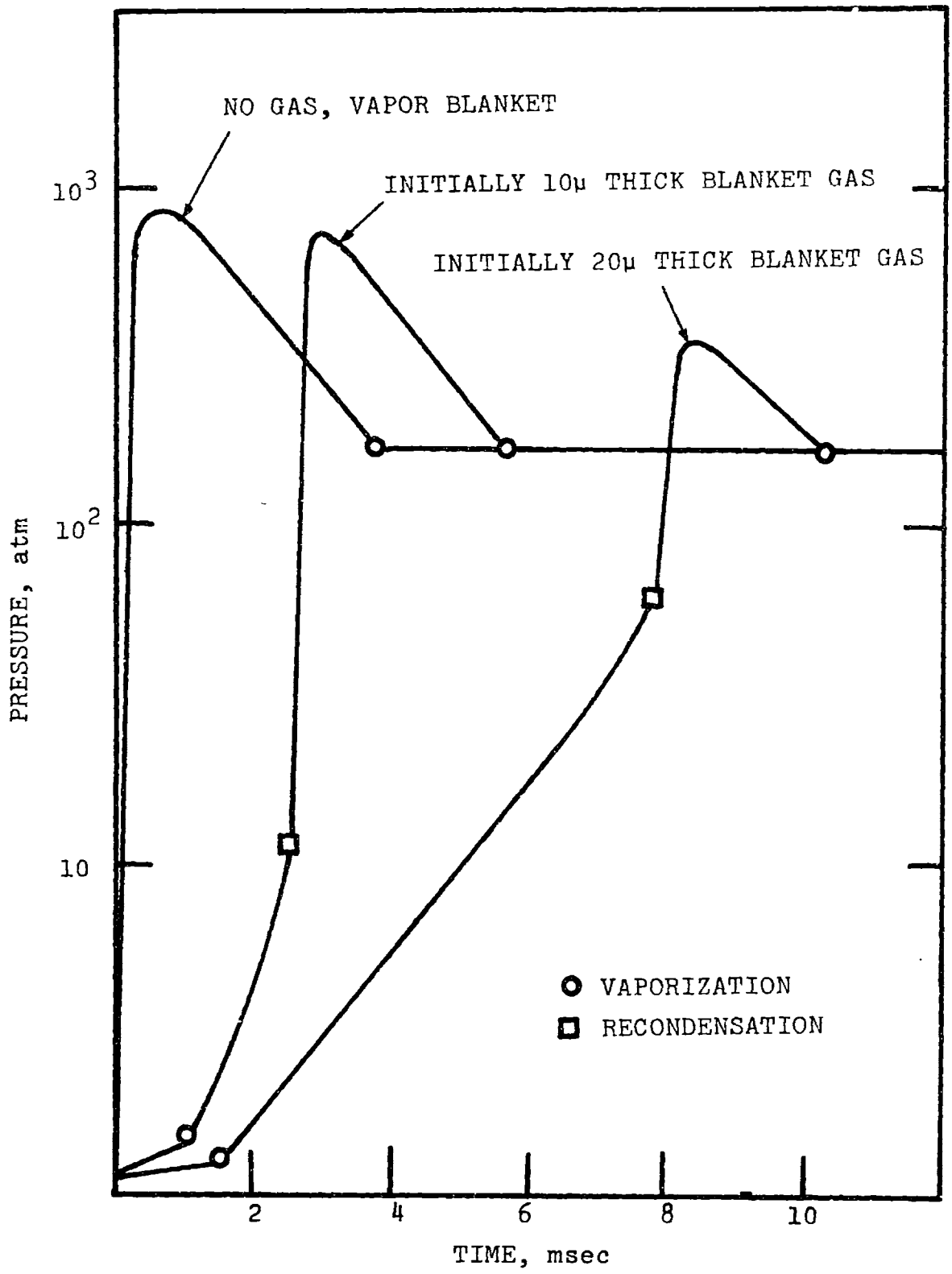

FIG. 3.3: EFFECT OF GAS BLANKETING ON PRESSURE-TIME HISTORY

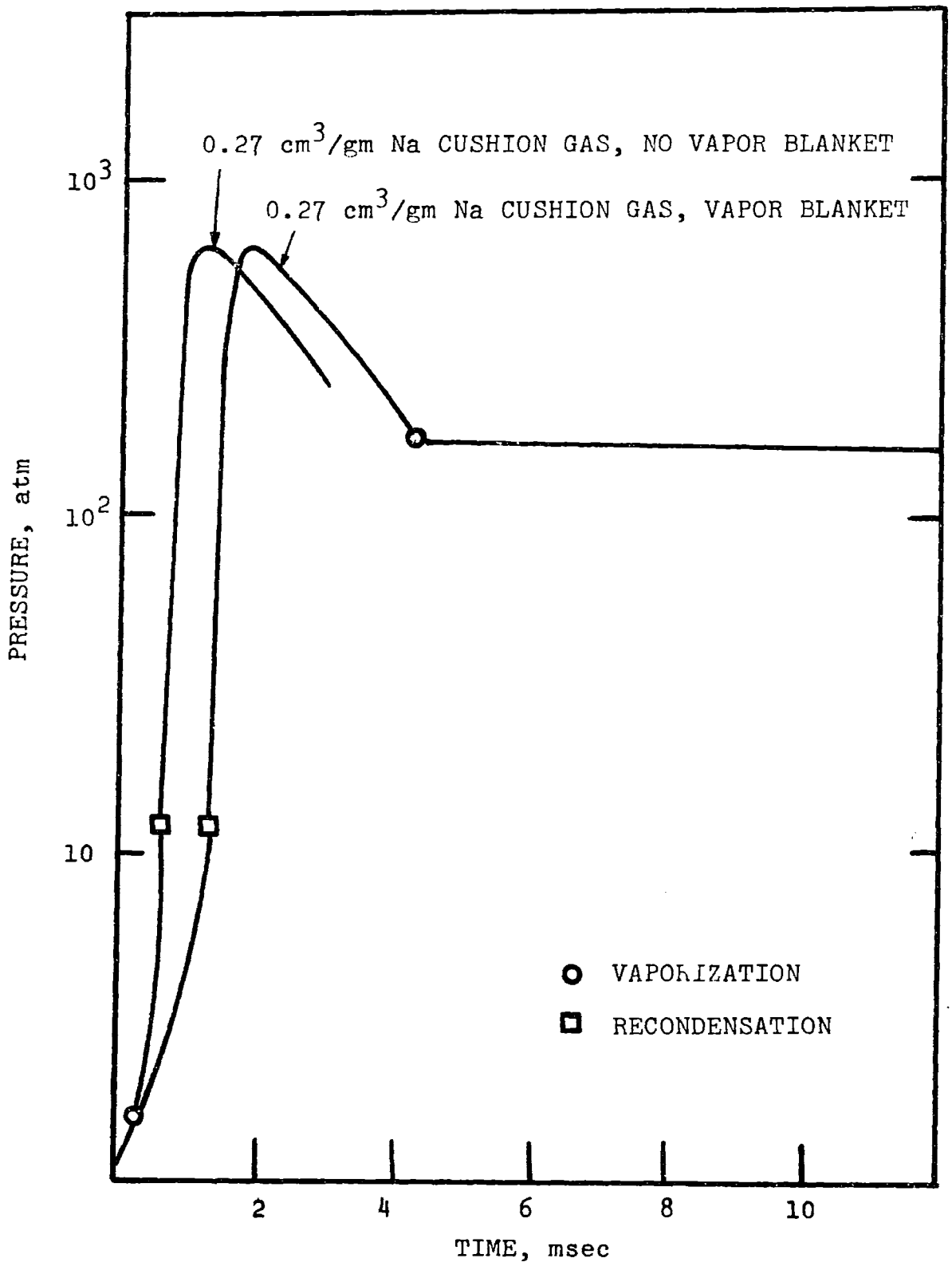

FIG. 3.4: EFFECT OF VAPOR BLANKETING ON PRESSURE-TIME HISTORY

Additionally, the peak pressure is reduced as the initial thickness of the gas blanket increases.

Consider the results shown in Fig. 3.4 for cases 4 and 5. It is seen that an equal value for the peak pressure is obtained with or without accounting for vapor blanketing. However, vapor blanketing seems to cause a delay in the pressure rise time.

The above results indicate, that, when all interacting sodium is initially liquid as is all the present cases, vapor and gas blanketing do not preclude the development of high shock pressures.

The generated mechanical work is calculated using the inertial formulation for the constraint. The length of the unheated sodium slug, L, in these calculations is taken to be 200 cm. The mechanical work is plotted in Fig. 3.5 as a function of the slug displacement for cases 6, 7 and 12. The mechanical work is equivalent to the slug kinetic energy since the interaction zone in the present model is assumed to expand under adiabatic conditions. It is seen that vapor blanketing reduces the mechanical work that is developed at each displacement.

For example, when no gas is initially present in the interaction zone (cases 6 and 7), the mechanical work at a displacement of 100 cm is reduced by about 40% when vapor blanketing is considered.

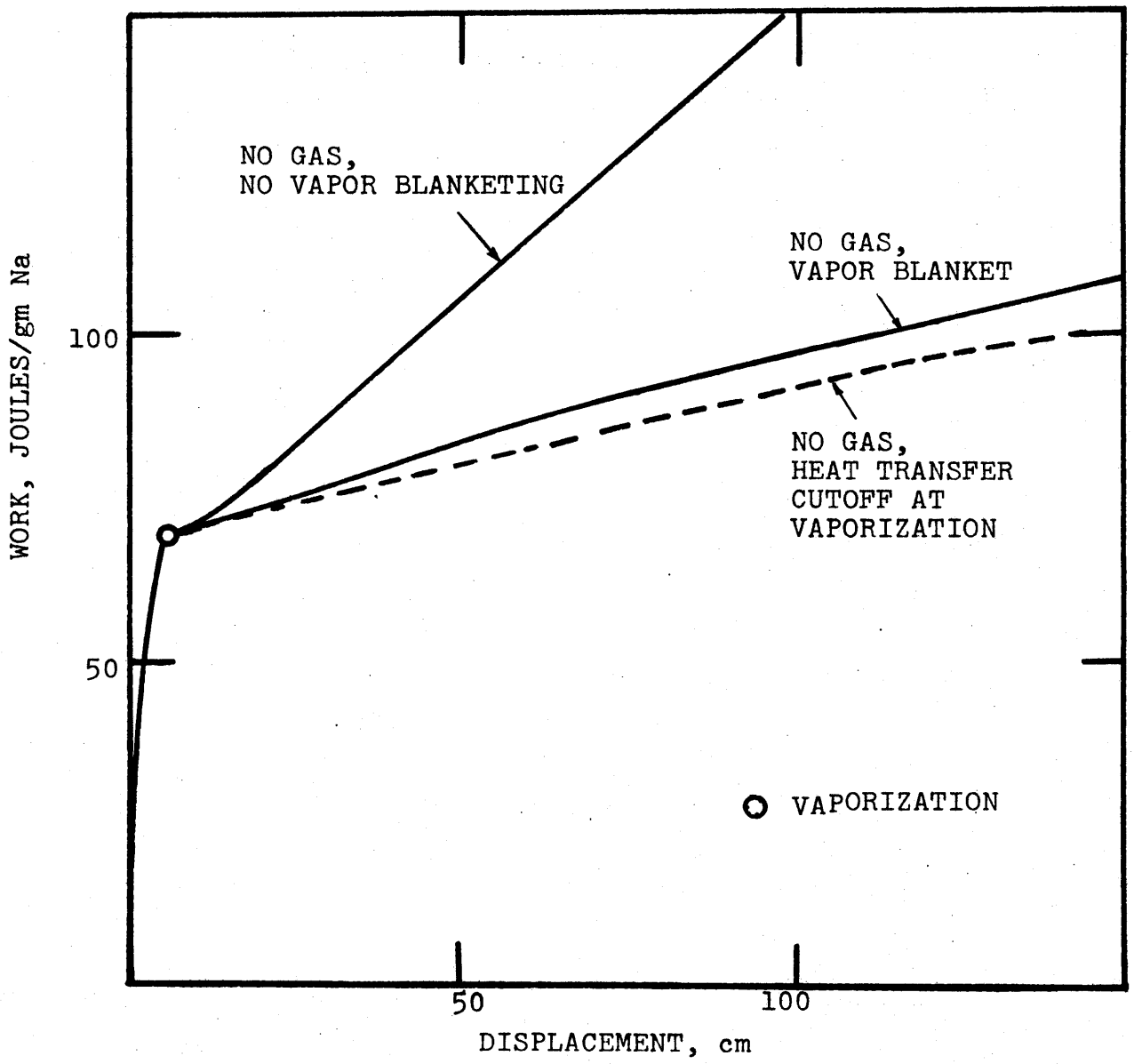

FIG. 3.5: EFFECT OF VAPOR BLANKETING ON MECHANICAL WORK

From the results of cases 7 and 12, plotted in Fig. 3.5, it is seen that in the calculations of mechanical work, vapor blanketing is nearly equivalent to a heat transfer cutoff at the onset of vaporization. It should be noted however that for the calculated cases vapor was continuously produced with the movements of the unheated sodium slug. Therefore, the equivalence of vapor blanketing to a heat transfer cutoff is observed when recondensation of sodium vapor does not take place.

The results for cases 8 and 9 are plotted in Fig. 3.6. The results also show the marked reduction in the generated mechanical energy when vapor blanketing is taken into account.

The effect of gas blanketing is seen in Fig. 3.7 to reduce the mechanical work for the initial displacement. The reduction in the developed work is greater the larger the initial thickness of the gas blanket. The reduction in the mechanical work is larger at smaller displacement values. It is interesting to note here that the limited data of the in-pile fuel pin failure experiments in the TREAT reactor (see Chapter 2, Section 2.2.6) indicate that larger thermal-to-mechanical energy conversion ratios may be obtained by molten fuel-sodium thermal interaction in the absence of a gaseous bond in the fuel pin.

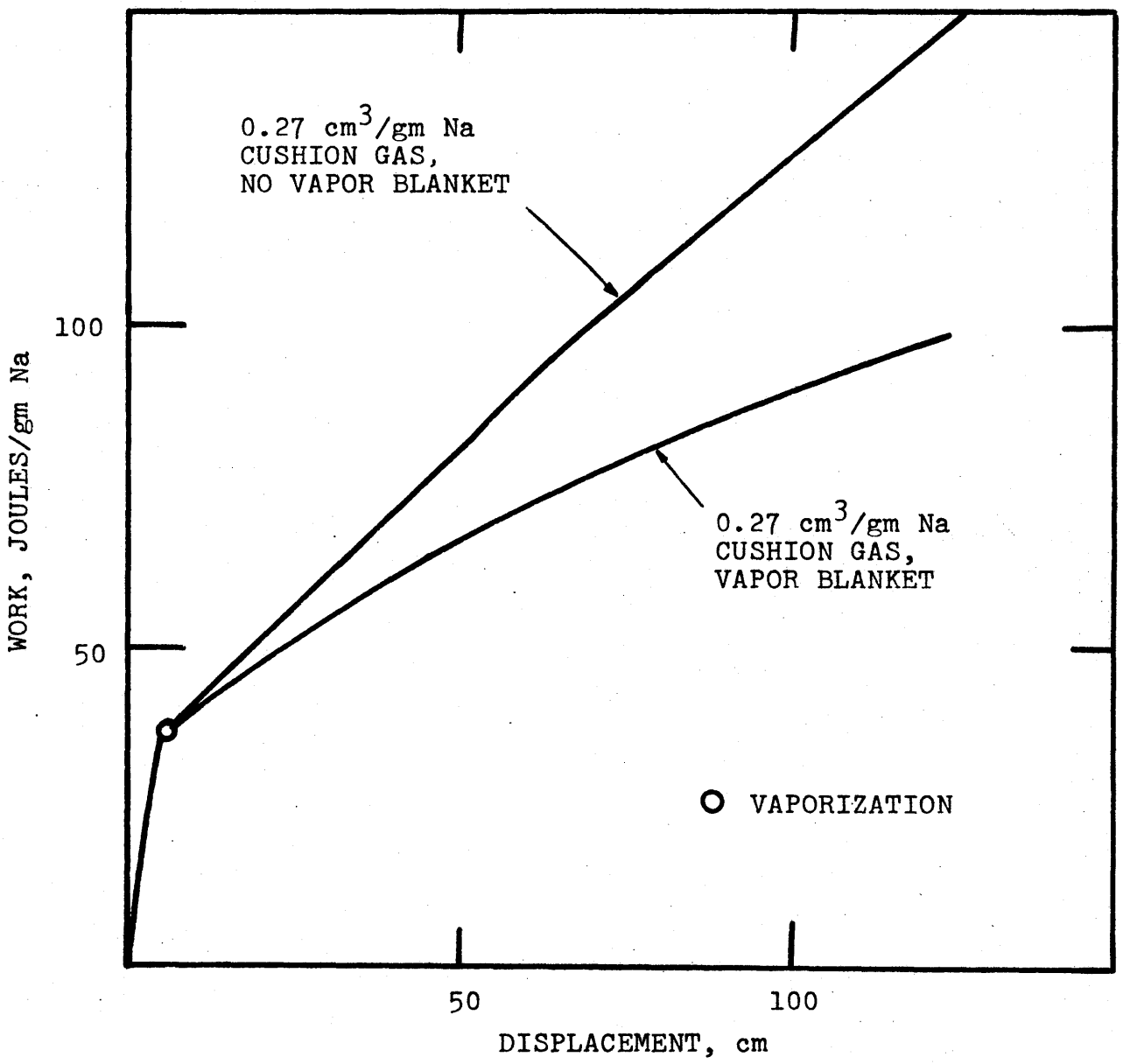

FIG. 3.6: EFFECT OF VAPOR BLANKETING ON THE MECHANICAL WORK IN PRESENCE OF A CUSHION GAS

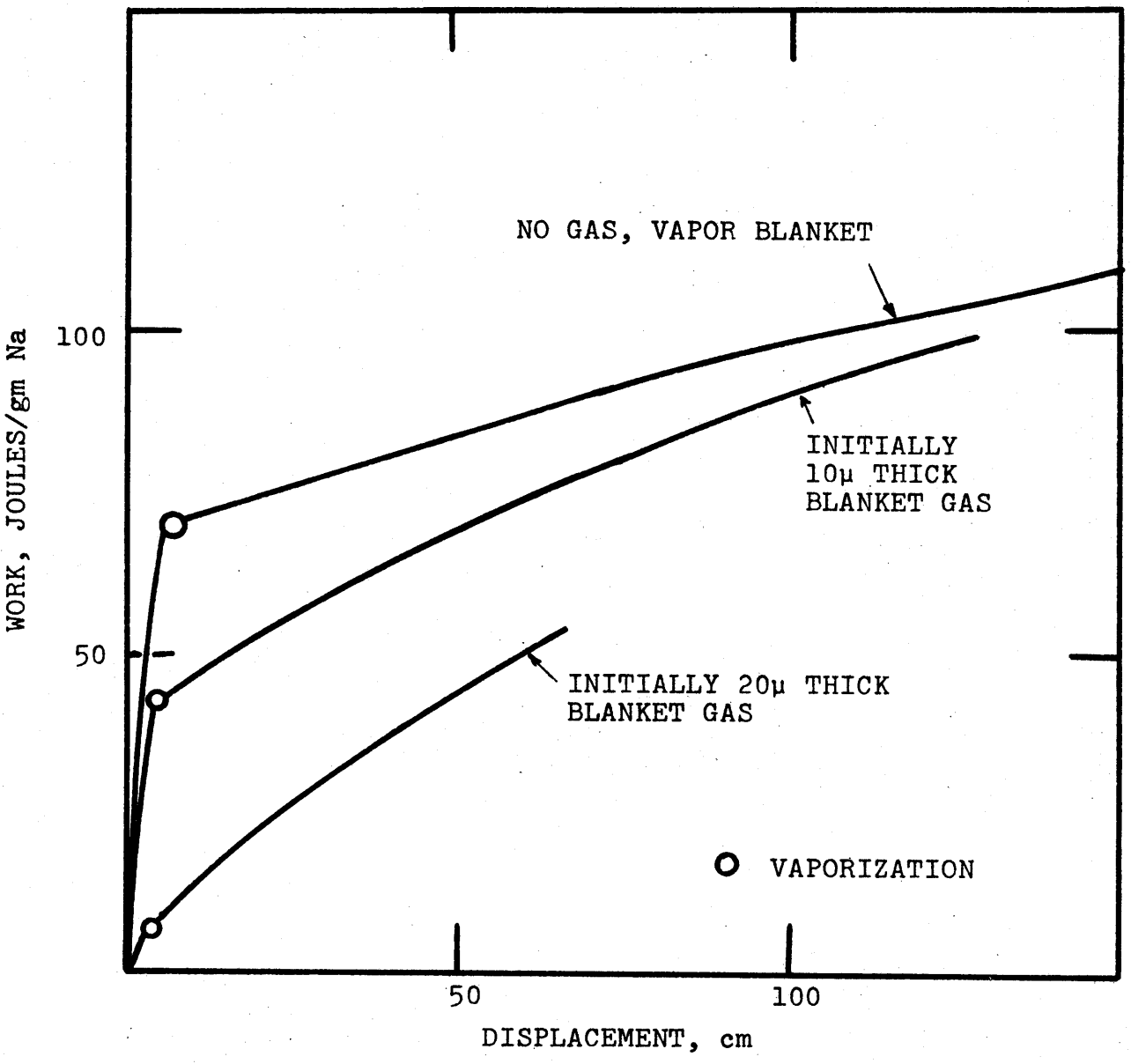

FIG. 3.7: EFFECT OF GAS BLANKETING ON MECHANICAL WORK

The above observations may be summarized as follows:

1. Gas/vapor blanketing of fuel does not preclude the development of high pressure pulses by post fragmentation thermal interaction of molten fuel and liquid sodium.
2. The peak pressures produced by the interaction are, however, reduced by the presence of an initial gas blanket.
3. Gas/vapor blanketing results in an increase in the pressure rise time.
4. Vapor blanketing results in a substantial reduction in the mechanical work that can be developed by the interaction. For the cases considered in the calculation of the mechanical work, vapor blanketing was tantamount to a heat transfer cutoff.
5. The effect of initial gas blanketing is to further reduce the mechanical work developed by the interaction. The larger the blanket thickness the greater is the reduction in the mechanical work.

Chapter Four

DYNAMICS OF VAPOR FILM GROWTH AROUND A HOT PARTICLE IN A COOLANT

Chapter Four

DYNAMICS OF VAPOR FILM GROWTH AROUND A HOT PARTICLE IN A COOLANT

4.1 Introduction

In this chapter the dynamic behavior of a vapor film growing at the surface of a hot sphere which has been suddenly immersed in a coolant is considered. The purpose of this study is to investigate the effects of the initial temperature and the properties of both the sphere and the coolant on the dynamic behavior of the growing film. The results of this study are used in Chapter 5 to investigate a possible correlation between the pressure history of the growing film and the observed fragmentation of hot molten materials when dropped in relatively cold liquids.

The formulation of the model used in the study is first discussed. The model is then applied to hot spheres in water and sodium coolants. The sphere materials are chosen from the materials used in reported experiments of dropping molten materials in water and sodium. (See Section 2.2.4)

4.2 Formulation of the Model

4.2.1 Basic Assumptions

Consider a sphere which has been suddenly immersed in a large amount of a relatively cold liquid. The

sphere is initially at a high enough temperature to induce film boiling of the liquid at the hot surface. The liquid is initially subcooled with respect to the ambient pressure. Part of the heat flux from the sphere is consumed in vapor formation at the film/liquid interface, the rest is conducted away from the film into the liquid. The growth of the film is governed by the evaporation rate as well as the inertial effects of the liquid motion induced by unbalanced pressure across the liquid. Thus, the film may grow due to formation of new vapor as well as to a film pressure in excess of the ambient pressure. Conversely, the film may collapse due to vapor condensation as well as to a film pressure less than the ambient pressure. Additionally, the following assumptions are made:

1. The system may be treated as spherically symmetric.
2. All the generated vapor is retained in the film, i.e. no vapor is allowed to detach.
3. A small gaseous film initially exists at the surface of the sphere.
4. The pressure in the film may be considered uniform.
5. The liquid and the vapor are at equilibrium at the film/liquid interface. Hence, the vapor pressure at any time determines the temperature at the film/liquid interface.

6. The heat is transferred across the film only by conduction. The heat flux corresponds to a linear temperature profile in the film:

$$q''_v = k_v \Delta T/\delta$$

7. The vapor and gases in the film may be treated as perfect gases at the average temperature of the sphere surface and the film/liquid interface.
8. Buoyancy effects may be neglected.
9. Convective heat transfer in the liquid may be neglected.
10. The liquid may be treated either as incompressible or as acoustically infinite.
11. The physical properties of the sphere and the liquid may be considered temperature independent.

4.2.2 Discussion of Assumptions

In the present model, the coolant is assumed to undergo "film boiling" rather than "nucleate boiling" when exposed to the hot sphere. It should be emphasized that "film boiling" as used here does not mean "stable film boiling" but the mode of boiling in which evaporation takes place at all points of the hot surface and

not at preferred locations. It is generally accepted that film rather than "nucleate boiling" takes place when the surface is at a high enough temperature[83]. The conditions under which film boiling (both stable and unstable) observed in experiments of quenching hot spheres in water and sodium are summarized in Table 4.1. The motion picture observations of the boiling modes by Walford[86] (700 frames/second) and Stevens et al.[47,88] (2000 - 4000 frames/second) indicate that transition between stable film boiling and nucleate boiling takes the form of a pulsating film. This is supported by the observations of Board et al.[90] in experiments of rapid heating of a 0.001 inch thick nickel foil. Additionally, the observations of Walford and Stevens et al. indicate that film boiling may not be preceeded by nucleate boiling. Therefore, the assumption of film-wise evaporation seems suitable for the range of sphere and coolant pool temperatures studied in the present analysis.

The assumption of spherical symmetry implies that the variation of the film thickness is small compared to the thickness itself. The assumptions of spherical symmetry (Assumption 1) and the retention of all the vapor in the film (Assumption 2) are supported by several experimental observations of film boiling in subcooled

Table 4.1

Experiments of Quenching of Spheres in Subcooled Coolants

Investigator (Reference)	Sphere Material (Dia., inch)	Range of Temperature in Experiment, °C		Temperatures of Critical Heat Flux, °C		Range of Temperatures For Film Boiling	Coolant Velocity ft/sec	COOLANT
		Coolant T_ℓ	Sphere T_h	Coolant T_ℓ	Sphere T_h			
Bradfield (84, 85)	Cr-plated Cu (2.35)	27-95	160-870	27 53 95	600 332 204	Stable film boiling in 27, 53, 95 °C water for sphere temperatures above 704, 593 and 260 °C respectively	0.0	WATER
Walford (86)	Nickel (0.25)	18-99	104-466	–	–	For $T_\ell \geq$ 18°C film boiling takes place when $T_h \leq$ 460°C	1.8-5.0	
Jacobson and Shair (87)	Steel (0.5)	10-49	–	–	–	A film was always maintained by continuous heating of the sphere. Temperatures not reported	0.7-5.0	

Table 4.1 (continued)

Experiments of Quenching of Spheres in Subcooled Coolants

Investigator (Reference)	Sphere Material (Dia., inch)	Range of Temperature in Experiment, °C		Temperatures of Critical Heat Flux, °C		Range of Temperatures For Film Boiling	Coolant Velocity ft/sec	COOLANT
		Coolant T_ℓ	Sphere T_h	Coolant T_ℓ	Sphere T_h			
Stevens et al. (47, 88)	Ag-plated Cu (0.75)	24,60	190-246†	–	–	Stable or pulsating film was always observed initially	9.6-20	WATER
	Ag (0.356)	24-95	565†	–	–		0.0	
	Ag (1.0)	24, 60, 77	260-537†	24 60 77	271 260 221		5.0	
Farahat (89)	Tantalum (0.5, 0.75 and 1.0)	156-875	up to 2315	875 400 156	∿954 ∿1426 –	Stable film boiling for sphere temperatures above T^* †† given by: $T^*-T_\ell=421+6.28(T_s-T_\ell)$ °C	0.0	SODIUM

†Initial sphere temperatures are given

††The correlation specifies the sphere temperature at which minimum heat flux was observed.

liquids. The assumptions are less justified for saturated boiling which we do not consider. Bradfield[84] observed "...as the subcooling is increased, the normally wavey interface gradually changes in appearance and becomes glassy smooth". Jacobson and Shair[87] observed that "Water subcoolings to 10°C and 50°C resulted in a stable vapor film and no bubbles left the film ... The cool liquid prevented the emission of vapor from the film due to buoyant forces". Stevens et al.[47] also observed that in many instances their silver sphere "appeared to travel through the pool enclosed in an almost perfectly spherical shell of vapor, without a trailing vapor wake behind the sphere".

Assumption 3 of initial existence of a small gaseous film at the surface of the sphere is made in light of the practical conditions for which the model would be applied: namely, the study of the characteristics of boiling around molten particles dropped in coolants. In the reported experiments of this type the particles were usually dropped through a gaseous atmosphere. Thus, a gaseous film may exist at the surface due to physical adsorption[91,92] as well as to "sweeping" some of the gas into the coolant pool. There is no experimental data on the thickness of the gas film that would be swept into the pool under such conditions.

The initial thickness of the gas film is therefore treated parametrically and is varied between 10^{-6} and 10^{-4} cm. The existance of a non-condensable gas at the surface is also justified for nuclear fuel contacting liquid sodium under LMFBR environment, where non-condensable gases (fuel pin bond gas or fission gases) may adhere to the fuel surface.

It should be pointed out, however, that the present model is incapable of treating the cases where intimate contact between the hot sphere and the coolant may be assumed. In such cases, when the change of phase is accompanied by a change in the specific volume of the coolant, vaporization cannot take place initially under the assumed equilibrium conditions at the film/liquid interface.

The assumption of uniform pressure in the film (Assumption 4) can be considered acceptable as long as a pressure disturbance at one end of the film reaches the other end in a time less than the time involved in appreciably changing the average pressure in the film. The pressure equalization time τ_p is given by $\tau_p = 2\delta/c$, where δ is the film thickness and c is the velocity of sound in the film. The calculated periods of oscillation of the uniform pressure in the present analysis have been typically greater than τ_p by two orders of magnitude.

For the cases considered in this study the assumed equilibrium at the film/liquid interface (Assumption 5) seems adequate since the interface temperature is expected to vary negligibly from that of saturation at the film pressure. (See Appendix C)

The contribution of radiative heat transfer to the total heat transfer is small for the considered temperatures and film thicknesses (see Appendix A), and may therefore be neglected. The effect of convective heat transfer in the film was shown negligible in studies of transient growth of a vapor film around hot wires[94]. The approximation of a linear temperature profile in the film is a common approximation in studies of steady state film boiling[95-97]. There are indications[90], however, that the conduction value ($k_v \Delta T/\delta$) underestimates the transient heat flux for subcooled water film boiling, when the film thickness is $> 3 \times 10^{-3}$cm.

The treatment of the vapor as a perfect gas (Assumption 7) is an approximation of the state equation of the vapor. However, unless the pressure in the film gets to values near the critical pressure, the error introduced by this approximation is not of appreciable significance. The use of the average of the sphere surface temperature and the film/liquid interface temperature to evaluate an effective gas density is again an

approximation that introduces a maximum error of 13% in estimation of the perfect gas density under the assumed linear temperature in the film (See Appendix B).

In pool boiling the assumptions of negligible effects of buoyancy and convective heat transfer in the liquid (Assumptions 8 and 9) are justified only for short-time after the initiation of the film growth[93,94]. It should be noted that the two assumptions are affected differently by the liquid subcooling. Subcooling retards the vapor generation rate and hence the buoyancy effects. On the other hand, with larger subcoolings the density variation leading to the convective currents is enhanced. As a consequence of the two assumptions, however, only short term behavior of the vapor film can be predicted by the present model. For forced convection conditions, as encountered in the dropping experiments, the thermal resistance of the liquid would be less than the conduction resistance. This would retard the film growth by reducing the amount of evaporation, and would therefore lead to a higher cooling rate of the sphere than the pool boiling case[88].

Finally, to avoid the complexity of solving the explicit equations of the conservation of mass and momentum of the liquid coolant, the calculations are

made for the two limiting cases of (Assumption 10):

i - incompressible liquid

ii - compressible, acoustically infinite liquid.

Both assumptions are commonly made in analysis of vapor bubble dynamics[98-104]. For a rapidly changing pressure field in the film, the liquid compressibility should be taken into account in calculating the film/liquid interface velocity. When the liquid is so large that reflections of pressure waves, originated at the film interface, at free or rigid surfaces can be neglected in the time period of interest, the acoustically infinite liquid is the more appropriate approximation. However, if the time for pressure wave reflections to reach the film is small compared to the time period in which the transient pressure is appreciably changed, the incompressible liquid is more appropriate. The actual interface velocity lies between these two bounds.

4.2.3 Mathematical Formulation

The dynamic growth of the vapor film is determined by the simultaneous solution of the following equations:

a. The heat transfer equation in the hot sphere.

b. The heat transfer equation in the cold liquid.

c. The equations determining the rate of vaporization.

d. The equation of motion of the film/liquid interface.

e. The equations of state for the gases in the film.

The integral approach is used for the description of the heat transfer in the sphere and the liquid. This approach is used to overcome the difficulty of solving the differential heat transfer equations under the highly non-linear boundary conditions. The adequacy of the integral method for the description of the heat transfer is discussed in Appendix D.

The integral approach to the description of the heat transfer in the sphere yields two time dependent variables by which the rate of heat transfer from the sphere is determined at any time. These two variables are: $T_R(t)$, the temperature of the sphere surface, and $\lambda(t)$, the thickness of the thermally active region. When the thermally active region progresses to include all the sphere $\lambda(t)$ becomes constant (equal to the radius of the sphere), and is replaced as a variable by the temperature of the center of the sphere, $T_c(t)$. Similarly, the integral approach to the description of the heat transfer in the cold liquid yields two variables, $T_{\ell v}(t)$ and $\Delta(t)$, that determine the rate of heat transfer

into the liquid at any time. The variable $T_{\ell v}(t)$ is the temperature at the film/liquid interface. The variable $\Delta(t)$ is the thickness of the thermally active region in the liquid, which can progress indefinitely within the large body of liquid. Three additional variables are to be determined at any time: $R_\delta(t)$, the radius of the film/liquid interface; $U(t)$, the velocity of the film/liquid interface due to imbalances between the film pressure and the ambient pressure, and $P_f(t)$ the film pressure at any time.

The aforementioned equations a, b, c, d and e are utilized in the following to derive relations that couple the rate of change of the seven variables (T_R, $T_{\ell v}$, λ(or T_c), Δ, R_δ, U and P_f). A numerical solution is then obtained for the resulting set of first order differential equations for the rates of change of these variables with time.

Heat Transfer in the Sphere

For a spherical coordinate system with its origin at the center of the sphere (see Fig. 4.1), the heat transfer is governed by Fourier's equation[105,107]:

$$\frac{\alpha_h}{r^2} \frac{\partial}{\partial r} \left[r^2 \frac{\partial}{\partial r} T_h(r,t) \right] = \frac{\partial}{\partial t} T_h(r,t) \qquad 4.1$$

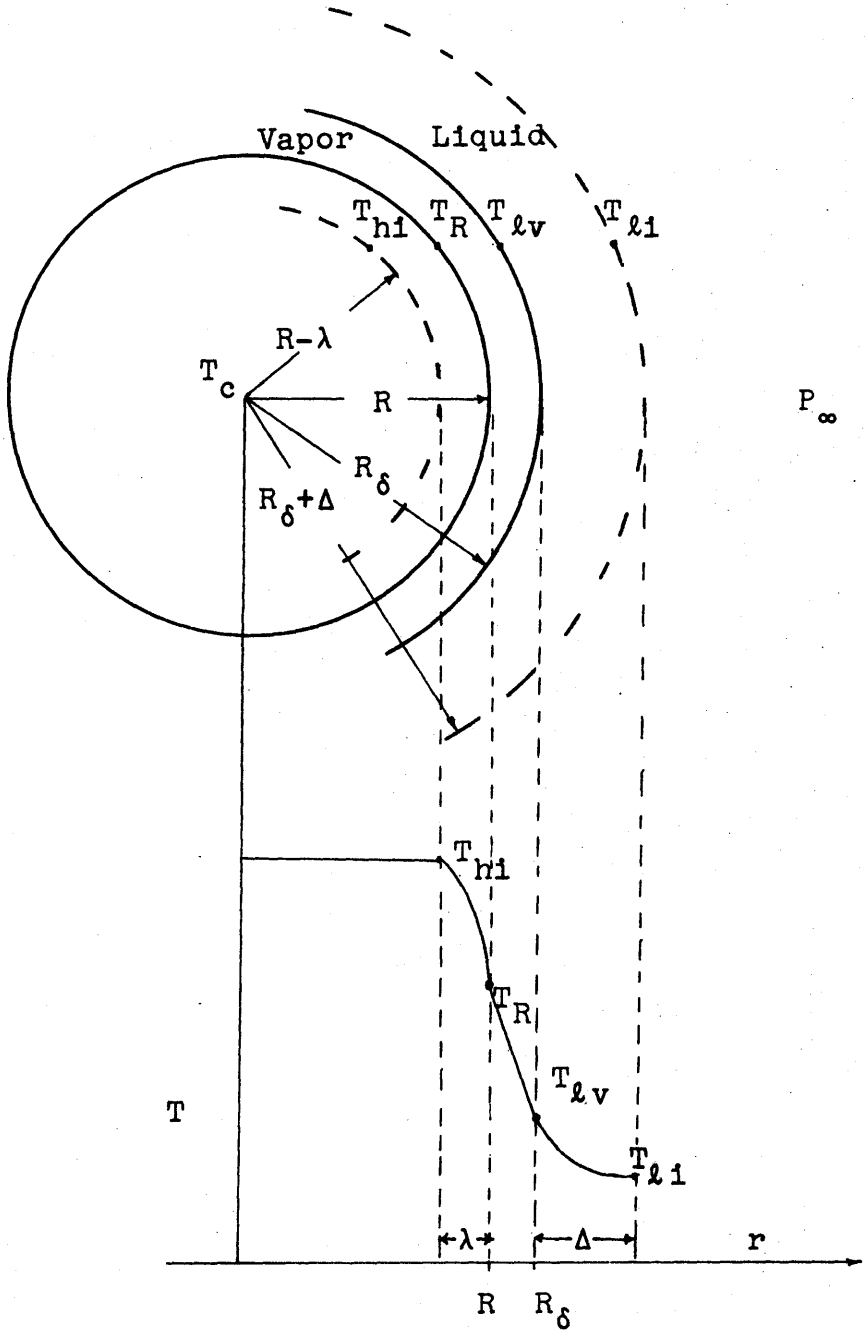

Fig. 4.1 A Schematic Diagram of the Temperature Field

where α_h is the thermal diffusivity of the hot sphere, and the spherical symmetry assumption has been applied.

Following the standard integral approach, the temperature is assumed to be affected only within a penetration, $\lambda(t)$, which progresses with time. The temperature at the center of the sphere, T_c, remains constant until the thermally active region progresses to include the whole sphere, i.e. until $\lambda(t) = R$. Equation 4.1 is to be satisfied in the integral form:

$$\alpha_h \int_0^R dr^2 \frac{\partial T_h(r,t)}{\partial r} = \int_0^R r^2 \frac{\partial T_h(r,t)}{\partial t} dr \qquad 4.2$$

Since the temperature in the sphere is initially uniform and is affected only within the thickness $\lambda(t)$ from the surface, equation 4.2 may be written as:

$$\alpha_h \int_{R-\lambda(t)}^R dr^2 \frac{\partial T_h(r,t)}{\partial r} = \int_{R-\lambda(t)}^R r^2 \frac{\partial T_h(r,t)}{\partial t} dr \qquad 4.3$$

Assume the temperature profile within the thermally active region is of the quadratic form:

$$T_h(r,t) = a_0(t) + a_1(t)r + a_2(t)r^2 \; ;$$

$$R \geq r \geq R-\lambda \qquad 4.4$$

By applying the conditions:

$$T_h(R,t) = T_R(t), \tag{4.4a}$$

$$\left.\begin{aligned} T_h(R-\lambda(t),t) &= T_{hi}; \quad \lambda < R \\ &= T_c \; ; \quad \lambda = R \end{aligned}\right\}, \tag{4.4b}$$

and

$$\left.\frac{\partial T_h}{\partial r}\right|_{R\,-\,\lambda(t)} = 0 \tag{4.4c}$$

Equation 4.4 can be written in the form:

for $\lambda < R$

$$\left.\begin{aligned} \frac{T_{hi}-T_h(r,t)}{T_{hi}-T_R} &= \left[1-\frac{y}{\lambda}\right]^2; \quad R > r > R-\lambda \\ &= 0 \qquad ; \quad R-\lambda > r > 0 \end{aligned}\right\}, \tag{4.5a}$$

and for $\lambda = R$

$$\frac{T_c-T_h(r,t)}{T_c-T_R} = \left[1-\frac{y}{R}\right]^2; \text{ all } r < R, \tag{4.5b}$$

where the notation of the dependence of λ, T_R, and T_c on t has been dropped and where $y = R-r$.

Note that as long as $\lambda < R$, the thermal field in the sphere is determined once the values of λ and T_R are obtained. When $\lambda = R$, the thermal field is determined when the values of T_c and T_R are obtained.

The rate of heat transfer from the sphere is given by:

$$\frac{dQ_h}{dt} = 4\pi R^2\left[-k_h \left|\frac{\partial T_h(r,t)}{\partial r}\right|_R\right], \qquad 4.6$$

where k_h is the thermal conductivity of the sphere. By substitution for $T_h(r,t)$ from Equation 4.5 in Equation 4.6, the heat transfer rate is determined by:

$$\frac{dQ_h}{dt} = \frac{8\pi R^2 k_h(T_{hi}-T_R)}{\lambda} \quad ; \quad \lambda < R, \qquad 4.6a$$

and

$$\frac{dQ_h}{dt} = 8\pi R k_h(T_c-T_R); \qquad \lambda = R. \qquad 4.6b$$

The rates of change of λ and T_c are determined by substitution for $T_h(r,t)$ from Equations 4.5 into Equation 4.3 yielding:

for $\lambda < R$

$$A_2 \frac{d\lambda}{dt} = \frac{\alpha_h}{\lambda} + \frac{\lambda A_1}{2(T_{hi}-T_R)} \frac{dT_R}{dt} , \qquad 4.7a$$

where

$$A_1 = \frac{1}{3} - \frac{\lambda}{6R} + \frac{1}{30}\left(\frac{\lambda}{R}\right)^2 ,$$

$$A_2 = \frac{1}{6} - \frac{\lambda}{6R} + \frac{1}{20}\left(\frac{\lambda}{R}\right)^2 ,$$

and for $\lambda = R$

$$\frac{dT_c}{dt} = \frac{3}{2}\left[\frac{10\alpha_h(T_R-T_c)}{R^2} - \frac{dT_R}{dt}\right] ; \quad \lambda = R \qquad 4.7b$$

As the sphere surface temperature, T_R, is not a priori defined, $\frac{dT_R}{dt}$ is determined from the heat flux boundary condition:

$$- k_h \frac{\partial T_h(r,t)}{\partial t}\bigg|_R = \frac{k_v(T_R-T_{\ell v})}{R_\delta - R} , \qquad 4.8a$$

i.e.,

$$\frac{1}{4\pi R^2}\frac{dQ_h}{dt} = \frac{k_v(T_R - T_{\ell v})}{R_\delta - R}\ , \qquad 4.8b$$

where k_v is the thermal conductivity of the vapor, and

$T_{\ell v}$ is the temperature at the film/liquid interface.

By substituting for $\frac{dQ_h}{dt}$ from Equation 4.6 into Equation 4.8b and differentiating the resultant equations with respect to time we get:

For $\lambda < R$

$$\left[\frac{k_v}{\delta} + \frac{2k_h}{\lambda}\right]\frac{dT_R}{dt} = \frac{k_v}{\delta}\frac{dT_{\ell v}}{dt} + \frac{k_v(T_R - T_{\ell v})}{\delta^2}\frac{dR_\delta}{dt}$$

$$- \frac{2k_h(T_{hi} - T_R)}{\lambda}\frac{d\lambda}{dt}\ , \qquad 4.9a$$

and for $\lambda = R$

$$\left[\frac{k_v}{\delta} + \frac{2k_h}{\lambda}\right]\frac{dT_R}{dt} = \frac{-2k_h}{R}\frac{dT_c}{dt} + \frac{k_v}{\delta}\frac{dT_{\ell v}}{dt}$$

$$+ \frac{k_v(T_R - T_{\ell v})}{\delta^2}\frac{dR_\delta}{dt} \qquad 4.9b$$

where $\delta = R_\delta - R$, the thickness of the film.

Heat Transfer in the Liquid

For a liquid in motion, the Fourier equation for heat conduction in fixed spherical coordinates takes the form[107]:

$$\frac{\alpha_\ell}{r^2}\frac{\partial}{\partial r}\left[r^2\frac{\partial}{\partial r}T_\ell(r,t)\right] = \frac{\partial}{\partial t}T_\ell(r,t) + \frac{\partial r}{\partial t}\cdot\frac{\partial}{\partial r}T_\ell(r,t), \quad 4.10$$

where α_ℓ is the thermal diffusivity of the liquid.

The Fourier equation is to be satisfied in the integral form:

$$\alpha_\ell \int_{R_\delta(t)}^{\infty} d\, r^2 \frac{\partial}{\partial r}T_\ell(r,t) = \int_{R_\delta(t)}^{\infty} r^2 \frac{\partial}{\partial t}T_\ell(r,t)\, dr$$

$$+ \int_{R_\delta(t)}^{\infty} r^2 \cdot \frac{\partial r}{\partial t} \cdot \frac{\partial T_\ell(r,t)}{\partial r}\, dr \,. \quad 4.11$$

Assume a quadratic temperature profile in the thermally active region of thickness $\Delta(t)$, (see Figure 4.1):

$$\left.\begin{aligned} T_\ell(r,t) &= C_0(t) + C_1(t)r + C_2(t)r^2; \quad R_\delta \leq r \leq R_\delta + \Delta \\ &= T_{\ell i} \qquad\qquad\qquad\qquad ; \quad r \geq R_\delta + \Delta \end{aligned}\right\} \quad 4.12$$

where the notation of the dependence of R_δ and Δ on t has been dropped.

By applying the conditions:

$$T_\ell(R_\delta,t) = T_{\ell v}(t), \qquad 4.12a$$

$$T_\ell(R_\delta+\Delta,t) = T_{\ell i}\ , \qquad 4.12b$$

$$\left.\frac{\partial T_\ell(r,t)}{\partial r}\right|_{R_\delta + \Delta} = 0\ , \qquad 4.12c$$

Equation 4.12 can be written in the form:

$$\left.\begin{aligned} \frac{T_\ell(r,t)-T_{\ell i}}{T_{\ell v}(t)-T_{\ell i}} &= \left(1 - \frac{X}{\Delta}\right)^2 \quad ; \quad R_\delta \leq r \leq R_\delta + \Delta \\ &= 0 \qquad\qquad ; \qquad r \geq R_\delta + \Delta \end{aligned}\right\} \quad 4.13$$

where $X = r - R_\delta$.

The integration of Eqn. 4.11 can be greatly simplified if the liquid within the thermally active region is considered

incompressible so that, from conservation of mass considerations.

$$r^2 \frac{\partial r}{\partial t} = R_\delta^2 \left.\frac{\partial r}{\partial t}\right|_{R_\delta} = R_\delta^2 \, U \quad . \tag{4.14}$$

Note that U is the film/liquid interface velocity due to dynamic pressure in the film only; i.e. not including the velocity of the interface due to change of phase. Substitution in Eq. 4.11 for $T_\ell(r,t)$ from Eq. 4.13 and for $\frac{\partial r}{\partial t}$ from Eq. 4.14 and performing the integration yields:

$$C_2 \frac{d\Delta}{dt} = \frac{\alpha_\ell}{\Delta} - \frac{\Delta C_1}{2(T_{\ell v}-T_{\ell i})} \frac{dT_{\ell v}}{dt} - C_3 \frac{dR_\delta}{dt} + \frac{1}{2} U \, , \tag{4.15}$$

where

$$C_1 = \frac{1}{3} + \frac{1}{6} \frac{\Delta}{R_\delta} + \frac{1}{30} \left(\frac{\Delta}{R_\delta}\right)^2 \quad , \tag{4.15a}$$

$$C_2 = \frac{1}{6} + \frac{1}{6} \frac{\Delta}{R_\delta} + \frac{1}{20} \left(\frac{\Delta}{R_\delta}\right)^2 \quad , \tag{4.15b}$$

$$C_3 = \frac{1}{2} + \frac{1}{3} \frac{\Delta}{R_\delta} + \frac{1}{12} \left(\frac{\Delta}{R_\delta}\right)^2 \quad . \tag{4.15c}$$

The rate at which the heat is conducted away from the film into the bulk liquid is given by:

$$\frac{dQ_\ell}{dt} = 4\pi R_\delta^2 \cdot \left[-k_\ell \left.\frac{\partial T_\ell(r,t)}{\partial r}\right|_{R_\delta} \right] \qquad 4.16a$$

which, when substituting for $T_\ell(r,t)$ from Eqn. 4.13, gives:

$$\frac{dQ_\ell}{dt} = \frac{8\pi R_\delta^2 \cdot k_\ell (T_{\ell v} - T_{\ell i})}{\Delta} \quad . \qquad 4.16b$$

Rate of Vaporization

Assuming the energy consumed in heating (or cooling) the gas and vapor in the film is negligible as compared to the energy consumed in vaporization (or condensation), the rate of vaporization, $\frac{dM_v}{dt}$, is determined by the net available heat

$$\frac{dM_v}{dt} = \frac{1}{h_{fg}} \left[\frac{dQ_h}{dt} - \frac{dQ_\ell}{dt} \right] , \qquad 4.17$$

where h_{fg} is the latent heat of vaporization. The mass of the vapor in the film, M_v, is given by:

$$M_v = \rho_v V_f = \rho_v \cdot \frac{4}{3}\pi \left(R_\delta^3 - R^3\right) \qquad 4.18$$

where ρ_v is the vapor density in the film and is given by the perfect gas law:

$$\rho_v = \frac{P_v}{G_v T_f} \quad , \tag{4.19}$$

where G_v is the gas constant for the vapor, and

T_f is the average film temperature given by

$$T_f = \frac{T_R + T_{\ell v}}{2} \quad . \tag{4.20}$$

Note that P_v is the partial vapor pressure in the film, the total film pressure being composed of the partial pressures of the gas and the vapor. Thus, in this treatment the pressure of the film is partitioned between the gas and the vapor, both of which having the total volume V_f. An alternate approach has been used in Chapter 3, where the film volume was partitioned between the gas and the vapor, both of which having the total pressure P_f.

From the assumption of equilibrium at the film/liquid interface, the vapor pressure is given by:

$$P_v = P(T_{\ell v}) \quad . \tag{4.21}$$

The change in the vapor mass, M_v, is accommodated by changing the vapor density and the film radius. Thus, differentiating Equation 4.18 with respect to time yields:

$$\frac{dM_v}{dt} = \frac{4}{3}\pi(R_\delta^3 - R^3)\frac{d\rho_v}{dt} + 4\pi R_\delta^2 \rho_v \frac{dR_\delta}{dt} \quad . \qquad 4.22$$

Substitution from Equations 4.18, 4.19, 4.20 and 4.21 into Equation 4.22 gives:

$$\frac{dM_v}{dt} = \frac{V_f}{G_v T_f}\left[\frac{dP\ (T_{\ell v})}{dT_{\ell v}} - \frac{P_v}{2T_f}\right]\frac{dT_{\ell v}}{dt} - \frac{V_f P_v}{2G_v T_f^2}\frac{dT_R}{dt}$$

$$+ 4\pi R_\delta^2 \rho_v \frac{dR_\delta}{dt} \quad . \qquad 4.23$$

Velocity of the Film/Liquid Interface

The equation of motion of the film/liquid interface is given by:

$$\frac{dR_\delta}{dt} = U + \frac{1}{4\pi R_\delta^2 \cdot \rho_\ell}\frac{dM_v}{dt} \quad . \qquad 4.24$$

The first term represents the motion of the interface due to the dynamic imbalances between the film

pressure, P_f, and the ambient pressure, P_∞. The second term represents the motion due to the change in phase at the interface.

An exact determination of the velocity component U requires simultaneous solution of the equations of conservation of mass and conservation of momentum of the liquid. For a spherically symmetric system the conservation of mass is given by[107]:

$$\frac{\partial \rho_\ell}{\partial t} + u \frac{\partial \rho_\ell}{\partial r} + \rho_\ell \frac{1}{r^2} \frac{\partial}{\partial r} (r^2 u) = 0 \ , \qquad 4.25$$

and the conservation of momentum, when the viscosity is ignored, is given by [107]:

$$\rho_\ell \left[\frac{\partial u}{\partial t} + u \frac{\partial u}{\partial r}\right] = - \frac{\partial P}{\partial r} \ , \qquad 4.26$$

where u is the radial velocity at any radius, r.

a) Case of Incompressible Liquid:

For incompressible liquids, the conservation of mass yields

$$u = U \frac{R_\delta^2}{r^2} \ . \qquad 4.14$$

By substituting from Eqn. 4.14 into Eqn. 4.26 and integrating over radius between the film/liquid interface and infinity, the well known Rayleigh equation[108] is obtained:

$$R_\delta \frac{dU}{dt} + \frac{3}{2} U^2 = \frac{P_f - P_\infty}{\rho_\ell} \quad . \tag{4.27}$$

b) Case of Compressible, Acoustically Infinite Liquid:

When only outgoing pressure waves exist in the liquid, the liquid is said to be acoustically infinite. For such a system Kirkwood and Bethe[109] proposed that the kinetic enthalpy $r(h+\frac{u^2}{2})$ is propagated in the liquid with a speed u + c, in such a manner that the kinetic enthalpy value remains unchanged. Here c is the local speed of sound and is given by

$$c = \sqrt{\frac{dP}{d\rho_\ell}} \quad , \tag{4.28}$$

and h is the specific enthalpy of the liquid and is given by:

$$h = \int_{P_\infty}^{P} \frac{dP}{\rho_\ell} \quad . \tag{4.29}$$

When the Kirkwood-Bethe assumption is made, the equation of motion of the interface of a spherical cavity has been derived by Gilmore[110] as:

$$R_\delta \frac{dU}{dt}\left(1-\frac{U}{C}\right) + \frac{3}{2} U^2\left(1-\frac{U}{3C}\right) = H\left(1+\frac{U}{C}\right) + \frac{R_\delta}{C}\left(1-\frac{U}{C}\right)\frac{dH}{dt} , \qquad 4.30$$

where C is the speed of sound in the liquid at the interface and H is now given by

$$H = \int_{P_\infty}^{P(R_\delta,t)} \frac{dP}{\rho_\ell} = h(P_f) . \qquad 4.31$$

Note that Eqn. 4.30 reduces to Rayleigh's equation for incompressible liquid if C becomes infinite.

Ignoring the effects of density changes due to the temperature changes within the thermal region, the relation between the pressure and the density of the liquid can be related as[98, 101]:

$$\rho_\ell^m = P + B \quad , \qquad 4.32$$

where m and B are constants.

Thus, by substituting from Eqn. 4.32 into Eqn. 4.28, the speed of sound at the interface may be given by:

$$C^2 = \left[\frac{P_f + B}{P_\infty + B}\right]^{\frac{m-1}{m}} C_\infty^2 \quad . \qquad 4.33$$

Substitution from Eqn. 4.33 in Eqn. 4.31 gives

$$H = \frac{C^2 - C_\infty^2}{m-1} \quad . \qquad 4.34$$

Making use of Eqn. 4.34, Eqn. 4.30 can now be written as

$$R_\delta \frac{dU}{dt}\left(1-\frac{U}{C}\right) + \frac{3}{2}U^2\left(1-\frac{U}{3C}\right) = \frac{C^2-C_\infty^2}{m-1}\left(1+\frac{U}{C}\right)$$

$$+ \frac{R_\delta C}{m}\left(1-\frac{U}{C}\right)\left(\frac{1}{P_f+B}\right)\frac{dP_f}{dt} \quad . \qquad 4.35$$

Equation 4.35 provides the equivalent equation to that of Rayleigh for incompressible liquid.

The Film Pressure

The pressure in the film is determined by Dalton's law for partial pressures:

$$P_f = P_v + P_g \ . \qquad 4.36$$

Assuming the non-condensable gas may be treated adiabatically, the partial gas pressure at any time is given by:

$$P_g = P_g^o \left[\frac{V_f^o}{V_f}\right]^n , \qquad 4.37$$

where P_g^o is the initial partial pressure of the gas in the film,

V_f^o is the initial film volume, and

n is the adiabatic index of the non-condensable gas.

From the assumption of vapor-liquid equilibrium at the film/liquid interface, the vapor pressure is given by:

$$P_v = P\ (T_{\ell v}) . \qquad 4.21$$

The rate of change of the film pressure is obtained by substitutions for P_v and P_g from Equations 4.37 and 4.21 in Equation 4.36 and differentiation with respect to time:

$$\frac{dP_f}{dt} = \frac{dP(T_{\ell v})}{dT_{\ell v}} \cdot \frac{dT_{\ell v}}{dt} - n \frac{P_g}{V_f} \frac{dV_f}{dt} \cdot \qquad 4.38$$

Method of Solution

Equations 4.7, 4.9, 4.15, 4.23, 4.24, 4.27 (or 4.35) and 4.38 constitute a set of non-linear first order differential equations in the seven time-dependent variables T_R, $T_{\ell v}$, λ or (T_c), Δ, R_δ, U and P_f. These equations are expressed in the form

$$\sum_{i=1}^{7} K_i \frac{dY_i}{dt} = f_i \; ; \qquad i = 1 \ldots, 7 \qquad 4.39$$

where Y_i is one of the variables T_R, $T_{\ell v}$, λ (or T_c), Δ, R_δ, U and P_f, and

K_i and f_i are expressions involving the variables Y_i.

By successive substitutions among the seven equations of 4.39, the time rate of change for each variable, Y_i, can be expressed in the form:

$$\frac{dY_i}{dt} = F_i(Y_1, Y_2, \ldots, Y_7) \; ; \; i = 1, \ldots, 7. \qquad 4.40$$

A simultaneous solution of the equations in the form 4.40 has been obtained by numerical integration. The computer program developed in Fortran IV language for the solution is given in Appendix E. The numerical integration subroutine, DHPCG, was provided by the Code Library of M.I.T. Information Processing Center. In the subroutine DHPCG the numerical integration is carried out using a standard predictor corrector method[130]. An essential feature of DHPCG is the ability to estimate the local truncation error and to chose a smaller time step for the integration if the truncation error exceeds a preset value. In the cases presented in this chapter, the maximum acceptable truncation error has been chosen to keep the overall relative error in the calculated variables less than 0.1%.

Since Equations 4.7 and 4.15 initially involve infinite derivatives, an analytic solution suitable for an initial small period of time is used to start the numerical integration. The initial time solution assumes a constant heat flux across the film and ignores the small value of film/liquid interface velocity developed in this initial period. The derivation of the expressions used in calculating the starting values is given in Appendix F. The sensitivity of the resultant film behavior to the assumed starting time was checked in

several cases. The results seemed to be insensitive to the starting time values as long as the change in the temperature drop across the film, $T_R - T_{\ell v}$, during this initial period did not exceed 10% of the initial value.

The time steps for starting the numerical integration had to be extremely small (10^{-8} to 10^{-11} second). Larger values of the time steps would lead to instabilities due to a reversal in the evaporation rate. (Too large a time step would overestimate the increment in the film pressure and, hence, an overestimated temperature at the film/liquid interface. This increases the rate of heat conduction in the liquid causing condensation of vapor. Refer to Equation 4.17.) The time steps could be increased (up to 10^{-6} seconds) after the pressure reaches its first peak, as the rate of change of the pressure in the film is then considerably smaller than the initial values. In general the required time steps were smaller for cases of large coolant subcoolings. In such cases the net heat consumed in vaporization is a smaller fraction of the total rate of heat transfer from the sphere. For the largest case of subcooling of sodium (Case 17 of a stainless steel sphere in 250°C sodium, to be discussed in Section 4.4), the time steps have been restricted to a maximum of 10^{-10} seconds throughout the calculations.

A block diagram for the numerical integration scheme is shown in Fig. 4.2.

4.3 Application of the Model to Hot Spheres in Water

The model developed in Section 4.2 has been applied to the growth of a vapor film around hot spheres in water, under various conditions. The temperature of the water pool, the initial temperature of the hot sphere, the thickness of the assumed initially present gaseous film around the sphere, the material of the sphere and the sphere radius have been varied to cover the ranges of variation of these parameters in the reported experiments of dropping hot molten materials in water (see Section 2.2.4). Table 4.2 summarizes the values of parameters in the cases considered.

In all cases the rapid vaporization initially results in a pressure rise in the film which accelerates the film/liquid interface. However, the outward motion of the interface continues beyond the equilibrium position (at which the film pressure is equal to the ambient pressure). Thus, the film pressure falls below the ambient level leading to deceleration of the interface motion. The film/liquid interface motion is then reversed, and the film starts to collapse. The continued evaporation in the film leads to a second pressure rise in the collapsing film and the collapse is stopped before sphere/liquid

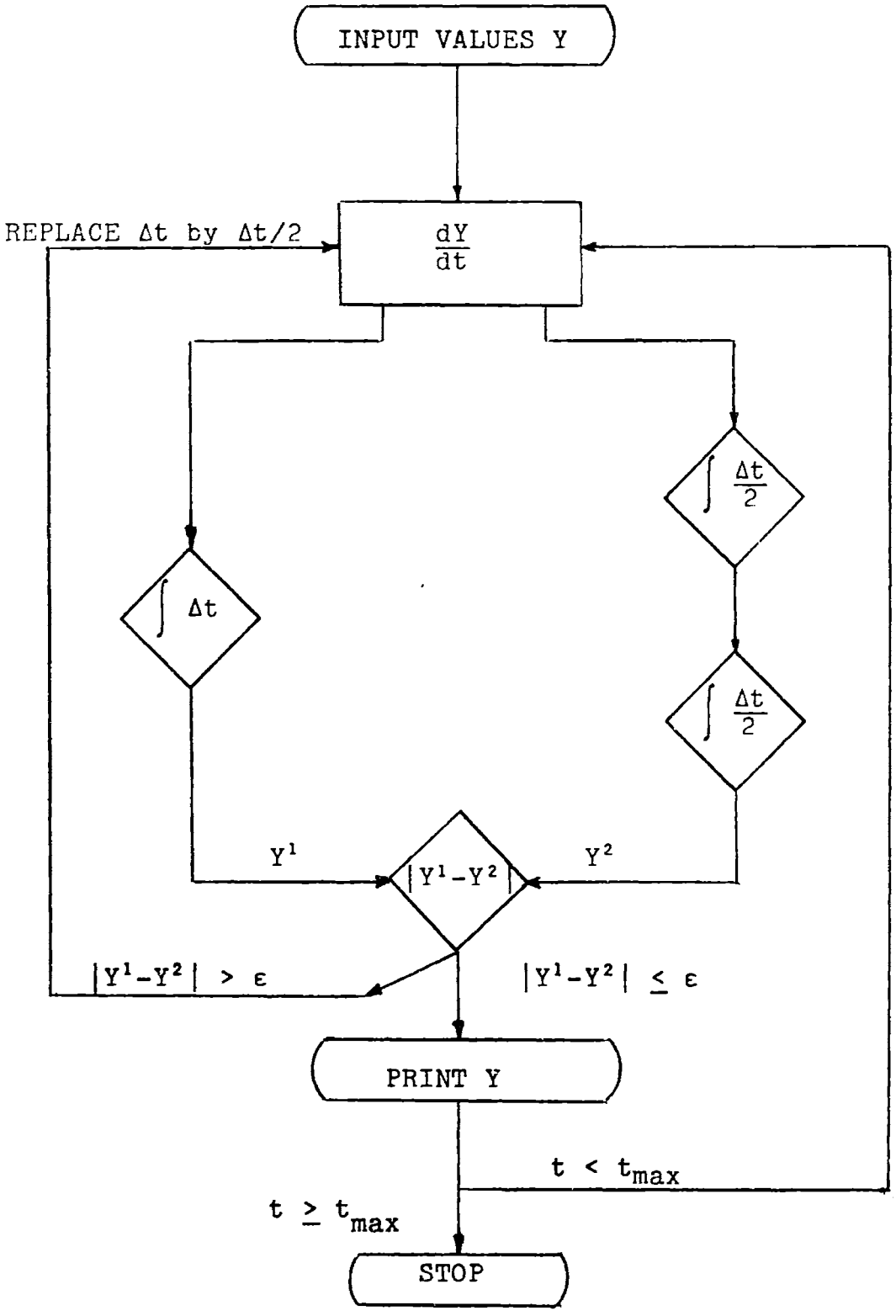

FIG. 4.2: BLOCK DIAGRAM FOR THE NUMERICAL INTEGRATION SCHEME FOR THE VARIABLES (Y)

Table 4.2

Values of the Parameters Varied for the Cases of Hot Spheres in Water[+]

Variables \ Case Number	1	2	3	4	5	6	7	8	9	10	11	12	13
Sphere Material	Sn	Sn	Sn	Sn	Sn	Sn	Sn	AgCl	Sn	Sn	Sn	Sn	Sn
Initial Sphere Temperature, °C	500	500	500	400	700	700	700	700	700	700	700	500	500
Water Pool Temperature, °C	20	50	80	20	20	20	20	20	20	20	20	20	80
Sphere Radius, cm	0.3	0.3	0.3	0.3	0.3	0.3	0.3	0.3	0.1	1.0	0.3	0.3	0.3
Initial Film Thickness, cm	10^{-5}	10^{-5}	10^{-5}	10^{-5}	10^{-5}	10^{-4}	10^{-6}	10^{-5}	10^{-5}	10^{-5}	10^{-5}	10^{-5}	10^{-5}
Coolant Compressibility I = incompressible C = compressible	I	I	I	I	I	I	I	I	I	I	C	C	C

[+]For all cases the initial film pressure and the ambient pressure are taken to be 1 atm.

contact is achieved. The cycle of growth and partial collapse is repeated several times with decreasing amplitude of the pressure fluctuations. The amplitude and frequency of the film pressure during the oscillatory growth depend on the conditions of interaction, as discussed in the following paragraphs.

A. Effect of Water Temperature

The time history of the pressure in the vapor film for cases 1, 2 and 3 are shown in Figure 4.3. It is clear that in spite of the initially larger pressure pulse, the oscillatory behavior of the pressure is damped quickly when the water subcooling is small. The reason for the damped oscillations at lower subcooling is the more rapid vaporization obtained, which tends to prevent the pressure in the film from reaching low subatmospheric values. The energy consumed in vaporization and the growth history of the vapor film are shown for cases 1, 2 and 3 in Figure 4.4 and Figure 4.5 respectively. The trend of increased frequency of the growing film as water subcooling is increased is similar to the experimentally observed trend of oscillations of the vapor film reported by Board et al[90].

The rates of heat transfer from the hot sphere for cases 1, 2 and 3 are shown in Figure 4.6. When the heat transfer rate (Fig. 4.6) is compared with the energy consumed in vaporization (Fig. 4.4) it is seen that only a small fraction of the transferred heat is consumed in

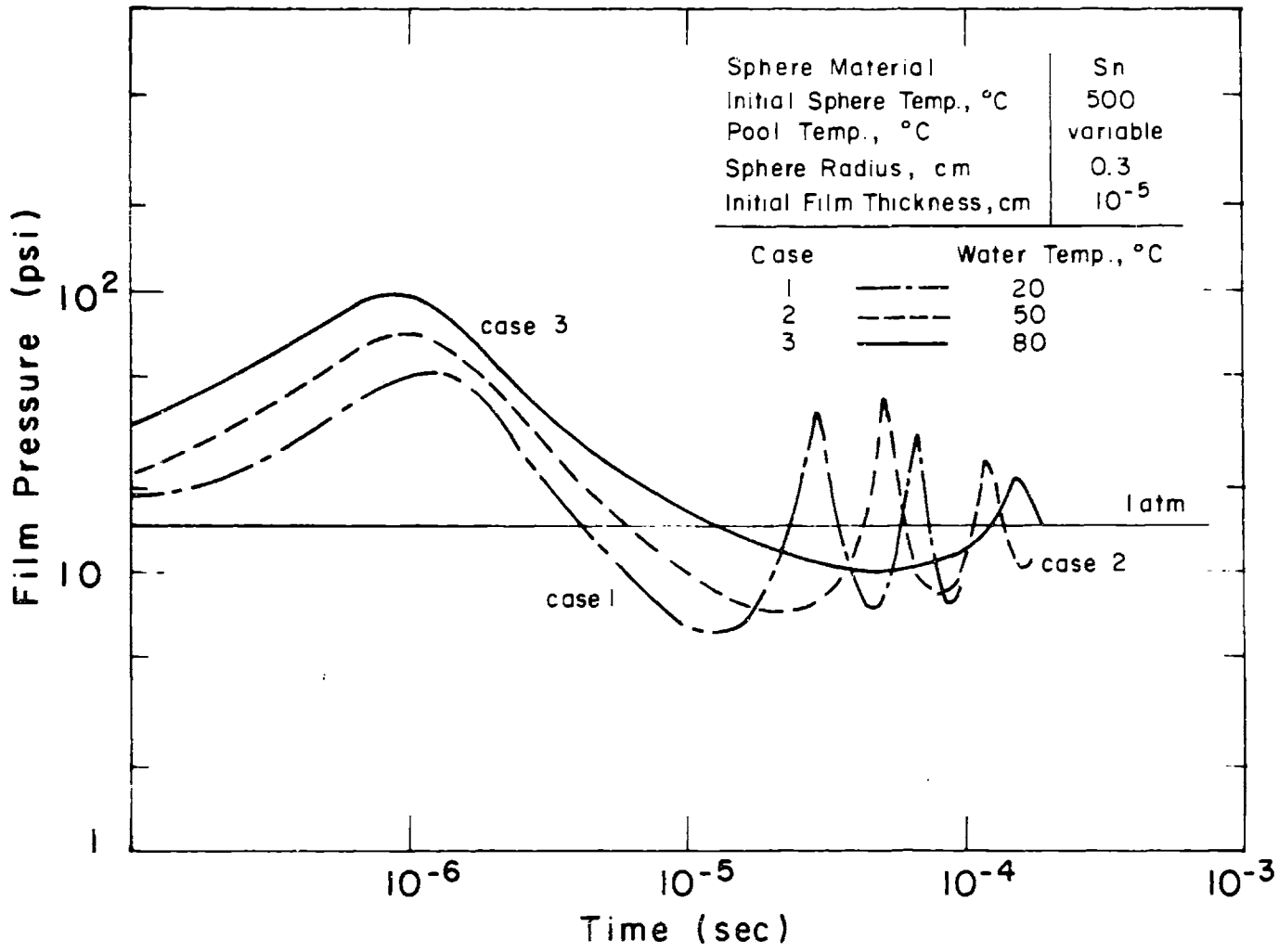

Fig. 4.3 Effect of Water Pool Temperature on the Pressure-Time History of the Growing Film

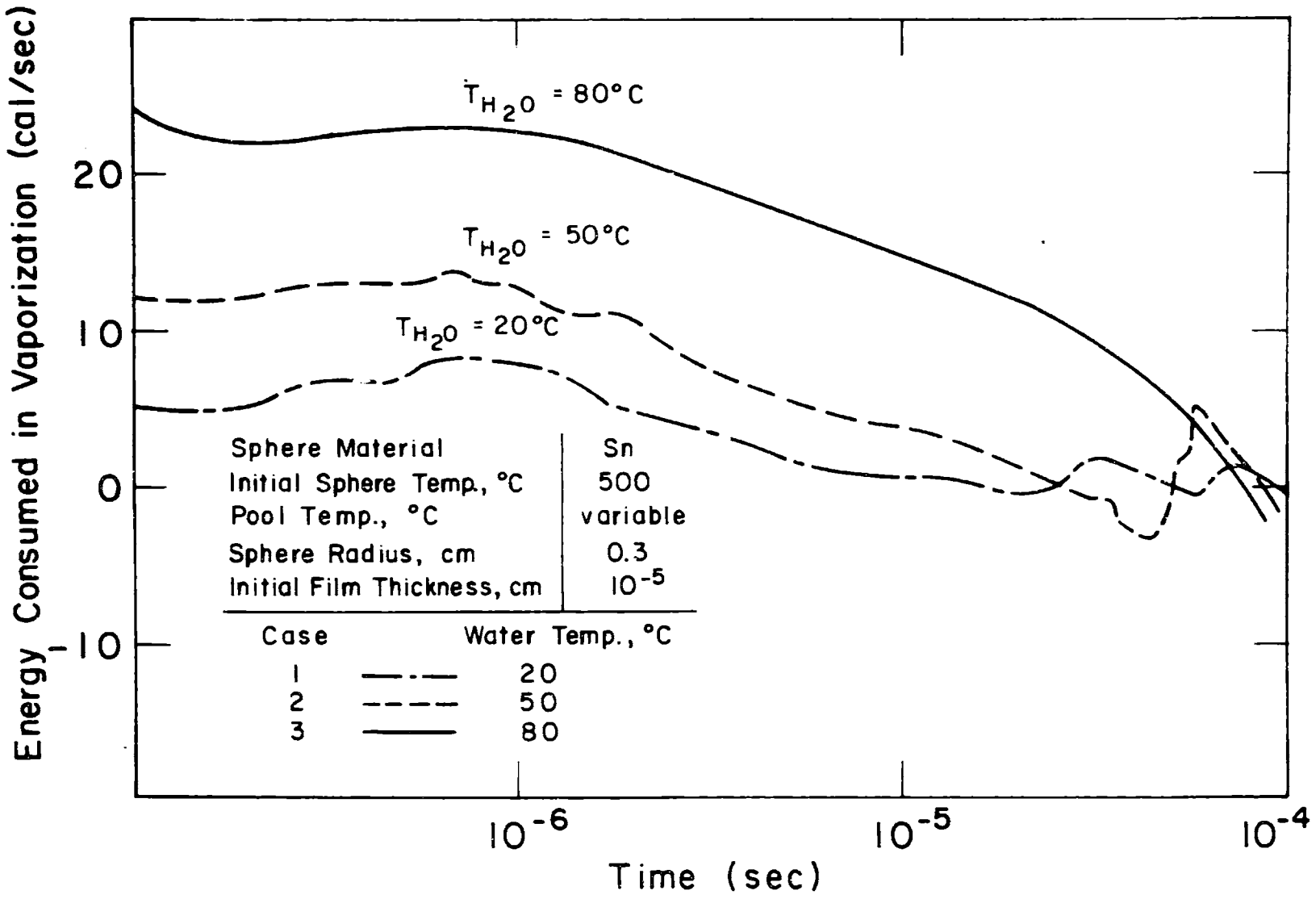

Fig. 4.4 Effect of Water Pool Temperature on Vaporization Rate

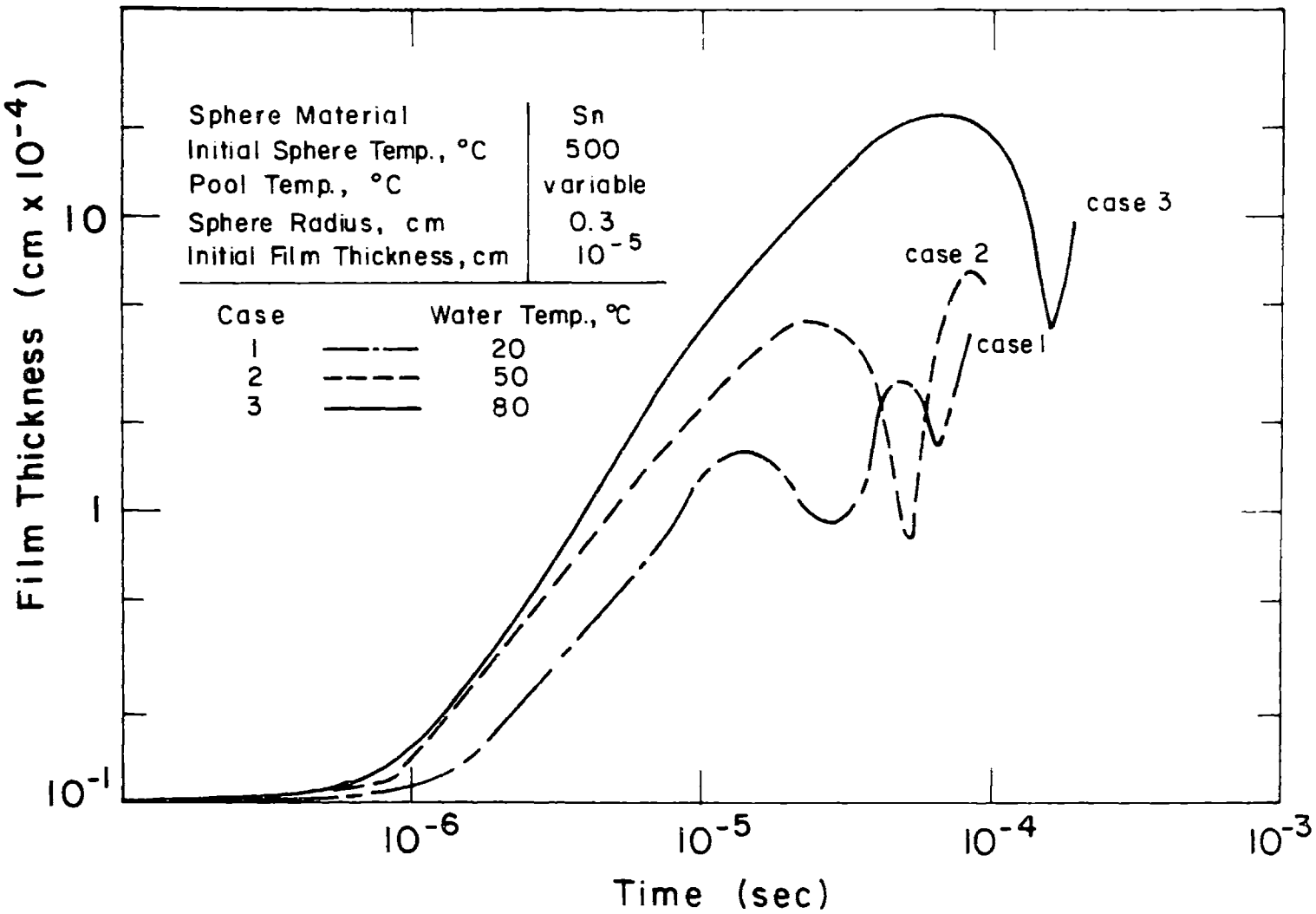

Fig. 4.5 History of Vapor Film Growth

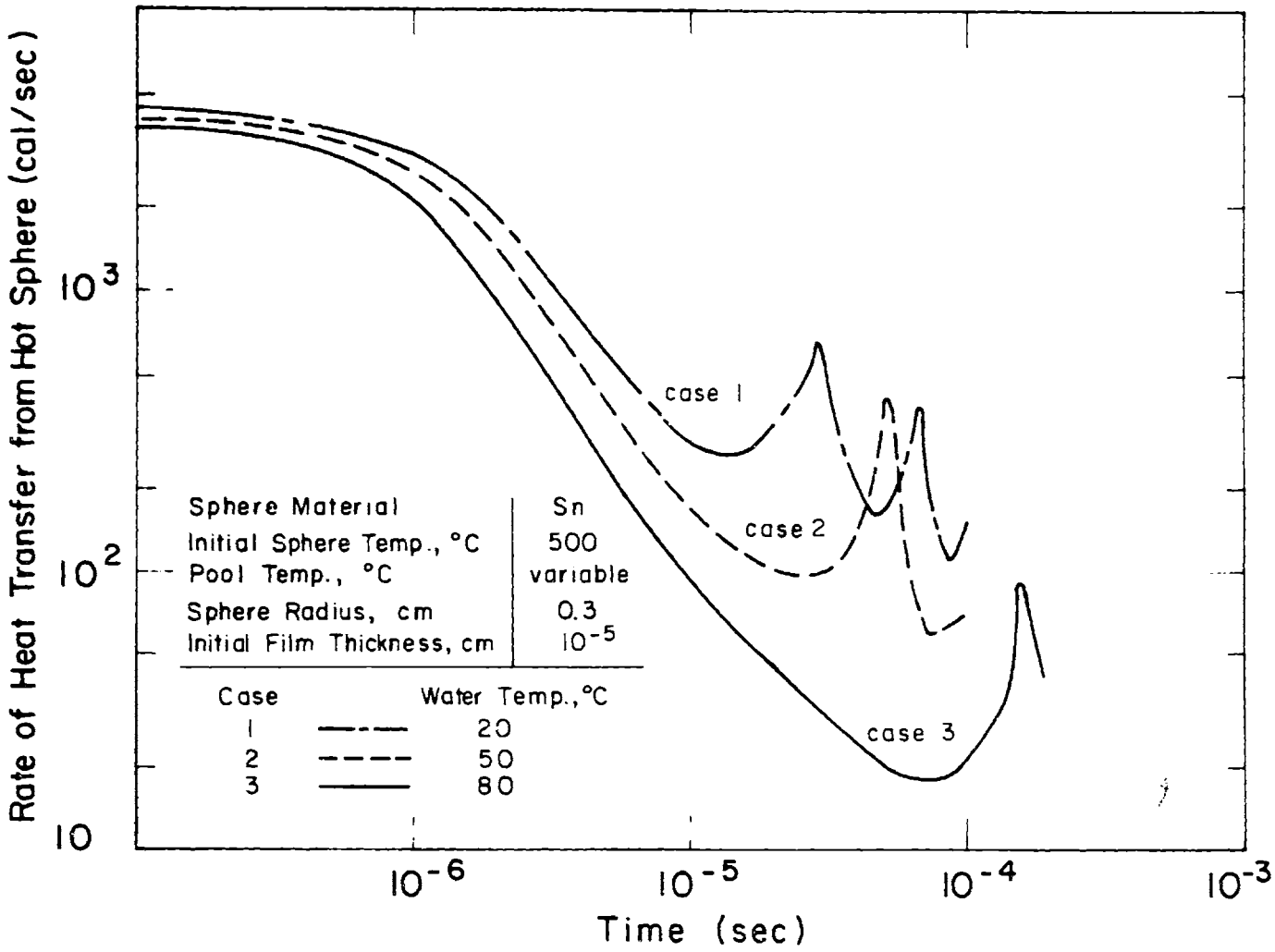

Fig. 4.6 Effect of Water Pool Temperature on the Rate of Heat Transfer from Hot Sphere

vaporization. The larger the water subcooling the smaller is the fraction consumed in vaporization. The system eventually approaches a near-zero vaporization rate. Transient film boiling around spheres with no net vaporization has been observed by Jacobson and Shair[87] and Stevens et al.[47] for water subcoolings of 90°C to 50°C.

B. Effect of Hot Sphere Temperature

The pressure time histories for the vapor film in cases 1, 4 and 5 are shown up to 0.1 msec in Fig. 4.7. In Fig. 4.8 the envelopes of the pressure oscillations between 0.1 msec and 1.0 msec for these cases (1, 4 and 5) are shown. As the tin temperature is increased, the pressure oscillations have larger amplitudes initially, but their frequency is decreased. The pressure oscillations are damped faster for the sphere of initial temperature of 700°C, as shown in Fig. 4.8. The present model neglects the effects of convection in both the water pool and the vapor film. It also neglects the bouyancy effects. These two effects become more important at larger times and hence the model cannot predict the eventual stability of the film. Henry's correlation for stable film boiling (see Appendix G) predicts eventual stable film boiling for tin at 700°C, (in water at 20°C) but not for tin at 400°C or 500°C.

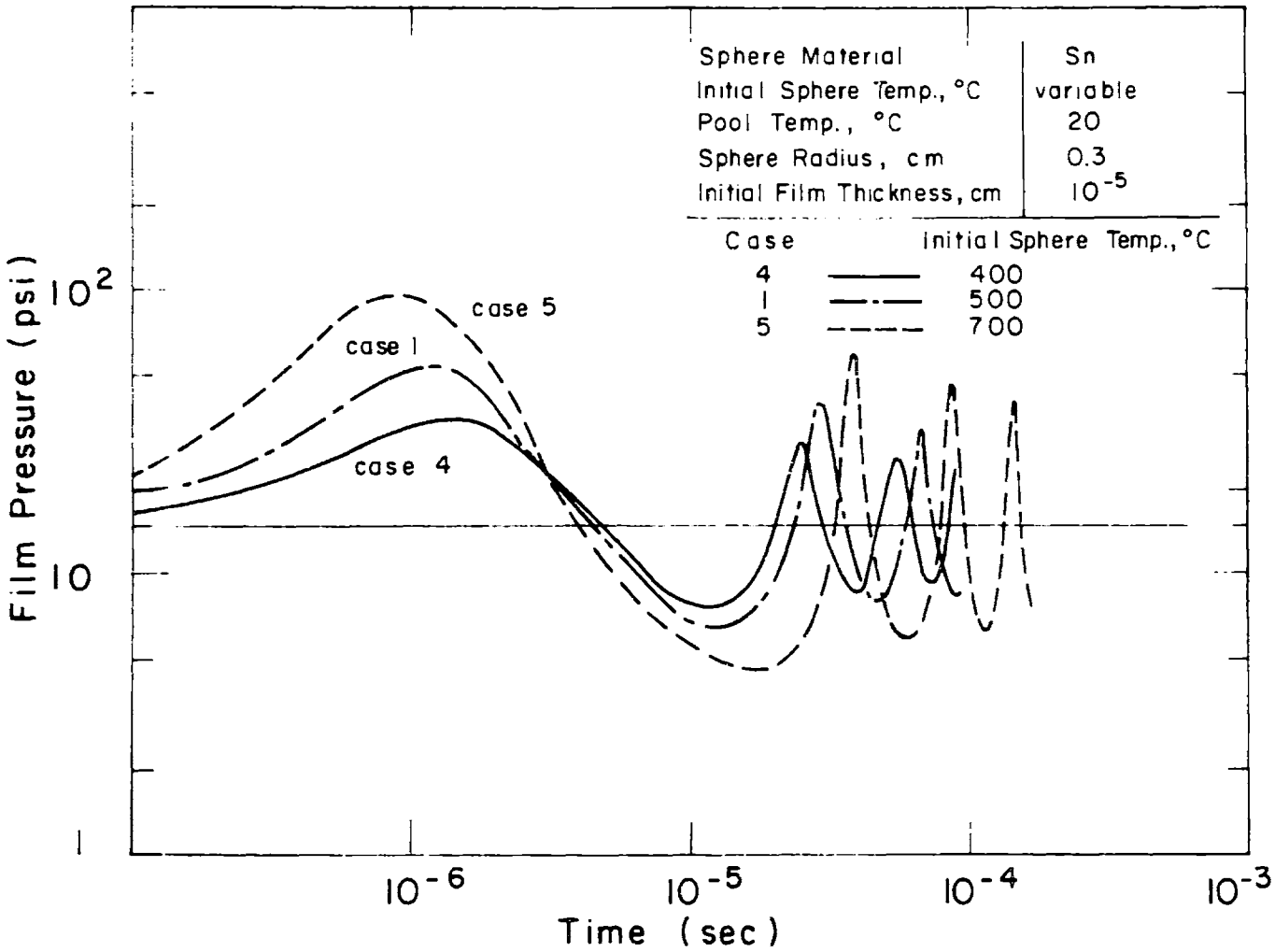

Fig. 4.7 Effect of Initial Temperature of the Sphere on Pressure-Time History

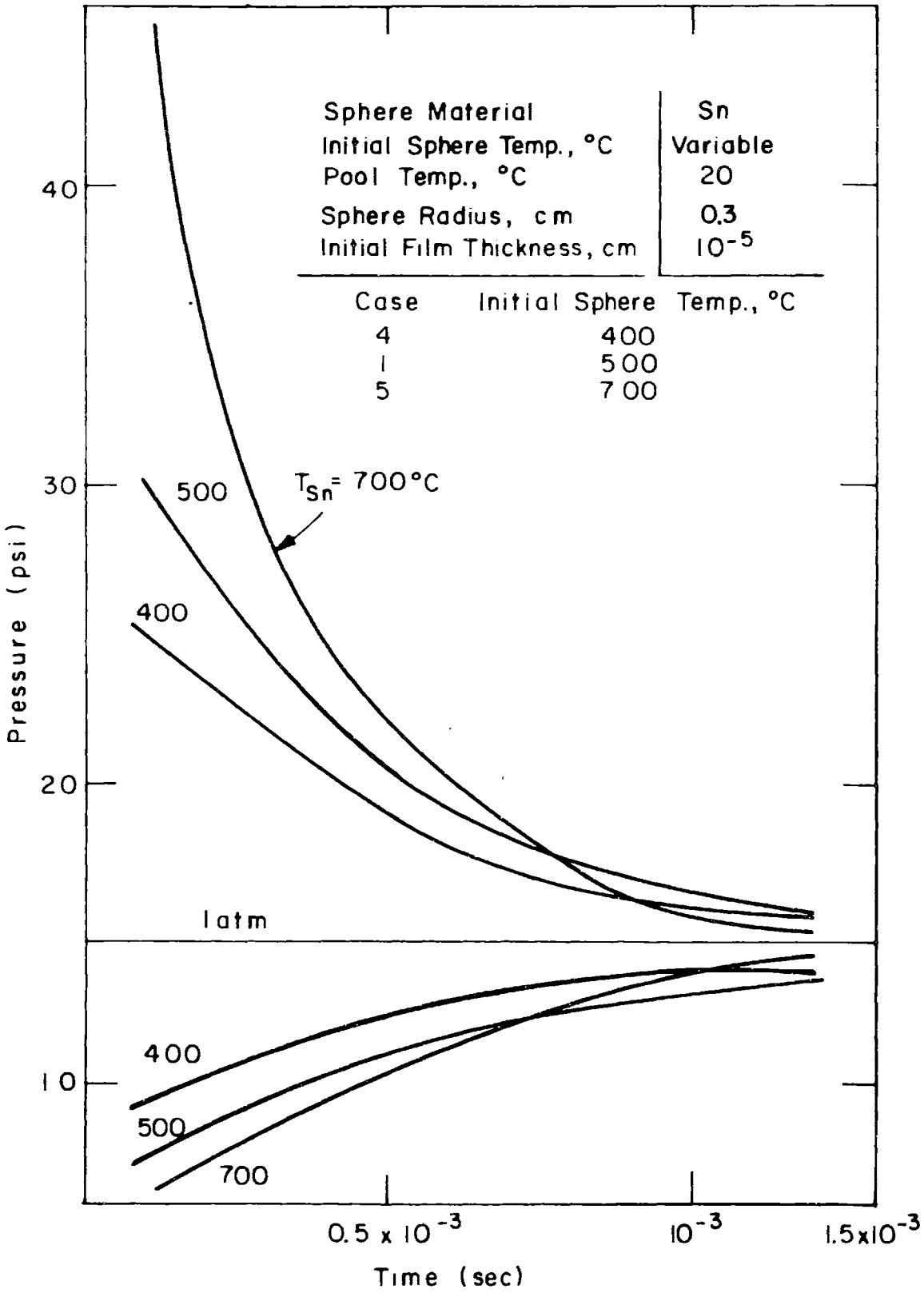

Fig. 4.8 Effect of Sphere Temperature on Envelope of Pressure Oscillations

C. Effect of Initial Gas Film Thickness

Figure 4.9 shows the pressure time history in a film growing around a tin sphere at 700°C immersed in water at 20°C, assuming the initial gaseous film around the sphere has a thickness of 10^{-6}cm, 10^{-5}cm and 10^{-4}cm (case 5, 6 and 7). The influence of the initial thickness on the pressure history is very significant. If a relatively large amount of gas was swept with the drop into the liquid, the initial boiling around the sphere would be "quiet", since the large gaseous film retards the fast transfer of heat to the liquid coolant which causes the initial pressurization event.

D. Effect of the Sphere Material

Calculations have been performed for the case of an AgCl sphere at 700°C (Case 8). AgCl has been used in dropping experiments at ANL[39]. The thermal diffusivity of AgCl is 0.0055 cm^2/sec while that of Sn is 0.17 cm^2/sec. The ρkc value of AgCl is also much lower than that of Sn (.001 vs .033 in cal^2/cm^4 sec deg^4). The results of the calculations were nearly identical to those of a Sn sphere in water under the same conditions (Case 5). This strongly suggests that the heat transfer rate for such cases is determined by the water side. Further discussion of this observation will be given in Section 4.4 of this chapter.

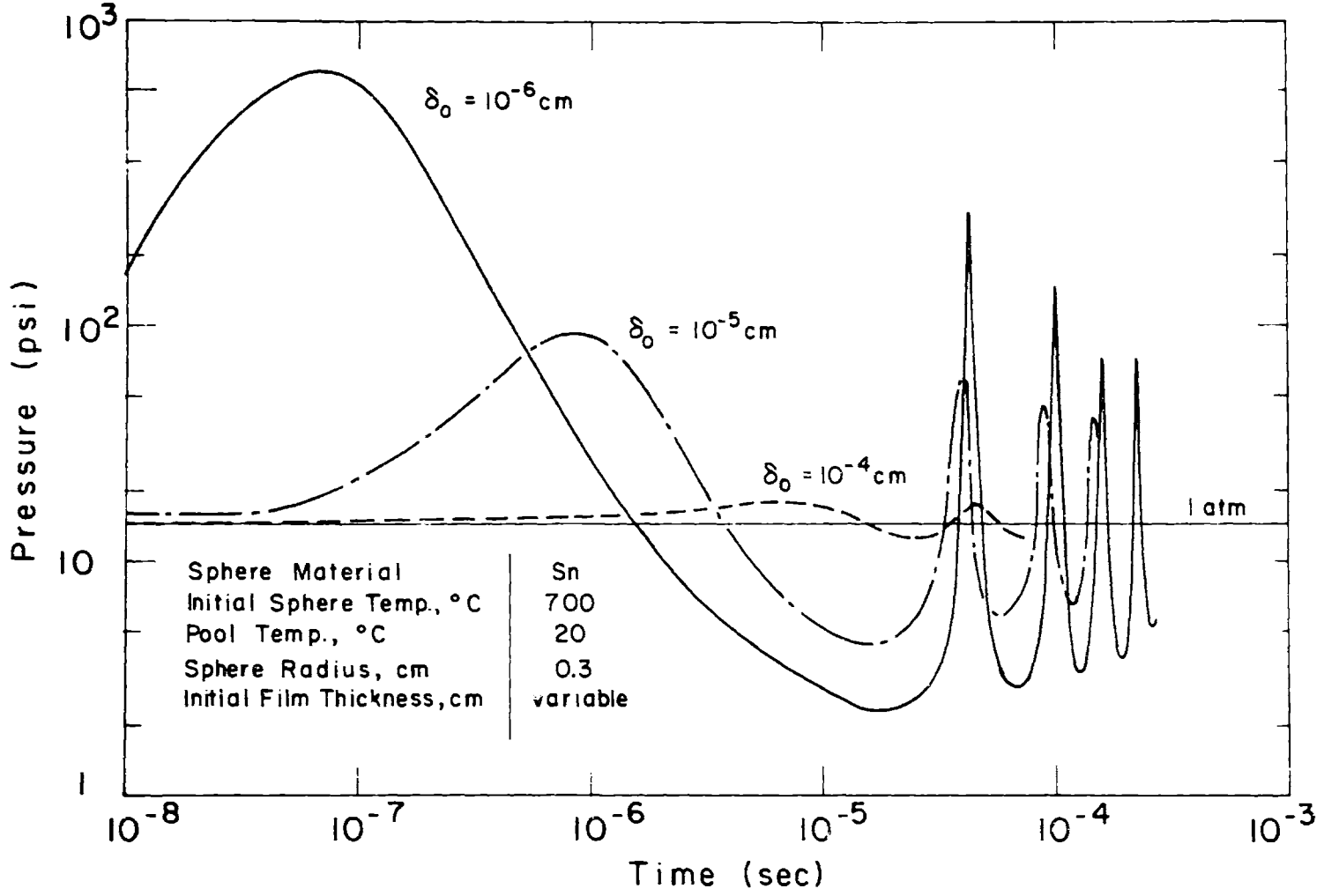

Fig. 4.9 Effect of Initial Gas Film Thickness, δ_0 on Pressure – Time History

E. Effect of the Sphere Radius

The results for cases 8, 9 and 10 are shown in Fig. 4.10. In these calculations the radius of the sphere is the only varied parameter. The radius is varied between 0.1 cm and 1.0 cm to cover the range of particle radii used in dropping experiments at ANL[39,12] and G.C.E.B (U.K.)[48]. The results indicate that the amplitude of pressure pulsations is enhanced by the increase in the sphere radius, however the frequency of the oscillation is retarded. Board et al.[90] have reported an increase in the frequency of the oscillating film with the decrease of the total heated area in experiments of rapid laser heating of a nickel foil in water. The theoretical trend of frequency change with the heating area agrees with their results.

F. Effect of Liquid Compressibility

In cases 1 to 8 the water has been considered incompressible. In Fig. 4.11 a comparison is shown between the pressure histories predicted for case 8 and case 11, for which all the initial conditions are identical. In case 11 the water is considered to be compressible. It is clear from Fig. 4.11 that the treatment of water as compressible leads to a significant reduction in the pressure pulse amplitudes, and a faster stabilization of the film pressure. As seen in Fig. 4.12 and Fig. 4.13 the trends of the pressure time history with the change

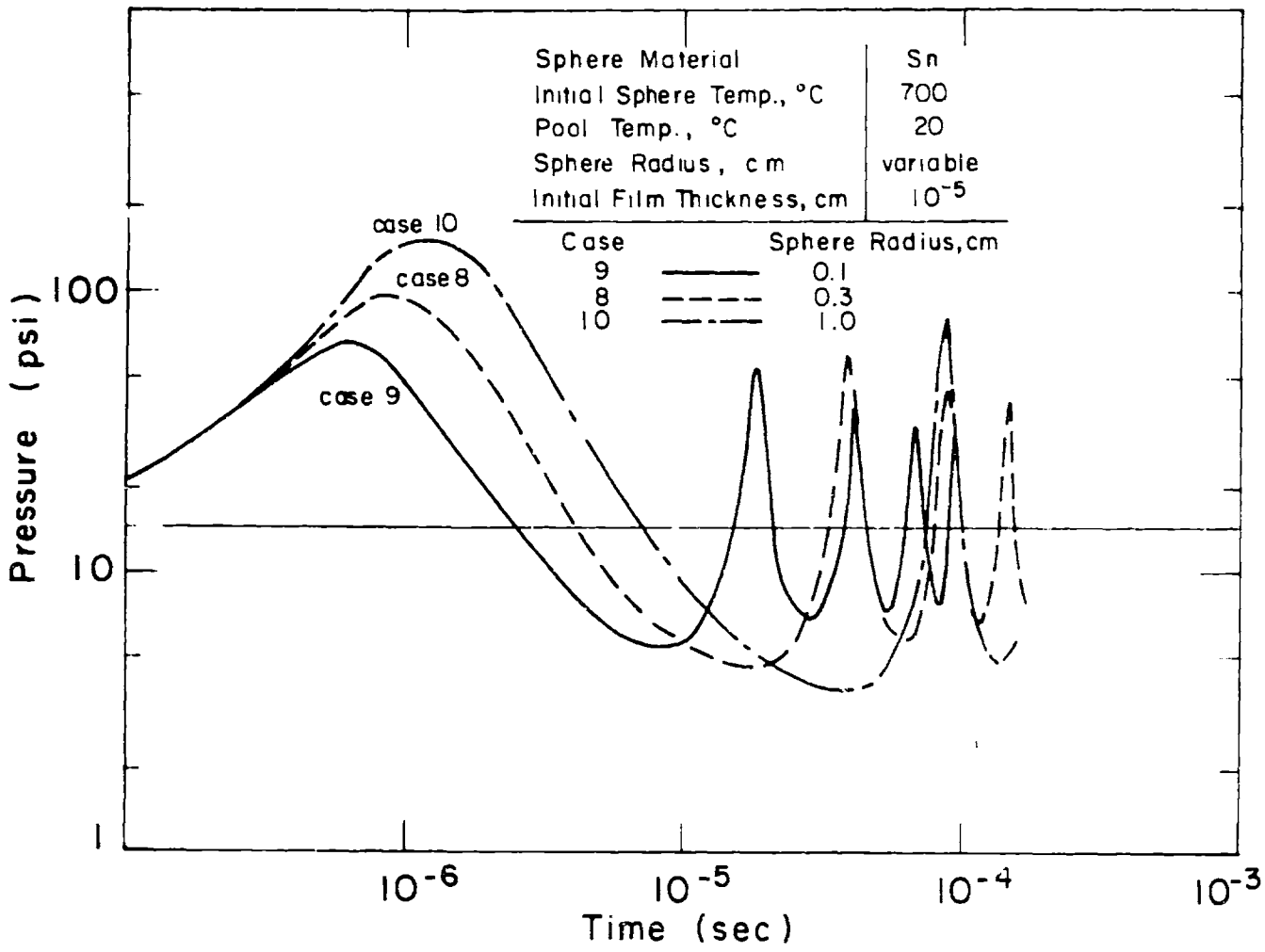

Fig. 4.10 Effect of Sphere Radius on Pressure – Time History

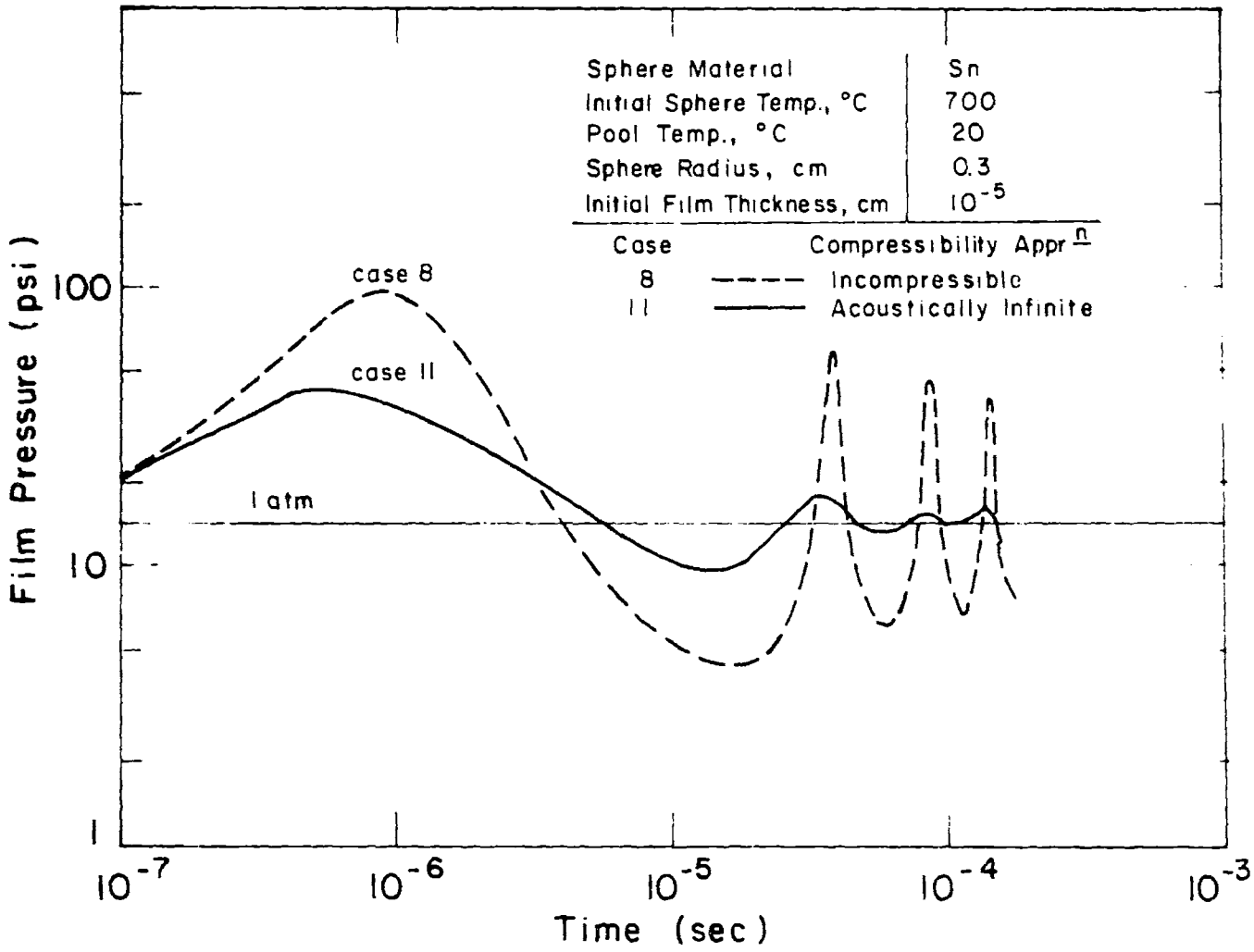

Fig. 4.11 Effect of the Liquid Compressibility on Pressure - Time History

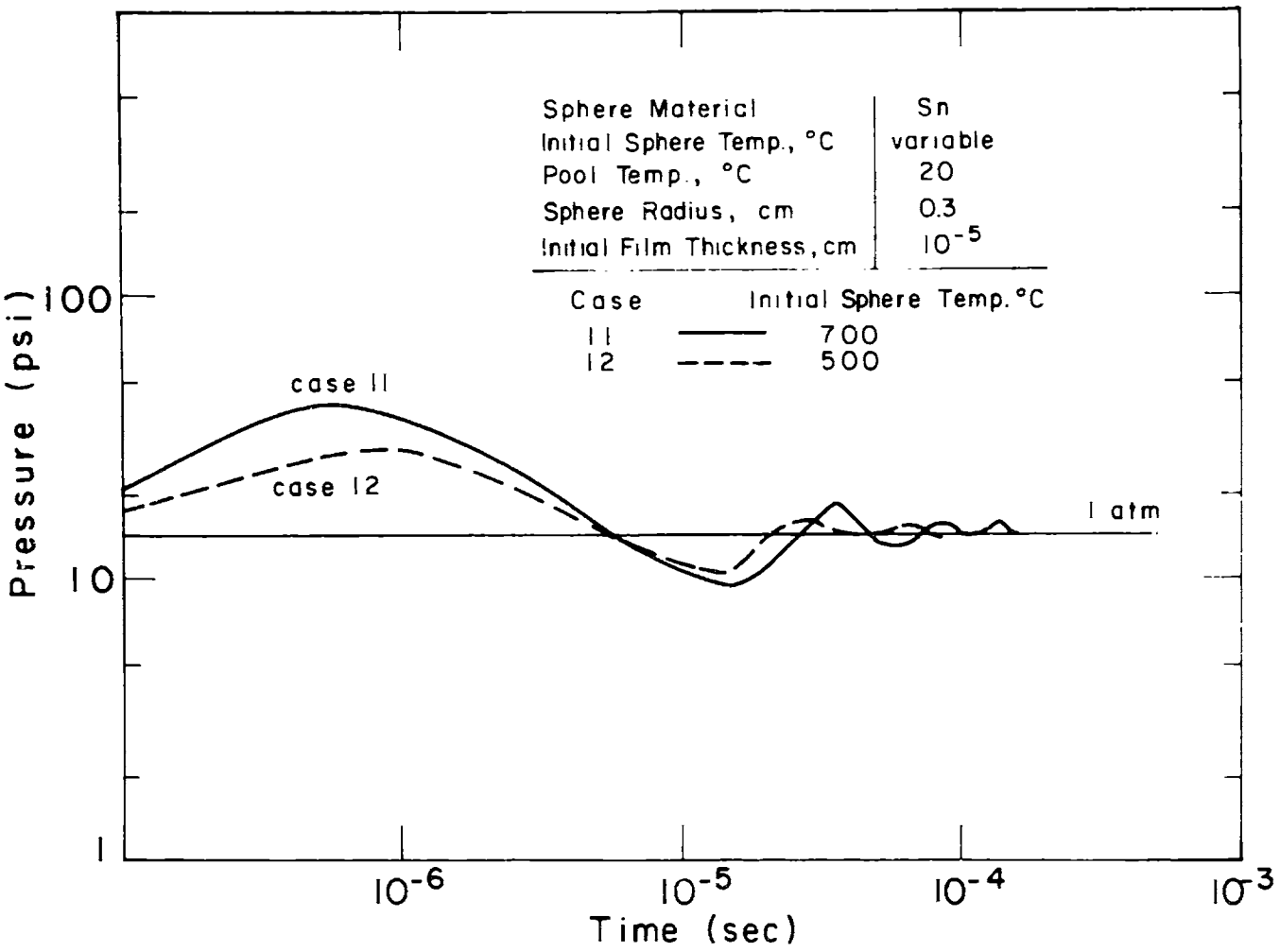

Fig. 4.12 Effect of the Sphere Initial Temperature on Pressure-Time History Using the Acoustic Approximation

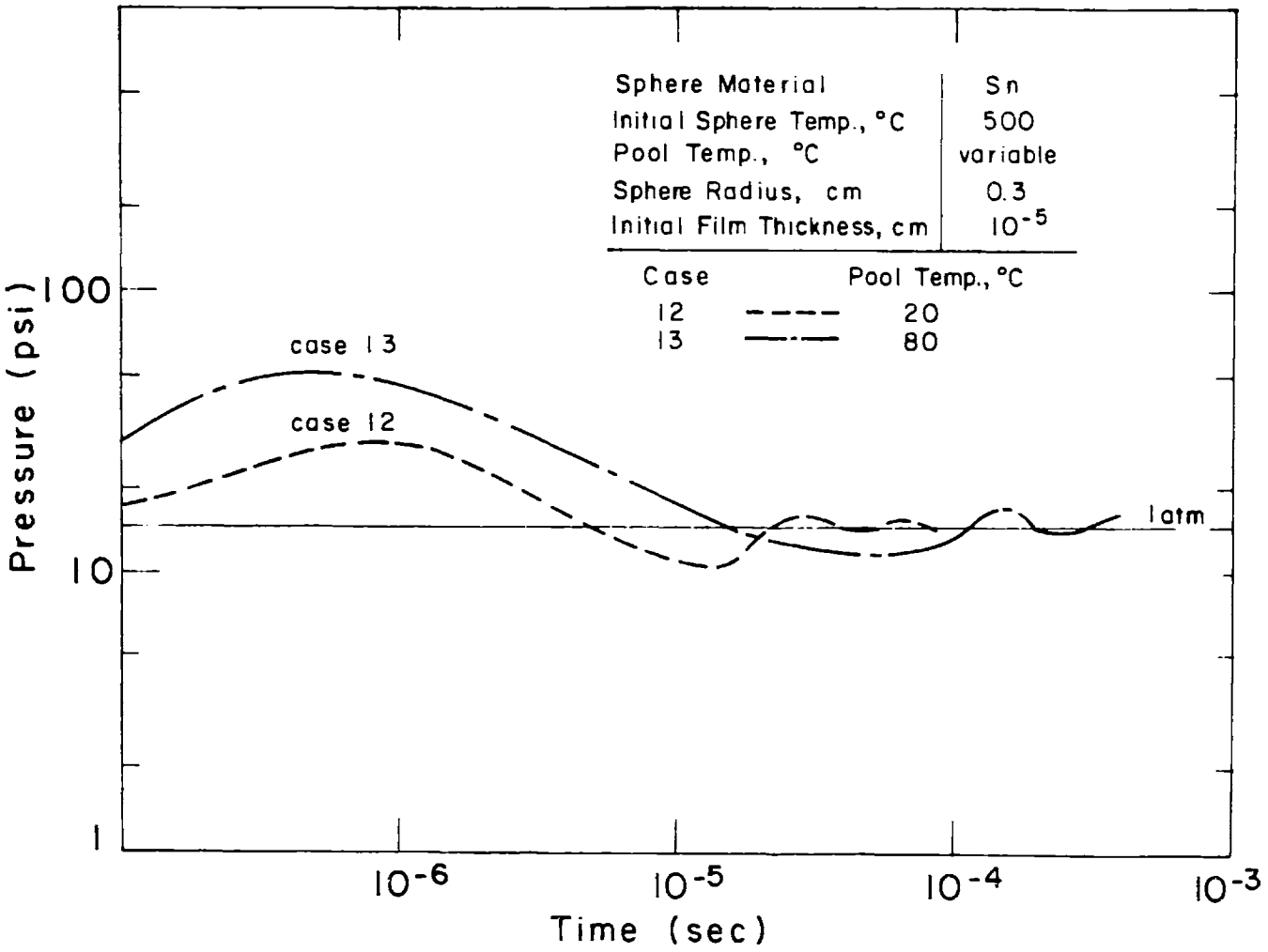

Fig. 4.13 Effect of the Water Pool Temperature on the Pressure–Time History Using the Acoustic Approximation

in the initial sphere temperature and the water temperature when the compressibility of water is included are similar to the cases where the water was considered incompressible. Because of the Kirkwood-Bethe assumption employed in the treatment of compressibility (see Section 4.2.3), the results of the compressible water treatment may be invalidated by the presence of reflected pressure waves in the liquid. For example, for a reflecting surface at a 3 cm distance from the sphere surface the Kirkwood-Bethe assumption would be invalidated in $\sim 2 \times 10^{-5}$ seconds.

4.4 Application of the Model to Hot Spheres in Sodium

The model has also been applied to hot stainless steel and UO_2 spheres in liquid sodium. The initial temperatures of the spheres and the liquid sodium have been chosen from the range over which dropping experiments have been reported in literature[12,13,35]. The sphere radius and the initial thickness of the gaseous film have been kept constant in this study, since the effect of their variation is expected to be similar to that studied in the water cases. The sphere radius is chosen to approximate the radii of particles used in ANL dropping experiments[35]. The initial film thickness is chosen arbirtarily as 5×10^{-6} for lack of experimental data on the gas films that is swept with the molten particles in dropping experiments. The values of the parameters

Table 4.3

Values of Parameters Varied for the Cases of Hot Spheres in Sodium[†]

Variable \ Case Number	14	15	16	17	18	19	20	21
Sphere Material	SS	SS	SS	SS	UO_2	UO_2	UO_2	UO_2
Initial Sphere Temperature, °C	2200	2200	2200	2200	3200	3200	3200	2200
Sodium Pool Temperature, °C	850	800	600	250	850	800	600	800

[†]For all cases the sphere radius is 0.35 cm, the initial gas film thickness is 5×10^{-6} cm; the initial film pressure and ambient pressure are at 1 atm, and the liquid sodium is considered incompressible.

in the cases considered are summarized in Table 4.3.

The results for the cases indicate the growth of the vapor film will also follow an oscillatory pattern. The amplitude and frequency of oscillation depend on the conditions of the case as discussed in the following:

A. Effect of Sodium Temperature

The pressure time histories for cases 14 through 17 are shown in Fig. 4.14. The first pressure pulse is seen to be higher for smaller sodium subcooling, because of the larger initial pressurization rate. However, the amplitude of the pressure oscillations following the initial pressure rise exhibit a maximum for an intermediate sodium subcooling. In other words, starting at near-saturated sodium (i.e. case 14), as the subcooling is increased the amplitude of the pressure fluctuations is enhanced initially. Further subcooling, however, leads to smaller amplitude of fluctuations. Farahat[89] has reported that the largest pressure pulse recorded in his experiments during transition boiling showed a maximum for sodium at about 715°C. He suggested an explanation which applies for the present case also. In the case of small sodium subcooling, as in case 14, the availability of a large volume for the present vapor (see Fig. 4.15) prevents large pressurization of the vapor due to the partial film collapse. At the other end, i.e. for large sodium sub-

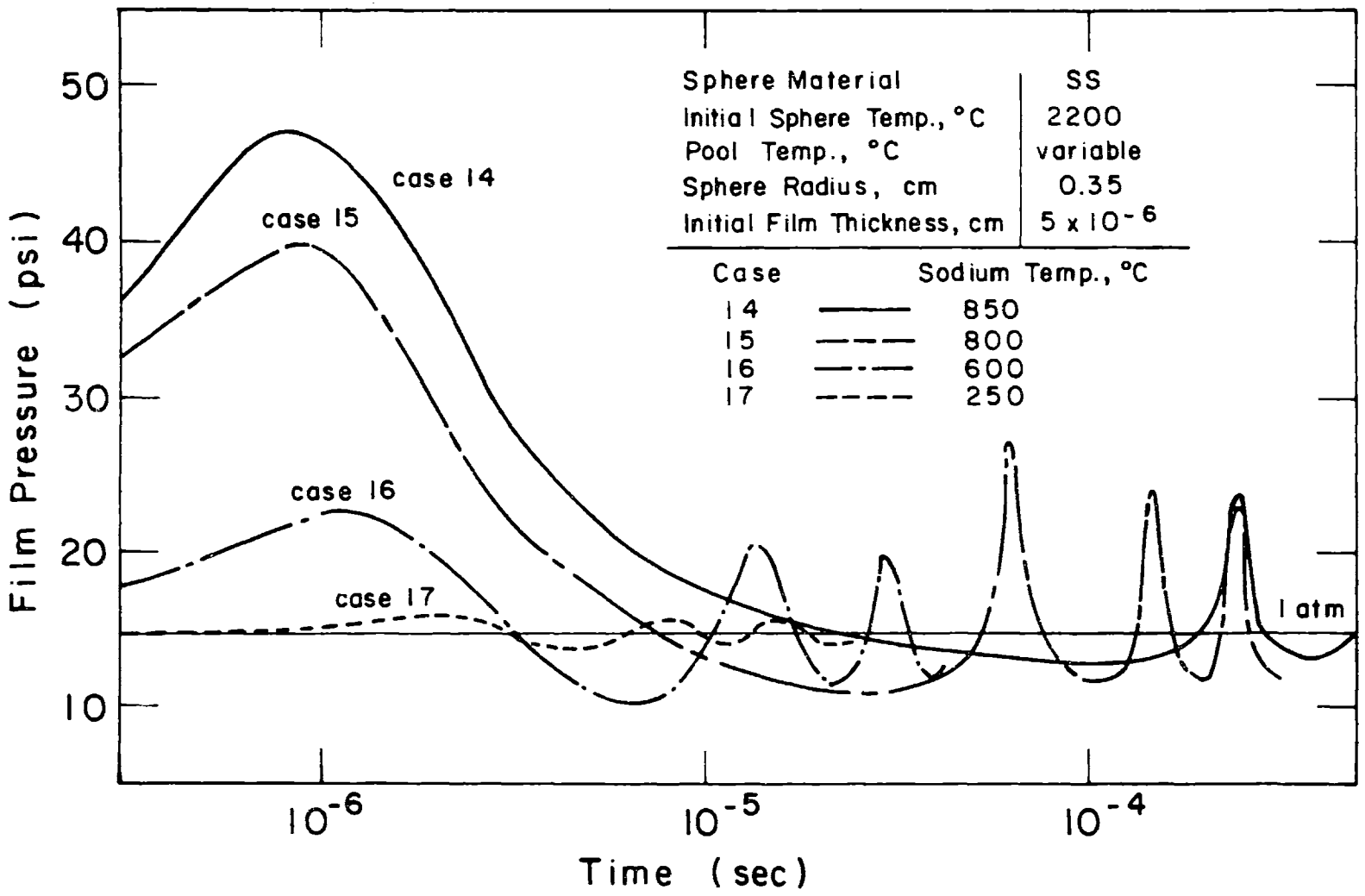

Fig. 4.14 Effect of Sodium Pool Temperature on the Pressure - Time History of the Film Growing at a Stainless Steel Sphere

cooling as in case 18, the ability of liquid sodium to absorb the heat of condensation is higher. Thus the faster vapor condensation rate during the collapse prevents the development of large pressurization. The trend of enhancement of the amplitude of the pressure pulses for an intermediate subcooling range is different from the water cases, where the pulses increased in amplitude with water subcooling, without a reversal at low subcoolings.

In Figure 4.15, the history of vapor film growth for cases 14 through 16 is shown. The film thickness for case 17 remained less than 10^{-5}cm for the time period of 2.5×10^{-5} sec for which the calculation was performed, and, therefore, lie outside the scale of Fig. 4.15. The rate of heat transfer from the sphere for cases 14 through 17 is shown in Fig. 4.16. The rate of heat transfer is seen to be more rapidly decreasing for lower sodium subcoolings because of the faster growth of the film. In Fig. 4.17, the rate of heat consumption in evaporation is shown for cases 14 through 16. Comparison of the total heat transfer rate from the sphere (Fig. 4.16) and the rate of heat consumption in evaporation (Fig. 4.17) indicate that the heat consumed in evaporation is a small fraction of the total heat transfer rate from the sphere.

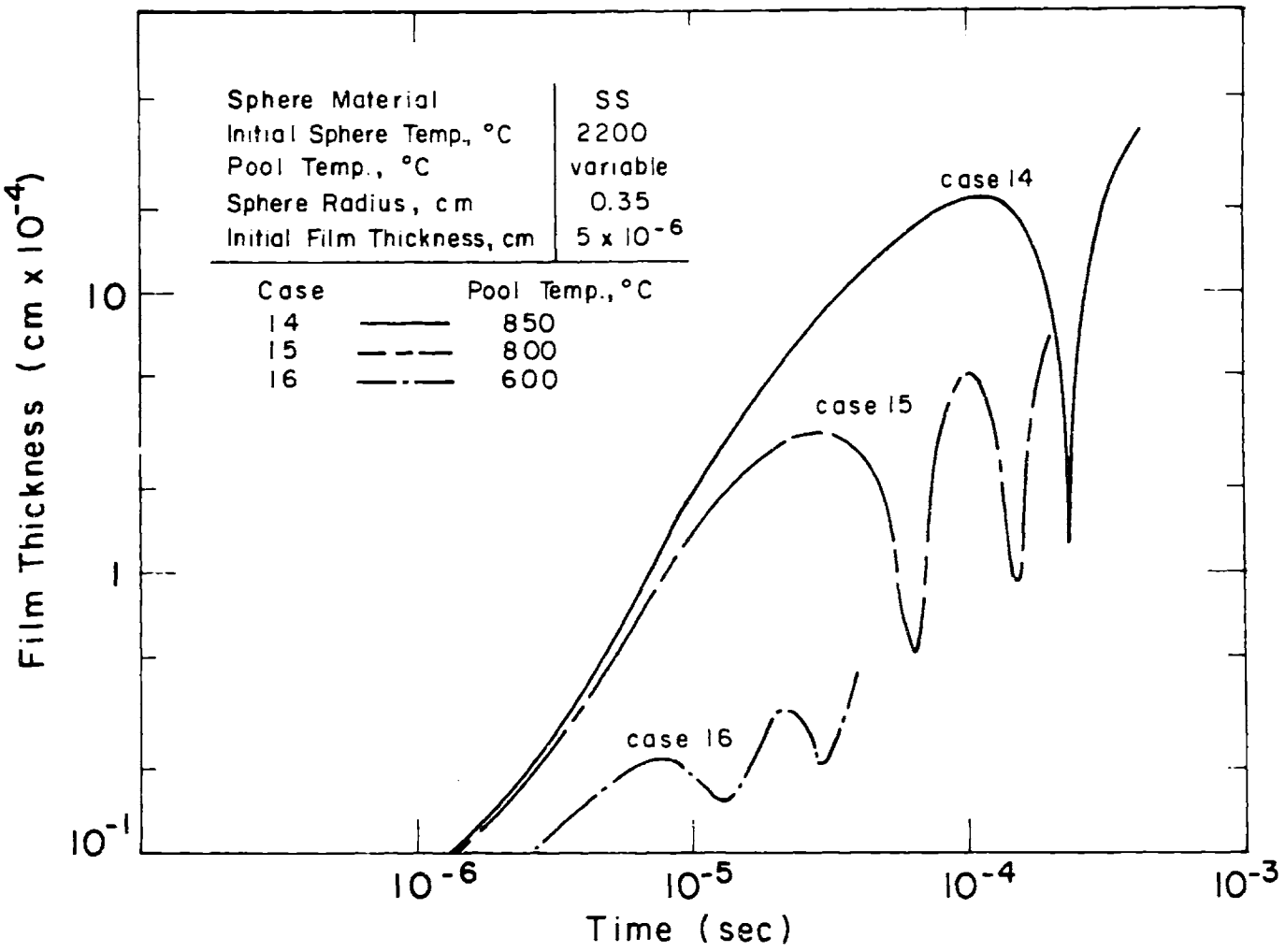

Fig. 4.15 History of Vapor Film Growth

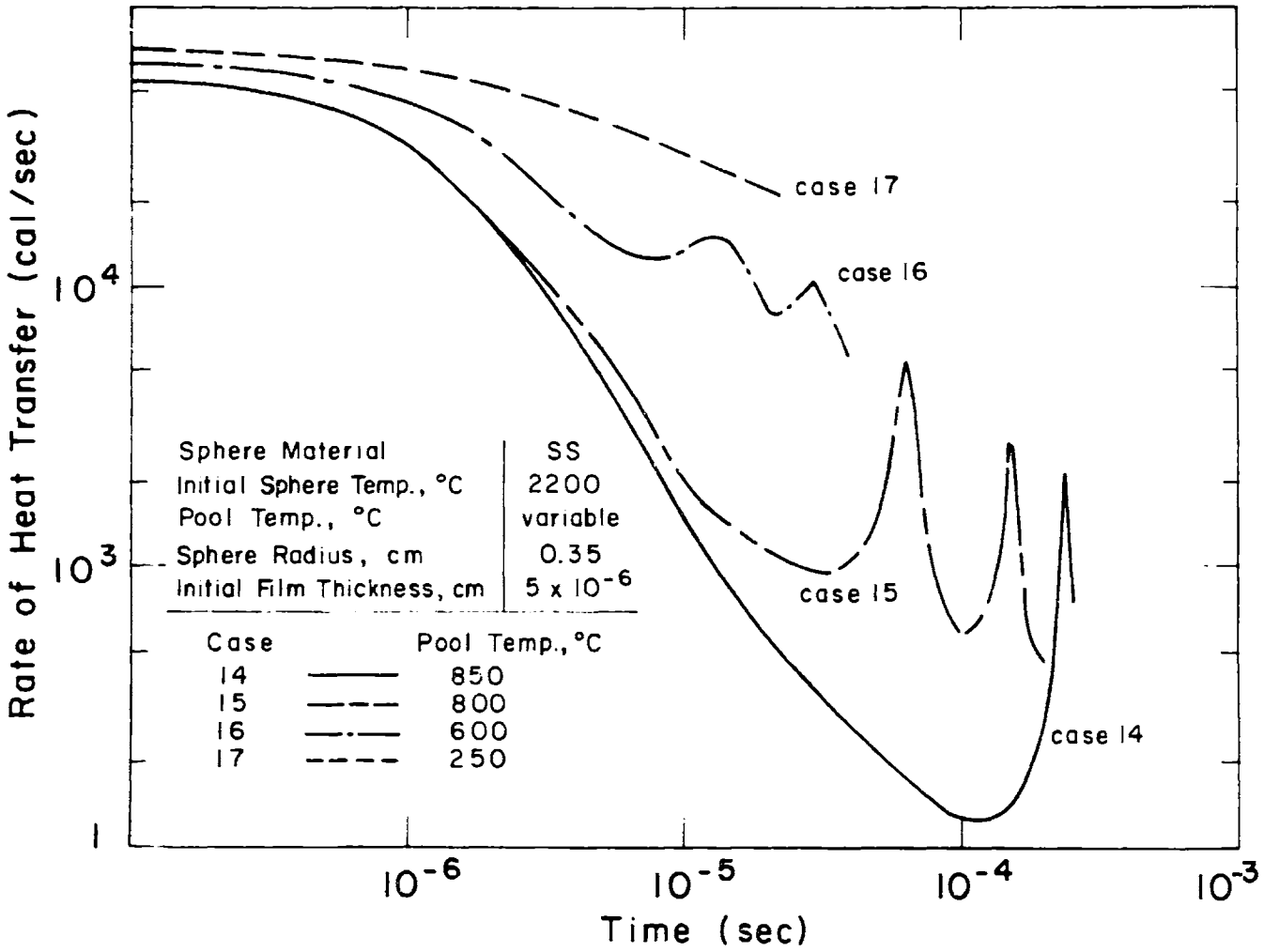

Fig. 4.16 Effect of Sodium Pool Temperature on Rate of Heat Transfer from the Hot Sphere

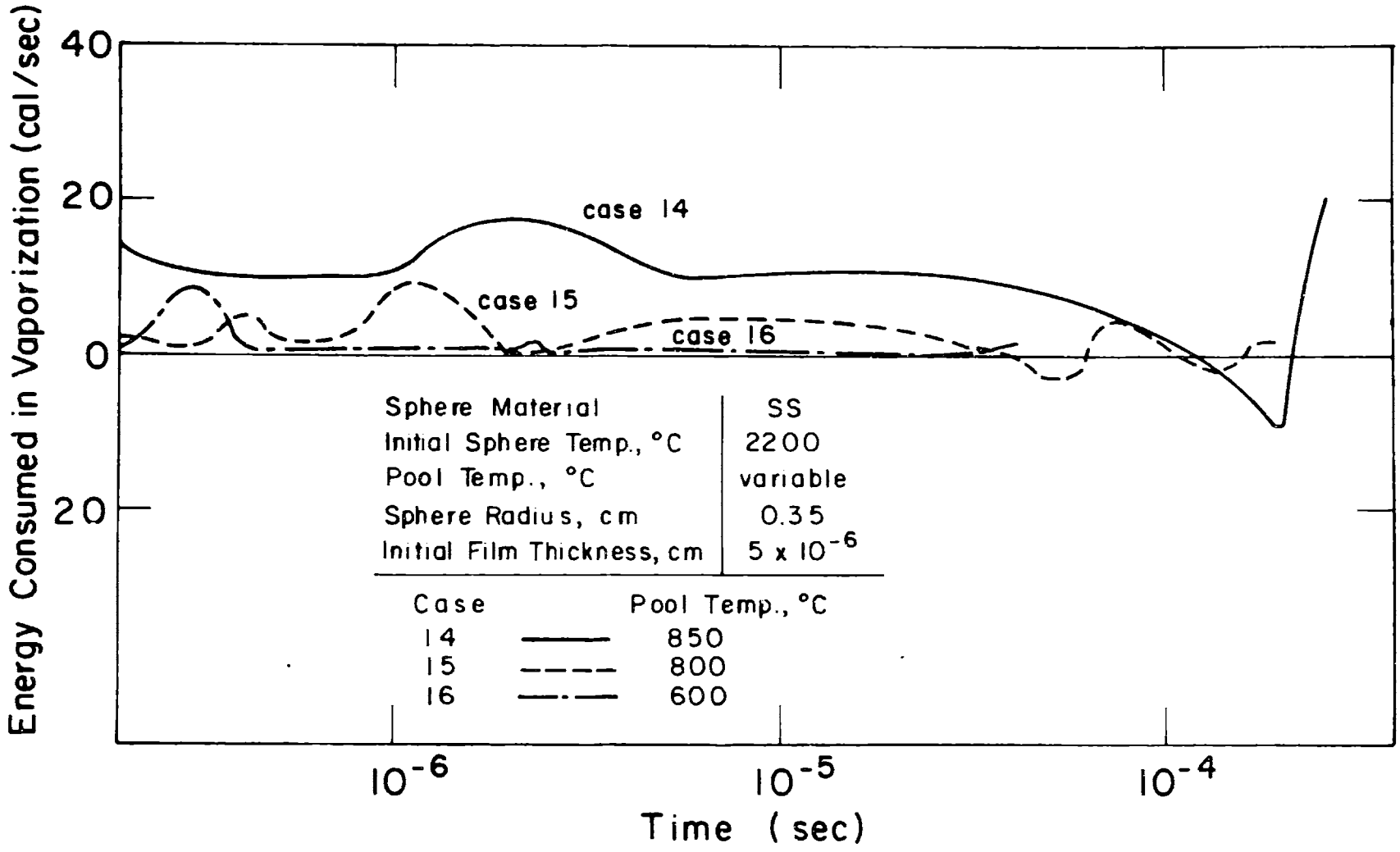

Fig. 4.17 Effect of Sodium Pool Temperature on Rate of Vaporization

The effect of sodium pool temperature on the pressure history of a film growing around a UO_2 sphere in sodium is shown in Fig. 4.18. The results indicate the pressure pulses produced when the sodium temperature is at 800°C are larger than those for sodium at either 850°C and 600°C, as observed for stainless steel in Fig. 4.14.

B. Effect of Hot Sphere Temperature

The effect of the initial hot sphere temperature on the pressure time history for a vapor film growing in sodium is obtained by comparing the results for cases 18 and 21. In Fig. 4.19 the pressure time history for both cases is shown. It is seen that as the sphere initial temperature is increased, the amplitude of the pressure pulses is increased but the frequency is decreased. This trend is similar to the trend observed for the cases of water (Fig. 4.7).

C. Effect of Sphere Material

The pressure time histories for the film in cases 14 and 21 are plotted in Fig. 4.20. All the parameters in these two cases are identical except for the sphere material. The results indicate that the sphere material has some influence on the pressure history, which was not observed for the water cases. The stainless steel sphere (thermal diffusivity of 0.038 cm^2/sec) encounters higher pressure pulses than the UO_2 sphere (thermal

diffusivity of 0.005 cm^2/sec). The effect of the material properties of the sphere is apparently more important for a film growing in sodium than in water.

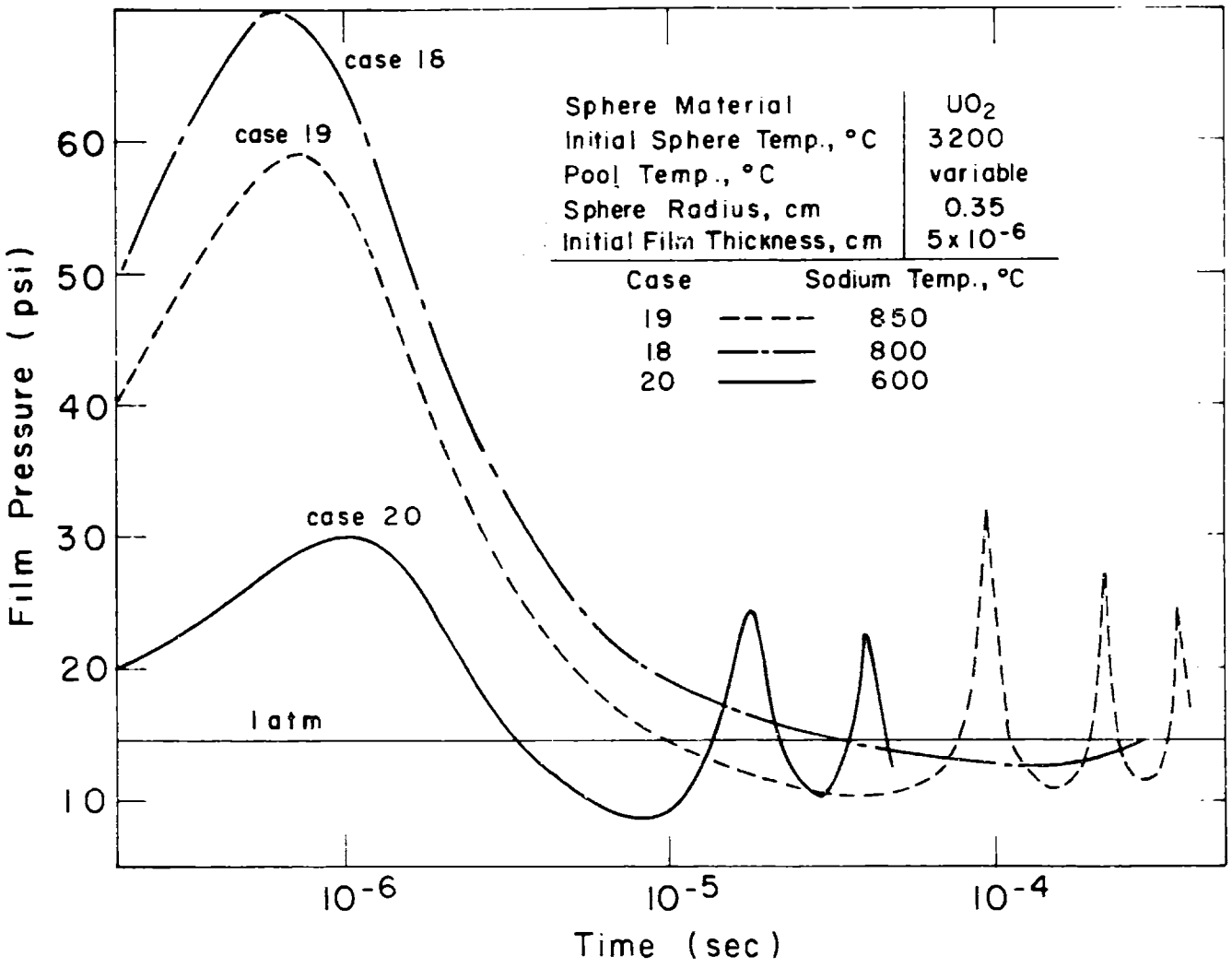

Fig. 4.18 Effect of Sodium Pool Temperature on the Pressure - Time History of a Film Growing at a Uo_2 Sphere

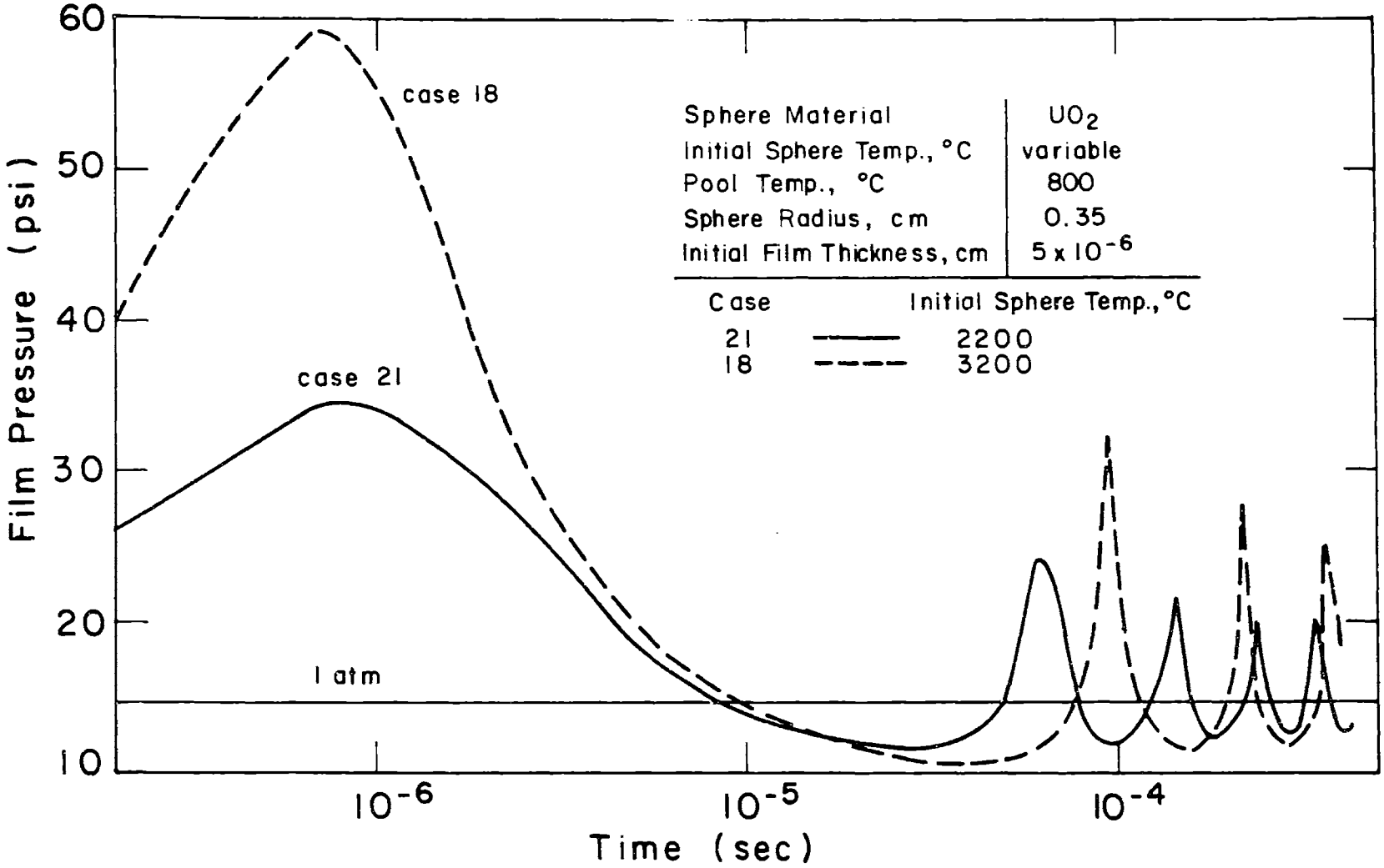

Fig. 4.19 Effect of Initial Sphere Temperature on Pressure-Time History

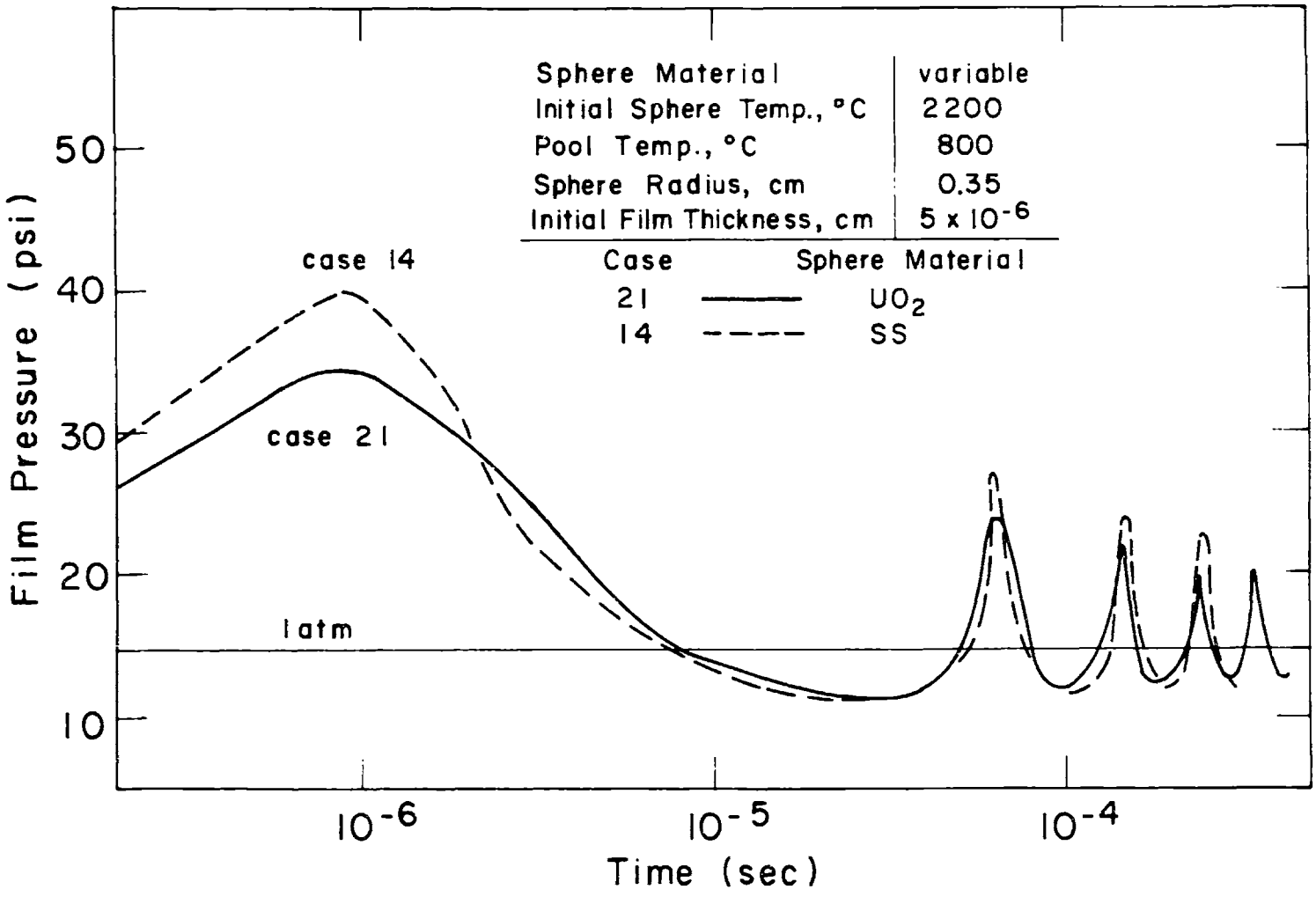

Fig. 4.20 Effect of Sphere Material Properties on Pressure-Time History

Chapter Five

THE MECHANISM OF FREE-CONTACT FRAGMENTATION OF HOT MOLTEN MATERIALS IN COOLANTS

Chapter Five

THE MECHANISM OF FREE-CONTACT FRAGMENTATION OF HOT MOLTEN MATERIALS IN COOLANTS

5.1 Introduction

The fragmentation of hot molten materials as they contact relatively cold liquids has been observed under several experimental conditions. A review of these experiments is given in Chapter 2: Sections 2.2.2, 2.2.3 and 2.2.4. The experimental observations indicate the presence of four modes of fragmentation as described in Section 5.2. These modes of fragmentation depend on the conditions of contact of the two fluids. In this chapter, the physical mechanism inducing fragmentation of hot molten materials under free-contact conditions is investigated. A mechanism based on cavitation within the molten material due to the pressure pulses of transient film boiling at the molten surface is shown to predict most of the observed fragmentation behavior.

5.2 Modes of Fragmentation

The observed fragmentation of hot molten materials in coolants can be categorized according to four distinguishable conditions of contact of the two fluids:

1. Entrapment Fragmentation was demonstrated in the experiments of Long[6] involving dropping of large quantities (∿ 50 lbs) of molten aluminum in water (See Section 2.2.2). This mode of fragmentation is induced by the evaporation of coolant entrapped between the hot molten material and a solid surface. In Long's experiments, when the entrapment of water was made difficult by greasing or painting the bottom of the water container, fragmentation of the aluminum was prevented.

2. Impact Fragmentation was demonstrated in the shock tube experiments of Wright[34] and others[15] (See Section 2.2.3). In those experiments a column of water held in a tube impacted on hot molten metals at the bottom of the tube. Impact fragmentation has been attributed to the effects of the mechanical impact[34]. Recently, the observed fragmentation and vapor explosions in shock tube experiments have been associated with spontaneous nucleation of the coolant[11] and with the dispersal of the coolant within the molten material[48]. The limited data available from shock tube experiments does not provide conclusive evidence for any of these proposed mechanisms of fragmentation. However, since aluminum fragments under shock-tube conditions but does not fragment when dropped in small quantities in water

(as other metals do), the impact of the water column seems to be necessary for producing this mode of fragmentation.

3. Hydrodynamic Fragmentation was demonstrated in the experiments of Ivins[38] and Delhaye[15] involving the fragmentation of mercury in water under isothermal conditions[15,38] (See Section 2.2.4). This mode of fragmentation is caused by the nonuniformity of the forces resisting the motion of a deformable body in a fluid. Hydrodynamic fragmentation is sometimes referred to as the Weber Number Effect since a critical Weber Number has to be exceeded if hydrodynamic fragmentation is to take place. This mode of fragmentation has been thoroughly analyzed by Hinze[40].

4. Free-Contact Fragmentation was demonstrated in several experiments involving the dropping of small amounts (of the order of one gram) of hot molten materials in relatively cold liquids. The observed fragmentation occurred under conditions that do not lead to fragmentation by the preceding three modes. Free-contact fragmentation is highly influenced by the temperatures of the two fluids, which indicates the thermal nature of the mechanism inducing this mode of fragmentation. Several mechanisms have been advanced to explain free-contact fragmentation, but none

seem to be successful in predicting the observed trends of fragmentation. The previously advanced mechanisms are discussed in Section 5.4. In Section 5.5 a hypothesis that is capable of predicting the experimentally observed behavior of fragmentation is advanced.

5.3 Summary of the Experimental Observations of Free-Contact Fragmentation

The following observations are summarized from reported experiments involving dropping a small amount of molten material in a pool of relatively cold liquid. A detailed review of such experiments has been given in Section 2.2.4. The interpretation of the dropping experiments must take into consideration the possible contribution of hydrodynamic fragmentation to the over-all observed fragmentation. The trends of fragmentation as the initial temperature of the hot material or the temperature of the coolant pool changes can be attributed to the free-contact mode of fragmentation. When the Weber Number is kept below the critical value ($\sim$ 13), fragmentation is due only to the free-contact mechanism. With these qualifications, the following experimentally determined behavior can be considered characteristic of the free-contact mode of fragmentation:

1. Fragmentation occurs for some but not all hot

molten materials dropped with equal initial temperature in water.

2. Some hot materials, at the same temperature , fragment in sodium but not in water.
3. For all tested materials, fragmentation in water is reduced by the increase of the water temperature between 0°C and 80°C.
4. For highly subcooled sodium (200°C - 400°C), fragmentation of stainless steel is enchanced by the increase of the sodium temperature. In some experiments[35] the trend of fragmentation enhancement with the increase in the sodium temperature seems to be continued up to a temperature of 820°C. Other experiments[12] indicate a reversal in this trend as the sodium temperature is increased from 400°C to 600°C.
5. As the initial temperature of the molten material is increased, fragmentation of some of the molten materials in water is enhanced. In some cases, the enhancement of fragmentation occurs only within a certain range of temperatures (See Figs. 2.7 through 2.11).
6. The fragmentation seems to result from internal pressure generation in the molten material, as

evidenced by the outward burst of metals in the experiments of Flory et al.[43] (See Fig. 2.12), and Bradley et al.[46]

5.4 Discussion of Previously Advanced Mechanisms

Numerous physical mechanisms have been suggested to explain the free-contact mode of fragmentation. Table 5.1 summarizes these mechanisms. Some of these mechanisms are discounted by experimental observations as pointed out in the following.

5.4.1 Shell Solidification

Fragmentation may be postulated to result from pressurization of the molten core of the hot material due to shrinkage of the solidifying surface. This mechanism, however, is incapable of explaining the observed fragmentation of bismuth in water[39,45], since bismuth volume increases about 3% upon solidification. Furthermore, the fragmentation of hot mercury (melting point -38.8°C) in water[45] is also inexplicable by this mechanism.

5.4.2 Coolant Encapsulation

Fragmentation has been suggested to result from the evaporation of an amount of coolant that penetrates the molten material[31,43,48]. There is difficulty, however,

Table 5.1

Suggested Mechanisms of Free-Contact Fragmentation

1. Shell Solidification
2. Coolant Encapsulation:
   a. by cracks in a solidifying shell
   b. by Helmholtz instabilities
   c. by penetration of a coolant jet
3. Acoustic Pulse in the Coolant
4. Spontaneous Nucleation of the Coolant
5. Vapor Bubble Growth and Collapse
6. Cavitation within the Molten Material (Proposed in the present study)

In defining the mechanism by which the coolant penetrates the molten material which, in many cases, is at a temperature higher than the critical temperature of the coolant (e.g., Tin at 500°C fragments in 20°C water while the water critical temperature is 374°C). At such high temperatures, mere contact of the liquid coolant with the molten material induces spontaneous nucleation in the coolant.

Sallack[31] suggested encapsulation takes place in cracks in the solidified surface. Hsiao's[77] calculations indicate that the thermal and contraction stresses are of maximum values at the instant at which the solid shell starts to develop. Thus, the solidifying shell is most likely to develop cracks when the shell thickness is very small. If such is the case, no significant penetration of coolant can occur. Also, the fragmentation of bismuth and mercury cannot be explained by this penetration mechanism.

Flory et al.[43] suggested encapsulation of coolant is due to the development of surface instabilities in the molten material. Again, the ripples formed at the molten surface by these instabilities, called Helmholtz instabilities, were of small size. Even when liquid coolant is assumed to be encapsulated within the ripples, the penetration of the coolant would be too small to explain the

central cavities observed in some of the aluminum drops in the experiments of Flory et al. (See Fig. 2.12).

Board et al.[48] have recently suggested that penetration of a jet of coolant into the hot molten material may result when a vapor film collapses at the molten surface. (Stevens et al.[47] have also suggested an association of the film collapse with fragmentation, but have not advanced a defined mechanism for the process.) The jet would hydrodynamically disperse within the hot material, and the energy transfer to the small dispersed coolant droplets would then result in fragmentation of the hot material. Plesset and Chapman[114] have considered the formation of a jet of coolant by a collapse of a vapor bubble near a solid (rigid) wall. Their results indicate that the jet will be formed at the later stages of the collapse when the bubble radius has become even less than half its original value. Considering the blanket collapse around a hot molten drop may be approximately treated, at least initially, as a collapse of a vapor bubble, the initial radius of the vapor blanket would have to be at least twice the radius of the molten drop to form the penetrating jet. Such thick vapor blankets are not observed to exist around the molten drops prior to their fragmentation (See Fig. 2.12).

5.4.3 Acoustic Pulse in the Coolant

It has been suggested[73] that fragmentation may be associated with the pressure pulse that develops in the liquid coolant due to instantaneous heating of the coolant at the interface with the hot molten material. If a constrained volume of liquid suddenly undergoes a temperature change of ΔT, the pressure in the liquid volume is changed by an amount ΔP given by:

$$\Delta P = \left(\frac{\partial P}{\partial T}\right)_v \Delta T. \qquad 5.1$$

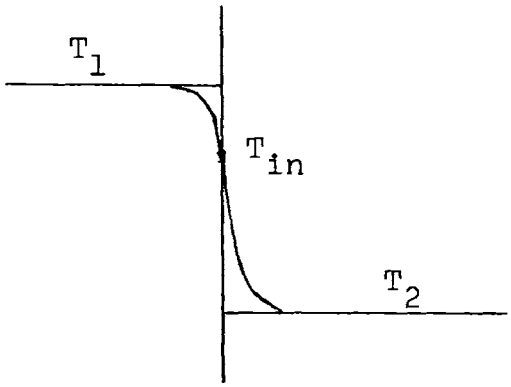

If perfect contact is postulated between the hot material (initially at a temperature T_1) and the coolant (initially at a temperature T_2), the interface temperature, T_{in}, assumes an intermediate value that may be calculated considering each of the materials semi-infinite in extension.

The solution of the heat conduction problem of this type is given by Carslaw and Jaeger[115] (page 70). The interface temperature is found to be constant in time and given by:

$$T_{in} = T_1 - \frac{\sqrt{(\rho kc)_2}}{\sqrt{(\rho kc)_1} + \sqrt{(\rho kc)_2}} (T_1 - T_2), \qquad 5.2$$

where ρ, k, and c are the density, thermal conductivity and specific heat respectively.

Thus, at the time of contact, the coolant at the interface develops a pressure increase given by:

$$\Delta P = \left(\frac{\partial P}{\partial T}\right)_v (T_{in} - T_2). \qquad 5.3$$

By substitution from equation 5.2 into equation 5.3, equation 5.3 may be written as:

$$\Delta P = \left(\frac{\partial P}{\partial T}\right)_v \left[\frac{f}{1 + f}\right] (T_1 - T_2), \qquad 5.4$$

where

$$f = \sqrt{(\rho kc)_1/(\rho kc)_2} \; . \qquad 5.5$$

This pressure pulse at the interface with the hot surface propagates in the coolant as a pressure wave, and the pressure at the interface is reduced very rapidly. (The acoustic velocity in water is $\sim$ 1500 m/sec at 20°C

and in sodium is ∿ 2500 m/sec at 550°C.) From equation 5.4, it is clear that the pressure pulse developed at the interface of a certain combination of hot and cold materials would be larger the larger is the difference (T_1-T_2). It is then expected that the extent of fragmentation by this mechanism, for a certain material combination, would increase proportional to (T_1-T_2). This is contradictory to the observed decrease in the fragmentation of stainless steel (initially at 2200°C) in sodium as the sodium temperature decreases between 820°C and 200°C in the experiments of Swift and Pavlik[35] and between 400°C and 200°C in the experiments of Armstrong.[12]

5.4.4 Spontaneous Nucleation of the Coolant

It has been suggested that if the interface temperature defined by equation 5.2 is higher than the spontaneous nucleation temperature of the coolant, the high localized pressures resulting from the nucleation would extensively fragment the hot material also.[116] The spontaneous nucleation temperature of sodium and water are calculated in Appendix H. In Table 5.2 the spontaneous nucleation temperatures are compared to the interface temperatures for the conditions of some fragmentation experiments. It is evident that for molten uranium dioxide and stainless steel in sodium the

Table 5.2

Comparison of Spontaneous Nucleation Temperatures of Sodium and Water with Temperatures at the Interface of Some Molten Materials*

Coolant (Temp., °C)	Molten Material (Temp., °C)	T_{in}, °C (Eq. 5.2)	$T_{s.n.}$, °C (App. H)
Sodium (600)	UO_2 (2900)	1130	1850
	Stainless Steel (2200)	1346	1850
Water (20)	Pb (700)	543	314
	Bi (700)	543	314

*All the molten materials are reported to fragment under the experimental conditions.

interface temperatures are much below the spontaneous nucleation temperature, and hence the observed fragmentation cannot be explained by this mechanism.

5.4.5 Bubble Growth and Collapse

Vapor bubble growth and collapse at the surface of the molten materials have been suggested to induce free-contact fragmentation.[36] This mechanism is incompatible with the observed fragmentation of molten metals in water, when the metal water is at temperatures higher than the critical temperature of water.

For sodium, Judd[101] has shown that the pressure pulse generated by the collapse of a vapor bubble is higher for lower temperatures of sodium. Thus an association of fragmentation with the pressure pulses of the collapsing bubbles predicts an increase in the extent of fragmentation of stainless steel at lower sodium temperatures, contrary to the observed trend of fragmentation at large subcoolings of sodium.

5.5 A Proposed Mechanism of Fragmentation

In Chapter 4 a model has been developed to simulate the dynamics of the growth of a vapor film around a hot spherical particle in a coolant. The results of the model indicate that large pressure pulsations accompany, under

certain conditions, the growth of the vapor film. A rapidly changing pressure at the surface of a molten material gives rise to pressure waves within the molten material. As the pressure fluctuations created at the surface of a spherical (or cylindrical) particle travel towards the center (or axis) of the particle, the pressure fluctuations are expected to be magnified. Camp[125] (page 64) treats the problem of pressure distribution inside a nonviscous compressible fluid for a spherically symmetric, time-wise sinusoidally varying pressure wave. He finds the spatial distribution may be given by:

$$P(r) = \frac{A}{r} e^{+ikr}, \qquad 5.6$$

where P(r) is the pressure at radius r, and

A, k are constants depending on the particular problem.

Equation 5.6 substantiates the possibility of magnifying the pressure fluctuations created at the surface of the molten drop. The pressure at the molten surface due to the growth of a vapor film would exhibit, as calculated in Chapter 4, positive and negative fluctuations about the initially uniform pressure in the molten drop-coolant system, which in the calculations of Chapter 4 was taken to be 1 atm. Therefore, subatmospheric pressures obtained at the surface can momentarily reach very large "negative"

values near the drop center, thus facilitating internal cavitation in the molten material which leads to the observed fragmentation. (Cavitation is used here to denote the process of growth of vapor nuclei within a liquid when the liquid pressure is reduced. The vapor nuclei in a liquid may also grow if the liquid, at the original pressure, is sufficiently superheated; a process usually called spontaneous or homogeneous nucleation.) Internal cavitation in a liquid due to negative liquid pressure has been the subject of several experimental studies.[117-120] It is particularly interesting that the possibility of inducing cavitation in a liquid by an oscillatory pressure field, in which the reduction of the liquid pressure required for cavitation is obtained intermittently, has been well deomonstrated in experiments involving the application of high intensity sound fields to several liquids.[120,121] This phenomenon is usually referred to as acoustic cavitation.

In Appendix H, the theoretical negative pressures required to facilitate cavitation in molten metals are estimated using an expression developed by Bernath[122]. The theoretical negative values required for cavitation are very large. Cavitation, however, may be obtained at smaller values of negative pressures should the molten material contain impurities or dissolved gases. For

water at room temperature under negative pressures of few atmospheres[119], i.e., below the theoretical value required for cavitation by two orders of magnitude. This proposed mechanism for free-contact fragmentation seems particularly suitable to explain the internal cavities produced in aluminum in the experiments of Flory et al.[43], and the expansion in the size of the molten jet prior to the fragmentation in the experiments of Bradley et al.[46] Other observed fragmentation behavior can also be predicted by this mechanism, as demonstrated in the following:

1. The analytic results of Chapter 4 indicate that lower water temperatures lead to lower sub-atmospheric values of pressure in the vapor film growing around a tin sphere in water. The film pressure behavior was also observed to be insensitive to the thermal diffusivity of the sphere material. Thus it is expected that larger "negative" pressures could be obtained, in all materials, as the water temperature is decreased. Therefore, more extensive fragmentation is expected at lower water temperatures, in agreement with the observed behavior of all materials that fragmented in water. In Fig. 5.1, the maximum reduction in the film pressure as calculated by

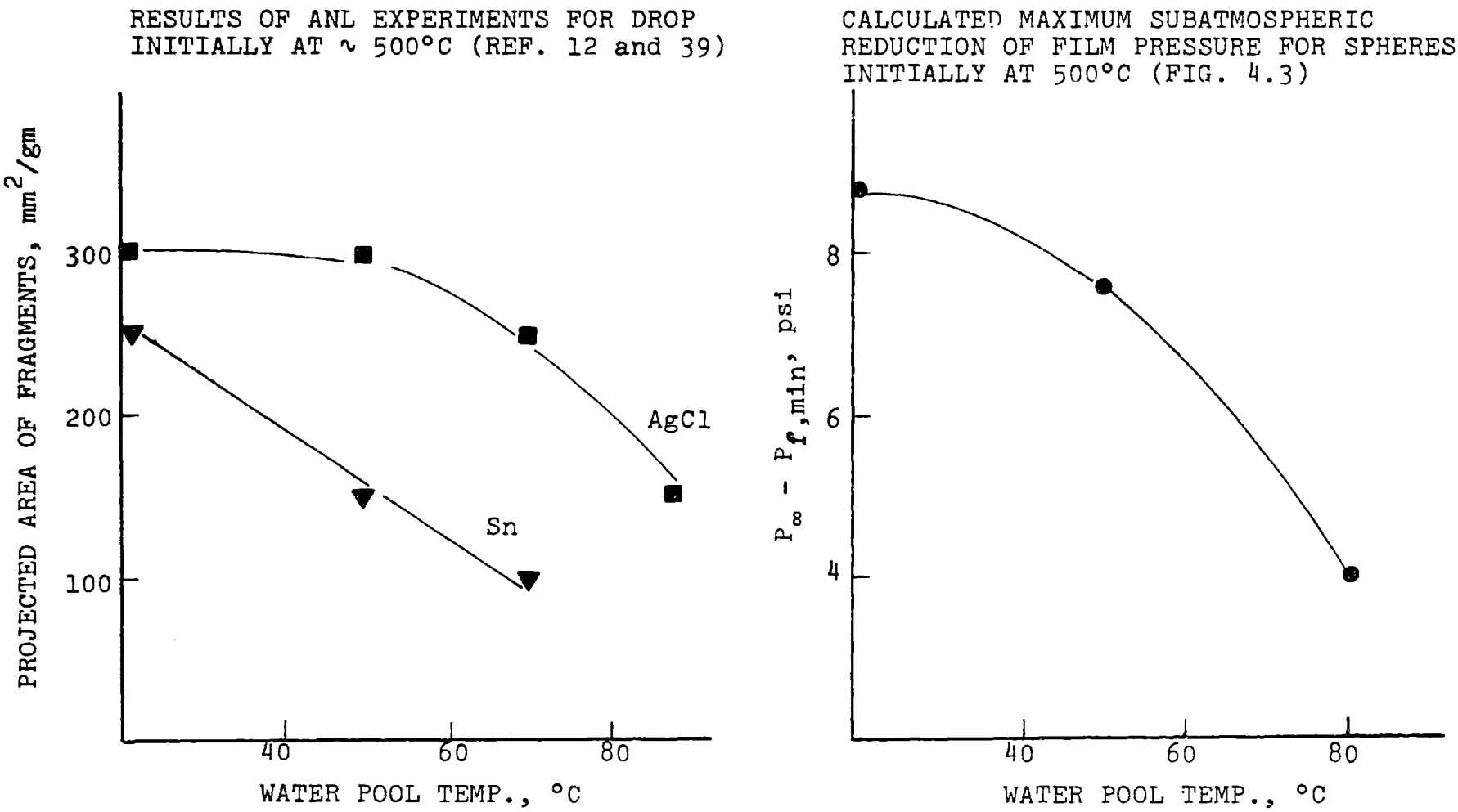

FIG. 5.1: COMPARISON OF THE EFFECT OF WATER POOL TEMPERATURE ON THE FRAGMENTATION IN WATER AND ON THE MAXIMUM SUBATMOSPHERIC PRESSURE REDUCTION IN A VAPOR FILM GROWING AROUND A HOT PARTICLE IN WATER.

the model of Chapter 4 is compared to the projected area of fragments for Sn and AgCl as obtained in experiments conducted at ANL.[12,39] The data for fragmentation of Bi in 80°C water is unavailable but the general trend of the fragmentation of Bi in water at 4°C, 22°C and 50°C (Fig. 2.9) is diminshed with the increase in water temperature.

2. As the temperature of liquid sodium is decreased in the range 250-850°C, the analytic results indicate that there is an intermediate sodium temperature below which the subatmospheric reduction in pressure is decreased with the decrease in the sodium temperature. Therefore, the extent of fragmentation is to be enhanced within an intermediate range of temperatures. This is in agreement with the observed trend of fragmentation in Armstrong's[12] experiments (See Fig. 5.2). The diminished fragmentation of stainless steel in sodium as the sodium temperature is reduced has also been qualitatively observed by Swift and Pavlik[35,36] for a sodium temperature range of 250-820°C. The qualitative results of Amblard's[13] experiment of dropping UO_2 in sodium also indicate more extensive fragmentation took place in 400°C sodium than in 200°C sodium.

RESULTS OF ANL EXPERIMENTS (AREA IS BASED ON MEAN DIAMETER OF FRAGMENTS GIVEN IN REF. 12)

CALCULATED MAXIMUM SUBATMOSPHERIC REDUCTION OF FILM PRESSURE (FIG. 4.14)

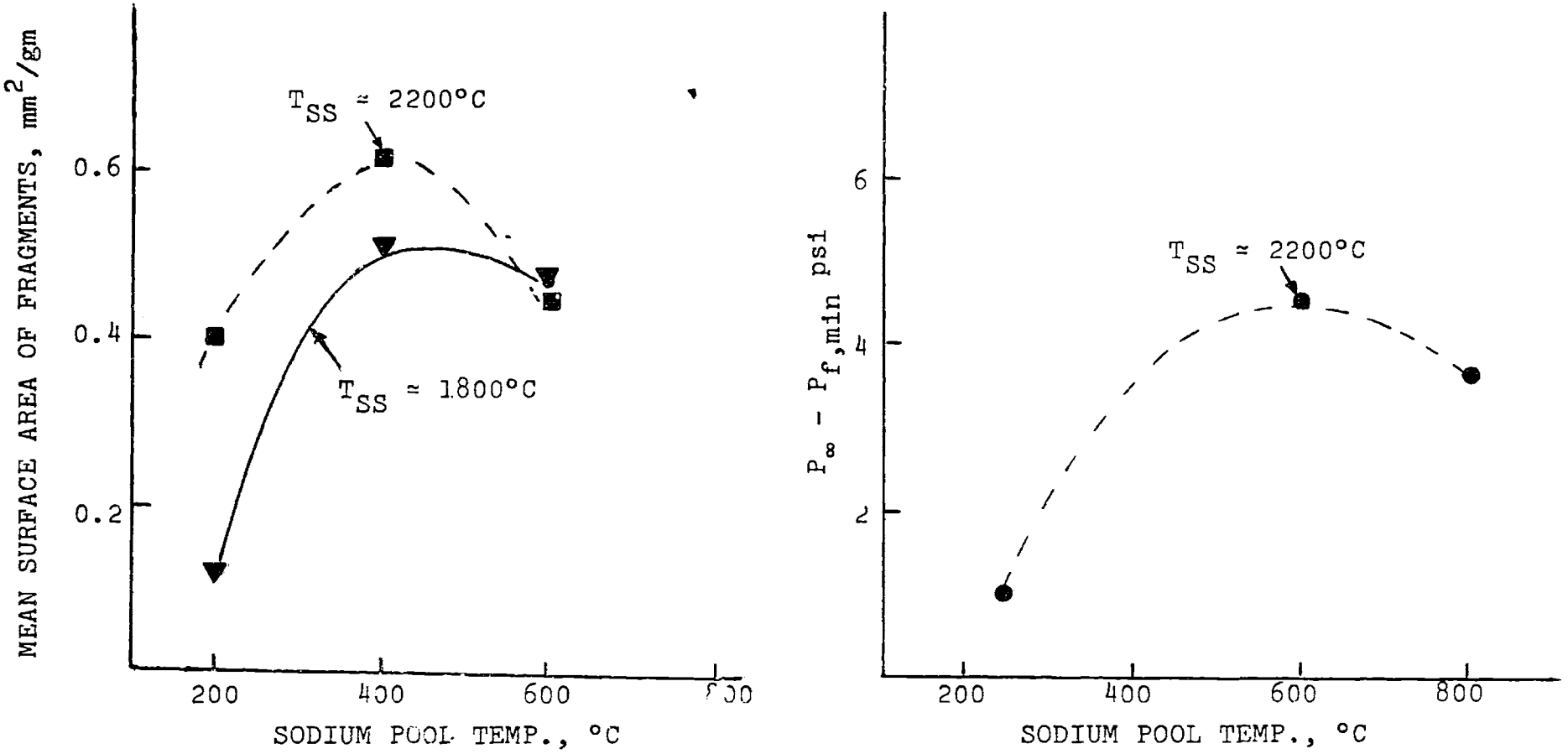

FIG. 5.2: COMPARISON OF THE EFFECT OF SODIUM POOL TEMPERATURE ON THE FRAGMENTATION OF STAINLESS STEEL IN SODIUM AND THE MAXIMUM SUBATMOSPHERIC PRESSURE REDUCTION IN A VAPOR FILM GROWING AROUND A STAINLESS STEEL PARTICLE IN SODIUM.

3. Under the same conditions of pressure pulsation at the sphere surface (i.e., for the same negative pressures obtained in the molten material), fragmentation should be easier to produce in molten materials of lower surface tension (See Appendix H). The results of the analytic model of Chapter 4 suggest the thermal diffusivity of the hot sphere material does not have appreciable influence on the pressure oscillations of the vapor film growth in H_2O. Thus, for initial drop temperature of 700°C, the extent of fragmentation of Aℓ, Zn, Pb and Bi should increase in that order. (Surface tension values are given in Appendix I.) Indeed the results of the ANL experiments show that no fragmentation occurs at free-contact conditions with 20°C water for Aℓ ($\sigma \simeq 900$ dyne/cm) and Zn ($\sigma = 750$ dyne/cm) but that fragmentation occurs for Pb ($\sigma = 400$ dyne/cm) and Bi ($\sigma \simeq 350$ dyne/cm). The fragmentation of Bi is observed to be more extensive than that of Pb.
4. For the same coolant temperature, larger amplitude of the pressure oscillations in the film are predicted as the initial temperature of the molten

drop is increased (See Fig. 4.7 and Fig. 4.19). The predicted enhancement of the extent of fragmentation of stainless steel in sodium with the increase in the initial drop temperature is in good agreement with the observed trend[35,36] (Fig. 2.2). For water at 20°C, the predicted enhancement of fragmentation of Bi and Pb is also in agreement with the observed trend (See Fig. 5.3). The data of ANL for Sn/H_2O system show enhancement with the increase in the initial tin temperature up to 500°C, followed by a reversal of this trend for initial tin temperatures in the experimentally observed range of 500-800°C. The Sn behavior is not readily explainable, but could be related to the rapid stabilization of the vapor film at temperatures above 500°C (See Fig. 4.8). The minimum temperature at the hot surface that is required to stabilize film boiling, T^*, for several hot surface/liquid material combinations seems to be best correlated by the expression proposed by Henry[113] (Appendix G). The values of T^* for Sn, Pb and Bi as predicted by Henry's correlation are shown in Fig. 5.3. It is interesting to note that the film stabilization temperature for Sn in 20°C water

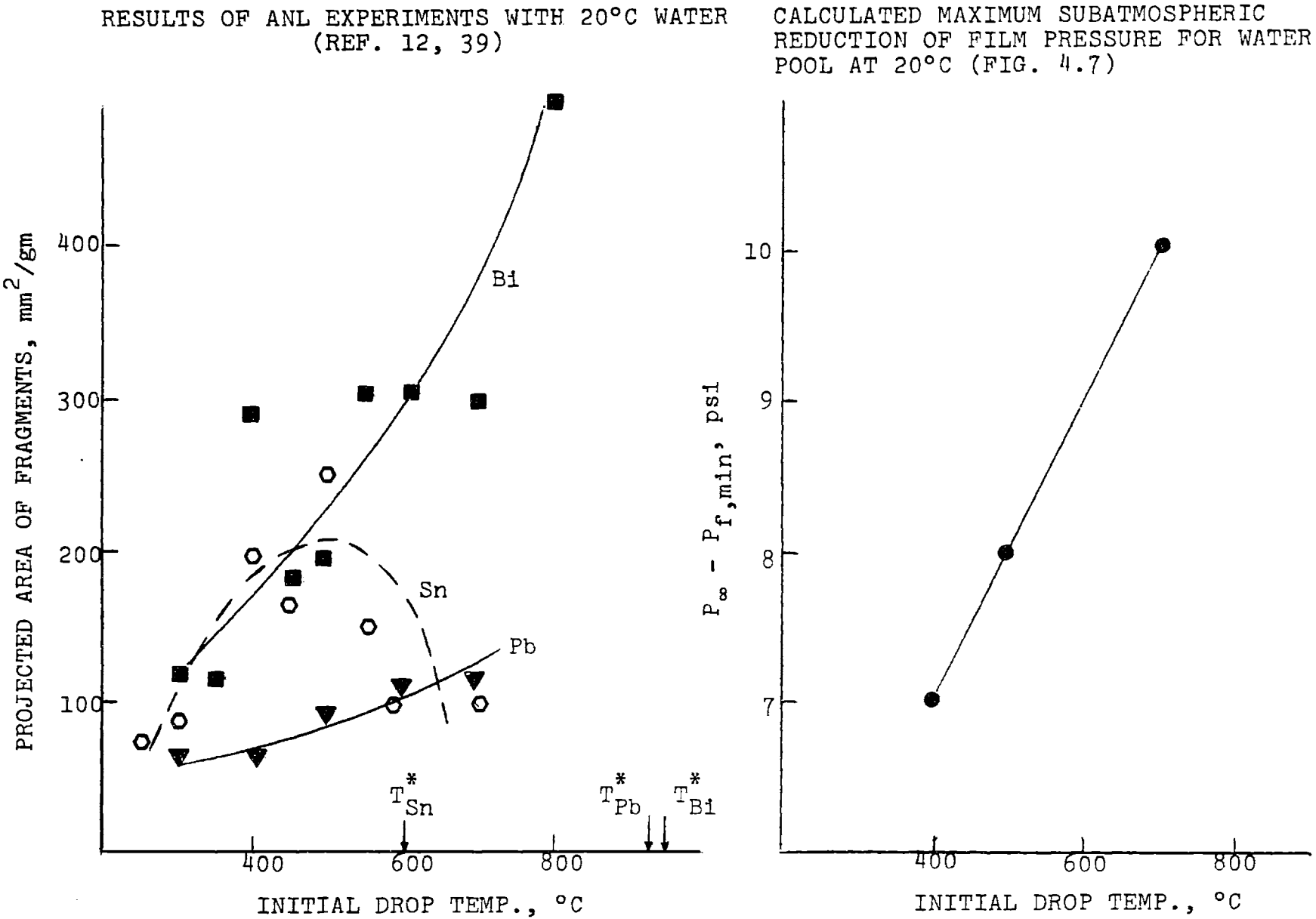

FIG. 5.3: COMPARISON OF THE EFFECT OF THE INITIAL TEMPERATURE OF THE HOT MATERIAL ON THE FRAGMENTATION IN WATER AND THE MAXIMUM SUBATMOSPHERIC FILM PRESSURE REDUCTION IN A WATER POOL AT 20°C

(600°C) limits the range for which extensive free-contact fragmentation of tin was observed. While the values of T^* for Bi (960°C) and Pb (940°C) lie beyond the experimental range of the initial drop temperature of 500-800°C.

Based on the above discussed behavior of the fragmentation of tin, it can be hypothesized that fragmentation takes place only if the initial temperature of the molten material, T_{hi}, was below the film stabilization temperature, T^*. Then fragmentation occurs if

$$T_{m.p.} < T_{hi} < T^*. \qquad 5.6$$

The criterion 5.6 is capable of explaining the observed fragmentation behavior of tin in the ANL experiments. However it cannot be further supported by the available data on fragmentation of other materials, because of the limited range of the initial temperature, T_{hi}, used in the experiments. From equation 5.6 it is seen however that free-contact fragmentation is expected only if the melting point of a material is less than the film stabilization temperature, i.e., if

$$T_{m.p.} < T^*. \qquad 5.7$$

The fragmentation data can be used to verify the relaxed criterion of 5.7. In Fig. 5.4 this criterion is tested

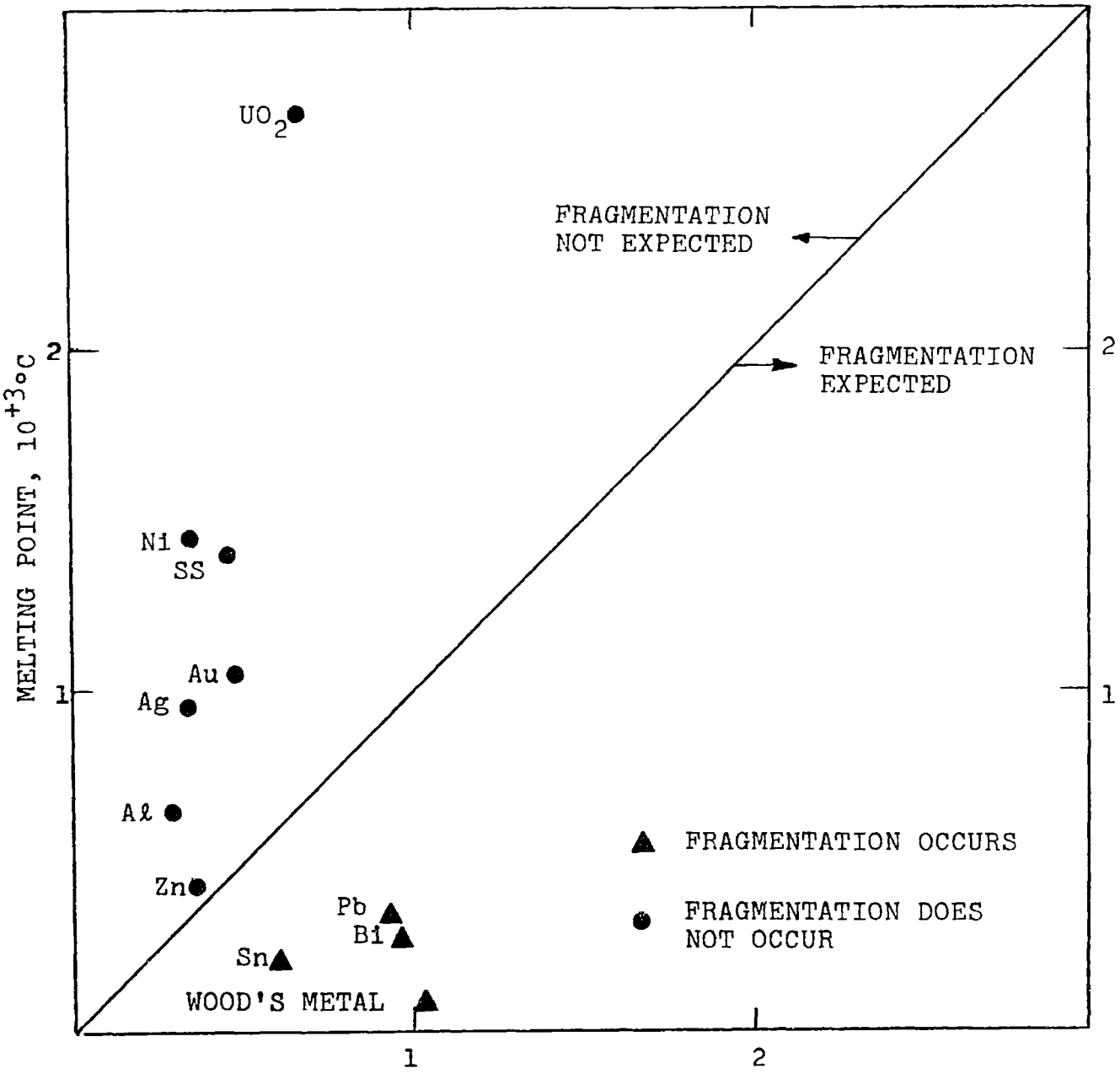

FIG. 5.4: COMPARISON OF THE OBSERVED FRAGMENTATION BEHAVIOR IN 20°C WATER WITH THE STABLE FILM CRITERION

for the fragmentation of molten materials in 20°C water. The criterion shows good agreement with the experimental results. In Fig. 5.5 it is seen that the criterion also satisfies the observed fragmentation in 250°C sodium.

It is interesting to note that the materials predicted to fragment in Fig. 5.4 (Sn, Bi, Pb and Wood's metal) have surface tension values lower than the materials predicted not to fragment (Zn, Aℓ, Ag, Au, SS, Ni and UO_2). The validity of criterion 5.7 should be further tested in future experiments by observing the fragmentation of a material that satisfies the criterion but has a surface tension value less than that of Bi and Pb (i.e., $\sigma < 300$ dyne/cm). Should such a material fragment, then the agreement between the criterion 5.7 and the water experiments of Fig. 5.4 is coincidental only.

Equation 5.6 represents even a more restricted criterion for fragmentation. The criterion satisfies the results of the ANL Sn/H_2O experiments. However, fragmentation of Sn at initial temperatures higher than the film stabilization temperature is reported to take place in experiments at other laboratories.[43,48] The conflicting results could be due to the difference in the size of the molten tin drops used in the experiments. For example, in the experiments of Board et al.[48] the tin drops were

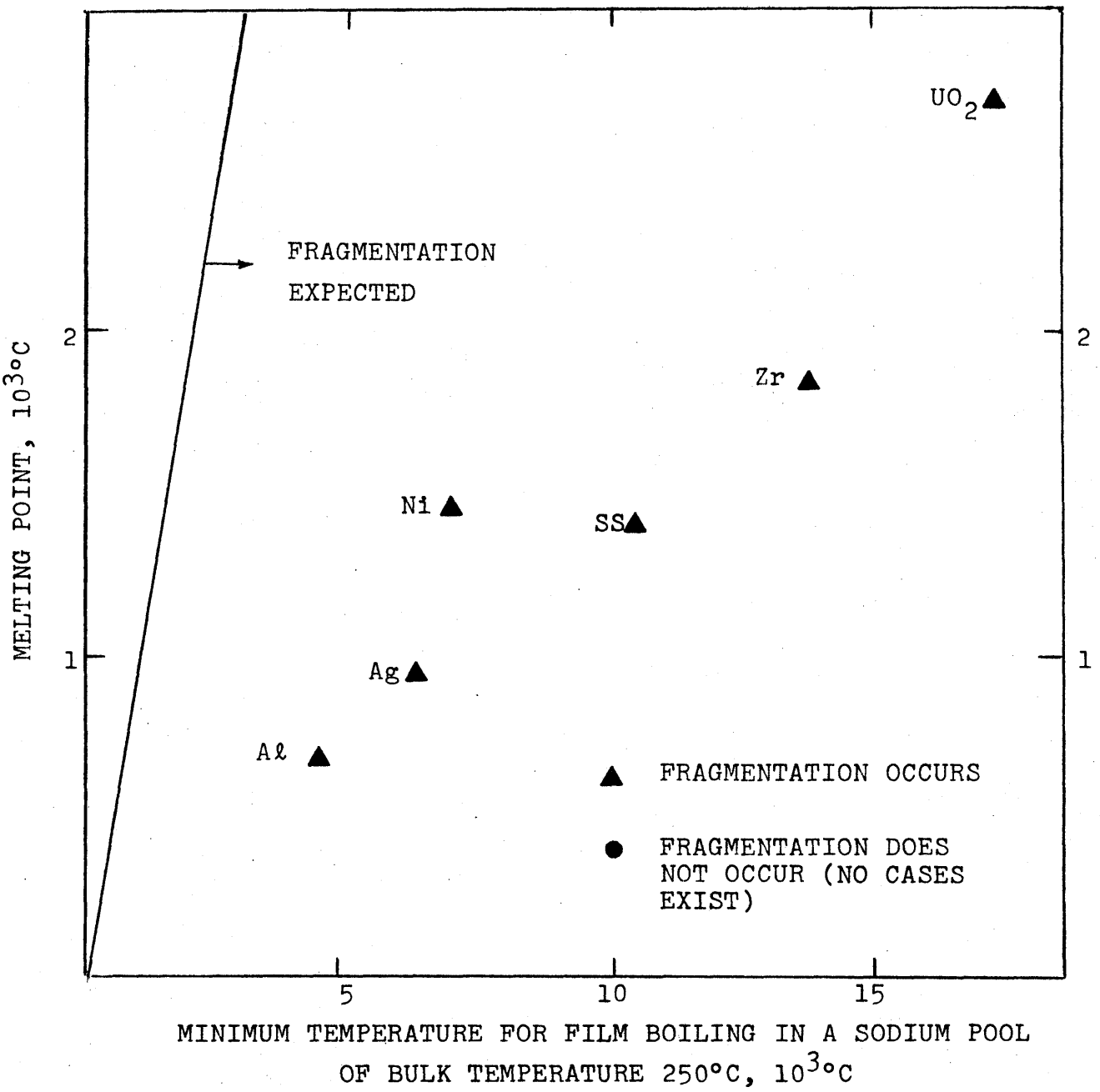

FIG. 5.5: COMPARISON OF THE OBSERVED FRAGMENTATION BEHAVIOR IN 250°C SODIUM WITH THE STABLE FILM CRITERION

"few grams" in weight while in the ANL experiments the tin drop was "approximately 0.3 gm in weight".[12] The more extensive fragmentation of the larger drops may be due to hydrodynamic fragmentation (higher Weber Number). Another possible explanation is the larger amplitude of pressure pulsation in the film growing around larger particles as indicated by the results of the analytic model (Fig. 4.9). Both larger surface subatmospheric pressure reduction and volume of the molten drop increase the internal volume of the liquid which may be subjected to the large negative pressures required for cavitation.

Finally, if cavitation due to the pressure pulses of the growing film is the mechanism inducing the fragmentation, then fragmentation should be observed within a short time of the initial contact of the molten material and the coolant. The accurate estimate of the time which would theoretically be expected to elapse between the initial contact of the two fluids and the fragmentation phenomenon requires a solution of the problem of a cavity growing within the molten material under the expected dynamic pressure conditions. An order of magnitude estimate of the time for growth of a cavity may be obtained by considering the calculations that have been conducted by Flynn[121] for cavities growing in water under acoustic pressure fields. For an acoustic pressure field of an

amplitude of 0.8 atm and of a frequency of 24.5 kc/sec., a cavity of 0.027 cm radius was shown by Flynn to approximately double its size in 1 msec. The calculations of Flynn[121], however, indicate the sensitivity of the maximum radius to which a bubble may grow to the initial radius of the cavity as well as the frequency of the oscillatory pressure. For smaller frequencies (longer periods), larger radii may be achieved.

It should be noted that the case considered by Flynn is different from our case in two respects: 1) the surface tension values of the molten materials of interest are higher than the water surface tension; which implies that larger values of negative pressures are required in the present case to maintain the same rate of cavity growth, and 2) the amplitudes of the pressure fluctuations above 1 atm are higher, in our case, than the subatmospheric pressure amplitudes which would tend to retard the cavity growth rate calculated for an acoustic pressure field. The calculations of Flynn should, therefore, be considered representative only of the order of magnitude of the times involved inthe growth of cavities in the molten materials of interest.

The experimental data on the time elapsed between the initial contact of the molten material and the coolant are not always reported. Flory et al.[43] find the most

violent cases of fragmentation to occur "almost instantaneously" upon contact of the molten material and the water. Witte et al.[45] observed delay time ranging between 3 and 80 milliseconds. The fragmentation process itself takes place in a shorter time (< 1 msec., See Fig. 2.12a). The time required for growth of cavities under dynamic pressure conditions, as discussed above, seem to be of the same magnitude of the limited reported experimental data.

In summary, the proposed mechanism of cavitation induced free-contact fragmentation due to pressure pulsation at the surface of the molten material is capable of explaining the experimentally observed trends of fragmentation:

1. Enhanced fragmentation of molten materials for greater subcoolings of water.
2. Enhanced fragmentation of stainless steel for an intermediate subcooling of sodium.
3. The apparent internal pressure generation within the quenched molten material.
4. The observed fragmentation of some but not all molten materials in water.
5. The increased fragmentation of Pb, Bi and AgCl in water and stainless steel in sodium for increased initial drop temperatures.

There are some difficulties in explaining the behavior of the fragmentation of Sn in water with increasing initial Sn temperature. The ANL results indicate that the fragmentation is greatly diminished when the initial drop temperature is higher than the film stabilization temperature. The results of the experiments at other laboratories seem to indicate fragmentation of tin will continue to be enhanced with increasing tin temperature.

Chapter Six

CONCLUSION

Chapter Six

CONCLUSION

6.1 Summary

Two aspects of the thermal interaction of hot molten fuel and coolant that may take place under LMFBR accident conditions have been investigated:

1. The effect of gas/vapor blanketing of the fuel on the pressure and mechanical work that may develop due to fragmentation of the molten fuel in sodium, and
2. The association of the phenomenon of fragmentation of molten fuel as it contacts sodium with the pressure pulses that accompany transient vapor film formation at the molten surface.

In Chapter 3, a model developed at Argonne National Laboratory to analyze the fragmentation-induced vapor explosions in LMFBR accidents has been modified to include the effect of gas/vapor blanketing of the fuel. The modified model accounts for both thermal resistance and the compliance of the gas/vapor blanket. The modified model has been applied to several cases involving a hypothetical accident in an FFTF subassembly to assess the

effects of gas/vapor blanketing of fuel on post-fragmentation generation of pressure and mechanical work. The major conclusions of this study are:

1. Gas/vapor blanketing of the fuel reduces, but does not preclude the high pressure that may be developed by the thermal interaction.
2. The mechanical work generated by the thermal interaction is considerably reduced when gas/vapor blanketing is accounted for.

In Chapter 4, a model has been formulated to simulate the dynamic growth of a vapor film around a hot spherical particle which is suddenly immersed in a large pool of relatively cold liquid. The model has been applied to several cases of hot spheres in both water and sodium. The results indicate that the rapid vaporization initially leads to a pressure rise in the film which drives the film growth in an oscillatory manner. The film pressure exhibits a damped oscillatory behavior in which sub-atmospheric values of pressure are repeatedly reached. The conclusions of this study are:

1. In water, the pressure oscillations are more quickly damped as the subcooling is decreased.
2. In sodium, the amplitude of the pressure oscillations exhibits a maximum for an intermediate range of subcooling.

3. In both water and sodium, for a fixed coolant temperature, the increase in the initial sphere temperature leads to increased amplitude of pressure fluctuations.
4. The thermal properties of the hot sphere seem not to influence the pressure history of the film in water, but have a small effect in sodium.
5. Higher pressures accompany the growth of the vapor film for increased sphere radius.

In Chapter 5, a hypothesis has been advanced to explain the observed fragmentation of hot molten materials in coolants under free-contact conditions. The hypothesis relates the observed fragmentation to internal cavitation within the molten materials due to the dynamic conditions of pressure at the molten surface. The observed fragmentation behavior in reported experiments involving dropping of small molten particles in both sodium and water has been compared in Chapter 5 to the predicted behavior by this hypothesis. The predicted behavior is in general agreement with the observed one. It is noted, however, that the available experimental data on free-contact fragmentation in some instances shows conflicting fragmentation behavior. Possible explanations for this contradictory behavior have been advanced in Chapter 5.

Further experimental investigation seems to be required for confirming the proposed explanations as discussed in Section 6.2.

6.2 Recommendations for Future Work

The hypothesis of cavitation-induced fragmentation, advanced in Chapter 5, merits further investigation. Both theoretical and experimental work may be suggested to further examine the hypothesis.

Theoretical studies can be directed to analysis of the pressure field established within the molten material under conditions of pulsating pressure at the surface. The knowledge of the time varying pressure field within the molten material could be utilized in the assessment of the time required for internal cavities to grow within the hot molten materials to large sizes, at which fragmentation can be expected. Such information should be of direct interest in the description of the rate of generation of the fuel surface area in the models developed for LMFBR accident analysis.

Experimental investigations are needed for both reexamining what seems to be conflicting trends of fragmentation and verification of the proposed mechanism of fragmentation. As have been discussed in Chapter 5, the fragmentation of molten tin in water in the ANL experiments[12] seem to be enhanced as the initial temperature of tin is

increased up to a temperature of ~500°C, beyond which free-contact fragmentation is diminished. Other qualitative data[43,48] indicates fragmentation of tin is increased with the increase in the initial temperature up to 900°C. Additionally, fragmentation of bismuth, lead and silver chloride have been observed in other ANL experiments to, in general, be enhanced with the increased initial temperature of the molten material up to a temperature of 800°C. Future experiments should involve dropping of molten materials other than Sn in subcooled water such that the initial temperature of the molten drop be higher than the temperature required to stabilize film boiling in the water. Bismuth and lead initially at 1000°C may be dropped in 20°C water to satisfy such a condition (See Fig. 5.3). If the fragmentation of such high temperature molten materials is diminished, then the tin fragmentation behavior may be induced by the stabilization of the vapor film as proposed in the present study. The influence of the size of the molten drop has been suggested in Chapter 5 as a possible explanation for the conflicting results of tin fragmentation in water. An experimental investigation involving dropping tin particles at the same initial temperature from the same height above a water pool can be conducted to establish

the effect of the radius of the molten particle.

Another investigation may be necessary to establish the effect of sodium temperature on the fragmentation of stainless steel. Quantitative results of fragmentation in a range higher than the available Armstrong data[12] (200-600°C) would verify the trend of enhancement of fragmentation at an intermediate sodium subcooling. In all future experiments, data on the time elapsed between initial contact and actual fragmentation should be sought, as it serves as basis for comparing theoretical fragmentation mechanisms, which could then be useful in specifying the time-rate of fuel area generation in models of LMFBR accident analysis.

An experimental investigation of the possibility of inducing fragmentation in hot molten materials by rapid reduction of the surface pressure is required to verify the proposed mechanism of fragmentation. The dynamic pressure conditions in the growing film may be simulated by a sound field acting at the surface of a molten hot material. In effect, this would serve to confirm that acoustic cavitation, which is a well-established phenomenon for liquids of small surface tension values,[121] can also occur in the molten materials of high surface tension values as those used in fragmentation studies.

Appendix A

Contribution of Radiative Heat Transfer to Total Heat Transfer in Film Boiling

Consider a spherical hot particle in a liquid undergoing film boiling at the hot surface. Heat will be transferred across the film by radiation and conduction. Assuming the thickness of the film is small compared with the sphere radius, the thermal flux due to radiation is given by [131]:

$$q''_r = \frac{\sigma}{1/\varepsilon_h + 1/\varepsilon_\ell - 1} \left(T_h^4 - T_{\ell v}^4\right) \quad , \qquad \text{A.1}$$

where σ = Stephen's constant = 1.38×10^{-12} cal/cm^{2}sec$^\circ$K^4 ,

ε_h, ε_ℓ = the emissivity of the sphere and the liquid respectively,

T_h, $T_{\ell v}$ = the temperatures of the sphere surface and the film/liquid interface.

The thermal flux due to conduction is given by:

$$q''_c = \frac{k_v}{\delta} \left(T_h - T_{\ell v}\right) \quad , \qquad \text{A.2}$$

where k_v = vapor conductivity

δ = vapor film thickness.

From A.1 and A.2, the ratio of q''_r and q''_c is:

$$\frac{q''_r}{q''_c} = \frac{\delta\sigma}{k_v(1/\varepsilon_h + 1/\varepsilon_\ell - 1)} \frac{T_h^4 - T_{\ell v}^4}{T_h - T_{\ell v}} \quad . \qquad \text{A.3}$$

The ratio of radiative to conductive heat flux is directly proportional to the film thickness δ. Consider the film thickness at which the ratio $q_r'' : q_c'' = 0.1$:

$$\delta_{0.1} = \frac{0.1k_v\ (T_h - T_{\ell v})}{\frac{\sigma}{1/\varepsilon_h + 1/\varepsilon_\ell - 1}\ (T_h^4 - T_{\ell v}^4)} \quad . \qquad \text{A.4}$$

Consider a Uo_2 sphere (3200°K) in sodium (1153°K) Since no data is available for ε_{Na} and ε_{Uo_2}, assume conservatively that $\varepsilon_{Uo_2} = 1.0$ (black body) ,

$\varepsilon_{Na} = 0.1$ (all metals reported in Ref. 131 have emissivity values less than 0.1) ,

$k_v = 2 \times 10^{-4}$ cal/cm sec°K ,

The value of $\delta 0.1$ is obtained from equation A.4 as:

$$\delta_{0.1} = 33 \times 10^{-4} \text{ cm} . \qquad \text{A.5}$$

Consider a metallic sphere (1000°K) in water (373°K). Again let $\varepsilon_{metal} = 0.1$,

$\varepsilon_{H_2O} = 1.0$,

$k_v = 9 \times 10^{-5}$ cal/cm sec °K ,

Then, by substitution in equation A.4 we obtain

$$\delta_{0.1} = 400 \times 10^{-4} \text{ cm} . \qquad \text{A.6}$$

For the range of surface temperatures and film thicknesses encountered in this study, the error in estimating the rate of heat transfer across the film introduced by

neglecting the radiation heat transfer does not exceed 10%.

Appendix B
On the Average Film Temperature

In both chapters 3 and 4 of this study, the temperature profile in the gaseous film was assumed a linear function of distance. The average temperature of the gases in the film can be estimated under such conditions as follows:

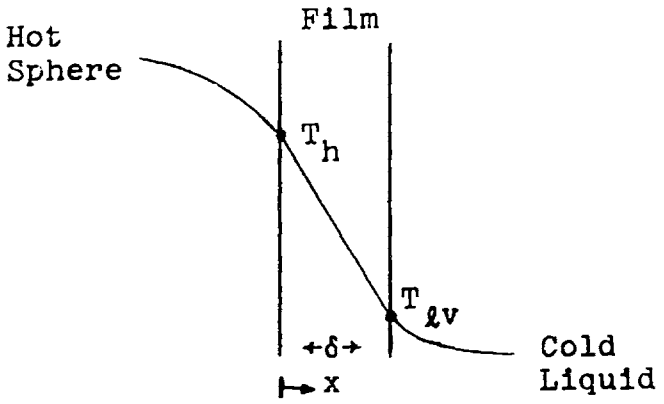

The average temperature in the film for any profile, T(r), is given by:

$$T_f = \frac{\int_0^{\delta} \rho T(r)\ 4\pi r^2\ dx}{\int_0^{\delta} \rho\ 4\pi r^2\ dx} \quad , \qquad \text{B.1}$$

where x = r-R, and

R = radius of the hot sphere.

For a relatively thin film (i.e. x<<R), r ≈ R and hence equation B.1 reduces to

$$T_f = \frac{\int_0^{\delta} \rho T\ dx}{\int_0^{\delta} \rho\ dx} \quad . \qquad \text{B.2}$$

The density of a perfect gas is given by:

$$\rho = \frac{P}{GT} \qquad \text{B.3}$$

Substituting from equation B.3 in equation B.2 gives:

$$T_f = \frac{\int_o^\delta dx}{\int_o^\delta \frac{dx}{T}} \qquad \text{B.4}$$

The assumption of linear temperature in the film yields:

$$\frac{T_h - T}{T_h - T_{\ell v}} = \frac{x}{\delta} \, . \qquad \text{B.5}$$

By differentiation of equation B.5 we get

$$dx = - \frac{\delta}{T_h - T_{\ell v}} dT \qquad \text{B.6}$$

Thus, changing the variable from x to T in equation B.4 yields:

$$T_f = \frac{\int_{T_h}^{T_{\ell v}} dT}{\int_{T_h}^{T_{\ell v}} \frac{dT}{T}} = \frac{T_h - T_{\ell v}}{\ell n (T_h / T_{\ell v})} \qquad \text{B.7}$$

In Table B.1 the values of T_f as obtained from equation B.7 are compared to the values obtained from the approximation:

$$T_f = \frac{T_h + T_{\ell v}}{2} \qquad \text{B.8}$$

TABLE B.1

Comparison of the Exact and Approximate Film Temperature

$\frac{T_h}{T_{\ell v}}$	$\frac{T_f}{T_{\ell v}} = \frac{T_h/T_{\ell v}-1}{\ell n(T_h-T_{\ell v})}$	$\frac{T_f}{T_{\ell v}} = \frac{T_h/T_{\ell v}+1}{2}$
2	1.44	1.5
3	1.82	2.0
4	2.16	2.5

For the cases encountered in this study, the value of $T_h/T_{\ell v}$ has always been less than 3 for the water coolant and less than 4 for the sodium coolant. Therefore, the error in T_f when estimated by equation B.7 is at most 13.6%, which gives negligible effect on the calculated parameters of interest.

Appendix C

Estimation of the Effects of Nonequilibrium Conditions on the Dynamic Vapor Film Growth

The kinetic theory can be used to obtain the following expression for the net evaporation at a vapor/liquid interface[128]:

$$\frac{dM_v}{dt} = \frac{1}{\sqrt{2\pi G}} \left[\frac{\eta_e P_i}{\sqrt{T_i}} - \Gamma' \frac{\eta_c P_v}{\sqrt{T_v}}\right] , \qquad C.1$$

Where P_i = the saturation pressure at the liquid interface temperature, T_i,

P_v = the vapor pressure,

T_v = the saturation temperature at a pressure P_v,

G = the vapor gas constant,

η_e = accomodation factor for evaporation,

η_c = accomodation factor for condensation, and

Γ' = a correction factor for the net vapor mass at the interface, reflecting the effect of the vapor "progress" velocity away from the interface given by:

$$\Gamma' = 1 - \frac{\frac{dM_v}{dt}}{P_v \sqrt{\frac{2}{\pi G T_v}}} . \qquad C.2$$

By substitution from equation C.2 into equation C.1 we obtain:

$$\frac{dM_v}{dt} = \frac{2}{2-\eta_c} \left[\frac{1}{\sqrt{2\pi G}} \right] \left[\frac{\eta_e P_i}{\sqrt{T_i}} - \frac{\eta_c P_v}{\sqrt{T_v}} \right] \quad . \qquad C.3$$

If the accomodation coefficients for evaporation and condensation are assumed equal:

i.e. $\eta_e = \eta_c = \eta$,

then equation C.3 reduces to:

$$\frac{dM_v}{dt} = \frac{2\eta}{2-\eta} \left[\frac{1}{\sqrt{2\pi G}} \right] \left[\frac{P_i}{\sqrt{T_i}} - \frac{P_v}{\sqrt{T_v}} \right] . \qquad C.4$$

Let $P_i = P_v + \Delta P_v$, and $\qquad C.5$

$T_i = T_v + \Delta T$. $\qquad C.6$

If ΔP is smaller than P_v and ΔT is smaller than T_v, then by substitution from equations C.5 and C.6 into equation C.4 the net rate of evaporation may be given by:

$$\frac{dM_v}{dt} = \frac{2\eta}{2-\eta} \frac{P_v}{\sqrt{2\pi G T_v}} \left[\frac{\Delta P}{P_v} - \frac{\Delta T}{2T_v} \right] \quad . \qquad C.7$$

For pressures as low as 0.001 atm, for metal vapors and water, the magnitude of $\Delta T/2T$ is around 3 to 4% of $\Delta P/P$. At higher pressures this relative magnitude is smaller. Thus, if $\Delta T/2T_v$ is neglected in equation C.7, the equation

reduces to:

$$\frac{dM_v}{dt} = \frac{2\eta}{2-\eta} \frac{\Delta P}{\sqrt{2\pi G T_v}} \quad . \qquad C.8$$

Equation C.8 permits the estimation of the amount of superheat required in the liquid to supply a net evaporation rate of $\frac{dM_v}{dt}$.

In the calculations performed in chapter 4, the maximum rate of heat consumption in vaporization around hot spheres in water was 26 cal/sec (See Fig. 4.4). This belongs to a maximum evaporation flux at the film radius, R≈0.3 cm, of

$$\left(\frac{dM_v}{dt}\right)_{max} = \frac{26}{4\pi R^2 h_{fg}} = 0.083 \text{ lb}_m/\text{ft}^2.\text{sec} \quad .$$

By substituting the values G=86 ft - $lb_f/lb_m°R$ and T_v = 672°R in equation C.8 we obtain

$$\Delta P = 8.8 \left(\frac{2-\eta}{2\eta}\right) \text{ lb}_f/\text{ft}^2$$

$$= 0.061 \left(\frac{2-\eta}{2\eta}\right) \text{ psi} \qquad C.9$$

The values of the accomodation coefficients have been summarized by Wylie and Brodkey[129], and range between very low (.001) to very high (1.0). Rohsenow[128] has suggested that when attention is paid to the cleanliness of the vapor/liquid interface in the experiments and to precision in measurements, the value of η tends to be close to unity. If η is taken to be unity in equation C.10 the expected

value of ΔP is only 0.061 psi. Thus the corresponding superheat required to maintain the observed evaporation rate is less than 1°C. Thus the assumption made in chapter 4 that the vapor/liquid interface is at equilibrium does not introduce appreciable error.

For the cases of hot spheres in sodium, the maximum rate of heat consumption in vaporization was 40 cal/sec (for case 18). Using the same steps outlined above for the water case we obtain the value of ΔP to sustain such a rate of evaporation (around a sphere of 0.35 cm radius and for the values $G = 67.3\ lb_m/ft^2.sec$ and $T_v = 2020°R$) to be:

$$\Delta P = 0.075 \text{ psi.}$$

The corresponding value of ΔT is again less than 1°C which indicates the suitability of the equilibrium assumption.

Appendix D

On the Adequacy of the Integral Method for Describing the Heat Transfer in the Model for Dynamic Vapor Film Growth

In chapter 3, a model has been developed to simulate the growth of a vapor film around a sphere immersed in a coolant. The integral approximation has been used for the description of the heat transfer in the hot sphere and the coolant. In the integral approximation, the heat conduction equation is satisfied over thermally-active regions in both the sphere and the liquid, assuming a certain temperature profile exists in the active region. The integral approximation thus leads to a coupling between the total amount of heat transferred across both interfaces of the vapor film and the rate at which the heat is transferred at any time, without satisfying the heat conduction equation at each infinitesimal volume element within the sphere or the liquid. Such an approach is employed to overcome the difficulty of solving the heat transfer equation in each medium with the nonlinear boundary conditions. Quadratic temperature profiles have been assumed in both the sphere and the liquid. The assumption of a monotonic temperature profile along with the integral approach has been used by Judd[100,101] and Theofanous et al.[102,103] to describe the heat transfer in the liquid surrounding growing or collapsing vapor bubbles. Both models have reported successful application of the method

to the cases of growing bubbles in superheated liquids but encountered cases where the method would fail to describe the heat transfer around collapsing bubble in subcooled liquids[101,103]. In both treatments the net change of the vapor bubble energy had to be supplied (or withdrawn) by the heat flux at the liquid/vapor interface. Thus the heat flux at the interface is specified. Additionally the temperature of the liquid/vapor interface is specified by the conditions in the bubble (through the equilibrium condition in Judd's model and the nonequilibrium condition in the model of Theofanous et al.). As reported by Judd[101], the integral method with a monotonic temperature profile would fail when the specified heat flux at the bubble interface would mean the transfer of heat across the thermally active region from the boundary of a lower temperature to the boundary of a higher temperature. Theofanous et al.[103], do not elaborate on the reason for the failure of the method in their study beyond stating that the treatment is inadequate in case vaporization develops in a collapsing bubble as it rebounds. It is seen, however, that in their model vaporization can not be accounted for should it develop while the liquid temperature at the bubble interface is higher than the bulk liquid temperature, since then the required vaporization energy cannot be supplied.

In the present model the rate of change of the vapor energy is equal to the difference between the rates of heat

supply by the hot sphere and the heat transmission to the liquid (i.e., evaporation takes place when the difference between the heat supply and heat transmission rates is positive and condensation takes place when the difference is negative). Thus a reversal of the temperature gradient at the interface is not required when vaporization changes to condensation or vise versa. Difficulties as those described by Judd[101], have not resulted in any of the calculated cases of this study.

Two additional remarks about the integral method are worth mentioning here. First, the method gives indefinite values for the heat fluxes at both sides of the film at the zero-time moment. A solution applicable for short times after the start of the interaction was used to specify the starting conditions for the code (see Appendix F). Secondly, very short time steps have to be used at the beginning as the film pressure starts to depart from the initial condition so as not to reverse the evaporation rate. The required time steps vary with the rate at which the film pressure is undergoing change initially. The time steps can be increased after the first peak pressure is reached. In the numerical subroutine used, a maximum allowable time step is specified but the time advancement can use shorter steps to keep the truncation errors within a specified maximum value. In all cases, the value of the specified maximum truncation error has been chosen to keep the overall relative error

less than 0.1%.

As a part of this study, attempts were also made to describe the heat transfer in the sphere and the liquid by a finite-difference formulation. In this method the sphere and the liquid are divided into a number of concentric shells, each at a uniform temperature. The heat transfer between each two adjacent shells depends on the temperature difference between the two shells and their inter-resistance. Thus one is immediately faced with the question of appropriate selection of shell thickness. The large thermal gradients involved require small shell thicknesses which limits the time step that can be used. The time steps are limited throughout the calculation and cannot be increased as the vapor film grows. Thus, for the cases calculated up to about 5×10^{-5} sec, the calculations of the film growth by the finite-difference formulation were about three to five times more expensive than the calculations using the integral method. With the finite difference formulation, two options have been tried for the boundary conditions of equal temperatures on both sides of the sphere/film interface and the film/liquid interface. As one option, the vapor temperature at both interfaces may be equated to the temperature of the shell in contact with the vapor film as shown in Fig. D.1.a. As the second option, the vapor temperature may be equated to interface temperatures dissociated from the first shell temperatures, as shown in Fig. D.1.b. The two

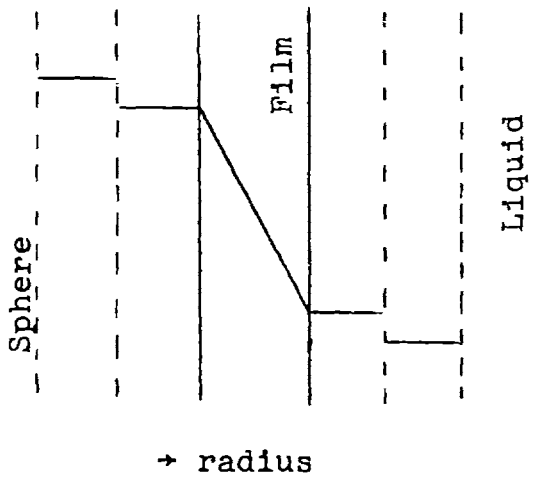

Fig. D.1a

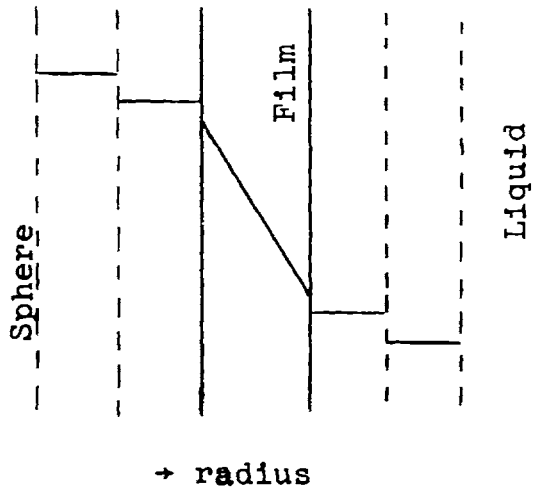

Fig. D.2b

Fig. D.1 Illustration of Options for Film Boundary Temperature

treatments result in somewhat different pressure-time history, as shown in Fig. D.2. In fact the pressure-time history of the film predicted by the finite difference method is influenced by the choice of the shell thicknesses (in all calculations the ratio of the shell-thickness in the sphere to that in the liquid has been taken to be equal to the square root of the ratio of their thermal diffusivities, i.e., $(\Delta r)_h/(\Delta r)_\ell = \sqrt{\alpha_h/\alpha_\ell}$). No "saturation" of the influence of shell thickness was seen even when the water shell thickness was decreased to equal 3×10^{-5} cm. The pressure time history as calculated by the finite difference approximation, with the water shell thickness as small as 3×10^{-5} cm, also departs from the results of the integral method. However, because of the arbitrariness of the finite-difference results, depending on the shell thickness, no confidence can be assigned to its results.

The finite difference formulation with interface temperatures dissociated from the adjacent shell temperatures exhibited small fluctuations of pressure about the "average" trend of pressure. Taking smaller time-steps produces a "smoother" development of pressure.

Using even smaller shell thicknesses than the ones already used in calculations and changing the numerical integration scheme from a predictor-corrector method (which is equivalent to a partially explicit and partially implicit integration scheme) to a fully implicit method to

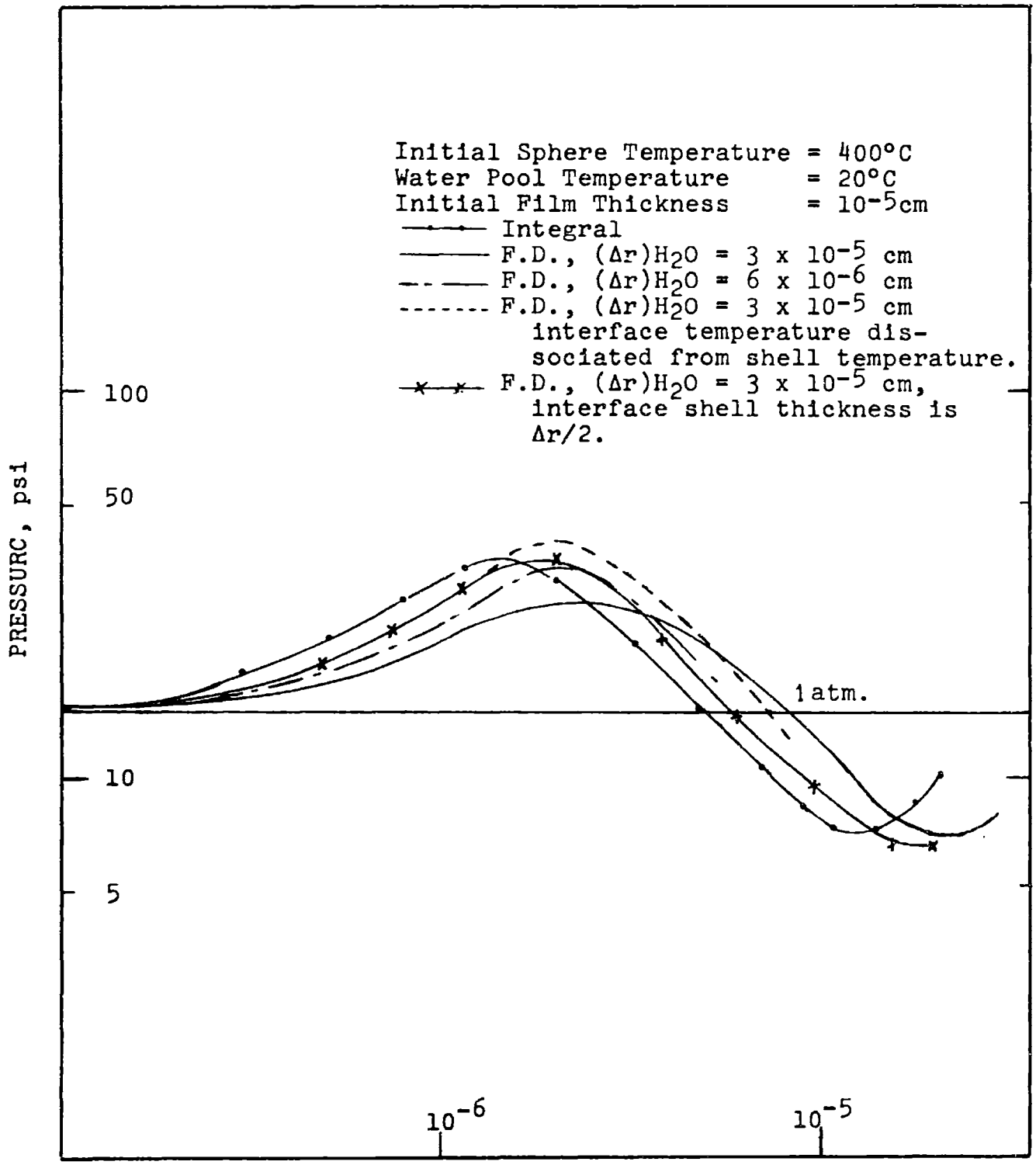

Fig. D2 Results of the Calculations of the First Pressure Pulse Using Integral and Finite Difference Approximations to Describe the Heat Transfer

ensure stability may have improved the agreement between the results of the finite difference and the integral formulation. Using both smaller shell thicknesses and an implicit method of integration would have also increased the expenses of the calculation. The solution of the heat transfer problem by finite difference methods was, therefore, discontinued in this study in favor of the integral method.

Appendix E. Listing of the Computer Program for Dynamic Vapor Film Growth, FILDYN

```
C      VAPOR FILM DYNAMICS =FILDYN
C
C      THE MODEL DESCRIBES THE DYNAMIC GROWTH OF  A VAPOR FILM AROUND A
C      HOT PARTICLE IMMERSED IN A LARGE AMOUNT OF LIQUID. THE INTEGRAL
C      METHOD IS USED TO DESCRIBE THE HEAT TRANSFER IN BOTH THE SPHERE
C      AND THE LIQUID. AN INITIAL GASEOUS FILM IS ASSUMED TO EXIST AT THE
C      INTERFACE OF THE SPHERE AND THE LIQUID. THE FILM/LIQUID INTERFACE
C      IS ASSUMED TO BE AT THERMODYNAMIC EQUILIBRIUM CONDITIONS AT ALL
C      TIMES. THE EQUATION OF MOTION OF THE INTERFACE IS OPTIONAL BETWEEN
C      THAT ASSOCIATED WITH AN INCOMPRESSIBLE LIQUID OR THAT ASSOCIATED
C      WITH AN ACOUSTICALLY INFINITE COMPRESSIBLE LIQUID
C
C
C             THE  PROGRAM CONSISTS OF FOUR PARTS : A MAIN PART AND THREE
C      SUBROUTINES.  SUBROUTINE FCT SUPPLIES THE DIFFERENTIAL EQUATIONS
C      DESCRIBING THE PHYSICAL PROCESSES IN THE SYSTEM. SUBROUTINE DHPCG
C      IS A STANDARD INTEGRATION SUBROUTINE SUPPLIED BY M.I.T. CODE
C      LIBRARY AT THE INFORMATION PROCESSING CENTER.  SUBROUTINE OUTP
C      SPECIFIES THE OUTPUT FORMAT AND ANY OTHER QUANTITIES TO BE PRINTED
C       BY MANIPULATION OF THE MAIN VARIABLES.
C
C
      IMPLICIT REAL*8 (A-H,O-Z)
      REAL*8 KH,KL,KV
      INTEGER*4 CCM
      DIMENSION Y(7),DERY(7),PRMT(9),ALX(16,7),TIT(20)
      COMMON /R1/R,AH,KH,THI,AL,KL,KV,G,TB,RUL,PINF,S,PGO,GAM,VFC,LIQ,CC
     1M
      EXTERNAL FCT,OUTP
C
C      READ INPUT PARAMETERS AND INITIAL VALUES
C
      READ(5,5) (TIT(I),I=1,20)
      READ (5,10) (PRMT(I),I=1,4),NDIM,LIQ,CCM
      READ (5,20) R,AH,KH,THI
      READ (5,30) AL,KL,KV,G,TB,RUL,PINF,S
```

```
      READ (5,40) (Y(I),I=1,7),(DERY(I),I=1,7)
      READ (5,50) PGO,GAM,VFC
    5 FORMAT (20A4)
   10 FORMAT (4D10.4,3I3)
   20 FORMAT (4D10.4)
   30 FORMAT (8D10.4)
   40 FORMAT (7D10.4)
   50 FORMAT (3D10.4)
C
C     WRITE SYSTEM PARAMETERS
C
      WRITE (6,204) (PRMT(I),I=1,4)
  204 FORMAT (//,' VAPOR FILM DYNAMICS ',//,' FROM TIME T = ',D10.4,10X,
     1 ' TO TIME T = ',D10.4,' SEC ',//,' INITIAL TIME INCREMENT IS  ',D
     210.4,' SEC ',//,' UPPER ERROR BOUND IS ',D10.4)
      WRITE (6,202) (TIT(I),I=1,20)
  202 FORMAT (/,5X,20A4)
      WRITE (6,205) R,AH,KH,THI
  205 FORMAT (//,' PROPERTIES OF HOT SPHERE ',/,' SPHERE RADIUS (CM) = '
     1,D10.4,/,' THERMAL DIFFUSIVITY (CM SQ/SEC) = ',D10.4,/,' THERMAL CO
     2NDUCTIVITY (CAL/CM.SEC.DEG K) = ',D10.4,/,' INITIAL SPHERE TEMPERA
     3TURE (DEG K) = ',D10.4)
      WRITE (6,206) AL,KL,KV,G,TB,RUL,PINF,S
  206 FORMAT (//,' PROPERTIES OF FLUID ',/,' THERMAL DIFFUSIVITY (CM SQ
     1/SEC)  = ',D10.4,/,' LIQUID THERMAL CONDUCTIVITY (CAL/CM.SEC.DEG K
     2) = ',D10.4,/,' VAPOR THERMAL CONDUCTIVITY (CAL/CM.SEC.DEG K) = ',
     3D10.4,/,' GAS CONSTANT (PSI.CM*3/DEG K) = ',D10.4,/,' INITIAL LIQU
     4ID TEMPERATURE (DEG K) = ',D10.4,/,'  LIQUID DENSITY (GM/CM*3) = '
     5,D10.4,/,' AMBIENT PRESSURE (PSI) = ',D10.4,/,' SOUND VELOCITY IN
     6 LIQUID (CM/SEC) = ',D10.4)
      WRITE (6,207) PGO,GAM,VFC
  207 FORMAT (/,' INITIAL GAS PROPERTIES ',/,' PARTIAL GAS PRESSURE (PSI) = '
     1I) = ',D10.4,/,' ADIABATIC GAS INDEX = ',D10.4,/,' INITIAL FILM VO
     2LUME (CM*3) = ',D10.4)
      IF (LIQ.NE.1) GO TO 222
      WRITE (6,221)
```

```
  221 FORMAT (/,5X,15HLIQUID IS WATER,/)
      GO TO 224
  222 WRITE (6,223)
  223 FORMAT (/,5X,16HLIQUID IS SODIUM,/)
  224 IF (COM.NE.1) GO TO 212
      WRITE (6,211)
  211 FORMAT (/,5X,35HLIQUID IS CONSIDERED INCOMPRESSIBLE,/)
      GO TO 214
  212 WRITE (6,213)
  213 FORMAT (/,5X,33HLIQUID IS CONSIDERED COMPRESSIBLE,/)
  214 CONTINUE
C
C     START CALCULATIONS
C
      PRMT(9)=210.
      Y(1)=R+Y(1)
  201 CALL DHPCG(PRMT,Y,DERY,NDIM,IHLF,FCT,OUTP,AUX)
C
C     ERROR MESSAGES
C
      IF (X.GE.PRMT(2)) GO TO 99
      IF (PRMT(5).NE.0.0) GO TO 51
      GO TO 52
   51 WRITE (6,61) PRMT(5)
   52 IF (IHLF.GT.10) GO TO 53
      GO TO 60
   53 WRITE (6,62) IHLF
   60 CONTINUE
   61 FORMAT (' PARAMETER 5 IS ', D10.4)
   62 FORMAT (' IHLF IS ',I3)
   99 STOP
      END
```

```
      SUBROUTINE FCT(X,Y,DERY)
C
C
      IMPLICIT REAL*8 (A-H,O-Z)
      REAL*8 KH,KL,KV
      INTEGER*4 COM
      DIMENSION Y(8),DERY(8)
      COMMON /R1/R,AH,KH,THI,AL,KL,KV,G,TB,RUL,PINF,S,PGO,GAM,VFC,LIQ,CO
     1M
      RC=Y(1)
      U=Y(2)
      TW=Y(4)
      TR=Y(5)
      THC=Y(3)
      TV=.50*TW+.50*TR
      IF (Y(6).GE.(R-1.D-04)) Y(6)=R
      IF (LIQ.NE.1) GO TO 5
C
C        WATER CASE : CALCULATION OF VAPOR PRESSURE
C
      HFG=545.
      P=14.7*DEXP(HFG/.1103*(1./373.-1./TW))
      DP=HFG*P/(.1103*TW**2)
      GO TO 6
C
C        SODIUM CASE : CALCULATION OF VAPOR PRESSURE
C
    5 P=DEXP(15.3838-(12767.8/TW))/TW**0.61344*14.7
      DP=P*(12767.8/TW**2-0.61344/TW)
      HFG=930.
    6 RUV=P/(G*TW)
      IF(Y(6)-R) 1,2,2
      GO TO 3
    2 DQDT=12.565*R**2*(THC-TW)/((RC-R)/KV+R*.5/KH)
    3 D1=RC-R
      D2=(RC**2-R**2)/2.
```

```
      D3=(RD**3-R**3)/3.
      D4=(RD**4-R**4)/4.
      D5=(RD**5.-R**5)/5.
      A1=Y(6)/R
      A2=1./3.-A1/6.+A1**2/30.
      A3=1./6.-A1/6.+A1**2/20.
      C1=Y(7)/Y(1)
      C2=1./3.+C1/6.+C1**2/30.
      C3=1./6.+C1/6.+C1**2/20.
      C4=1./2.+C1/3.+C1**2/12.
      DQC=25.13*KL*RD**2*(TW-TB)/Y(7)
      VF=12.565*D3
      PG=PGO*(VFO/VF)**GAM
      PF=P+PG
      DMV=(DQDT-DQC)/HFG
    8 DRO=Y(2)+DMV/(12.565*RO**2*RUL)
      IF (Y(6)-R) 10,20,20
C
C       THERMAL PENETRATION IS LESS THAN THE RADIUS OF THE SPHERE
C
    1 DQDT=12.565*R**2*(THI-TW)/((RD-R)/KV+Y(6)*.5/KH)
   10 G1=(2.+A2/A3)*KH/Y(6)+KV/D1
      G2=(AH/(A3*Y(6)**2)-DRO/D1)/(12.565*R**2)
      G3=12.565*D3*(DP-.5*P/TV)/(G*TV)
      G4=12.565*D3*P/(2.*G*TV**2)
      DTW=(DMV-12.565*RD**2*RUV*DRD-G2*G4*DQDT/G1)/(G3-KV*G4/(D1*G1))
      DTR=(KV*DTW/D1-G2*DQDT)/G1
      DERY(1)=DRO
      IF (COM.NE.1) GO TO 102
C
C       CASE OF INCOMPRESSIBLE LIQUID
C
      DERY(2)=((PF-PINF)/RUL*6.894D  4-1.5*Y(2)**2)/Y(1)
      GO TO 103
C
C       CASE OF COMPRESSIBLE LIQUID
```

```
C
  102 DPF=DP*DTW-GAM*PG*12.565*RC**2*DRD/VF
      B=4.4D  4
      C=S*((PF+B)/(PINF+B))**.428
      UC=1.-U/C
      UCC=1.+U/C
      DERY(2)=(UCC/6.*(C**2-S**2)+RD*UC*C/(7.*(PF+B))*DPF-1.5*U**2*(1.-U
     1/(3.*C)))/(RD*UC)
  103 CONTINUE
      DERY(3)=0.0
      DERY(4)=DTH
      DERY(5)=DTR
      DERY(6)=(A2*Y(6)*DTR+2.*AH*(THI-TR)/Y(6))/(2.*(THI-TR)*A3)
      DERY(7)=0.5/C3*(2.*AL/Y(7)+U-C2*Y(7)*DTW/(Y(4)-TB)-2.*C4*DRD)
      GO TO 30
C
C       THERMAL PENETRATION IS EQUAL TO THE RADIUS OF THE SPHERE
C
   20 G1=5.*KH/R+KV/D1
      G2=(15.*AH/R**2-DRD/C1)/(12.565*R**2)
      G3=12.565*C3*(DP-.5*P/TV)/(G*TV)
      G4=12.565*C3*P/(2.*G*TV**2)
      DTH=(DMV-12.565*RD**2*RUV*DRD-G2*G4*DQDT/G1)/(G3-KV*G4/(D1*G1))
      DTR=(KV*DTH/D1-G2*DQDT)/G1
      DERY(1)=DRD
      IF (COM.NE.1) GO TO 105
C
C       CASE OF INCOMPRESSIBLE LIQUID
C
      DERY(2)=((PF-PINF)/RUL*6.894D  4-1.5*Y(2)**2)/Y(1)
      GO TO 106
C
C       CASE OF COMPRESSIBLE LIQUID
C
  105 DPF=DP*DTW-GAM*PG*12.565*RD**2*DRD/VF
      B=4.4D  4
```

```
      C=S*((PF+B)/(PINF+B))**.428
      UC=1.-U/C
      UCC=1.+U/C
      DERY(2)=(UCC/6.*(C**2-S**2)+RD*UC*C/(7.*(PF+B))*DPF-1.5*U**2*(1.-U
     1/(3.*C)))/(RD*UC)
  106 CONTINUE
      DERY(3)=(10.*AH*(TR-THC)/R**2-DTR)*1.5
      DERY(4)=DTW
      DERY(5)=DTR
      DERY(6)=0.C
      IF (DERY(6).LT.0.0) DERY(6)=0.C
      DERY(7)=0.5/C3*(2.*AL/Y(7)+U-C2*Y(7)*DTW/(Y(4)-TB)-2.*C4*DRD)
   30 RETURN
      END
```

```
      SUBROUTINE OUTP(X,Y,DERY,IHLF,NDIM,PRMM)
C
C
      IMPLICIT REAL*8 (A-H,O-Z)
      REAL*8 KH,KL,KV
      INTEGER*4 COM
      DIMENSION Y(7),DERY(7),PRMM(9),AUX(16,7)
      COMMON /R1/R,AH,KH,THI,AL,KL,KV,G,TB,RUL,PINF,S,PGO,GAM,VFC,LIQ,CO
     1M
      IF (Y(1).LT.R) PRMM(5)=1.0
      TW=Y(4)
      RO=Y(1)
      IF (Y(6)-R+1.D-04) 203,213,213
  203 PRMM(6)=12.565*R**2*(THI-TW)/((RO-R)/KV+Y(6)*.5/KH)
      GO TO 223
  213 PRMM(6)=12.565*R**2*(Y(3)-TW)/ ((RO-R)/KV+R*.5/KH)
      Y(6)=R
  223 PRMM(7)=25.13*KL*RO**2*(TW-TB)/Y(7)
      PRMM(8)=RO-R
      PRMM(9)=PRMM(9)+1.0
      IF (PRMM(9)-210.) 80,81,81
   80 RETURN
   81 PRMM(9)=1.0
      IF (LIQ.NE.1) GO TO 82
      HFG=545.
      P=14.7*DEXP(HFG/.1103*(1./373.-1./TW))
      GO TO 83
   82 P=DEXP(15.3838-(12767.8/TW))/TW**0.61344*14.7
   83 VF=4.189*(RO**3-R**3)
      PG=PGO*(VFC/VF)**GAM
      PF=P+PG
      WRITE (6,207) (Y(I),I=1,7),(DERY(I),I=1,7),(PRMM(I),I=6,8),X
  207 FORMAT (1X,7D10.4)
      WRITE (6,208) PF,P
  208 FORMAT (1X,' PF (PSI) = ',D10.4,3X,' PV (PSI) = ',D10.4)
      RETURN
```

Appendix F

Derivation of the Starting Values for the Numerical Integration of the Equations of Vapor Film Dynamics

F.1 Heat Transfer From the Hot Sphere

The rate of heat transfer from the hot sphere is given by:

$$\frac{1}{4\pi R^2}\frac{dQ_h}{dt} = \frac{2k_h\ (T_{hi}-T_R)}{\lambda}\ . \qquad 4.6a$$

The heat flux is subject to the boundary condition

$$\frac{2k_h\ (T_{hi}-T_R)}{\lambda} = \frac{k_v\ (T_R-T_{\ell v})}{\delta}\ , \qquad 4.8b$$

where the notation is kept as given in chapter 4.

The difference in temperature $T_R-T_{\ell v}$ and the film thickness, δ, may be assumed approximately constant for a short period of time, t_o. Thus, the heat flux across the film may be considered constant in this small period of time.

Hence,

$$\frac{dQ_h}{dt} = \dot{Q}_h \text{ constant};\ t<t_o\ . \qquad F.1$$

By substituting from equation F.1 into equation 4.6a and differentiating with respect to time, the following relation between the rate of change of T_R and λ is obtained:

$$\frac{dT_R}{dt} = \frac{\dot{Q}_h}{4\pi R^2}\cdot\frac{1}{2k_h}\ \frac{d\lambda}{dt}\ . \qquad F.2$$

For short times $\lambda << R$, and hence equation 4.7a reduces to:

$$\frac{d\lambda}{dt} = \frac{6\alpha_h}{\lambda} - \frac{\lambda}{T_R - T_{hi}} \frac{dT_R}{dt} \quad . \qquad F.3$$

Substitution for $\frac{dT_R}{dt}$ from equation F.2 in equation F.3 gives:

$$\frac{d\lambda}{dt} = \frac{6\alpha_h}{\lambda} - \frac{\lambda}{T_R - T_{hi}} \cdot \frac{2k_h(T_{hi} - T_R)}{\lambda} \cdot \frac{1}{2k_h} \frac{d\lambda}{dt} \quad ,$$

which reduces to:

$$\lambda \frac{d\lambda}{dt} = 3\alpha_h \quad . \qquad F.4$$

Integrating equation F.4 gives:

$$\lambda = \sqrt{6\alpha_h t} \quad ; \; t < t_o \quad . \qquad F.5$$

Substituting for λ from equation F.5 into equation 4.6a and rearranging the resultant equation:

$$T_R = T_{hi} - \frac{Q_h \sqrt{6\alpha_h t}}{8\pi k_h R^2} \quad ; \; t < t_o \quad . \qquad F.6$$

F.2 Heat Transfer into the Cold Liquid

For short times $\Delta << R_\delta$, hence equation 4.15 reduces to:

$$\frac{d\Delta}{dt} = \frac{6\alpha_\ell}{\Delta} - \frac{\Delta}{T_{\ell v} - T_{\ell i}} \frac{dT_{\ell v}}{dt} + U - \frac{dR_\delta}{dt} \quad ; \; t < t_o \quad . \qquad F.7$$

Neglecting the velocity of the film/liquid interface that can be developed within time to;

$$\text{i.e.} \quad U = \frac{dR_\delta}{dt} = 0 \quad ; \; t<t_o \quad , \qquad \text{F.8}$$

equation F.7 reduces to:

$$\frac{d\Delta}{dt} = \frac{6\alpha_\ell}{\Delta} - \frac{\Delta}{T_{\ell v}-T_{\ell i}} \frac{dT_{\ell v}}{dt} \cdot \qquad \text{F.9}$$

For subcooled boiling most of the heat flux from the hot surface is conducted away from the film into the liquid. Assuming the heat flux from the sphere and the heat flux into the liquid are approximately equal, then

$$\frac{1}{4\pi R^2} \frac{dQ_h}{dt} = \frac{1}{4\pi R_\delta^2} \frac{dQ_\ell}{dt} \cdot \qquad \text{F.10}$$

Equation 4.16b yields:

$$\frac{1}{4\pi R_\delta^2} \frac{dQ_\ell}{dt} = \frac{2k\ (T_{\ell v}-T_{\ell i})}{\Delta} \cdot \qquad \text{4.16b}$$

Differentiating equation 4.16b with respect to time gives:

$$\frac{1}{2k_\ell} \cdot \frac{1}{4\pi R_\delta^2} \frac{dQ_\ell}{dt} \frac{d\Delta}{dt} = \frac{dT_{\ell v}}{dt} \cdot \qquad \text{F.11}$$

Using equation F.10, 4.16b and F.11, equation F.9 can be reduced to the form:

$$\Delta \frac{\delta\Delta}{\delta t} = 3\alpha_\ell \ .$$

which, when integrated gives

$$\Delta = \sqrt{6\alpha_\ell t} \; ; \quad t<t_o \qquad \text{F.12}$$

By substitution from equation F.12 into equation 4.16b, we obtain

$$T_{\ell v} = T_{\ell i} + \frac{\dot{Q}_h \sqrt{6\alpha_\ell t}}{8\pi k_\ell R^2} \; ; \; t<t_o \; . \qquad \text{F.13}$$

The starting values for the variables T_R, $T_{\ell v}$, λ, Δ, and U are determined from equations F.6, F.13, F.5, F.12 and F.8 respectively. The value of $R_\delta(o)$ is given by

$$R_\delta(o) = R + \delta_o \; , \qquad 5.14$$

where R is the sphere radius and δ_o is the optional initial film thickness.

The value of $P_f(o)$ is obtained using equation 4.36:

$$P_f(o) = P_g(o) + P(T_{\ell v}) \qquad 5.15$$

Appendix G

COMPARISON OF EXPERIMENTAL DATA TO THE PREDICTIONS OF VARIOUS CORRELATIONS FOR THE MINIMUM WALL TEMPERATURE TO STABILIZE FILM BOILING

In the past few years, several correlations have been advanced for the prediction of the minimum wall temperature required to stabilize film boiling at a heating wall, T^*. Table G.1 summarizes the proposed correlations. Berenson[95] obtained his correlation from a Tayler instability analysis of film boiling on a horizontal surface. Berenson's correlation shows that T^*_B (the subscript denotes the originator(s) of the correlation for predicting T^*) depends on the thermodynamic properties of the liquid but not the surface material. Spiegler et al.[111] based their analysis on a spontaneous nucleation theory and deduced that T^*_S is dependent only on the critical temperature of the liquid, T_{cr} Kalinin et al.[112] assumed that the film boiling stabilization requires a certain interface temperature to be obtained when the liquid and the heating wall get in contact. Hence, Kalinin et al. concluded that the ratio of the ρkc product of the liquid and the hot material is an important parameter for film boiling. Henry's[113] correlation is based on the assumption that the hydro-

Table G.1

Summary of Correlations for Prediction of Minimum Wall Temperature to Sustain Film Boiling, T^* †

Berenson	$T_B^* - T_{sat} = 0.127 \frac{\rho_{vf} h_{fg}}{k_{vf}} \left[\frac{g(\rho_\ell - \rho_v)}{\rho_\ell + \rho_v}\right]^{\frac{2}{3}} \left[\frac{g_c \sigma}{g(\rho_\ell - \rho_v)}\right]^{\frac{1}{2}} \left[\frac{\mu_{vf}}{g_c(\rho_\ell - \rho_v)}\right]^{\frac{1}{3}}$
Spiegler et al.	$T_S^* = 0.84\ T_{cr}$
Kalinin et al.	$\frac{T_K^* - T_{sat}}{T_{cr} - T_\ell} = 0.165 + 2.48 \left[\frac{(\rho kc)_\ell}{(\rho kc)_w}\right]^{0.25}$
Henry	$\frac{T_H^* - T_B^*}{T_B^* - T_\ell} = 0.42 \left[\sqrt{\frac{(\rho kc)_\ell}{(\rho kc)_w}}\ \frac{h_{fg}}{c_w(T_B^* - T_{sat})}\right]^{0.6}$

†1. The subscripts given to T^* in the correlations refer to the originator(s) of the correlation.
2. The engineering system of units is to be used in Berenson's correlation. Absolute temperatures are to be used in the correlation of Spiegler et al. The other correlations include only dimensionless parameters.
3. Properties with subscript vf are to be evaluated at the average temperature in the film.

dynamically determined T_B^* of Berenson is to be obtained at the interface as the liquid contacts the heating wall. Henry also assumed the influence of an evaporating microlayer of liquid adhering to the heating wall and hence deduced that $h_{fg}/c_w(T_B^* - T_{sat})$ is a significant parameter for film boiling.

Table G.2 summarizes some of the data reported in literature on the minimum temperature for stable film boiling, T^*, and Leidenfrost temperature, T_{Leid}. Baumeister et al.[127] have considered both temperatures and concluded T^* and T_{Leid} may be considered equivalent when T_{Leid} is determined from the evaporation rates of large saturated drops. The wall superheat, $T^* - T_{sat}$, determined from the data in Table G.2 and the superheat predicted by the different correlations are summarized in Table G.3. The predicted superheat of each correlation is compared to the experimental superheat on Figures G.1, G.2, G.3 and G.4. In Figure G.1 it is seen that, in general, Berenson's correlation underestimates the needed wall superheat for film stabilization. For sodium the needed superheat is underestimated by a factor as large as 15. Kalinin's correlation (Fig. G.3) shows a reverse trend by overestimating $T^* - T_{sat}$. The disagreement between the predictions and the experimental

data is again largest for sodium. Spiegler's correlation (Fig. G.2) shows better agreement with the experimental data than the correlations of Berenson and Kalinin et al., although the degree of scatter of the data remains appreciable. In Fig. G.4 it is seen that Henry's correlation shows a better agreement with the data than the other correlations, especially so for the sodium data. A clearer comparison with the sodium data of Farahat[89] is given in Fig. G.5. The correlation accurately predicts the trend of increasing wall superheat with subcooling in Farahat's experiments. The correlation is less accurate in describing the trend of the wall superheat in the Ag/H_2O experiments of Stevens et al.[88], as shown in Fig. G.6.

In conclusion, over a wide range of material combinations, Henry's correlation shows a better agreement with the experimental observations than the other available correlations.

Table G.2

Experimental Data on Minimum Wall Temperature to Stabilize Film Boiling, T^*

Data No.	Heating Surface Material	Liquid	Temperatures in °C					Symbols Used In Figures	
			Liquid Characteristic Termperatures		Experimental Data				
			T_{sat} (1 atm)	T_{cr}	T_ℓ	T^*	Ref.		
1	Cu	n-pentane	36	197	36	94	95	■	Saturated Liquid
2	Cu	CCl_4	77	283	77	157	95	▼	
3	SS	Benzene	80	288	80	185	126	▲	
4	SS	Ethanol	78	243	78	178	126	◆	
5	SS	Water	100	374	100	305	127	▶	
6	Al	Water	100	374	100	235	127	◀	
7	Ag	Water	100	374	24	406	88	▽	Subcooled Liquid
8	Ag	Water	100	374	60	266	88	▽	
9	Ta	Sodium	880	2300	849	1700	89	○	
10	Ta	Sodium	880	2300	859	1576	89	○	

Table G.3

Values of Predicted and Observed Wall Superheat for Data Summarized in Table G.2

Data No.	Superheat in °C				
	T^*-T_{sat}	$T^*_B-T_{sat}$	$T^*_S-T_{sat}$	$T^*_K-T_{sat}$	$T^*_H-T_{sat}$
1	58	54	85.7	68	72.5
2	80	90	117	92	96.8
3	105	54	118	161	73.5
4	100	55.8	82	138	94.0
5	205	78	170	341	214.5
6	135	78	170	211	126.0
7	306	78	170	241	265.0
8	166	78	170	217	222.0
9	820	53.5	1008	2692	905.0
10	696	53.5	1008	2674	803.6

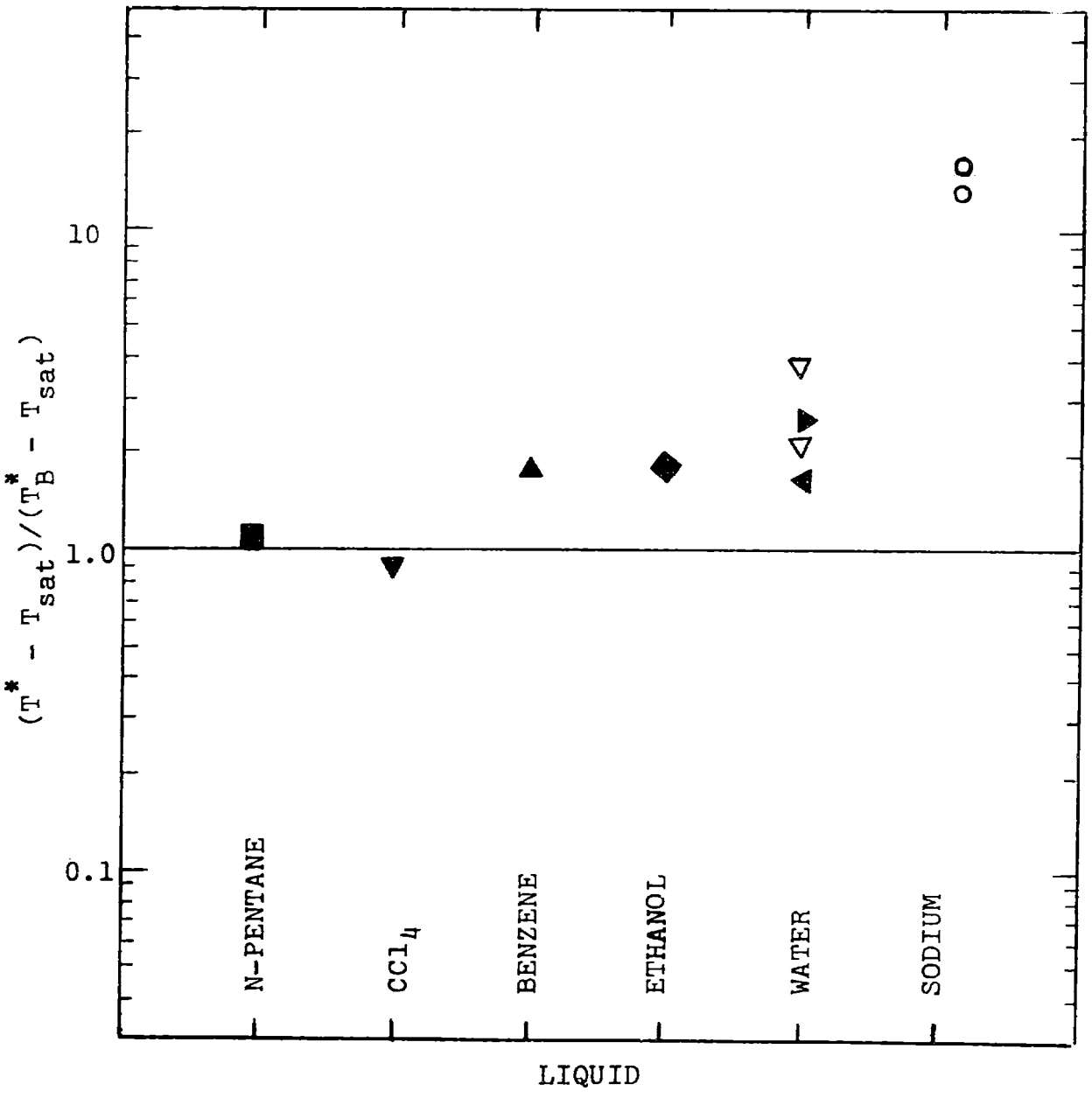

FIG. G.1: DATA FROM LITERATURE COMPARED TO PREDICTIONS OF BERENSON

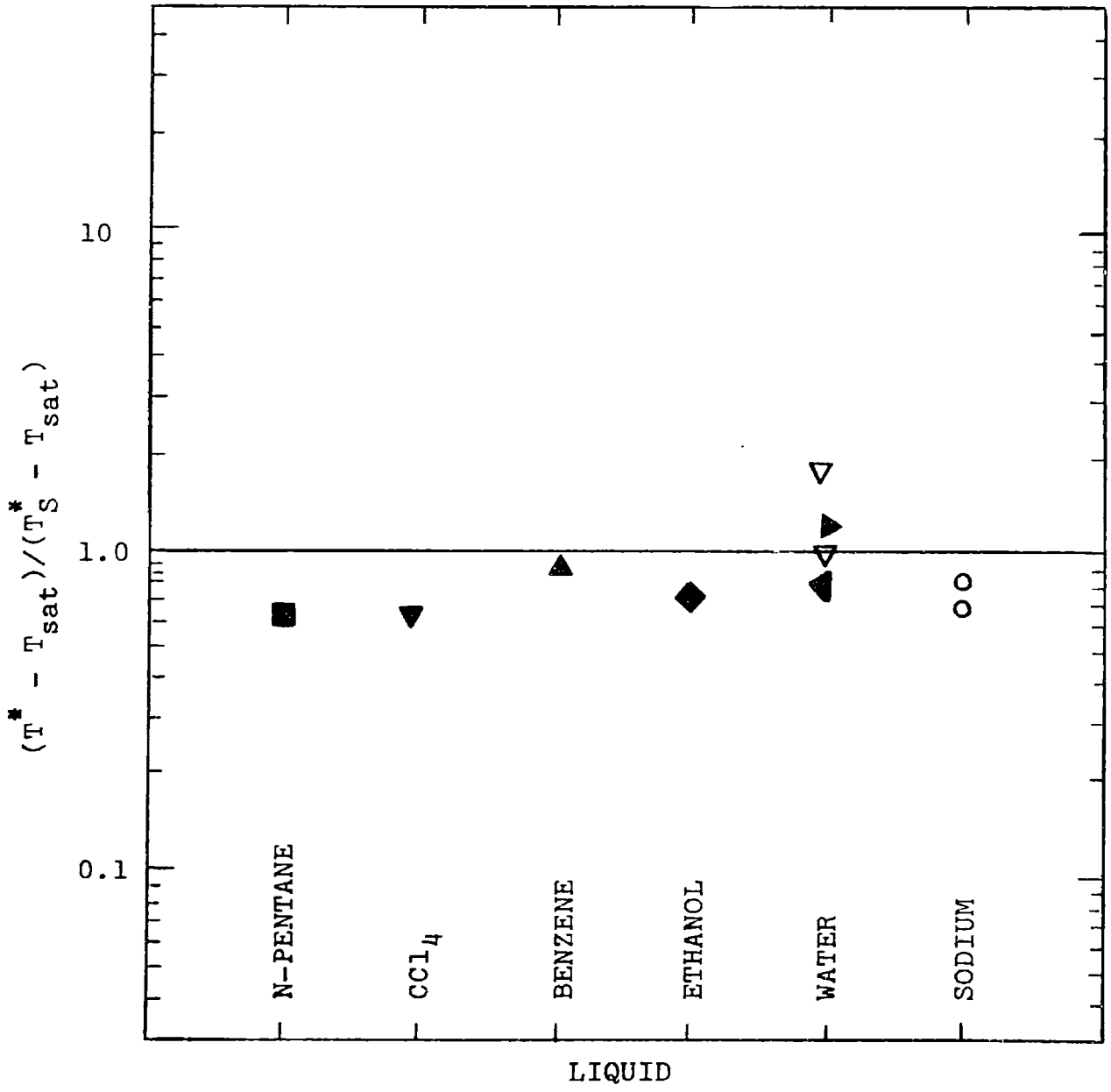

FIG. G.2: DATA FROM LITERATURE COMPARED TO PREDICTIONS OF SPIEGLER ET AL.

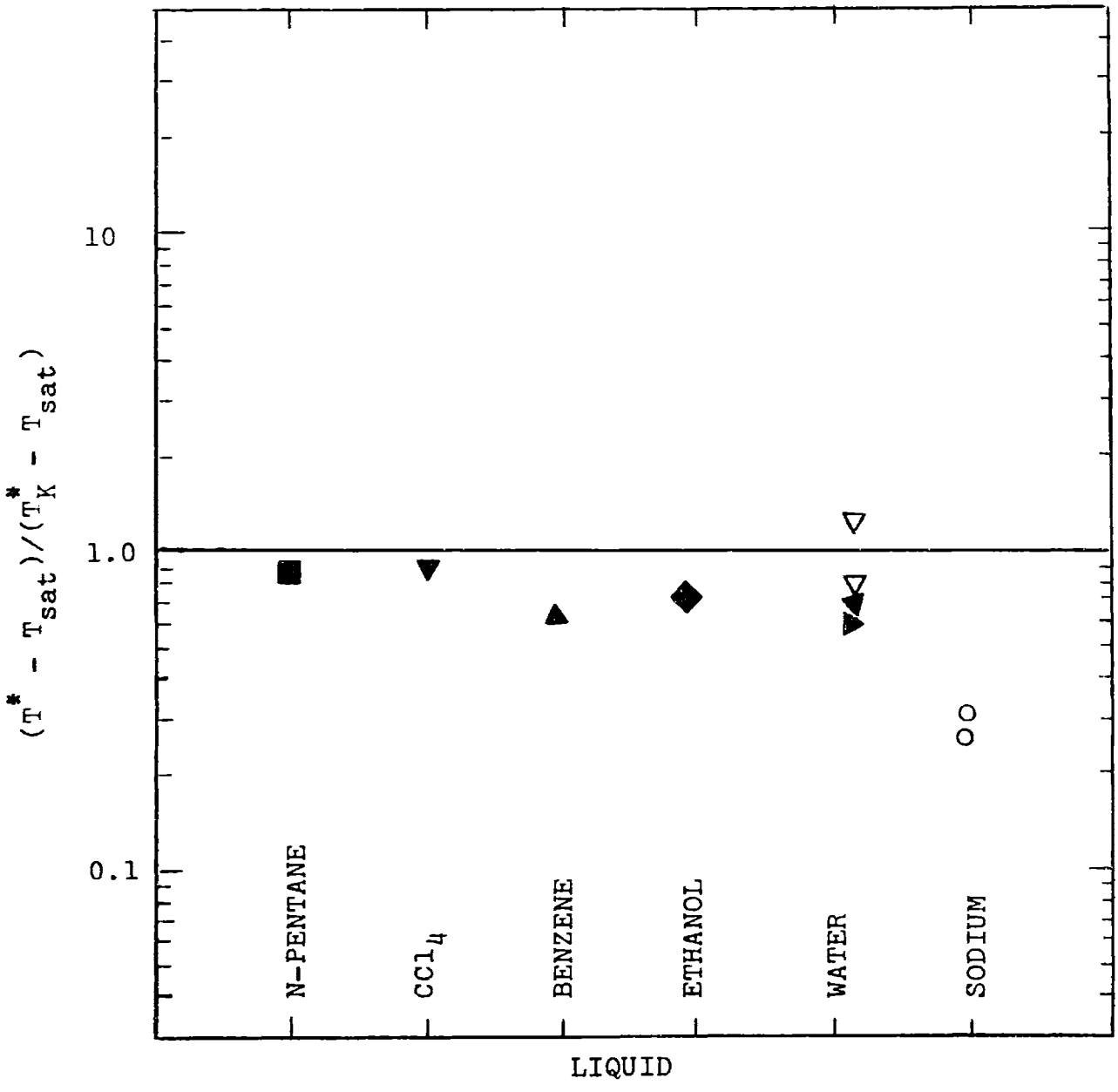

FIG. G.3: DATA FROM LITERATURE COMPARED TO PREDICTIONS OF KALININ ET AL.

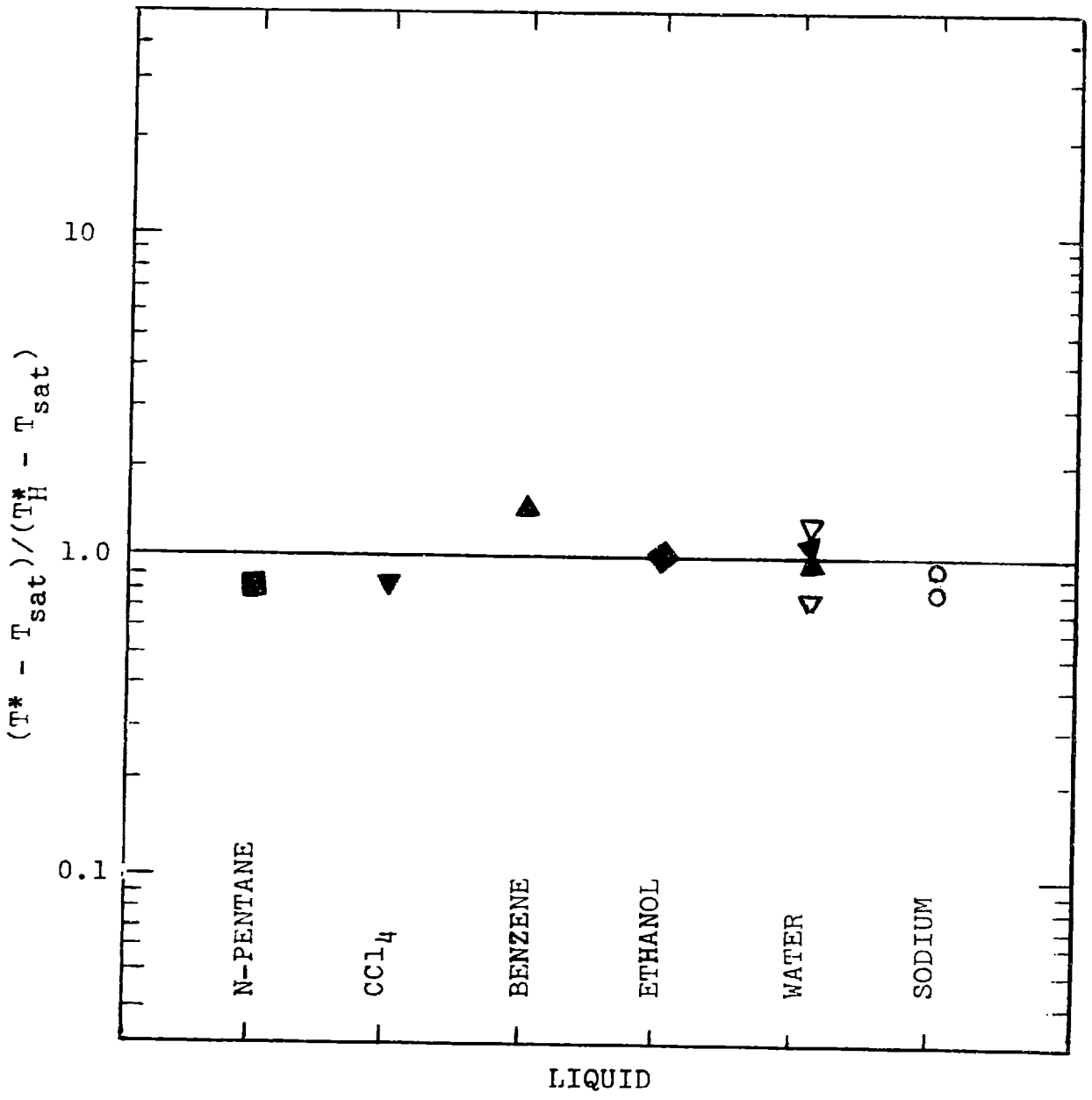

FIG. G.4: DATA FROM LITERATURE COMPARED TO PREDICTIONS OF HENRY

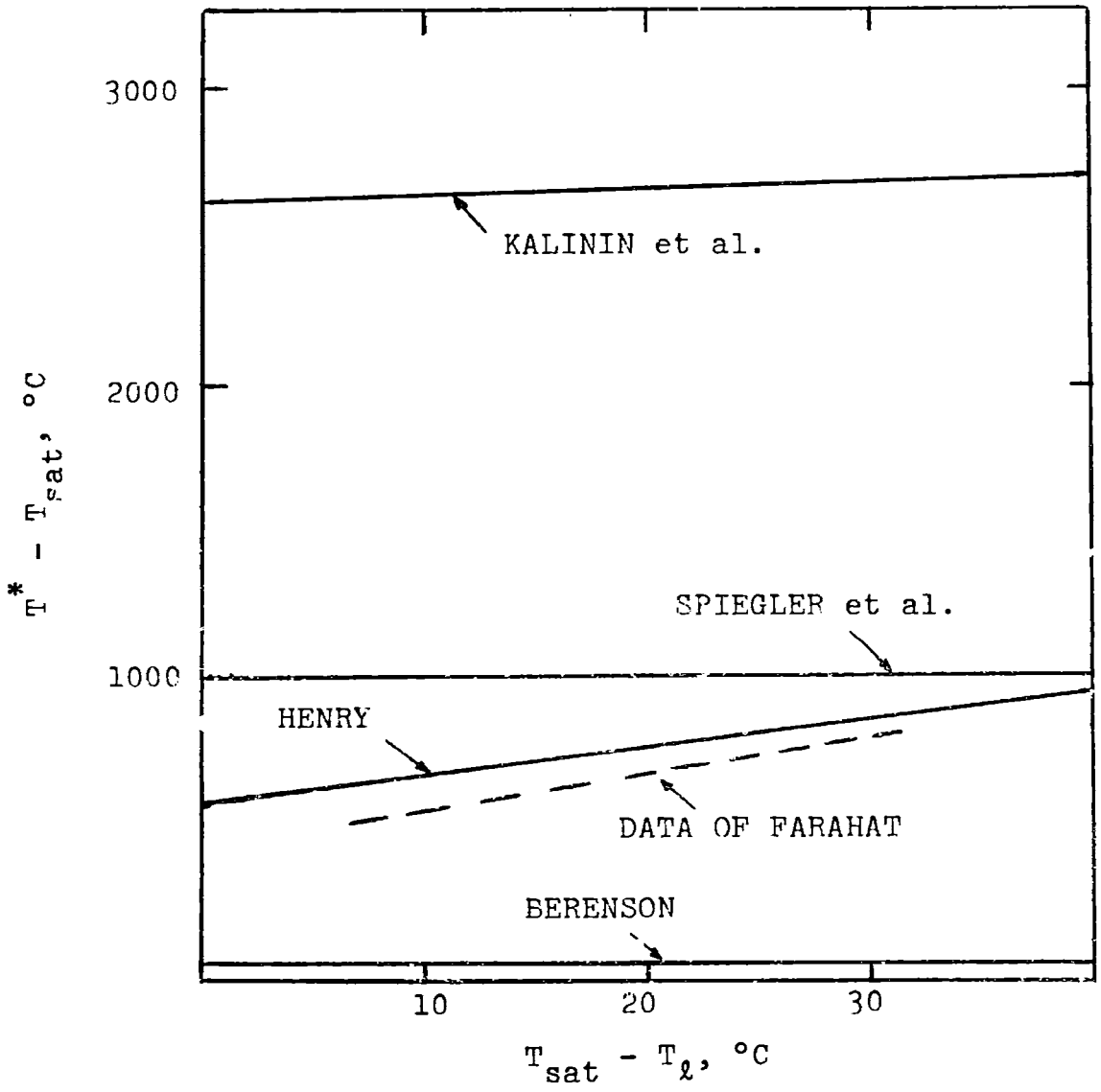

FIG. G.5: COMPARISON OF THE PREDICTION OF DIFFERENT CORRELATIONS WITH THE DATA OF FARAHAT FOR A Ta SPHERE IN SODIUM

FIG. G.6: COMPARISON BETWEEN THE PREDICTION OF THE DIFFERENT CORRELATIONS WITH THE DATA OF STEVENS ET AL. FOR A Ag SPHERE IN WATER

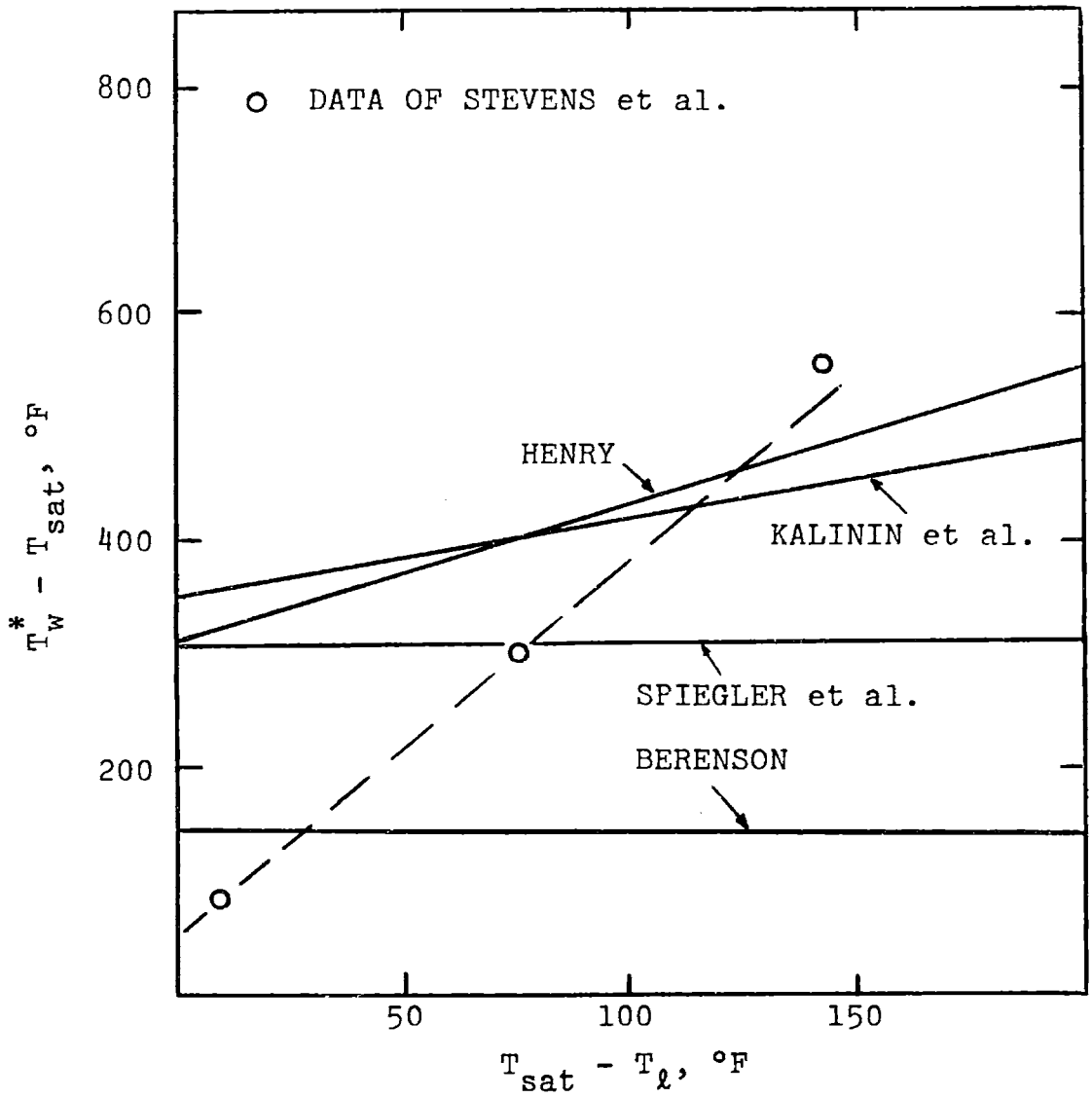

Appendix H

Nucleation in Liquids

When a liquid under normal pressure is heated beyond its saturation temperature in the absense of bounding walls with cavities, vapor bubbles appear in the bulk of the fluid at a certain temperature usually referred to as the spontaneous nucleation temperature. Vapor bubbles can be produced with the liquid at its original temperature by subjecting the liquid to negative (tensile) pressure. In this case, cavitation is said to have occurred.

A thermodynamic limit can be set for both processes by considering the equation of state of a pure real fluid (see for example Ref. 132, page 233) as illustrated in Fig. H.1. The curve abcdef represents an isotherm for a fluid at temperature T_1. Consider a liquid initially at the state b. By heating the liquid at constant pressure, the liquid approaches the point g beyond which the liquid temperature can not be increased at the same pressure. Therefore, the temperature T_2 is the thermodynamic limit for the temperature at which "spontaneous nucleation" would take place for a liquid at pressure P_1.

If the liquid, initially at b, is maintained at the temperature T_1 but its pressure is reduced, the liquid approaches the point c beyond which the pressure can not be further reduced at the same temperature. The negative pressure P_2 is then the thermodynamic limit for the "cavitation"

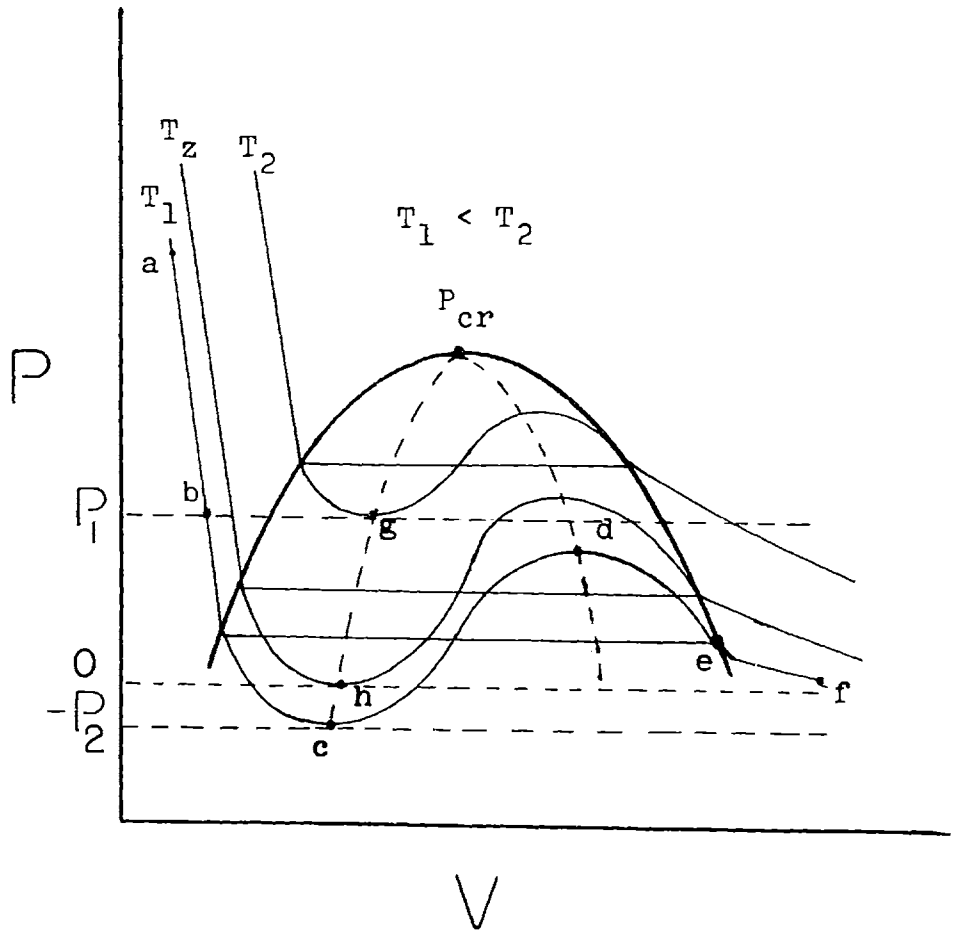

FIG. H.1: P-V-T DIAGRAM FOR A PURE FLUID

pressure for the liquid at the temperature T_1. The points g and c represent what Gibbs[133] called "the limit of essential instability", and are defined by

$$\left.\frac{\delta P(v,T)}{\delta v}\right|_T = 0 \ ,$$

where P(v,T) is the equation of state of the liquid.

The above approach to the estimation of the conditions at which vapor bubbles will appear in a liquid, by either spontaneous nucleation or cavitation, ignores the possibility of transient production of vapor nuclei by molecular thermal fluctuations in the liquid. The approach of Bernath[122] (based on work by Volmer[123]) for the determination of the limits of spontaneous nucleation and cavitation in liquids takes into account the probability of production of vapor nuclei at any temperature. Expressions given by Bernath are used here to estimate the required superheat for spontaneous nucleation and the required negative pressures for cavitation.

H.1 Spontaneous Nucleation Temperature, $T_{s.n.}$

At any temperature, T, the average number of vapor nuclei originated in a unit volume of the liquid per unit time, J, is given by:

$$J = \xi \left[\frac{6\sigma}{\pi m(3-b)}\right]^{1/2} e^{-\lambda/kT}\, e^{-W/kT} \quad , \qquad \text{H.2}$$

where ξ is the number of molecules of liquids per unit volume,

m is the mass of one molecule (gm),

σ is the surface tension (dyne/cm),

λ is the heat of vaporization of one molecule (erg),

k is Boltzman's constant (1.38×10^{-16} erg/^{o}K),

T is the absolute temperature of the liquid (^{o}K),

b is a pressure parameter defined by $b = (P_v - P_\ell)/P_v$, where P_v is the pressure in the nucleus and P_ℓ is the pressure in the liquid, and W is the work done in the formation of one nucleus.

W is given by:

$$W = \frac{16\ \pi\ \sigma^3}{3(P_v - P_\ell)^2} \qquad \text{H.3}$$

Equation H.2 can be rearranged to give the excess pressure $P_v - P_\ell$ required to produce J vapor nuclei at temperature T:

$$(P_v-P_\ell)^2 = \frac{16\pi\ \sigma^3}{3kT[\ell n\xi+1/2\ell n(6\sigma/\pi m(3-b)-\ell nJ]-3\lambda} \qquad H.4$$

For a unit volume of the liquid, the number of molecules is given by:

$$\xi = \frac{\delta A_v}{M} , \qquad H.5$$

where δ is the density (gm/cm^3), A_v is Avogadro's Number (0.6×10^{24} moleculer/gm-mole), and M is the molecular weight of the liquid (gm). The mass of the molecule is given by:

$$m = \frac{M}{A_v} . \qquad H.6$$

By substitution for ξ from equation H.5 and for m from equation H.6, equation H.4 may be written as:

$$(P_v-P_\ell)^2 = \frac{16\pi\ \sigma^3}{3kT[3/2\ell nA_v+1/2\ell n(6\sigma\rho^2/\pi M^2)-1/2\ell n(3-b)-\ell nJ]-3\lambda} \qquad H.7$$

Equation H.7 is a transcendental equation since b is a function of (P_v-P_ℓ) also. However, for practical purposes, spontaneous nucleation takes place at high values of P_v such that

$$b = \frac{P_v-P_\ell}{P_v} \approx 1 . \qquad H.8$$

Additionally, the value of $6\sigma\rho^2/\pi M^2$ for the temperature range of interest in sodium and water may be taken as

0.35. Equation H.7 is then simplified to:

$$(P_v - P_\ell)^2 = \frac{16\pi\sigma^3}{3kT[1.5\ell nA_v - \ell nJ - 1.35] - 3\lambda} \quad . \qquad \text{H.9}$$

To determine the temperature T that satisfies equation H.9, we assume the pressure of the vapor P_v is that of saturation at the prevailing liquid temperature. Thus, for a liquid pressure P_ℓ of 1 atm, and a vapor current, J, of 10^6 nuclei/cm^3 sec equation H.9 may be given as:

$$[P_v(T) - 1] = \sqrt{\frac{16.3\sigma^3}{9.11\times10^{-15}T - \lambda}} \times 10^{-16} \text{ atm.} \qquad \text{H.10}$$

For sodium, λ and σ are given by

$\lambda \simeq 1.68\times10^{-12}$ erg, and

$\sigma = 234 - 0.1T$ dyne/cm.

The saturation pressure is calculated from the Stone's equation[81].

$$P_v(T) = T^{-0.61344} \exp(15.3828 - 12767.8/T), \qquad \text{H.11}$$

where $P_v(T)$ is in atmospheres.

The spontaneous nucleation temperature is determined by equating $P_v(T)$ from H.11 to $P_v(T)$ from H.10 (see Fig. H.2) thus giving

$$T_{s.n.}(1 \text{ atm}) = 1850°C \ .$$

For water, λ and σ are given by:

$\lambda = 0.82\times10^{-12}$ erg, and

$\sigma = 153.4 - 0.237$ T dyne/cm.

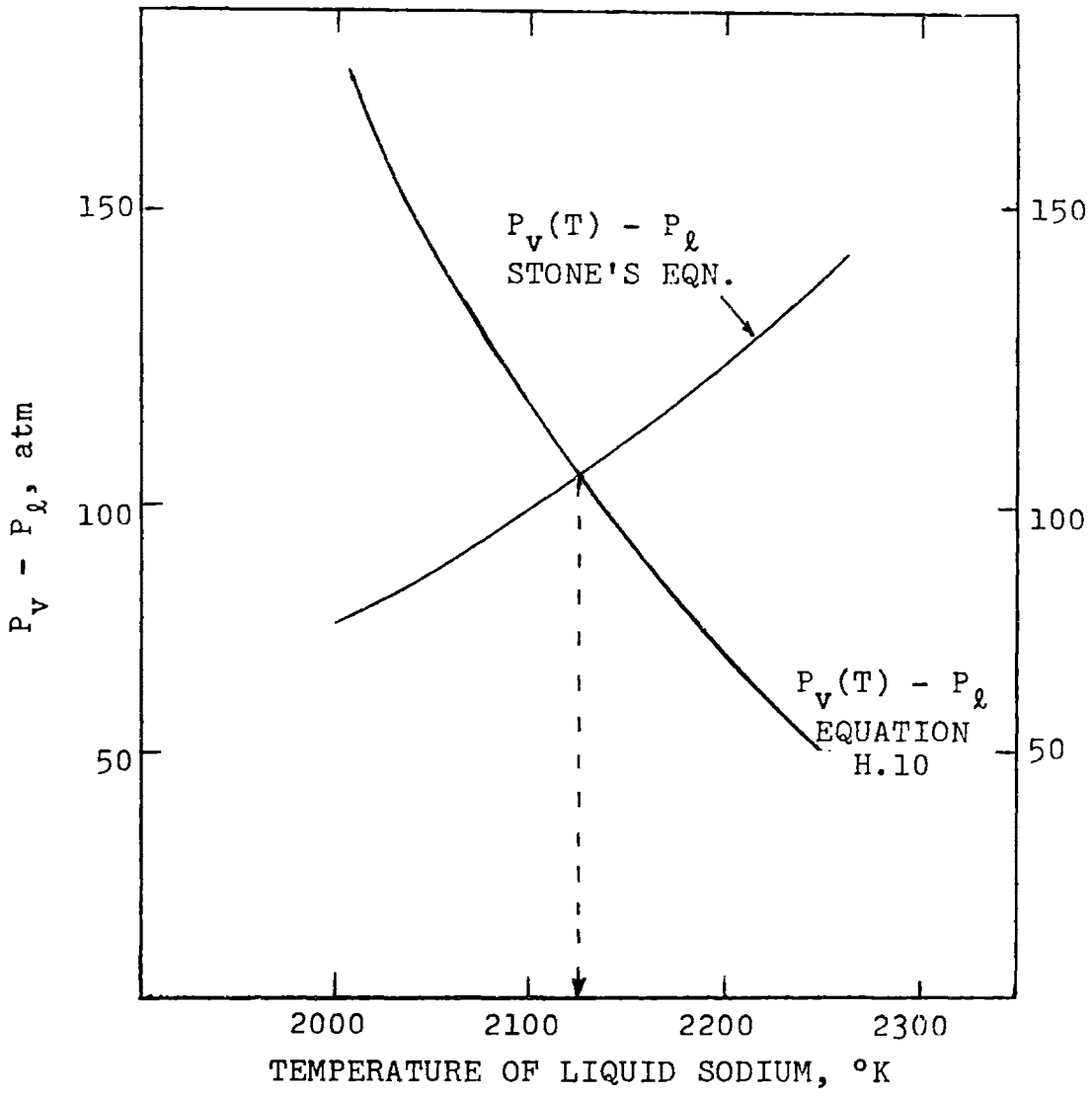

FIG. H.2: DETERMINATION OF THE SPONTANEOUS NUCLEATION TEMPERATURE OF SODIUM (P_ℓ = 1 atm)

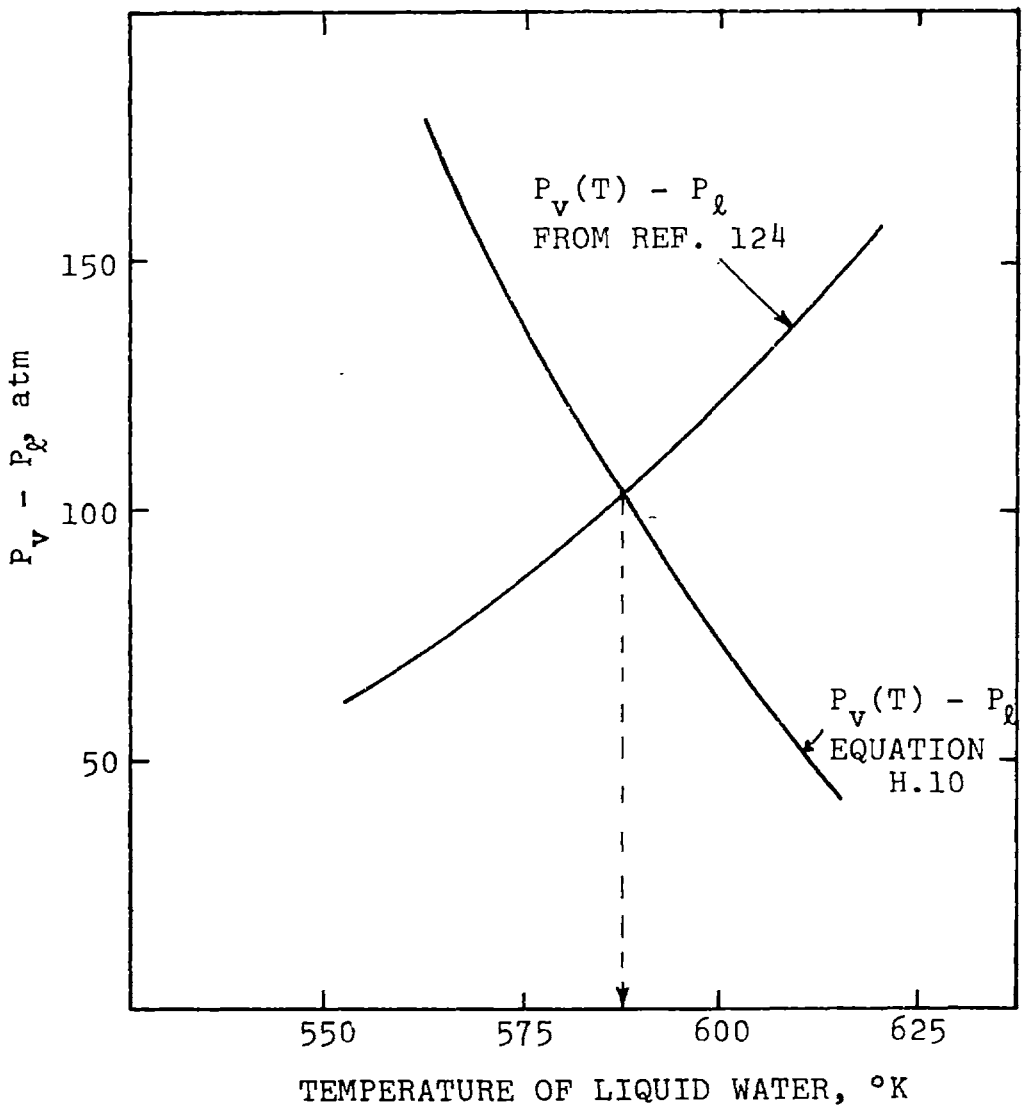

FIG. H.3: DETERMINATION OF THE SPONTANEOUS NUCLEATION TEMPERATURE OF WATER (P_ℓ = 1 atm)

The saturation pressure is obtained from Ref. 124. The spontaneous nucleation temperature is determined to be

$$T_{s.n.}(1 \text{ atm}) = 314°C$$

H.2 Cavitation Pressures

The following expression has been obtained by Bernath[122] for the minimum negative pressure required, theoretically, to induce cavitation in liquids:

$$\gamma_\ell = \left[\frac{9.06\ \sigma^3/kT}{\ell n \dfrac{1.45\delta A_v^2\ \sigma^2}{\gamma_{\ell M}{}^{3/2}\ GT} - \dfrac{\lambda}{kT}} \right]^{1/2} \qquad \text{H.12}$$

where γ_ℓ is the absolute value of the required negative pressure (dyne/cm^2),

ρ is liquid density (gm/cm^3),

G is the universal gas constant (erg/°K),

and the other symbols as defined above.

Using equation H.12, the values of the theoretically required negative pressure for cavitation in materials used in the fragmentation experiments are shown in Table H.1. Where existing, the experimental values of the maximum negative pressure that have been experimentally sustained in the liquids are shown also. It is clear that the theoretical values greatly exceed the experimentally observed ones. It is usually suggested that small amounts of impurities or dissolved gases act as sites for nucleation, thus reducing the negative pressures required to fracture the liquids under

practical conditions.

TABLE H.1

Values of Negative Pressures Required for Cavitation

Material	Melting Point °C	Cavitation Pressure, atm		
		Temperature °C	Calculated Eqn H.12	Experimental Maximum*
H_2O	0.0	20	- 1,039	- 281
Hg	-38.87	300	- 11,900	- 460
Sn	232	500	- 24,500	---
Bi	271	500	- 10,500	---
Pb	327	500	- 14,200	---
Al	660	800	- 35,000	---
Ag	961	1000	- 30,800	---
Au	1083	1100	- 44,800	---

*Reference 119

It should be noted that equation H.12 is valid only if the liquid is at a temperature lower than the temperature T_z, for which a zero pressure would be enough to produce cavitation (see Fig. H.1). The thermodynamic limit for the temperature T_z may be determined from the state equation of the liquid by requiring the two conditions:

$$\left.\frac{\delta P(v,T)}{\delta v}\right|_T = 0, \text{ and} \qquad \text{H.13}$$

$$P(v,T) = 0 \qquad \text{H.14}$$

be satisfied simultaneously.

If the Van Der Wall's equation is used as an approximate state equation for the liquid, then the P-v-T relation is given by

$$P = \frac{GT}{v-b} - \frac{a}{v^2} \quad , \qquad \text{H.15}$$

where G is the gas constant, and a, b are constants that are related to the critical properties of the fluid by:

$$a = \frac{27GbT_{cr}}{8}, \text{ and} \qquad \text{H.16}$$

$$b = v_{cr}/3 \ . \qquad \text{H.17}$$

When the condition H.13 is applied to equation H.15 we obtain

$$P^* = \frac{a}{v^{*2}}\left(1 - \frac{2b}{v^*}\right) \ , \qquad \text{H.18}$$

where P* and v* are the pressure P and the volume v at the point where $\frac{\delta P}{\delta v} = 0$. When the condition H.14 is applied to P* as given in equation H.18 we get

$$v^* = 2b \ . \qquad \text{H.19}$$

By substituting from equation H.19 into equation H.15 and applying the condition H.14 we get

$$P = 0 = \frac{GT_z}{b} - \frac{a}{4b^2} \ ,$$

which can be rearranged to:

$$T_z = \frac{a}{4Gb} \ . \qquad \text{H.20}$$

When the value of the constant "a" from equation H.16 is substituted in equation H.20 the value of T_z is determined to be

$$T_z = \frac{27}{32} T_c \ . \qquad \text{H.20}$$

The temperature T_z is the maximum liquid temperature for which equation H.12 can be applied. The temperatures at which the cavitation pressures were calculated for different materials in Table H.1 are all below the respective limiting values of T_z.

Appendix I

PROPERTIES OF MATERIALS

I.1 Properties Used in Chapter 3

I.1.a Temperature Dependent Thermophysical Properties of Sodium Unsed in Chapter 3

The properties of sodium used in the model for fragmentation-induced vapor explosions of Chapter 3 are the same values that were incorporated in the Parametric Model for Fuel-Coolant Interaction.[14,79] These properties are based on the values recommended by Golden and Takar.[81] The properties are defined by the following expressions. (The temperature, T, in the following is in °K)

A) On-Phase Liquid Sodium

1. The specific heat at constant pressure, $C_{p\ell}$:

$$C_{p\ell}(\text{cal/gm °K}) = 0.389352 - 1.99078 \times 10^{-4}T + 11.0542 \times 10^{-8}T^2 \qquad \text{I.1}$$

2. The thermal expansion coefficient, α':

$$\alpha'(°K^{-1}) = 0.21968 \times 10^{-3} + 0.81226 \times 10^{-7}T + 0.97135 \times 10^{-11} + 0.68998 \times 10^{-15}T^3. \qquad \text{I.2}$$

3. The isothermal compressibility β:

$$\beta_\ell(°K^{-1}) = \beta^s + \frac{V\ T\ (\alpha')^2}{C_{p\ell}}\ , \qquad \text{I.3}$$

where

$$\beta^s(°K^{-1}) = 0.69651 \times 10^{-5} + 0.26741 \times 10^{-7} T - 0.14891 \times 10^{-10} T^2 + 0.82082 \times 10^{-14} T^3. \qquad \text{I.4}$$

B) Two-Phase Sodium

1. Saturation pressure, P:

$$P(atm) = T^{-0.61344} \exp\left[15.3828 - \frac{12767.8}{T}\right] \qquad \text{I.5}$$

2. Saturated liquid and vapor enthalpies, H_ℓ and H_v:

$$h_\ell(cal/gm) = -0.9213 \times 10^3 + 1.9434T - 0.1051 \times 10^{-2} T^2 + 0.22418 \times 10^{-6}\ T^3 \qquad \text{I.6}$$

$$h_v(cal/gm) = 0.18605 \times 10^4 - 1.4691\ T + 0.10381 \times 10^{-2}\ T^2 - 0.23238 \times 10^{-6}\ T^3 \qquad \text{I.7}$$

3. The specific volume of the liquid, V_ℓ:

$$V_\ell(cm^3/gm) = V_{\ell o} \exp\left[\int_{T_{\ell o}} \alpha'\ d\ T\right], \qquad \text{I.8}$$

where α' is given above, and $V_{\ell o}$ is a reference

specific volume at the reference temperature $T_{\ell o}$. For the cases of Chapter 3 $T_{\ell o}$ = 1100°K and $V_{\ell o}$ = 1.35 cm^3/gm.

4. The specific volume of the Vapor, V_v

$$V_v = \frac{B_v G_v T_b}{P}$$, where

$$B_v = -0.97258 + 0.421417 \times 10^{-2} T - 0.28996 \times 10^{-5} T^2 + 0.55424 \times 10^{-9} T^3$$

and

G_v = 3.565 cm^3 - atm/°K gm, gas constant for 1 gm of vapor, I.10

and T_b is defined by equation 3.9.

I.1.b Other Properties Used in Chapter 3

Thermal conductivity of the gaseous blanket,

$k_b = 1.64 \times 10^{-4}$ cal/cm °K sec

Thermal conductivity of the fuel,

k_f = 0.005 cal/cm °K sec

Density of the fuel,

$\rho_u = 9.8\ cm^3/gm$

Speficif heat of the fuel,

C_u = 0.121 cal/gm °K

Adiabatic index of the non-condensable gas,

n = 1.4

Speed of sound in 1100°K sodium

$C_o = 2.15 \times 10^5$ cm/sec

Density of liquid sodium at 1100°K,

$\rho_o = 0.74$ gm/cm^3.

I.2 Properties Used in Chapter 4

In the model of Chapter 4, temperature-independent properties of both the hot spheres and the liquid coolants are used. The values of the thermal conductivity and thermal diffusivity of the material are taken to be those at an intermediate temperature in the range of temperature in the considered cases. These values are summarized in Table I.1. Other properties of water and sodium used in Chapter 4 are as follows:

Property	Water	Sodium
1. Density, ρ (gm/cm^3)	1.0	.83
2. Sound velocity in liquid, C_∞ (cm/sec)	1.49×10^5	2.5×10^5
3. Thermal conductivity of vapor, k_v (cal/cm °C sec)	9×10^{-5}	1.5×10^{-4}
4. Latent heat of vaporization, h_{fg} (cal/gm)	545.	930.

For water, the saturation pressure is taken to be given by the integral of the Clausius-Clapeyron equation (Ref. 131 page 217):

$$P(T) = 14.7 \exp\left[\frac{h_{fg}}{0.1103}\left(\frac{1}{373} - \frac{1}{T}\right)\right] \text{ psi} \qquad \text{I.11}$$

For sodium, equation I.5 is used to define the saturation pressure.

The constants of the equation 4.32 were taken to be: For water[98] $B = 4.4 \times 10^4$ psi, $m = 7$, and for sodium[101] $B = 6 \times 10^4$ psi, $m = 7$, the adiabatic gas constant, $n = 1.4$.

Table I.1

Values of the Thermal Conductivity and Diffusivity of Material used in Chapter 4

Property \ Material	Liquid		Hot Sphere			
	H_2O	Sodium	Sn	AgCl	SS	UO_2
Thermal Conductivity k(cal/cm °C sec)	.0012	.132	.08	.09	.035	.005
Thermal Diffusivity $\alpha(cm^2/sec)$	.0012	.573	.17	5.5×10^{-3}	.038	.005

Fig. I.1 Surface Tension of Molten Metals (Ref. 134)

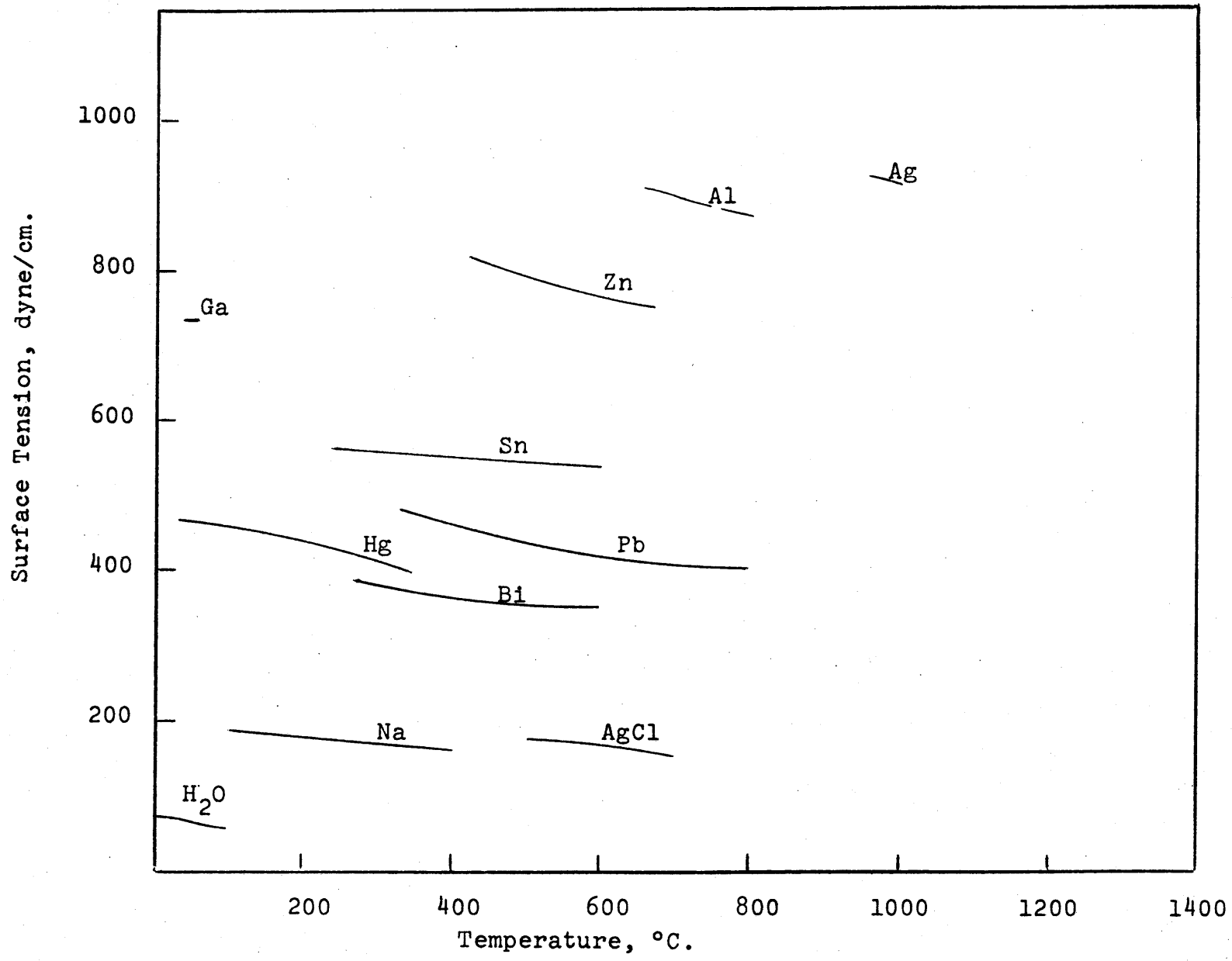

REFERENCES

1. C.N. Kelber et al., "Safety Problems of Liquid-Metal-Cooled Fast Breeder Reactors", ANL-7657, Feb. 1970.

2. F.R. Farmer et al., "An Appreciation of Fast Reactor Safety (1970)", UKAEA, Safeguards Division, A.S.H.B., NP-18487, 1970.

3. J. Graham, Fast Reactor Safety, Academic Press, New York, 1971.

4. E.P. Hicks and D.C. Menzies, "Theoretical Studies On The Fast Reactor Maximum Accidents", in Proc. Conf. Safety, Fuels and Core Design in Large Fast Power Reactors, ANL-7120, October 1965.

5. D.R. Armstrong, "Reactor Development Program Progress Report - February 1972", ANL-RDP-2, 8.31-8.32, March 1972.

6. G. Long, "Explosion of Molten Aluminum in Water - Cause and Prevention", Metal Progress 71, 107-112, May 1957.

7. R.O. Ivins and L. Baker, "Chemical Engineering Division Semiannual Report, January - June 1964", ANL-6900, 270-280, Aug. 1964.

8. L.C. Witte and J.E. Cox, "Nonchemical Explosive Interaction of LNG and Water", ASME 71-WA/HT-31, 1971.

9. E. Nakanishi and R.C. Reid, "Liquid Natural Gas-Water Reactions", Chem. Eng. Prog. 67 No. 12, 36-41, Dec. 1971.

10. T. Enger et al., "Explosive Boiling of Liquified Hydrocarbon Water Systems", Paper presented at Cryogenic Engineering Conference, Boulder, Colorado, August 1972.

11. H.K. Fauske, "The Role of Nucleation in Vapor Explosions", Trans. Am. Nucl. Soc. 15(2), p 813, Nov. 1972.

12. D. Armstrong and D. Cho, "LMFBR Nuclear Safety Program Annual Report", ANL-7800, 340-358, July 1971. Also see ANL-7765, 117-119, Dec. 1970.

13. M. Amblard et al., "Contact Effects Between Molten UO_2 and Sodium and Molten UO_2 and Water", EURFNR-811, March 1970.

14. D. Cho et al., "Pressure Generation by Molten Fuel-Coolant Interactions Under LMFBR Accident Conditions", Proc. Conf. New Developments in Reactor Mathematics and Applications, Idaho Falls, Idaho, March 1971, Conf-710302.

15. H.J. Teague,"Summary of the Papers Presented at the CREST Meeting on Fuel-Sodium Interaction at Grenoble in January 1972 and Report of Conference Papers 38a-k on Fuel-Sodium Interactions", Presented at Int. Conf. Engineering of Fast Reactors for Safe and Reliable Operation, Karlsruhe, Oct. 1972.

16. J. Percy, Metallurgy p 625, J. Murray, London, 1864.

17. S.G. Lipsett, "Explosions From Molten Materials and Water", Fire Technology 2, 118-126, May 1966.

18. L.F. Epstein, "Metal-Water Reactions: VII Reactor Safety Aspects of Metal-Water Reactions", GEAP-3335, Jan. 1960.

19. L.C. Witte et al., "The Vapor Explosion", J. of Metals 39-44, Feb. 1970.

20. T.J. Thompson, "Accidents and Destructive Tests", in The Technology of Nuclear Reactor Safety Vol 1, Ed. T.J. Thompson and J.G. Beckerley, M.I.T. Press, Cambridge, Ma., 1964.

21. D.G. Hurst, "The Accident of the NRX Reactor, Part II", AECL No. 233, reprinted Feb. 1956.

22. J.R. Dietrich, "Experimental Determination of the Self-Regulation and Safety of Operating Water-Moderated Reactors", Proc. Int. Conf. on Peaceful Uses of Atomic Energy Vol 13, 88-101 (see also p 125), 1955.

23. J.H. Kittel el al., "The EBR-I Meltdown Physical and Metallurgical Changes in the Core", Nucl. Sci. Eng. 4, 180-199, 1958.

24. "Final Report of SL-1 Recovery Operation", IDO-19311, July 1962.

25. R.W. Moller et al., "Report on the SPERT-I Destructive Test Program on an Aluminum, Plate-Type, Water-Moderated Reactor", IDO-16883, June 1964.

26. S.M. Zivi et al., "Kinetic Studies of Heterogeneous Water Reactors - Annual Summary Report 1964", STL 372-13, 45-68, TRW Space Technology Laboratories, Dec. 1964.

27. J.O. Elgert and A.W. Brown, "In-Pile Molten-Metal Water Reactions", IDO-16257, June 1956.

28. H.M. Higgins, "A Study of the Reaction of Metal and Water", AECD-3664, April 1955 and "The Reaction of Molten Uranium and Zirconium Alloys With Water", Aerojet General Report AGC-AE-7, 1965.

29. E.F. Epstein, "Metal Water Reactions: VI Analytical Formulations for the Reaction Rate", GEAP-3272, Sept. 1959.

30. P.D. Hess and K.J. Brondyke, "Molten Aluminum Water Explosions, Metal Progress, 93-100, April 1969.

31. J.A. Sallack, "On Investigation of Explosions in the Soda Smelt Dissolving Operation", Canadian Pulp and Paper Association Meeting, Quebec, Canada, June 6-8, 1955.

32. S.M. Zivi et al., "Kinetic Studies of Heterogeneous Water Reactors", Annual Summary Report 1963, STL-6312, 5-49; Annual Summary Report 1964, STL-372-13, 5-44; Annual Summary Report 1965, STL-372-30, 7-23.

33. R.W. Wright, "Pressure Pulses in Rapid Transient Boiling", Trans. Am. Nucl. Soc. 6 (2), p 338, Nov. 1963 and also in STL-6312, 50-70, TRW Space Technology Laboratories, Dec. 1963.

34. R.W. Wright, "Kinetic Studies of Heterogeneous Water Reactors, Annual Summary Report 1965", STL-372-30, TRW Systems, Dec. 1965 and "Annual Summary Report 1966", STL-372-50, Dec. 1966.

35. D. Swift and J. Pavlik, "Chemical Engineering Division Semiannual Report, July-December 1965", ANL-7125, 187-193 May 1966.

36. "Reactor Development Program Progress Report, January 1966", ANL-7152, 90-96, Feb. 1966.

37. As reported in "Core Design Developments Needs in Relation to Fuel Failure Propagation, Sodium Boiling and Clad/Fuel-Sodium Thermal Interaction", GEAP-13639-2, 770-774, October 1970.

38. R.O. Ivins, "Reactor Development Program Progress Report, Nov. 1967", ANL-7399, 162-165, Dec. 1967.

39. D. Cho, Private Communications, January 1972.

40. J.O. Hinze, "Fundamentals of the Hydrodynamic Mechanism of Splitting in Dispersion Processes", A.I.Ch.E. Journal 1 3 pp 289-295, Sept. 1955. Also "Forced Deformations of Viscous Liquid Globules", App. Sci. Research A1, 263-288, 1948.

41. J.W. Westwater, Advances in Chemical Engineering Vol. 1, Academic Press, New York 1957.

42. F.E. Brauer, et al., "Metal/Water Explosions", Nucl. Sci. Eng. 31, 551-554, March 1968.

43. K. Flory, et al., "Molten Metal-Water Explosions", Chem. Eng. Progress 65, 50-54, Dec. 1969.

44. P. Grouveld, "Explosive Vapor Formation", Trans. ASME J. Heat Transfer, 236-238, May 1972.

45. L.C. Witte et al., "Rapid Quenching of Molten Metals", ORO-3936-6, August 1971.

46. R.H. Bradley et al., "Investigation of the Vapor Explosion Phenomena Using a Molten-Metal Jet Injection Into Distilled Water", ORO-3936-7, October 1971.

47. J.W. Stevens et al., "Transient Film and Transition Boiling From a Sphere", ORO-3936-9, September 1972.

48. S.J. Board et al., "Fragmentation in Thermal Explosions", Central Electricity Generating Board Report RD/B/N2423, Oct. 1972.

49. R. Anderson and L. Bova, "Experimental Investigation of Vapor Explosions in a Molten Salt-Water System", Trans. Am. Nucl. Soc. 14 (1), p 236, June 1971.

50. R. Anderson and D. Armstrong, "Laboratory Tests of Molten-Fuel-Coolant Interactions", Trans. Am. Nucl. Soc. 15 (1), p 313, June 1972.

51. R.C. Liimatainen and F.J. Testa, "Chemical Engineering Division Semiannual Report, July-December 1965", ANL-7125, 170-178, May 1966.

52. R.W. Miller and W.G. Lussie, "Power Bursts in Zircaloy-2 Clad Oxide Fuel Rods", Trans. Am. Nucl. Soc. 12 (1), 344-346, 1969.

53. Z.R. Martinson, "Behavior of 5-Inch Long, 1/4-Inch OD, Zircaloy-2 Clad Oxide Fuel Rods Subjected to High Energy Power Bursts", IN-ITR-107, August 1969.

54. C.E. Dickerman, "Studies of Fast Reactor Core Behavior Under Accident Conditions", Nuclear Safety 11, 195-205, May-June 1970.

55. J.J. Barghusen et al., "LMFBR Nuclear Safety Program Annual Report", ANL-7800, 321-339, July 1971.

56. R.W. Wright et al., "Reactor Development Program Progress Report, June 1971", ANL-7833, p 8.23, July 1971.

57. R.W. Wright et al., "Reactor Development Program Progress Report, August 1971", ANL-7854, 8.19-8.21, September 1971.

58. J.J. Barghusen, "Reactor Development Program Progress Report, March 1972", ANL-RDP-3, 8.34-8.38, April 1972.

59. C.E. Dickerman, et al., "Fuel Dynamics Experiments On Fast Reactor Oxide Fuel Performance Under Transient Heating Conditions Using the TREAT Reactor", Trans. Am. Nucl. Soc. Supplement No. 1 to Volume 14, p 28, April 1971.

60. A.E. Klickman, "Summary of Energy Release Analyses of the Hypothetical Meltdown Design Accident for Core A of the Enrico Fermi Reactor", APDA-LA-7, July 1969.

61. A.M. Judd, "Calculation of the Thermodynamic Efficiency of Molten-Fuel-Coolant Interactions", Trans. Am. Nucl. Soc. 13 (1), p 369, 1970.

62. A. Padilla, "Analysis of Mechanical Work Energy for LMFBR Maximum Accidents", Nucl. Technology 12 No. 4, 348-355, Dec. 1971.

63. H. Pfefferlen, "Analytical Evaluation of the Consequences of a Hypothetical Instantaneous Loss of Coolant Flow to a Fast Flux Test Facility Driver Fuel Assembly", Compiled by L.M. McWethy, GEAP-10059, July 1969.

64. L.C. Biasi et al., "Heat Transfer and Fluid Dynamics of Fuel-Sodium Interaction", Paper presented at the International Center for Heat and Mass Transfer, Trogior, Yogoslavia, Sept. 1971.

65. A. Padilla, "Transient Analysis of Fuel-Sodium Interaction", Trans. Am. Nucl. Soc. 13 (1), p 375, 1970.

66. D. Cho et al., "Effects of Gas/Vapor Blanketing On Pressure Pulses and Mechanical Work Produced By Molten Fuel-Coolant Interactions", Trans. Am. Nucl. Soc. 15 (1), p 314, 1972.

67. R.B. Duffy, "Channel Voiding Due to Fuel-Coolant Interactions in Sodium Cooled Fast Reactors", CEGB Report RD/B/N 1609, 1970.

68. J. Randles, "A Thermodynamic Model For The Theoretical Study of Boiling and Ejection of the Coolant From a Reactor Channel Due To Direct Contact With Hot Molten Fuel", EUR-4592e, 1971.

69. I. Puig and A. Szeless, "Evaluation De La Production De Vapeur Au Cours De La Dispersion Du Combustible Chaud Dans Du Sodium", Paper presented at the CREST Meeting on Fuel-Sodium Interaction at Grenoble, France, January 1972.

70. L. Caldarola, "A Theoretical Model for the Molten-Fuel-Sodium Interaction in a Nuclear Fast Reactor", Nucl. Eng. Design 22 (2), 175-211, October 1972.

71. M.D. Carelli, "Fission Gas and Molten Fuel Ejection From Failed Fuel Rods in an LMFBR", Proc. Conf. New Developments in Reactor Mathematics and Applications, Idaho Falls, Idaho, March 1971.

72. R.W. Tilbrook, "Coolant Voiding Transients in LMFBR's", Proc. Conf. New Developments in Reactor Mathematics and Applications, Idaho Falls, Idaho, March 1971.

73. A.W. Cronenberg, "A Thermodynamic Model for Molten UO_2-Na Interaction Pertaining to Fast Reactor Fuel-Failure Accidents", Ph.D. Thesis, Nucl. Eng. Dept., Northwestern University, June 1971.

74. P.G. Lorenzini and G.F. Flanagan, An Evaluation of Fuel-Coolant Interactions During Disassembly of an LMFBR", Proc. Conf. New Developments in Reactor Mathematics and Applications, Idaho Falls, Idaho, March 1971.

75. J.C. Mills and W.E. Kastenberg, "An Axial Kinetics Model for Fast Reactor Disassembly Accidents", Proc. Conf. New Developments in Reactor Mathematics and Applications, Idaho Falls, Idaho, March 1971.

76. L.L. Smith et al., "SAS/FCI: A Fuel-Coolant Interaction Model for LMFBR Whole-Core Accident Analysis", ANS Topical Meeting on Mathematical Models and Computational Techniques for Analysis of Nuclear Systems", Ann Arbor, Mich., April 1973.

77. K.H. Hsiao et al., "Pressurization of a Solidifying Sphere", J. App. Mechanics, ASME Paper No. APM-71-AAA.

78. K.V. Roberts, "Theoretical Calculations on Fuel-Coolant Interactions", Paper presented at CREST Specialist Meeting on Fuel-Sodium Interaction at Grenoble, France, January 1972.

79. D. Cho and R.W. Wright, "LMFBR Nuclear Safety Program Annual Report", ANL-7800, 358-369, July 1971.

80. A.H. Shapiro, The Dynamics and Thermodynamics of Compressible Fluid Flow, Vol. 1, p 46, The Ronald Press Company.1953.

81. G.H. Golden and J.V. Tokar, "Thermodynamical Properties of Sodium", ANL-7323, August 1967.

82. R. Bulrisch and J. Stoer, Proceedings of IFIP Congress, W.A. Kalenich Ed., Vol 2, Sparatan Books, 487-488, 1965.

83. W.M. Rohsenow, "Heat Transfer With Boiling", in Developments in Heat Transfer, M.I.T. Press, Cambridge, MA 1964.

84. W.S. Bradfield, "Liquid-Solid Contact in Stable Film Boiling", I. & E. C. Fundamentals 5 (2), 200-204, May 1966.

85. W.S. Bradfield, "On the Effect of Subcooling On Wall Superheat in Pool Boiling", J. Heat Transfer 89 (3), 269-270, August 1967.

86. F.J. Walford, "Transient Heat Transfer From a Nickel Sphere Moving Through Water", Int. J. Heat Mass Transfer 12, 1621-1625, 1969.

87. R.N. Jacobson and F.H. Shair, "Film Boiling from a Sphere During Forced Convection of Subcooled Water", I. & E.C. Fundamentals 9 (1), 183-185, Feb. 1970.

88. J.W. Stevens et al., "Transition Boiling From Spheres to Water", University of Houston ORO-3936-3, April 1970.

89. M.M.K. Farahat, "Transient Boiling Heat Transfer From Spheres to Sodium", Ph.D. Thesis, Dept. Nucl. Eng., Northwestern University, August 1971.

90. S.J. Board et al., "An Experimental Study of Energy Transfer Processes Relevant to Thermal Explosions", Int. J. Heat Mass Transfer 14, 1631-1641, October 1971.

91. G.L. Gains, Jr., Insoluble Monolayers at Liquid-Gas Interfaces, Interscience Publishers, New York, 1966.

92. N.K. Adam, The Physics and Chemistry of Surfaces, Oxford University Press, Third Edition 1941.

93. H. Lurie and H.A. Johnson, "Transient Pool Boiling of Water On a Vertical Surface With a Step in Heat Generation", J. Heat Transfer 84 (3), 217-224, August 1962.

94. D.P. Wehmeyer and T.W. Jackson, "Transient Film Boiling of Carbon Tetrachloride and Freon-113 on a Horizontal Cylindrical Surface", J. Heat Transfer, November 1972.

95. P.J. Berenson, "Film Boiling Heat Transfer From a Horizontal Surface", J. Heat Transfer 83, 351-358, August 1961.

96. E.K. Kalinin et al., "Heat Transfer in Tubes With Rod Regime in the Case of Film Boiling of a Subcooled Liquid", Cocurrent Gas-Liquid Flow, Plenum Press, 1969.

97. L.C. Witte, "Film Boiling From a Sphere", I&EC Fundamentals 7 (3), 517-518, August 1968.

98. R. Hickling and M.S. Plesset, "Collapse and Rebound of a Spherical Bubble in Water", Phy. of Fluids 1 (1), p 7, January 1964.

99. R.D. Ivany and F.G. Hammitt, "Cavitation Bubble Collapse in Viscous Compressible Liquids - Numerical Analysis", J. Basic Eng. ASME Series D, p 977, December 1965.

100. A.M. Judd, "Boiling and Condensation of Sodium in Relation to Fast Reactor Safety", Paper IV-A-4, International Conference on the Safety of Fast Reactors, Aix-en-Provence, September 1967.

101. A.M. Judd, "The Condensation of Sodium Vapour Bubbles", AEEW-M813, UKAEA-Reactor Group, Winfrith, 1968.

102. T. Theofanous et al., "A Theoretical Study on Bubble Growth in Constant and Time-Dependent Pressure Fields", Chem. Eng. Sci 24, 885-897, 1969.

103. T.G. Theofanous et al., "Nonequilibrium Bubble Collapse, A Theoretical Study", 11th National Heat Transfer Conference, Minneapolis, August 1969.

104. R.B. Duffy, "The Analytical Description of Vapour Bubble Dynamics in Water and Liquid Sodium", Central Electricity Generating Board Report RDIB/N1349, April 1969.

105. M.N. Ozisik, Boundary Value Problems of Heat Conduction, International Textbook Co., Scranton, Pa., 1968.

106. T.R. Goodman, "Application of Integral Methods to Transient Nonlinear Heat Transfer", in Advances in Heat Transfer Vol. 1, 1964.

107. R.B. Bird, W.E. Stewart and E.N. Lightfoot, Transport Phenomena, John Wiley and Sons Inc., 1960.

108. Lord Rayleigh, "Pressure Due to Collapse of Bubbles", Phil. Mag. 34, 94-98, 1917.

109. J.G. Kirkwood and H.A. Bethe, Report No. 588, 1942 Office of Scientific Research and Development, 1942.

110. F.R. Gilmore, Report No. 26-4, Hydrodynamics Laboratory, California Institute of Technology, Pasadena, 1952.

111. P. Spiegler et al., "Onset of Stable Film Boiling and the Foam Limit", Int. J. Heat Mass Transfer 6, 987-989, 1963.

112. E.K. Kalinin et al., "Investigation of the Crisis of Film Boiling in Channels", Moscow Aviation Institute, USSR, 1968.

113. R.E. Henry, "A Correlation for the Minimum Wall Superheat in Film Boiling", Trans. Am. Nucl. Soc. 15, p 420, 1972.

114. M.S. Plesset and R.B. Chapman, "Collapse of an Initially Spherical Vapor, Cavity in the Neighborhood of a Solid Boundary", J. Fluid Mechanics 47 (2) 283-290, 1971.

115. H.S. Carslaw and J.C. Jeager, Conduction of Heat In Solids, Oxford University Press, 1947.

116. R.E. Henry and D.H. Cho, "Reactor Development Program Progress Report, December 1972", ANL-RDP-12, p 9.34, February 1973.

117. L.J. Briggs, "Limiting Negative Pressure of Water", J. App. Phy. 21 (7), 721-722, July 1950.

118. D.C. Couzens and D.H. Trevera, "Critical Tension in a Liquid Under Dynamic Conditions of Stressing", Nature, 222, May 3, 1969.

119. A.T.J. Hayward, "Negative Pressure in Liquids: Can it be Harnessed to Serve Man?", American Scientist 59 (4), 434-443, July-August 1971.

120. M.G. Sirotyuk, "Experimental Investigations of Ultrasonic Cavitation", in High Intensity Ultrasonic Fields, L.D. Rozenberg Ed., Plenum Press, New York, 1971.

121. H.G. Flynn, "Physics of Acoustic Cavitation in Liquids", in Physical Acoustics Vol. I - Part B, W.P. Mason, Ed., Academic Press, New York, 1964.

122. L. Bernath, "Theory of Bubble Formation in Liquids", Ind. Eng. Chem. 44, 1310-1313, 1952.

123. M. Volmer, Kinetik der Phasenbildung, Theodore Steinkapft, Dresden and Leipsig, 1939.

124. J.H. Keenan et al, Steam Tables, John Wiley and Sons, Inc., New York, 1969.

125. L. Camp, "Underwater Acoustics", Wiley-Interscience, New York, 1970.

126. B.S. Gottfried et al., "The Leidenfrost Phenomenon: Film Boiling of Liquid Droplets on a Flat Plate", Int. J. Heat Mass Transfer 9, 1167-1187, Nov. 1966.

127. K.J. Baumeister et al., "Role of the Surface in the Measurements of the Leidenfrost Temperature", Proc. ASME Symp. on Augmentation of Convective Heat and Mass Transfer, 91-101, 1970.

128. W.M. Rohsenow, "Film Condensation of Liquid Metals", Paper presented at the International Center for Heat and Mass Transfer, Troigir , Yugoslavia, Sept. 1971 also Trans. CSME 1 (1), 5-12, March 1972.

129. K.F. Wylie and R.S. Brodkey, "Transport Phenomena at the Liquid-Vapor Interface of Mercury Using Radioactive Tracers", Int. Sym. Two Phase Flow, Haifa, Israel, August 1971.

130. A. Ralston, "Mathematical Methods for Digital Computers, H.S. Wilf Ed., 95-109, Wiley, New York, 1960.

131. W.M. Rohsenow and H.Y. Choi, Heat, Mass and Momentum Transfer , Prentice Hall, Inc., 1961.

132. G. Hatsopoulos and J. Keenan, Principles of General Thermodynamics, John Wiley & Sons, Inc., N.Y., 1965.

133. W.R. Gibbs, Collected Papers, Vol. I Thermo., Yale University Press, 1948 (as Referenced in W.M. Rohsenow, "Nucleation With Boiling Heat Transfer", in Role of Nucleation in Boiling and Cavitation, R. Nystrom and F. Hammitt, Ed., ASME Publications, 1970.

134. C.J. Smithells Ed., Metals Reference Book, Vol. III, Fourth Edition, Butterworth and Company, London, 1967.